

THE UNIVERSITY OF NOTTINGHAM

**SEMI-SYNTHESIS OF NOVEL
CARDAMONIN ANALOGUES AND
IDENTIFICATION OF A HIGHLY ACTIVE
Cu(II)-CARDAMONIN COMPLEX THAT
INHIBITS MIGRATION AND INDUCES
APOPTOSIS *VIA* INHIBITION OF MTOR
EXPRESSION**

Mohammed Khaled Ali Bin Break, MSc
(Chemistry)

Thesis submitted to The University of Nottingham for the degree of
Doctor of Philosophy

JULY 2018

Abstract

Lung cancer is considered a major health concern and is responsible for most cancer-related deaths. Nasopharyngeal carcinoma (NPC) is another type of cancer that is predominantly in China and has a low survival rate, which makes it a serious health issue. There is currently no cure for lung cancer and NPC, so it was decided to investigate derivatives of the highly bioactive natural product, cardamonin, for a potential drug candidate. 19 analogues of cardamonin were synthesised and tested against A549 (lung) and HK1 (NPC) cell lines. The techniques employed in synthesising the analogues were one-step reactions which included alkylation, acylation, reduction, condensation, cyclisation and complexation reactions. The analogues were fully characterised. MTS assay showed that several derivatives, such as the allyl derivative of cardamonin (**2**) and cardamonin's Cu (II) complex (**19**), had more potent cytotoxic activities than cardamonin. Furthermore, the active analogues have generally demonstrated lower toxicity towards normal MRC5 cells. Structure-activity relationship (SAR) analysis showed the importance of the ketone and alkene groups for bioactivity, while substituting cardamonin's phenolic groups with more polar moieties resulted in activity enhancement. As part of the SAR study and further exploration of chemical space, the effect of metal coordination on cytotoxicity was also investigated, but it was only possible to successfully obtain the Cu (II) complex of cardamonin (**19**), and the metal ion enhanced bioactivity. **19** was the most potent analogue possessing IC₅₀ values of 13.2 µM and 0.7 µM against A549 and HK1 cells, corresponding to a 5- and 32-fold increase in activity, respectively. It was also able to inhibit the migration of A549 and HK1 cells. Mode

of action studies revealed that **19** induced DNA damage in both cell lines resulting in G2/M-phase arrest, which further led to apoptosis *via* the activation of caspase-9 and caspase-3/7. Moreover, qPCR analysis showed that **19** inhibited the expression of the mammalian target of rapamycin (mTOR) by >50% in A549 and HK1 cells which indicated that it exerted its anticancer activity, at least in part, *via* inhibition of the mTOR signalling pathway. So molecular docking of cardamonin and **19** to mTOR was performed and the study showed that the higher activity of **19** might be due to formation of further hydrogen bond interactions with the receptor resulting in a higher binding free energy of -9.8 kcal/mol. Therefore, all these assays have further proven the high bioactivity of **19**. However, further *in vivo* and animal model studies would have to be conducted in order to confirm the potential of **19** as an anticancer agent.

Publications

M.K. Break, M.S. Hossan, Khoo, Y., Qazzaz, M.E., Al-Hayali, M.Z.K., Chow, S.C., Wiart, C., Bradshaw, T.D., Collins, H. and T.J. Khoo (2018). "Discovery of a highly active anticancer analogue of cardamonin that acts as an inducer of caspase-dependent apoptosis and modulator of the mTOR pathway." Fitoterapia **125**: 161-173.

Khoo, Y., **M. K. Break**, S. C. Chow and T. J. Khoo (2015). "In vitro cytotoxic potential of novel semi-synthesised clusianone and cardamonin analogues." Planta Med **81**(16): PM_49.

Acknowledgements

All praises to The Almighty Allah, the most Merciful, the most Beneficent, for providing me with the determination and strength that allowed me to accomplish this task. I would then like to extend my appreciation and thanks to my great mother, Najaat Baabbad, my father Khaled Bin Break, my uncle Abdullah Baabbad and my whole family who have always been on my side and encouraged me to accomplish this study.

I wish to thank my supervisor Dr.Khoo Teng-Jin for assisting me in my research, trusting me and granting me a great deal of freedom in conducting my research. I really appreciate this and I find it an important factor that contributed to my development as a researcher. Moreover, I wish to express my appreciation for all the lab technicians for their assistance during the course of my study; they were certainly of great help.

I would also like to thank Dr.Alan Khoo from Institute of Medical Research and prof. Tsao George Sai-Wah from the University of Hong Kong for providing us with the HK1 cell-lines

Finally, I would like to thank all the students at the Cell Culture Lab for their assistance, especially Mr.Shahadat Hossan for running the flow cytometric experiments and caspase-3/7 assay, and Ms. Yivonn Khoo for helping me in screening the analogues.

Table of Contents

Abstract	i
Publications	iii
Acknowledgements	iv
List of Figures	ix
List of Tables	xv
1 Introduction	1
1.1 Lung Cancer	7
<i>1.1.2 Types of Lung Cancer.....</i>	<i>8</i>
<i>1.1.3 Symptoms, Risk Factors, Diagnosis and Treatment</i>	<i>9</i>
1.2 Nasopharyngeal Cancer	11
<i>1.2.1 Symptoms, Risk Factors, Diagnosis and Treatment</i>	<i>12</i>
1.3 Chalcones.....	13
<i>1.3.1 Structure and Chemistry.....</i>	<i>13</i>
<i>1.3.2 Formation of Chalcones</i>	<i>15</i>
<i>1.3.3 Bioactivity of Chalcones.....</i>	<i>18</i>
2 Literature Review	25
2.1 Structure and Analysis of Cardamonin.....	25
2.2 Sources of Cardamonin.....	28
2.3 Medicinal Applications of Cardamonin.....	29
<i>2.3.1 Anti-inflammatory Activity.....</i>	<i>29</i>
<i>2.3.2 Antioxidant Activity</i>	<i>30</i>

2.3.3 Vasorelaxant Activity.....	31
2.3.4 Hypoglycaemic Activity	32
2.3.5 Anti-infectious Activity	32
2.3.6 Pain Management.....	33
2.3.7 Anticancer Activity	33
2.4 Pharmacokinetic and ADME Studies on Cardamonin.....	38
2.5 Cardamonin Analogues	39
3 Results and Discussion	42
3.1 Chemistry.....	42
3.1.1 Synthesis	42
3.1.2 Structure and Characterisation	47
3.2 Biological Studies.....	84
3.2.1 Cell Viability and Structure-activity Relationship Studies	84
3.2.2 Active Analogues Showed More Selectivity Towards the Cancer Cells	89
3.2.3 Compound 19 Inhibited the Migration of A549 and HK1 Cells	90
3.2.4 Induction of G2/M-phase Arrest by Compound 19 in A549 and HK1 Cells	94
3.2.5 Compound 19 causes DNA damage in A549 and HK1 cells	96
3.2.6 Induction of Apoptosis by Compound 19 via Activation of Caspase-3/7.....	98
3.2.7 Compound 19 Activated Caspase-9 Leading to Apoptosis via the Mitochondrial Pathway	101
3.2.8 Compound 19 Inhibited mTOR Expression in A549 and HK1 Cells	105
3.3 In Silico Studies	109

3.3.1 <i>Drug-likeness and ADMET Studies</i>	109
3.3.2 <i>Molecular Docking Studies</i>	115
4 Conclusion	120
5 Future Studies	123
6 Materials and Methods	124
6.1 General.....	124
6.2 Synthesis	125
6.3 Cell Culture.....	138
6.4 Cell Viability Assay.....	138
6.5 Migration Assay.....	139
6.6 Cell-cycle Analysis.....	139
6.7 Flow Cytometric Detection of γ -H2AX.....	140
6.8 Caspase-Glo 3/7 Apoptosis Assay	140
6.9 Caspase-Glo 8 and Caspase-Glo 9 Assays	141
6.10 qPCR Assay	141
6.11 In Silico Studies	142
6.11.1 <i>Drug-likeness and ADMET Studies</i>	142
6.11.2 <i>Molecular Docking Studies</i>	142
7 References	143
8 Appendix	173
8.1 HPLC Chromatograms	173

8.2 IR Spectra	182
8.3 Cell Viability Data for Compound 19 and Cardamonin at 24 h	192
8.4 Caspase-Glo 3/7 Assay Attempts in A549 and HK1 Cells.....	194

List of Figures

Figure 1.1 General structure of chalcones with their numbering scheme.....	14
Figure 1.2 Structural conformations of chalcones	14
Figure 1.3 Biosynthesis of chalcones naturally (<i>adapted from: Yadav et al. 2011</i>).....	16
Figure 1.4 General reaction scheme for the synthesis of chalcones by the Claisen-Schmidt condensation reaction	18
Figure 2.1 Structure of cardamonin	26
Figure 2.2 Cardamom seeds (<i>adapted from: Gonçalves, Valente and Rodrigues 2014</i>) ..	29
Figure 2.3 Examples of cardamonin analogues	39
Figure 3.1 Structure of SBDTC	43
Figure 3.2 Intramolecular hydrogen bonding in cardamonin	47
Figure 3.3 Overlaid IR spectra of cardamonin and 19	52
Figure 3.4 NMR spectrum of cardamonin	54
Figure 3.5 Resonance effect of cardamonin	55
Figure 3.6 NMR spectrum of 1	56
Figure 3.7 NMR spectrum of 2	57
Figure 3.8 NMR spectrum of 3	59
Figure 3.9 NMR spectrum of 4	60
Figure 3.10 NMR spectrum of 5	61
Figure 3.11 NMR spectrum of 6	62
Figure 3.12 NMR spectrum of 7	63
Figure 3.13 NMR spectrum of 8	64
Figure 3.14 NMR spectrum of 9	65
Figure 3.15 NMR spectrum of 10	66
Figure 3.16 thione-thiol tautomerism in 10	67
Figure 3.17 NMR spectrum of 11	68

Figure 3.18 NMR spectrum of 12	69
Figure 3.19 NMR spectrum of 13	71
Figure 3.20 NMR spectrum of 14	72
Figure 3.21 Tautomerism in pyrimidones/pyrimidthiones	73
Figure 3.22 NMR spectrum of 15	74
Figure 3.23 NMR spectrum of 16	75
Figure 3.24 NMR spectrum of 17	76
Figure 3.25 NMR spectrum of 18	77
Figure 3.26 NMR spectrum of 19	78
Figure 3.27 HRMS spectrum of 19	81
Figure 3.28 TGA curve of 19	82
Figure 3.29 UV-Vis spectrum of cardamonin and 19	83
Figure 3.30 A summary of the anticancer SAR study results of cardamonin.....	88
Figure 3.31 Compound 19 inhibited the migration of A549 and HK1 cells. Migration assay was conducted in a 6-well plate by forming a “wound” across a layer of cells followed by treatment with either solvent control, 25 μ M cardamonin or 25 μ M compound 19 . The figure shows representative wound closure images from three experiments.....	92
Figure 3.32 Quantification of cell migration assay results for A549 and HK1 cells was performed using the software ImageJ. Cell migration was calculated and expressed as the percentage of “wound” area covered by the cells to the initial cell-free “wound” area. The assay was repeated three times, and bars and error bars refer to mean \pm SEM. * $p < 0.05$, analysed using a two-tailed unpaired t-test.....	93
Figure 3.33 Flow cytometric analysis of cell-cycle parameters following 24 h of treatment with either solvent control or 19 at IC ₅₀ concentrations in A549 and HK1 cells. Data were gated to exclude apoptotic cells from calculations of the fraction of cells in G1,	

S and G2/M phases. Results are representative of two independent experiments for each cell-line.	95
Figure 3.34 Flow cytometric detection of γ -H2AX formation following 24 h of treatment with either solvent control or 19 at IC ₅₀ concentrations in A549 and HK1 cells. (A) Representative dot-plots illustrating γ -H2AX abundance versus total cellular DNA content of each cell. (B) Bar chart summarising results of the flow cytometry analysis. Results represent the mean \pm SEM of 2 independent experiments. ***p<0.001, analysed using a two-tailed unpaired t-test.	97
Figure 3.35 Caspase-3/7 activity of A549 cells and HK1 cells, treated with solvent control or 19 at about 10 μ M for 12 h. The experiment was performed in duplicate for each cell line and bars and error bars refer to mean \pm SEM. *p<0.05, analysed using a two-tailed unpaired t-test.	100
Figure 3.36 Intrinsic apoptosis and Extrinsic apoptosis signalling pathways (<i>adapted from: Loreto et al. 2014</i>).....	102
Figure 3.37 Caspase-8 and caspase-9 activity of A549 cells and HK1 cells, treated with either solvent control or 19 at about 10 μ M for 6 h. The experiment was performed in duplicate for each cell line and bars and error bars refer to mean \pm SEM. **p<0.01, analysed using a two-tailed unpaired t-test.	104
Figure 3.38 PI3-K/Akt/mTOR signalling pathway (<i>adapted from: Holmes 2011</i>)	105
Figure 3.39 mRNA expression of <i>mTOR</i> in A549 and HK1 cells after treatment with either solvent control or 50 μ M of compound 19 for 24 h, as determined by qPCR. mRNA expression levels were normalised to GAPDH and compared with the untreated solvent control. The qPCR experiment was repeated three times, and bars and error bars refer to mean \pm SEM. **p<0.01, analysed using a two-tailed unpaired t-test.....	108
Figure 3.40 Drug-likeness graph used by Molsoft. Drug-likeness score for 6 has been shown in this image as a red vertical line.	110

Figure 3.41 Binding pose of the co-crystallised ligand compared to the highest binding energy pose of the ligand generated by Autodock Vina (Yellow). The binding poses were found to be similar.....	116
Figure 3.42 (A and C): 2D diagram showing the interactions between mTOR and: (A) Cardamonin; (C) Compound 19 , the orange lines represent hydrophobic interactions, while the blue arrows represent hydrogen bonds. (B and D): 3D interaction map of mTOR, which has been mapped according to hydrophobicity, and: (B) Cardamonin; (D) Compound 19	119
Figure 4.1 Schematic representation of the proposed signalling pathways induced by 19 in the cancer cells to cause apoptosis.....	122
Figure 8.1 HPLC chromatogram of 1	173
Figure 8.2 HPLC chromatogram of 2	173
Figure 8.3 HPLC chromatogram of 3	174
Figure 8.4 HPLC chromatogram of 4	174
Figure 8.5 HPLC chromatogram of 5	175
Figure 8.6 HPLC chromatogram of 6	175
Figure 8.7 HPLC chromatogram of 7	176
Figure 8.8 HPLC chromatogram of 8	176
Figure 8.9 HPLC chromatogram of 9	177
Figure 8.10 HPLC chromatogram of 10	177
Figure 8.11 HPLC chromatogram of 11	178
Figure 8.12 HPLC chromatogram of 12	178
Figure 8.13 HPLC chromatogram of 13	179
Figure 8.14 HPLC chromatogram of 14	179
Figure 8.15 HPLC chromatogram of 15	180
Figure 8.16 HPLC chromatogram of 16	180

Figure 8.17 HPLC chromatogram of 17	181
Figure 8.18 HPLC chromatogram of 18	181
Figure 8.19 IR spectrum of Cardamonin	182
Figure 8.20 IR spectrum of 1	182
Figure 8.21 IR spectrum of 2	183
Figure 8.22 IR spectrum of 3	183
Figure 8.23 IR spectrum of 4	184
Figure 8.24 IR spectrum of 5	184
Figure 8.25 IR spectrum of 6	185
Figure 8.26 IR spectrum of 7	185
Figure 8.27 IR spectrum of 8	186
Figure 8.28 IR spectrum of 9	186
Figure 8.29 IR spectrum of 10	187
Figure 8.30 IR spectrum of 11	187
Figure 8.31 IR spectrum of 12	188
Figure 8.32 IR spectrum of 13	188
Figure 8.33 IR spectrum of 14	189
Figure 8.34 IR spectrum of 15	189
Figure 8.35 IR spectrum of 16	190
Figure 8.36 IR spectrum of 17	190
Figure 8.37 IR spectrum of 18	191
Figure 8.38 IR spectrum of 19	191
Figure 8.39 Cell viability (MTS assay) of A549 and HK1 cells pre-treated with cardamonin at different concentrations for 24 h. The assay was repeated three times, and bars and error bars refer to mean \pm SEM.....	192

Figure 8.40 Cell viability (MTS assay) of A549 and HK1 cells pre-treated with compound **19** at different concentrations for 24 h. The assay was repeated three times, and bars and error bars refer to mean \pm SEM..... 193

List of Tables

Table 1.1 Summary of the anticancer effects of some naturally-occurring chalcones.....	20
Table 2.1 Summary of the analytical methods used for cardamonin characterisation.....	27
Table 2.2 Cytotoxicity of cardamonin towards different cancer cell-lines	34
Table 3.1 IC ₅₀ values of cardamonin and its analogues against HK1 and A549 cells. Active analogues have been shaded.....	84
Table 3.2 Cytotoxic activity of the bioactive analogues against MRC-5 cells	89
Table 3.3 ‘Lipinski’s rule of 5’ with additional parameters for selected analogues	111
Table 3.4 <i>In silico</i> prediction of further ADMET properties of cardamonin and its most active analogues.....	114
Table 8.1 Caspase-3/7 activity of A549 cells and HK1 cells, treated with 19 at about 10 μM. The experiment was performed in duplicate for each cell line and mean results are reported.....	194
Table 8.2 Caspase-3/7 activity of A549 cells and HK1 cells, treated with 19 at about 30 μM. The experiment was performed in duplicate for each cell line and mean results are reported.....	194

1 Introduction

Cancer is considered to be a major health concern and a leading cause of death worldwide with about 14 million new cases and 8.2 million deaths due to cancer in 2012. It is expected that the number of new cancer cases would increase by 70% over the next two decades. Lung cancer is responsible for most cancer-related deaths globally with more than 1.3 million deaths yearly, while the number of deaths is continuously rising in the Far East in countries such as China. Another type of cancer that is mostly prevalent in Asia is nasopharyngeal carcinoma (NPC) and this cancer is known to have a low survival rate making it a serious health problem. NPC is more specifically prevalent in Southern China and Southeastern Asia with a peak incidence rate of 50 cases per 100,000 people per year. It is also common amongst the Inuits of Alaska and people in North Africa. There is currently no cure for any of these two types of cancer and the drugs approved for treatment are usually accompanied with undesired side effects such as vomiting, hair loss, diarrhoea and weakness in the body. Therefore there is a need for further research aimed at developing more effective anticancer compounds (Wei and Sham 2005; Pastorino 2010; Cancer Research UK 2014; Cancer Research UK 2016; World Health Organization 2017; Wang *et al.* 2018).

Natural products are considered to be a rich source of bioactive molecules and have been studied extensively for the purpose of finding potent anticancer compounds. This is due to their biologically active and diverse chemotypes that enable the discovery of novel drugs. In the field of cancer, natural products or their derivatives

still make a large percentage of the approved drugs. Chalcones are naturally occurring compounds that are characterised by the presence of an α,β -unsaturated ketone with two aromatic rings and belong to the flavonoid family of compounds. This group of compounds have been reported to possess a wide range of bioactivities including antitumour, antioxidant, antimitotic and anticancer activities (Albuquerque *et al.* 2014; Newman and Cragg 2016; Rodrigues *et al.* 2016).

Cardamonin is a chalcone that has been extracted from several plants including *Alpinia rafflesiana* and was proven to possess cytotoxic properties against a wide variety of cancer cells while its mode of action has been studied extensively (Gonçalves, Valente and Rodrigues 2014; Lu *et al.* 2018; Shi *et al.* 2018). However, there have been no studies performed on semi-synthetic analogues of cardamonin with anticancer properties nor were there any detailed investigations on the structure-activity relationship of cardamonin specifically. Therefore, it has been decided to investigate the anticancer potential of cardamonin and its analogues against lung cancer cells (A549) and NPC cells (HK1) with the aim of producing novel and potent compounds.

In this chapter, the objectives, rationale and hypothesis of the present research study will be covered. Furthermore, crucial basic concepts that should be known to fully understand and appreciate the current study will be introduced in this chapter. This will include a brief introduction on **lung cancer**, **nasopharyngeal cancer** and **chalcones**. Introducing these basic concepts will ensure that essential information have been covered before going into the main research study.

- **Summary of Research Problem and Hypothesis:**

- **Research Problem:** Lung cancer and NPC are responsible for the deaths of many people worldwide and there is currently no cure for any of these types of cancer. Therefore, it has been decided to investigate the natural product, cardamomin, to search for a potential treatment for these types of cancer.
- **Hypothesis:** Cardamomin has been proven to possess high cytotoxic activity across a variety of cancer cell-lines. Therefore, it has been hypothesised that it would be an appropriate starting material for the production of compounds or analogues with higher cytotoxic activity. The analogues were produced *via* semi-synthesis and tested for their anticancer potential against A549 (lung) and HK1 (NPC) cancer cell lines.

- **Objectives and Rationale of the Study:**

- 1) **Semi-synthesis of cardamomin analogues and testing them against A549 and HK1 cell lines**

As it has been mentioned earlier, the need for a cure for NPC and lung cancer has made these two types of cancer the main focus of this study. Therefore, it was decided to investigate cardamomin on these cancer types due to its high bioactivity as has been also mentioned earlier. However, in this study, it was intended to optimise cardamomin's cytotoxic activity *via* synthesising a variety of analogues and testing them against A549 and HK1 cells.

A549 cells were used as a disease model for lung cancer cells because they are derived from a human source and are readily cultured. Moreover, A549 cells belong to a subtype of lung cancer known as non-small cell lung cancer

(NSCLC), and this subtype is responsible for the majority of lung cancer cases. Therefore, another reason for A549 cells being a suitable disease model for lung cancer was because this cell type reflects the majority of lung cancer cases, which will increase the relevance of this study's results (Koparal and Zeytinoglu 2003; Shen *et al.* 2009; Li *et al.* 2011).

HK1 cells were used as a disease model for NPC. It has been often challenging to establish NPC cell lines due to the small size of the biopsy and because it is infiltrated with lymphoid cells and connective tissue. Therefore, this resulted in a very limited number of available cell lines for NPC. Moreover, the available NPC cell lines suffer from authentication issues, as usually this disease is mainly in China so there are no global authentication efforts for NPC cell lines. This authentication issue resulted in several cell lines being falsely identified as NPC cell lines, such as CNE-1, CNE-2, AdAH, NPC-KT and HONE1 which were found to be contaminated with HeLa cells. However, HK1 has been authenticated and is regarded as a valid disease model for NPC and this is the main reason for choosing it for studies concerning NPC (Cheung *et al.* 1999; Chan *et al.* 2008; Strong *et al.* 2014; Wasil *et al.* 2015).

2) Testing the toxicity of the active analogues towards normal MRC-5 cells

Most marketed anticancer drugs cause severe side-effects and this has been a major issue when developing these drugs. Therefore, one of the main aims of this study is to ensure that the active cardamonin analogues would have higher selectivity towards cancer cells and less effect on normal cells.

Human normal lung fibroblast cells (MRC-5) were chosen to represent healthy cells of the body and analogues would have to be tested against it. MRC-5 has been often used across the field of cancer research to assess compounds' toxicities, even when the cancer cells were from an organ other than the lungs, such as ovarian cancer cells, MRC-5 was still used to assess the compound's toxicity. In fact, MRC-5 cells were used even outside the field of cancer, such as in developing antivirals and antiprotozoals in order to assess the compounds' toxicities. One of the main reasons for using MRC-5 cells for toxicity studies is because they are sensitive to the toxicity of exogenous chemicals. Therefore, for these reasons, it was decided to use MRC-5 cells to test for the cytotoxicity of cardamonin's active analogues towards normal cells for this study (Shigeta *et al.* 2002; Vik *et al.* 2009; Damião *et al.* 2014; Lu *et al.* 2015).

3) Conduct the first ever Structure-Activity Relationship (SAR) study on cardamonin and its analogues

There have been no SAR studies on cardamonin and its analogues before, this study is the first one to have considered doing so. This would help in identifying crucial chemical groups for bioactivity and aid in future optimisation efforts of cardamonin.

4) Investigate the mode of action of the most active analogue, especially the analogue's effect on Mammalian Target of Rapamycin (mTOR)

One of the main aims of this study is to further study the cytotoxic mode of action of the most active analogue with more focus on its effect on the

mTOR. **mTOR** is a 289 kDa serine/threonine kinase and a major regulator of cell growth and proliferation. It functions in two complexes, mTORC1 and mTORC2, and together these complexes play a major role in regulating several cellular processes such as protein synthesis, cell-cycle, autophagy and lipid synthesis. However, it has been found that mTOR is abnormally activated in several types of cancer and inhibiting its activity has been a known strategy in cancer treatment. One of the inhibitors of mTOR activity is cardamonin. Several studies have shown that cardamonin exerts its cytotoxic activity *via* inhibiting the mTOR pathway, so it was suggested that the most active analogue in this study would act *via* a similar mechanism. This was the main reason for deciding to investigate the effect of cardamonin's most active analogue on mTOR (Ekman, Wynes and Hirsch 2012; Tang *et al.* 2014; Nui *et al.* 2015; Xue *et al.* 2015).

5) Perform *in silico* studies on cardamonin's most active analogue

This study also aims to perform computational studies on cardamonin's most active analogue for a better understanding of the way the compound would interact with its potential receptor (mTOR). This could provide a possible explanation for the observed bioactivity of the analogue. Furthermore, the study aims to predict the active analogues' pharmacokinetics, which is concerned with how a compound gets processed in the body.

1.1 Lung Cancer

Lung cancer is a type of cancer that involves the uncontrolled growth of abnormal cells in one or both lungs and can start in the cells lining the bronchi in addition to the alveoli and bronchioles. It is thought that the cancer starts with initial changes in the lung cells prior to the disease, whereby DNA of the lung cells causes them to grow faster but no tumour is formed at this stage and symptoms are not clear. However, it is possible that certain genetic mutations might cause these cells to develop into cancer cells and these cells might later develop their own blood supply system to ensure their survival and growth until a tumour forms which can be easily observed on imaging tests.

Moreover, lung cancer cells might spread (metastasise) from the original tumour to other parts of the body and this phenomenon is responsible for making lung-cancer a life-threatening disease as this process can occur at an early stage even before the cancer can be detected *via* any imaging tests such as chest X-ray. One of the main ways by which lung cancer cells spread is through the lymphatic system. In this case, cancer cells tend to enter the lymphatic vessels and grow in lymph nodes in addition to the mediastinum. Once these cells have reached the lymph nodes then it is highly probable that the cancer has spread to other parts of the body. It is also possible for the cancer to spread through the blood by entering the blood vessels and spreading to other parts of the body (American Cancer Society 2015).

1.1.2 Types of Lung Cancer

There are two types of lung cancer, namely; **Small-cell lung cancer (SCLC)** and **Non-small cell lung cancer (NSCLC)**. This classification is highly essential as both types are treated differently.

SCLC constitutes approximately 10%-15% of lung cancers and has been called as such due to the size of cancer cells as observed through the microscope. It is very different from other lung cancer types. It usually starts around the chest's centre in the bronchi but later tends to spread throughout the body. SCLC is the most aggressive of lung-cancer subtypes and is characterised by high response rates to chemotherapy in addition to having higher chances of metastasis. It is responsible for the death of around 250,000 people yearly. Smoking has been the major cause for developing SCLC whereby almost all patients with SCLC are current or former heavy smokers. There have not been significant therapeutic advances with regards to SCLC in the past 30 years mainly due to pharmaceutical disinterest as it has proven to be a graveyard for drug development (American Cancer Society 2015; Gazdar, Bunn and Minna 2017; Oronsky *et al.* 2017).

NSCLC makes up the majority of lung cancers with a proportion of 85%-90% and they consist of 3 types, but these types are not similar in size, chemical make-up or shape; they were placed under the same group due to their similarities when it comes to the approach to treatment and prognosis. The types are as follows (American Cancer Society 2015; Herbst, Morgensztern and Boshoff 2018):

- Squamous cell carcinoma: This type usually affects early versions of a type of flat cells called squamous cells, and these cells tend to line the inside of

the airways in the lungs. This type of cancer accounts for 20%-30% of all lung cancers and has been often linked to smoking.

- **Adenocarcinoma:** This type of cancer makes about 40% of lung cancers, and usually starts in cells that are known for secreting substances as mucus, and often affects smokers but is also considered the main type of lung cancer in non-smokers. Adenocarcinoma is mostly found in the outer part of lungs and its relatively slower growth progress enables its discovery before spreading outside the lungs. This is the most common type of cancer in non-smokers.
- **Large cell (undifferentiated) carcinoma:** This type of cancer can occur in any part of the lung and usually accounts for 10%-15% of all lung cancers. It grows and spreads very quickly which makes it difficult to treat.

1.1.3 Symptoms, Risk Factors, Diagnosis and Treatment

Symptoms of lung cancer include continuous coughing, chest pain, wheezing, blood in sputum, weight loss, feeling tired and trouble in breathing.

Smoking is the main factor which increases the risks of a person being diagnosed with lung cancer and this includes passive smoking, while air pollution can also contribute to the development of lung cancer. Moreover, the risks of developing lung cancer might increase if a person was infected with human immunodeficiency virus (HIV), undergone previous treatment with radiotherapy to the chest or neck or had a family history of lung cancer (National Cancer Institute 2014).

One of the main reasons for treatment failure in lung cancer is the late diagnosis of the disease. The disease would have usually reached the metastatic phase upon diagnosis which makes it extremely challenging to treat at that stage. There are several ways by which lung cancer can be diagnosed and one of the first detecting methods that are usually used are chest X-ray tests in order to ensure that nothing abnormal is present in the lungs. Further methods include computed tomography (CT) scan which involves taking several X-ray images to obtain more detailed information regarding the structure of the tumours. Moreover, another testing method known as Magnetic resonance imaging (MRI) detects tumours *via* radiowaves and strong magnets rather than X-rays. The doctors may also study samples of a person's sputum or any fluid build-up in the chest in order to check for the presence of any cancer cells, and such method of diagnosis might also include obtaining samples of suspicious matter within the lungs for examination (Pastorino 2010; National Cancer Institute 2014).

Almost 40% of diagnosed lung cancer cases are stage IV and treatment is more concentrated on increasing survival time and reducing effects of the disease. Treatment of lung cancer depends on the type of cancer, however, both SCLC and NSCLC can be treated *via* surgery, radiation therapy and chemotherapy. Chemotherapy involves the administration of drugs into the body to treat cancer and some of the currently approved drugs for treatment of both types of cancers include etoposide and methotrexate, while paclitaxel, cisplatin, carboplatin and docetaxel are used to for treating specifically NSCLC. In the case of NSCLC, it may be treated using a combination of a platinum (cisplatin or carboplatin) and another drug such

as paclitaxel and docetaxel. However, these therapies are usually accompanied with some side-effects. Radiation therapy could damage the nearby healthy cells resulting in side-effects such as fatigue, cough and shortness of breath. Side-effects resulting from surgery are not expected to be life-threatening and these could include bleeding and pain. As for chemotherapy, side-effects could be severe and include vomiting, fatigue, hair loss, diarrhoea, kidney and bladder problems (National Cancer Institute 2014; Zappa and Mousa 2016; American Cancer Society 2018).

1.2 Nasopharyngeal Cancer

Nasopharyngeal cancer is a type of cancer that usually starts in the squamous cells of the epithelial lining of the nasopharynx and is considered to be a type of head and neck cancer. The nasopharynx is the upper part of the throat behind the nose. Nasopharyngeal cancer starts initially as abnormal cells existing in the lining of the nasopharynx and these cells can later develop into cancer that is either located in the nasopharynx only or has started spreading to the oropharynx, nasal cavity and the lymph nodes. Later stages of the disease involve it spreading to other parts of the body beyond the nasopharynx such as the cranial nerves, hypopharynx, areas beside the skull or jawbone and to lymph nodes on the neck and behind the pharynx

There are several types of tumours that can develop in the nasopharynx, but they can generally be divided into benign and malignant, with the former being rare, not life-threatening and do not usually spread to other parts of the body. On the other hand, malignant tumours can spread to other parts of the body and the most common type of malignant tumours of the nasopharynx is NPC. In fact, NPC has the highest

invasive and metastasis potential relative to the other types of head and neck cancers whereby 15%-30% of cases develop distant metastasis (Wei and Sham 2005; National Cancer Institute 2014; American Cancer Society 2015; Wang *et al.* 2018).

1.2.1 Symptoms, Risk Factors, Diagnosis and Treatment

Symptoms of NPC include having difficulty in breathing or speaking, sore throat, nose bleeds, ringing in the ear and headaches. Factors that increase the risk of developing NPC include having Asian ancestry, previous exposure to the Epstein-Barr virus and drinking large amounts of alcohol.

There are several tests used to identify the presence of NPC in an individual, including biopsy and imaging tests such as MRI, positron emission tomography (PET) and CT scan. Moreover, a blood test can be performed in order to check for antibodies to the Epstein-Barr virus as well as DNA markers for the same virus while a hearing test can also be conducted to examine if each ear can hear different types of sounds.

There is currently no cure for NPC and advancements in the treatment of NPC have not resulted in an improvement in the 5-year survival rate of 34%-52% over the decades. Treatment options for NPC include radiotherapy, surgery or chemotherapy. Radiotherapy involves directing a beam of high energy radiation towards cancer cells in order to stop their growth. It may be external, whereby radiation is applied to the cancer cells from outside the body or it could involve placing a radioactive substance inside the body near to the tumour. Surgery can also be used to treat NPC, especially if radiation therapy was not effective, whereby cancer tissues and lymph nodes might be removed in order to treat cancer. Finally,

chemotherapy can be considered for NPC treatment, and some of the currently-approved drugs for NPC treatment include cisplatin, methotrexate, docetaxel and fluorouracil. However, it is important to note that high-dose radiotherapy is considered one of the most effective treatments. This is because NPC is highly sensitive to radiotherapy. Moreover, NPC usually occurs at an anatomical site that is not easily accessible to surgeons, making surgical treatment challenging, so radiotherapy becomes the most effective treatment. Side-effects related to treatment options for NPC are similar to the ones mentioned earlier for lung cancer in section 1.1.3. However, radiotherapy in this case could result in further side-effects than the ones that were mentioned in the case of lung cancer. Radiotherapy against NPC could affect the mouth and cause taste changes in addition to resulting in a less active thyroid gland (Yang *et al.* 2013; National Cancer Institute 2014; Wang *et al.* 2018).

1.3 Chalcones

1.3.1 Structure and Chemistry

Chalcones, also known as 1,3-diaryl-2-propen-1-ones, are a group of naturally occurring compounds that are usually responsible for the yellow pigmentation in plants and belong to the flavonoid family, while they are also considered as precursors of flavones. Chalcones are characterised by the presence of an α,β -unsaturated ketone with two aromatic rings. The aromatic rings are usually called A and B while the numbering system for such compounds involves the A-ring being numbered from 1' to 6' while the B-ring is numbered from 1 to 6 (**Figure 1.1**) (Yadav *et al.* 2011; Albuquerque *et al.* 2014).

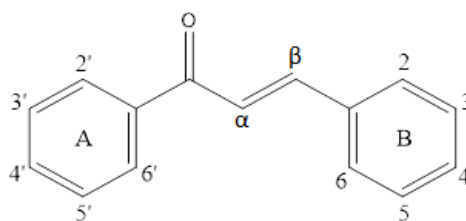


Figure 1.1 General structure of chalcones with their numbering scheme

The molecular structure of these compounds is very flexible enabling it to adopt several structural conformations. The $C\alpha=C\beta$ of the structure can exist in either the (*E*)- or (*Z*)- configuration with the former being more thermodynamically stable which explains the reason behind most of the isolated chalcones existing as (*E*)-isomers. Moreover the $O=C-C\alpha=C\beta$ can adopt the *s-cis* or *s-trans* conformation with the former being the more stable conformer, and there were also structures of chalcones possessing different degrees of planarity reported (**Figure 1.2**) (Albuquerque *et al.* 2014).

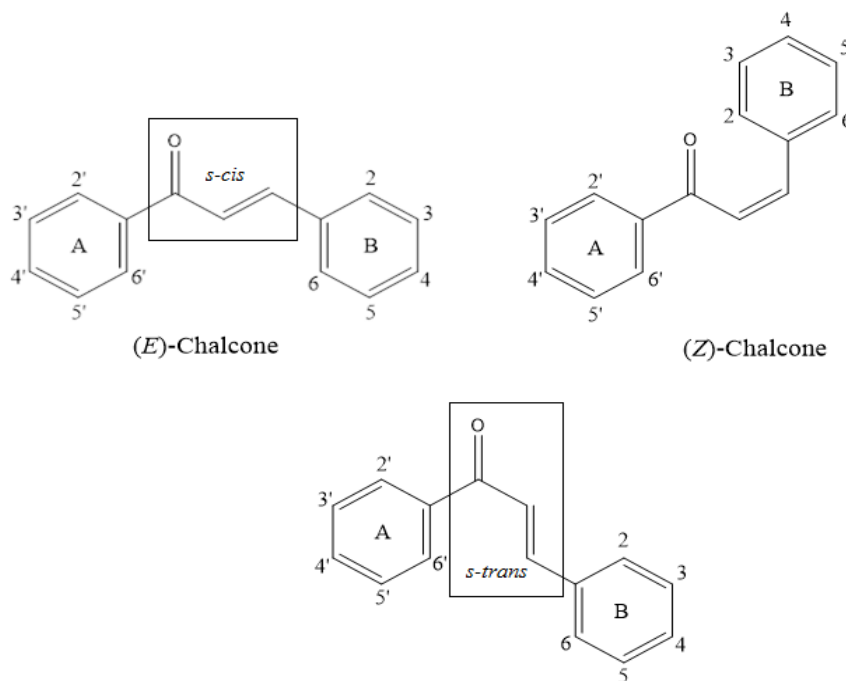


Figure 1.2 Structural conformations of chalcones

The α,β -unsaturated moiety of chalcones enables them to act as electrophilic reactive centres due to the delocalisation of electrons across the $O=C-C=C$ system and this manages to allow addition reactions *via* attacking the carbonyl group or the β -carbon. Therefore, chalcones can be used as synthons for the synthesis of several molecules such as pyrazolines, isoxazolines, pyrimidines, indoles and imidazoles (Albuquerque *et al.* 2014).

1.3.2 Formation of Chalcones

Chalcones can be either produced naturally or synthetically *via* several methods. The biosynthetic pathway for the formation of chalcones in plants involves initially the stepwise addition of L-phenylalanine with the simultaneous removal of one molecule of ammonia to produce trans-cinnamate which is later converted to *p*-coumarate. Ligation of *p*-coumarate with CoA-SH leads to the formation of 4-coumaroyl-CoA which later results in the formation of the flavonoid skeleton (Yadav *et al.* 2011). **Figure 1.3** Summarises the biosynthetic pathway for the formation of chalcones.

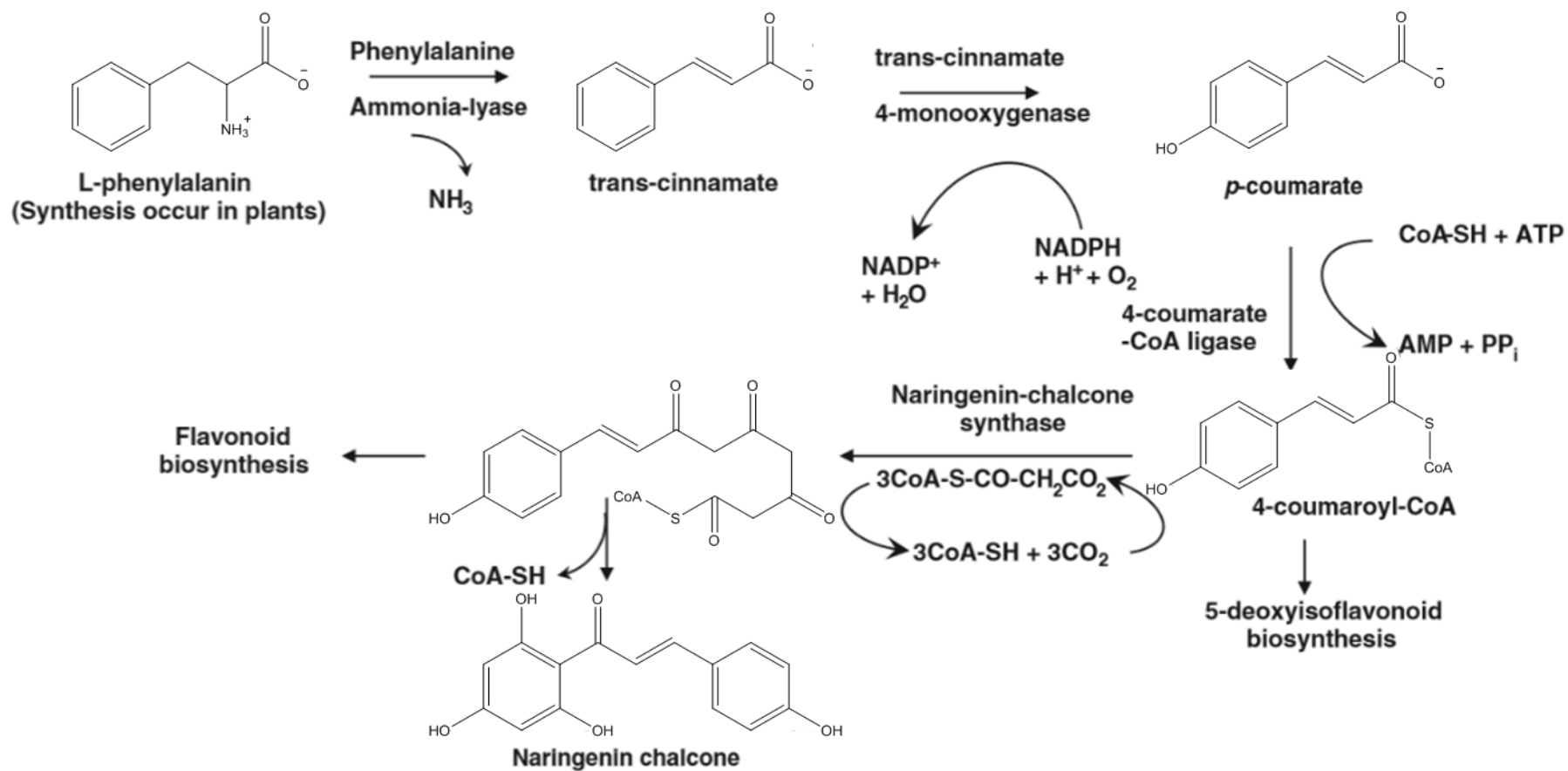


Figure 1.3 Biosynthesis of chalcones naturally (*adapted from: Yadav et al. 2011*)

It is also possible to produce chalcones synthetically and this can be done through various ways. One of the most widely used methods is the production of chalcones *via* the Claisen-Schmidt condensation reaction. This reaction involves the condensation of acetophenones and benzaldehydes to produce the desired chalcones (**Figure 1.4**) and that is usually performed under a base such as KOH or NaEtO⁻ at room temperature. It is also possible to conduct the reaction under acidic conditions by using HCl or *p*-toluenesulfonic acid for instance. Moreover, the reaction can be performed using solid-phase catalysts, heterogeneous catalysis or acidic ionic liquids, and recently better strategies have been implemented whereby it is possible to conduct the reaction under solvent-free conditions or by using microwave and ultrasound radiation (Albuquerque *et al.* 2014).

The base-catalysed Claisen-Schmidt condensation reaction is considered to be the primary method of choice for the synthesis of chalcones due to the feasibility of obtaining the reactants (acetophenones and benzaldehydes); while in acidic conditions, the most preferred method is the one involving BF₃•OEt₂. This is because the method involving BF₃•OEt₂ results in better yields, shorter reaction time and a simple work-up with no side reactions. Moreover, it can be used in solvent-free conditions and have been found to be suitable for compounds possessing functional groups that are sensitive to basic conditions (Albuquerque *et al.* 2014).

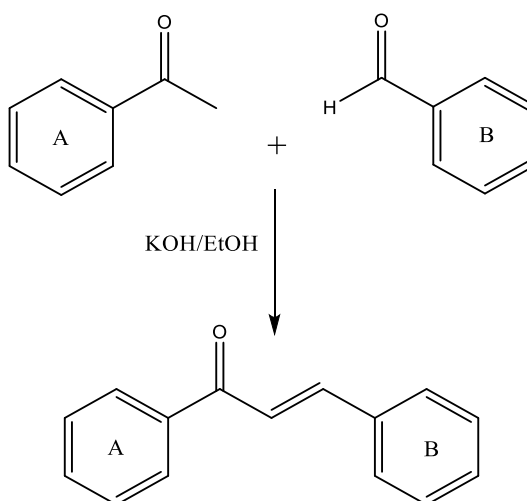


Figure 1.4 General reaction scheme for the synthesis of chalcones by the Claisen-Schmidt condensation reaction

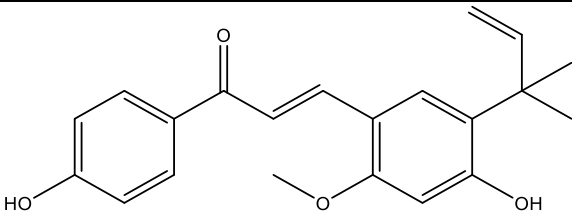
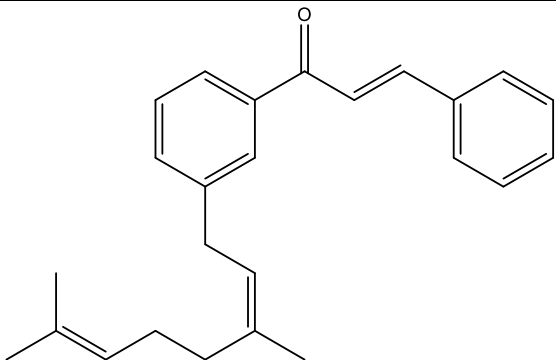
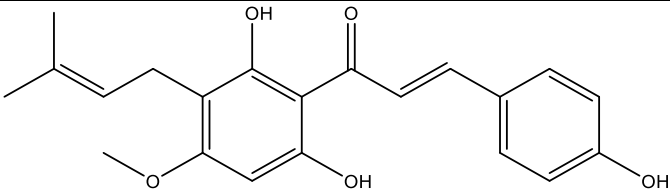
There are further reactions that can be used to produce chalcones such as the palladium catalysed coupling reaction of benzoyl chlorides and potassium styryltrifluoroborates under microwave heating. Furthermore, chalcones can also be synthesised *via* a Suzuki cross-coupling reaction involving benzoyl chlorides with arylvinylboronic acids under the presence of Pd(PPh₃)₄ and cesium carbonate. It has also been reported that the Friedel-Crafts reaction of phenols with cinnamoyl chloride can be regarded as a method for synthesis of chalcones (Albuquerque *et al.* 2014).

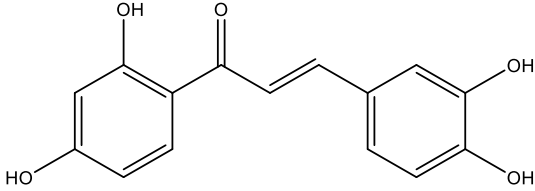
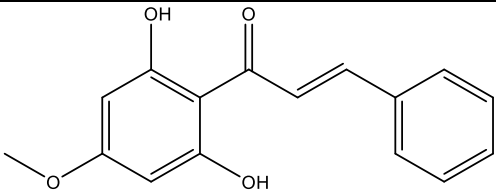
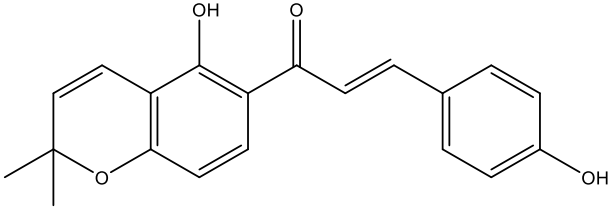
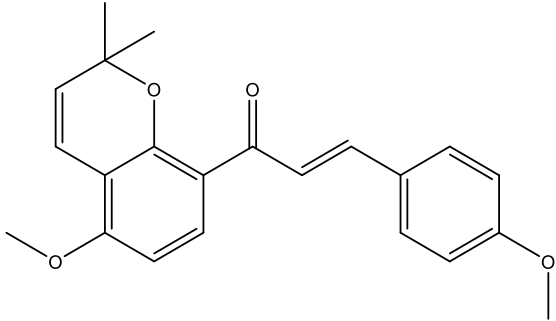
1.3.3 Bioactivity of Chalcones

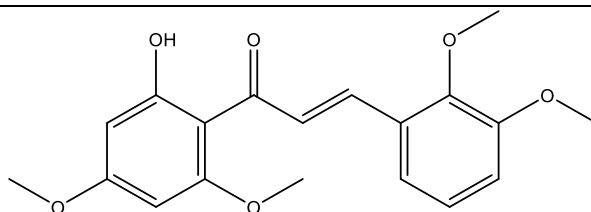
Chalcones have been found to possess a wide range of biological activities that made them seem attractive to medicinal chemists and such activities included antibacterial, anti-inflammatory, antifungal, antimalarial, antitumour, antimicrobial, antiviral, antitubercular, antioxidant, antimitotic, antileishmanial,

antiplatelet and anticancer activities (Albuquerque *et al.* 2014). The information on the bioactivity of chalcones in literature is vast, however, since this study focuses on the anticancer potential of cardamonin, it seemed appropriate to summarise the anticancer effects of some naturally-occurring chalcones (other than cardamonin) in **Table 1.1**. This should provide a glimpse on the potential of naturally-occurring chalcones as anticancer agents. Synthetic chalcones have also been shown to possess interesting bioactivities, but they are numerous and do not exactly lie within the scope of this study.

Table 1.1 Summary of the anticancer effects of some naturally-occurring chalcones

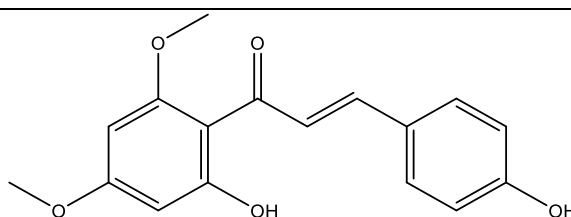
	Anticancer Activity	Reference
 <p>Licochalcone A</p>	A chalcone that was found in the roots of <i>Glycyrrhiza uralensis</i> . It exhibited anticancer activities and induced apoptosis in PC-3 cancer cells.	(Fu <i>et al.</i> 2004)
 <p>Xanthoangelol</p>	This is a chalcone that has been isolated from <i>Angelica keiskei</i> . It showed cytotoxic activity against neuroblastoma and leukemia cells <i>via</i> the activation of caspase-3.	(Tabata <i>et al.</i> 2005)
 <p>4-hydroxyderricin</p>	This compound has been also isolated from <i>Angelica keiskei</i> , and it induced apoptosis in HL60 cells <i>via</i> intrinsic and extrinsic pathways.	(Akihisa <i>et al.</i> 2011)

 <p style="text-align: center;">Butein</p>	<p>This is a polyphenol that was extracted from <i>Rhus verniciflua</i> and exhibited an antiproliferative effect on adenocarcinoma cells. Moreover, it caused apoptosis in HL-60 cells via the activation of caspase-3.</p> <p style="text-align: right;">(Yit and Das 1994; Kim <i>et al.</i> 2001)</p>
 <p style="text-align: center;">Pinostrobin chalcone</p>	<p>A chalcone which was extracted from <i>Alpinia mutica</i>. It demonstrated pronounced anticancer activity against KB, MCF7 and Caski cell lines.</p> <p style="text-align: right;">(Zhang <i>et al.</i> 2013)</p>
 <p style="text-align: center;">Isobavachromene</p>	<p>The compound has been isolated from <i>Millettia pachycarpa</i> and showed selective inhibition against 7860, A549, A2780, Hela, K562.</p> <p style="text-align: right;">(Su <i>et al.</i> 2012)</p>
 <p style="text-align: center;">Pyranochalcone</p>	<p>It has been isolated from <i>Millettia pachycarpa</i> and exhibited cytotoxic effects against HepG2, C26, LL2 and B16 cells.</p> <p style="text-align: right;">(Ye <i>et al.</i> 2012)</p>



HTMC

This is a natural chalcone extracted from *Caesalpinia pulcherrima*, and it demonstrated potent and selective activity against A549 cells. It showed G1-phase cell cycle arrest. (Rao *et al.* 2010)



Flavokawain C

The compound has been isolated from *Boesenbergia pandurata* and kava. It showed anticancer effects against bladder cancer cells and pancreatic cancer (PANC-1) cell line. (Zi and Simoneau 2005; Nwet *et al.* 2007)

It is important to note that despite the fact that there are several studies reporting the medicinal effects of chalcones, there have been few structure-activity relationship (SAR) studies conducted (Albuquerque *et al.* 2014). If there happened to be some SAR studies, then they often involved the synthesis of a set of chalcones to investigate the effect of certain substituents on biological activity but these studies usually do not refer to a specific chalcone and study it, rather they involve random derivatives which are different in their overall structure. For instance, they would not consider a specific chalcone like cardamonin and perform their study by modifying cardamonin's chemical groups specifically. Instead, these studies just focus on making chalcones that do not have a common starting material, such as cardamonin in this study, rather each chalcone is independently made from different starting materials. Therefore, this results in obtaining a more generalised SAR rather than an SAR specific to a certain chalcone.

The SAR of chalcones depends on the disease being targeted, and since this study focuses on the anticancer potential of chalcone (cardamonin) derivatives, it would seem appropriate to briefly discuss the anticancer SAR of chalcones. However, it is crucial to note that discussing SAR of chalcones with regards to their anti-cancer activity is also dependent on the type of cancer investigated and the molecular target being studied, which makes it difficult to define a general SAR for chalcones.

Despite the difficulty in defining a general SAR for chalcones due to the factors mentioned; it is still possible to identify certain chemical groups that have been shown to enhance cytotoxic activity in several studies. It has been shown that addition of methoxy groups, especially at the 3, 4 and 5 positions of the B-ring of

the chalcone, has managed to enhance cytotoxic activity and this has been attributed to the ability of this moiety to bind efficiently to the colchicine binding site of tubulin. Moreover, the presence of hydroxyl groups and electron-withdrawing groups such as halogens have also been found to increase cytotoxic activity while the α , β -unsaturated bond has been proven to be essential for bioactivity (Orlikova *et al.* 2011; Mahaptra, Bharti and Asati 2015).

2 Literature Review

In the previous chapter, crucial background concepts with regards to cancer and chalcones have been introduced, in addition to the objectives and rationale behind the present study. This was done in order to facilitate the understanding and appreciation of the main subject of the present study, which is the cytotoxic bioactivity of cardamonin and its analogues. In this chapter, cardamonin will specifically be further discussed and studies related to its chemistry and bioactivity will be reviewed in order to provide the latest research updates in the field. This literature review is crucial as the present study needs to build upon the previous studies that were done and avoid unnecessary repetition.

Cardamonin is a natural product belonging to the chalcone class of compounds under a larger family known as flavonoids (Gonçalves, Valente and Rodrigues 2014). Studies on cardamonin have recently increased, and the following review aims to initially cover the **chemistry** of cardamonin followed by a detailed literature review of cardamonin's **bioactivity**.

2.1 Structure and Analysis of Cardamonin

The structure of cardamonin (2',4'-dihydroxy-6'-methoxychalcone) involves an α,β -unsaturated ketone between two aromatic rings with "ring A" bearing two phenolic groups in addition to a methyl ether group. **Figure 2.1** shows the structure of cardamonin.

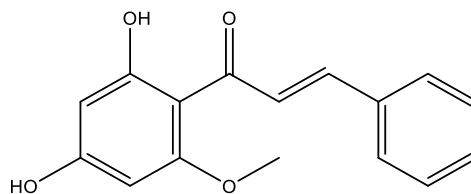


Figure 2.1 Structure of cardamonin

As for analysis, cardamonin has been detected and quantified *via* several techniques. A flow injection chemiluminescence method was employed for the determination or quantification of cardamonin based on the chemiluminescent reaction between cerium (IV) and rhodamine 6G in sulphuric acid. The chemiluminescence of this reaction is supposed to be enhanced by cardamonin (Zhang *et al.* 2005). Another analytical technique for cardamonin determination used an electokinetic capillary chromatography method with reverse sodium dodecyl sulfate micelles as a pseudo-stationary phase (Wang *et al.* 2007). Other researchers used a combination of flow injection and micellar electrokinetic chromatography coupled with direct UV detection at 214 nm for the first time for the determination of cardamonin in *Alpinia katsumadai* Hayata (Liu *et al.* 2007). Finally, a very recent study discussed a method for routine analysis of cardamonin in *Alpinia katsumadai* Hayata by using short-end injection microemulsion electrokinetic chromatography in combination with microwave-assisted extraction (Zhao, Lu and Xu 2017).

As for cardamonin's structure, there were several techniques used for characterising it. **Table 2.1** summarises the techniques employed by previous authors to elucidate cardamonin's structure as well as the data obtained from the techniques used.

Table 2.1 Summary of the analytical methods used for cardamonin

characterisation

Analytical method	Data
FTIR (KBr, cm ⁻¹)	<ul style="list-style-type: none"> - 3140, 1630, 1495, 1340, 1220, 1180, 1120, 980, 795, and 750 (Itokawa, Morita and Mihashi 1981) - 3154, 1628, 1542, 1486, 1286, 1320, 1224, 1188, 1114, and 926 (Sukari <i>et al.</i> 2007) - 3400 (OH), 2924 (C-H), and 1638 (C=O) (Derita and Zacchino 2011)
ESI-MS	<ul style="list-style-type: none"> - Negative mode: 269 (M-H)⁺, 177, 165, 139, 124 (He <i>et al.</i> 2009) - Positive mode: 271 (M+H)⁺, 167, 139 (Carvalho <i>et al.</i> 2012)
¹ H-NMR (δ ppm)	<ul style="list-style-type: none"> - (CD₃)₂CO: 3.87 (3H, <i>s</i>, MeO), 5.91 (1H, <i>d</i>), 6.00 (1H, <i>d</i>), 7.40-7.80 (5H, <i>m</i>), 7.63 (1H, <i>d</i>, α-position), 7.80 (1H, <i>d</i>, β-position), 13.65 (1H, <i>s</i>, broad) (Xiao <i>et al.</i> 2011) - DMSO-<i>d</i>₆: 3.87 (3H, <i>s</i>, MeO), 5.93 (1H, <i>d</i>), 6.02 (1H, <i>d</i>), 7.43-7.72 (5H, <i>m</i>), 7.67 (1H, <i>d</i>, α-position), 7.85 (1H, <i>d</i>, β-position), 13.71 (1H, <i>s</i>, broad) (Aderogba <i>et al.</i> 2012)
¹³ C-NMR (δ ppm)	<ul style="list-style-type: none"> - CDCl₃: 136.5 (C-1), 129 (C-2), 129.7 (C-3), 130.7 (C-4), 129.7 (C-5), 129 (C-6), 128.6 (C-7), 142.4 (C-8), 193 (C-9), 106.4 (C-1'), 168.3 (C-2'), 92.3 (C-3'), 165.8 (C-4'), 97 (C-5'), 164.3 (C-6'), 56.3 (OCH₃) (Itokawa, Morita and Mihashi 1981) - DMSO-<i>d</i>₆: 135.4 (C-1), 128.8 (C-2), 128 (C-3), 130.8 (C-4), 129.5 (C-5), 128.8 (C-6), 142.3 (C-7), 128 (C-8), 192.2 (C-9), 105.5 (C-1'), 166.7 (C-2'), 92.2 (C-3'), 165.6 (C-4'), 96.3 (C-5'), 163.1 (C-6'), 55.5 (OCH₃) (Derita and Zacchino 2011)
Melting point (°C)	<ul style="list-style-type: none"> - 195-196 (Itokawa, Morita and Mihashi 1981) - 199-200 (Jaipetch <i>et al.</i> 1982)

2.2 Sources of Cardamonin

Cardamonin's name is derived from one of its sources which is the cardamom spice (**Figure 2.2**), but it has been also extracted from other plant species. The following is a list of plant species from which cardamonin was successfully extracted (Gonçalves, Valente and Rodrigues 2014):

- *Alpinia blepharocalyx*
- *Alpinia conchigera*
- *Alpinia hainanensis*
- *Alpinia malaccensis*
- *Alpinia mutica*
- *Alpinia pricei*
- *Alpinia rafflesiana*
- *Alpinia speciosa*
- *Amomum subulatum*
- *Artemisia absinthium*
- *Boesenbergia pandurata*
- *Boesenbergia rotunda*
- *Carya cathayensis*
- *Cedrelopsis grevei*
- *Combretum apiculatum*
- *Comptonia peregrina*
- *Desmos cochinchinensis*
- *Elettaria cardamomum*
- *Helichrysum forskahlii*
- *Kaempferia parviflora*
- *Morella pennsylvanica*
- *Piper dilatatum*
- *Piper hispidum*
- *Polygonum ferrugineum*
- *Polygonum lapathifolium*
- *Polygonum persicaria*
- *Populus fremontii*
- *Syzygium samarangense*
- *Vitex leptobotrys*
- *Woodsia scopulina*



Figure 2.2 Cardamom seeds (*adapted from: Gonçalves, Valente and Rodrigues 2014*)

2.3 Medicinal Applications of Cardamonin

2.3.1 Anti-inflammatory Activity

Inflammation is a physiological immune response to an injury or infection of a tissue. The process involves the activation of macrophages and monocytes by components of the invading bacteria which also initiate several intracellular cascades of cytokines and chemokines. There are several inflammatory mediators secreted by the activated macrophages which include interleukin (IL)-6, tumor necrosis factor (TNF)- α , prostaglandin (PG)E₂, and nitric oxide (NO) (Lee *et al.* 2006).

Several studies have shown the anti-inflammatory effect of cardamonin (Lee *et al.* 2006; Lee *et al.* 2012; Chow *et al.* 2012; Kim *et al.* 2016) and further attempted to explain cardamonin's anti-inflammatory mode of action. Some studies attempted to link the anti-inflammatory effect of cardamonin to its effect over the signalling pathway of a protein complex that controls DNA transcription and regulates immune responses to infections called nuclear factor- κ B (NF- κ B) (Lee *et al.* 2006; Lee *et al.* 2012). Moreover, other studies have shown that cardamonin seemed to

inhibit prostaglandin E2, tumour necrosis factor α (TNF- α) release, thromboxane B2 production in addition to intracellular reactive oxygen species generation (Tewtrakul *et al.* 2009).

Sepsis is a type of inflammatory response that can result in organ failure, and lungs are usually the organs affected by this response which might lead to hypoxemia and pulmonary oedema (Gonçalves, Valente and Rodrigues 2014). It has been found that cardamonin can decrease systemic inflammatory responses during sepsis *via* the down-regulation of interleukins and TNF- α (Wei *et al.* 2012).

Carrageenan-induced (Carr-induced) paw oedema is a model used to measure the contribution of mediators that are involved in the production of acute inflammatory response in a rat hindpaw after the administration of carrageenan. A study has shown that cardamonin demonstrated anti-inflammatory activity by decreasing Carr-induced paw oedema (Li *et al.* 2015). This was accomplished by the inhibition of NF- κ B and MAPK signalling pathways, in addition to the induction of heme-oxygenase-1. Cardamonin was also found to have an effect on inflammatory bowel disease *via* a mechanism involving the suppression of toll-like receptor 4 expression and blockage of NF- κ B and MAPK pathways (Ren *et al.* 2015).

2.3.2 Antioxidant Activity

The antioxidant activity of cardamonin seemed to be dependent on the assay employed to study the activity as it showed potent activity in an oxygen radical absorbance capacity assay (Bajgai *et al.* 2011), however, no significant activity was observed in a DPPH and superoxide anion assay (Li *et al.* 2008). Moreover, it has been shown in another study that cardamonin had a fifth of the IC₅₀ of gallic acid's

antioxidant activity in a DPPH assay (Simirgiotis *et al.* 2008), while another study (Zhu *et al.* 2007) showed that cardamonin at a concentration of 50 μ M resulted in a 10%-20% antioxidant activity using Vitamin C as a positive control.

Selenoenzymes and nuclear factor erythroid 2-related factor 2 (Nrf2)-regulated phase II enzymes are considered to be important components of the cellular antioxidant systems. It was found that cardamonin was involved in the biosynthesis of important Nrf2-regulated antioxidant enzymes but the authors suggest further studies to be performed in order to determine other factors responsible for the observed effects of cardamonin on antioxidant enzymes (De Spirt *et al.* 2016). A similar result was achieved by another study which found that cardamonin was an activator of Nrf2 in PC12 cells and that resulted in upregulation in the expression of phase II antioxidant molecules (Peng *et al.* 2017)

2.3.3 Vasorelaxant Activity

It has been shown that cardamonin can act as a vasodilator by preventing the entry of calcium to the cell *via* the voltage-dependent $\text{Ca}_v2.1$ channel, while at the same time encouraging the exit of potassium by the calcium-activated KCa1.1 channel (Fusi *et al.* 2010). Such findings were further strengthened by other studies that showed the vasorelaxant activity of cardamonin (Wang *et al.* 2001). Cardamonin was also able to have a relaxing effect on agonist-induced vascular contraction *via* the inhibition of Rho-kinase and MEK activity (Je and Jeong 2016).

2.3.4 Hypoglycaemic Activity

It was found that cardamonin can enhance the uptake of glucose by glucose transporter-4 (GLUT4), whereby it was shown that a 30 μ M cardamonin solution could cause GLUT4 to be stimulated for 1-4 h, in levels comparable to that caused by a 0.1 μ M insulin solution (Yamamoto *et al.* 2011).

2.3.5 Anti-infectious Activity

Leishmaniasis is a disease caused by protozoan parasites from the genus *Leishmania* and is usually spread *via* bites of infected female sand-flies. Cardamonin showed strong activity against *Leishmania amazonensis* with an IC₅₀ of 8 μ M (Ruiz *et al.* 2011). Moreover, it has been found that cardamonin possessed anti-fungal activity against *Epidermophyton floccosum* and it was thought that the mode of action was that of a wall inhibitor type, but it did not exhibit any significant activity against other fungi such as *Candida albicans* (Lopez *et al.* 2011).

Cardamonin has been also found to possess activity against bacterial and viral infections. It has been found that cardamonin had antibacterial activity against *Staphylococcus aureus*, *Escherichia coli* and *Bacillus subtilis* with minimum inhibitory concentration (MIC) of 25 μ g/ml, 25 μ g/ml and 50 μ g/ml, respectively. Furthermore, cardamonin was shown to exhibit antiviral activity against HIV-1 by targeting its protease which is considered highly essential for the virus's lifecycle, and it showed an IC₅₀ of 115 μ M. Dengue was another virus that cardamonin was able to exert an effect on, as it was shown that cardamonin had some inhibitory action over the dengue virus type 2 (DV2) NS3 protease (Gonçalves, Valente and Rodrigues 2014).

2.3.6 Pain Management

It has been shown that cardamonin has the ability to manage pain. Cardamonin was able to demonstrate anti-nociceptive effects by blocking the expression of cyclooxygenase-2 and transglutaminase-2. This suggested that cardamonin can aid in controlling pain that arises from inflammatory diseases (Park *et al.* 2014).

Transient receptor potential ankyrin 1 (TRPA1) is a receptor that is involved in abnormal high sensitivity to pain (hyperalgesia), and it was found that cardamonin was a selective inhibitor of this receptor (Wang *et al.* 2016).

Neuropathic pain is a type of pain that arises from injury of the nervous system and has proven challenging to treat. A very recent study used chronic constriction injury (CCI)-induced neuropathic pain mice in order to study the effect of cardamonin on hyperalgesia and allodynia (experience of pain from a usually non-painful stimulation of the skin) (Sambasevam *et al.* 2017). The results showed that cardamonin exhibited antihyperalgesic and antiallodynic effects *via* the activation of the opioid system.

2.3.7 Anticancer Activity

Studies performed on cardamonin's bioactivity have, to a large extent, heavily investigated cardamonin's potential as an anticancer agent. **Table 2.2** summarises the cell-viability assays performed on cardamonin against some cancer cell lines and the results obtained for its cytotoxicity which was assessed based on its IC₅₀ values.

Table 2.2 Cytotoxicity of cardamonin towards different cancer cell-lines

Cancer cell-line	IC ₅₀ (Concentration at which 50% inhibition of cancer cells occurs)	Reference
MCF-7 (breast)	~50 µM (48 h MTT assay)	(Shrivastava <i>et al.</i> 2017)
BT-549 (breast)	~8 µM (48 h MTT assay)	
MDA-MB-231 (breast)	>100 µM (48 h Resazurin reduction assay)	(Kuate <i>et al.</i> 2014)
	~10 µM (48 h MTT assay)	(Shrivastava <i>et al.</i> 2017)
SW-480 (colon)	35 µM (72 h MTT assay)	(Simirgiotis <i>et al.</i> 2008)
	~6.5 µM (48 h CellTiter-Glo assay)	(Park <i>et al.</i> 2013)
HCT116 (colon)	~9 µM (48 h CellTiter-Glo assay)	(Park <i>et al.</i> 2013)
	~13 µM (48 h CCK8 assay)	(Kim <i>et al.</i> 2015)
LS174T (colon)	~13 µM (48 h CellTiter-Glo assay)	(Park <i>et al.</i> 2013)
DLD-1 (colon)	~24 µM (48 h CellTiter-Glo assay)	
HCT116 (<i>p53</i> ^{+/+}) (colon)	62.74 µM (48 h Resazurin reduction assay)	(Kuate <i>et al.</i> 2014)
SGC7901 (gastric)	61 µM (48 h MTT assay)	(Mi <i>et al.</i> 2016)
U87MG (glioblastoma)	>100 µM (48 h Resazurin reduction assay)	(Kuate <i>et al.</i> 2014)
CD133 ⁺ GSCs (glioblastoma)	~30 µM (72 h MTT assay)	(Wu <i>et al.</i> 2015)
CCRF-CEM (leukaemia)	8.59 µM (48 h Resazurin reduction assay)	(Kuate <i>et al.</i> 2014)
KB (mouth epidermal)	~20 µg/ml (48 h trypan blue exclusion assay)	(Lin <i>et al.</i> 2012)
HepG2 (liver)	22.63 µM (48 h MTT assay)	(Li <i>et al.</i> 2008)
	53 µM (48 h MTT assay)	(Mi <i>et al.</i> 2016)
AML12 (liver)	>100 µM (48 h Resazurin reduction assay)	(Kuate <i>et al.</i> 2014)
SMMC7721 (liver)	62 µM (48 h MTT assay)	(Mi <i>et al.</i> 2016)
A549 (lung)	~18 µM (48 h MTT assay)	(Tang <i>et al.</i> 2014)
	>100 µM (48 h MTT assay)	(Mi <i>et al.</i> 2016)
LLC (lung)	>10 µM (48 h MTT assay)	(Niu <i>et al.</i> 2015)
RPMI8226 (myeloma)	~10 µM (48 h CCK8 assay)	
U266 (myeloma)	~14 µM (48 h CCK8 assay)	(Qin <i>et al.</i> 2012)
ARH-77 (myeloma)	~10 µM (48 h CCK8 assay)	
PC-3 (prostate)	11.35 µg/ml (48 h sulforhodamine B assay)	(Pascoal <i>et al.</i> 2014)
DU145 (prostate)	~10 µM (72 h MTT assay)	(Zhang <i>et al.</i> 2017)

There were several studies performed on the mechanism of action of cardamonin, for instance, it has been found that cardamonin suppresses the proliferation of SW480 colon cancer cells *via* enhancing the degradation of β -Catenin and inhibiting the Wnt/ β -catenin pathway (Park *et al.* 2013). The down-regulation of Wnt/ β -catenin signalling cascade was also found to be the pathway responsible for cardamonin's inhibitory effect on the invasiveness of BT-549 human triple breast cancer cells (Shrivastava *et al.* 2017). However, another study (Kim *et al.* 2015) claimed that cardamonin exerted its antitumour activity on HCT116 cells colon cancer cells *via* the induction of autophagy which is executed by the activation of c-Jun N-terminal kinase (JNK) by tumour protein p53. JNK is a kinase responsible for the regulation of cell differentiation, proliferation, and death, while it is also considered a major mediator of autophagy that leads to cell death in some types of cancer cells (Kim *et al.* 2015).

Moreover, it has been shown that cardamonin exerted potent activity against multiple myeloma cells (RPMI 8226, U266 and ARH-77 cells) *via* the activation of caspase-3, which belongs to a larger group of caspases and possesses the ability to cause apoptosis; while it also managed to block the pathway of NF- κ B which is a transcription factor whose signalling pathway regulates cell survival and proliferation (Qin *et al.* 2012). The fact that NF- κ B pathway has been found to be inhibited by cardamonin was further supplemented by another study (Pascoal *et al.* 2014) which showed that cardamonin caused apoptosis and down-regulated the NF- κ B1 (a member of the NF- κ B family) gene in PC-3 prostate cancer cells. STAT3 is also a transcriptional factor belonging to a larger group of STAT proteins and was

found to be activated in a variety of cancers where it plays a major role in tumour initiation, promotion and progression. A study (Wu *et al.* 2015) found that cardamonin induced apoptosis in CD133+ glioblastoma stem cells (GSCs) *via* inhibiting STAT3 signalling pathway and was thus suggested as a potential anticancer agent for the treatment of the adult brain tumour disease known as glioblastoma multiforme (GBM). A similar result was reported by a more recent study in DU145 prostate cancer cells (Zhang *et al.* 2017) which showed that STAT3 was found to be negatively regulated by cardamonin, causing a repression in proliferation and invasion, and resulting in apoptosis.

It has been recently shown that cardamonin inhibited cell viability *via* blocking the testes-specific protease 50 (TSP50)-mediated nuclear factor-kappaB signalling pathway activation in MDA-MB-231 breast cancer cells . TSP50 is a gene that was thought to be specifically expressed in the testes, but it was also found to be overexpressed in several types of tumours and could promote cell proliferation, invasion, tumorigenesis, and tumour metastasis (Mi *et al.* 2016).

The mammalian target of rapamycin (mTOR) is a serine/threonine kinase that is the responsible for the regulation of cell metabolism, proliferation and apoptosis. Dysregulation of its activity has been linked to cancer. Rapamycin is an mTOR inhibitor which leads to apoptosis and anti-proliferative effects on cancer cells, so cardamonin was studied to investigate if it can also act as an mTOR inhibitor and results have shown that it actually did inhibit mTOR signalling when tested against A549 lung cancer cells (Tang *et al.* 2014). This inhibition of mTOR resulted in the inhibition of proliferation and induction of apoptosis in lung cancer cells, moreover,

the study further revealed the possibility of direct interaction of cardamonin with mTOR. The action of cardamonin on mTOR was further supplemented by another study which showed that cardamonin exhibited an anti-metastatic effect when tested against the highly metastatic Lewis lung carcinoma (LLC) cells. This study showed that proliferation, invasion and migration of LLC cells was inhibited upon treatment with cardamonin and this occurred partially *via* inhibition of the mTOR signalling pathway (Niu *et al.* 2015). There were other studies conducted that further demonstrated the effect of cardamonin on mTOR and emphasising its therapeutic potential as an mTOR inhibitor (Liao *et al.* 2010; Zheng *et al.* 2010; Niu *et al.* 2013).

In vivo and animal model studies with regards to cardamonin anticancer effects are much more limited than *in vitro* studies. It was found that cardamonin inhibited tumour growth and lung metastasis in C57BL/6 mice (Niu *et al.* 2015) while angiogenesis induced by SKOV3 cells was reduced by cardamonin in a chicken embryo allantois membrane model (Xue *et al.* 2015). Toll-like receptors (TLR) are a family of microbial sensors that make part of a host's immunity, and it is also involved in tissue repair and inflammatory signalling. However, they have been found to be highly expressed in cancer cells, and a study (Jia *et al.* 2015) showed that cardamonin could control TLR3 stimulation-induced tumour growth in human breast cancer xenografts. Cardamonin was also found to possess an inhibitory effect on TSP50 high-expressing tumour growth *in vivo* in 4T1 tumour-bearing mice (Mi *et al.* 2016). In another study (Shrivastava *et al.* 2017), murine breast cancer model in Balb/c mice was designed to assess the biological activity of cardamonin, and it

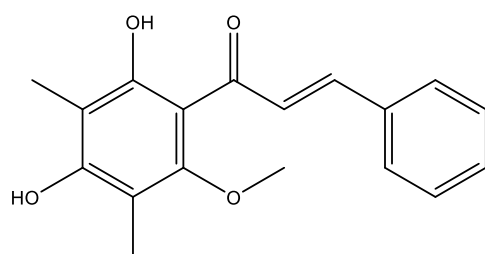
was found that cardamonin reduced tumour growth volumes at a dose of 5 mg/kg-treated mice.

2.4 Pharmacokinetic and ADME Studies on Cardamonin

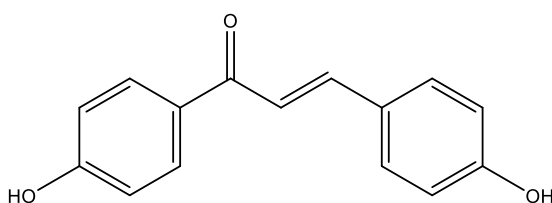
The interesting bioactivity demonstrated by cardamonin caused some researchers to investigate its pharmacokinetics. A study using human liver microsomes found that CYP 1A2 and 2E1 were the P450 isozymes that were involved in the metabolism of cardamonin. (He *et al.* 2009). Another study investigated the pharmacokinetics of cardamonin in Sprague Dawley (Jaiswal *et al.* 2015). The study showed that cardamonin reached peak serum concentration after about 2 h of an oral dose, but the bioavailability was low for both male (0.6%) and female (4.8%) rats. Moreover, the same study showed that cardamonin's bioavailability and pharmacokinetics were affected by gender. A more detailed study was recently performed on the pharmacokinetics of cardamonin (Jaiswal *et al.* 2016), and this study was able to provide much further information with regards to the pharmacokinetic and ADME properties of cardamonin. The study revealed that cardamonin possessed low solubility ($<10 \mu\text{M}$), high permeability ($>0.2 \times 10^{-4} \text{ cm/sec}$) and was found to moderately bind to plasma proteins ($<50\%$). When tested in mice, the study showed that cardamonin possessed a low oral bioavailability of 18% and it also exhibited high clearance, high volume of distribution and short mean residence time. As for its excretion, the study found that cardamonin was mostly excreted in faeces and negligibly in urine (Jaiswal *et al.* 2016).

2.5 Cardamonin Analogues

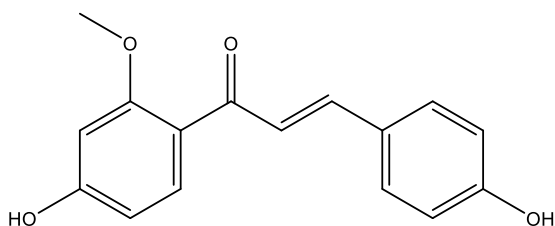
To the best of my knowledge there have been no previous attempts involving the production of cardamonin analogues *via* synthetic means. However, there are very few studies that reported the isolation of naturally-occurring cardamonin analogues (**Figure 2.3**) and assessed their bioactivities (Simirgiotis *et al.* 2008; Kim *et al.* 2010; Ko *et al.* 2011; He *et al.* 2014; Memon *et al.* 2014; Yu *et al.* 2015; Nesello *et al.* 2016; de Oliveira Cabral *et al.* 2017). The studies on these analogues are very limited and this makes them inferior to cardamonin as a well-established bioactive compound. In this section, only compounds that were regarded as cardamonin analogues by the authors would be discussed, as chalcones in general are analogues of each other, but over here, structures that highly resemble cardamonin except for minor changes would be considered.



Dimethyl cardamonin (DMC)



4,4'-dihydroxychalcone (DHC)



4,4'-dihydroxy-2'-methoxychalcone (DHMC)

Figure 2.3 Examples of cardamonin analogues

Dimethyl cardamonin (DMC) is a naturally occurring cardamonin analogue that has been isolated from *Syzygium samarangense* (Simirgiotis *et al.* 2008; Kim *et al.* 2010; Ko *et al.* 2011), *Syzygium campanulatum* Korth (Memon *et al.* 2014) and *C. operculatus* (Yu *et al.* 2015), and has been shown to possess a variety of biological activities. It has been shown that DMC possesses cytotoxic activity against SW-480 colon cancer cells with an IC₅₀ of 10 µM in a 72 h MTT assay (Simirgiotis *et al.* 2008), moreover, it also showed potent anti-inflammatory activity *in vitro* and *in vivo* which was exerted *via* the blockage of NF-κB activity (Kim *et al.* 2010). This anti-inflammatory effect of DMC was further confirmed by another study (Yu *et al.* 2015), whereby DMC exerted its anti-inflammatory effects by reducing early and late cytokines expressions *via* interfering with the PI3K-PDK1-PKCα signalling pathway. In another study (Ko *et al.* 2011), DMC was tested against HCT116 and LOVO human colorectal carcinoma cells, and the results showed that it was able to inhibit the proliferation of cancer cells *via* a G2/M phase cell-cycle delay with an IC₅₀ of approximately 18 µM and 28 µM for HCT116 and LOVO cells, respectively; these results were obtained from a 72 h CCK8 cell viability assay. The cytotoxic activity of DMC was further confirmed by a study (Memon *et al.* 2014) that showed its potent anti-proliferative effect on HT-29 colon cancer cells with an IC₅₀ of 12.6 µg/ml obtained *via* a 48 h MTT assay, and it also managed to inhibit the migration of HT-29 cells. It was also shown that DMC possessed anti-nociceptive effects when tested against two mice models (Nesello *et al.* 2016). Finally, it has been recently reported for the first time that DMC possessed gastroprotective potential (de Oliveira Cabral *et al.* 2017).

4,4'-dihydroxylchalcone (DHC) and 4,4'-dihydroxy-2'-methoxychalcone (DHMC) have been identified as cardamonin analogues isolated from *Cichorium intybus* and *Dracaena cochinchinensis*, respectively (He *et al.* 2014). The analogues were investigated using a 48 h MTT assay and were found to exert potent cytotoxic activity against A549, NCI-H1299, NCI-H460, NCI-H1688 and NCI-H446 lung cancer cells with IC₅₀ values in the range of 0.126–0.883 µM for DHC and 0.202–0.911 µM for DHMC. The mechanism of action involved the inhibition of NF-κB signalling pathway.

3 Results and Discussion

3.1 Chemistry

3.1.1 Synthesis

The analogues of cardamonin were synthesised according to **Scheme 3.1**. It can be clearly seen that one-step reactions were employed for synthesising the analogues, which proved to be economical as less reagents were used, and it also resulted in more product yields. Initially, the phenolic groups of cardamonin were targeted for modification by alkylation and acylation reactions. Alkylation proceeded by refluxing cardamonin with an alkyl halide and K_2CO_3 in acetone, while acylation generally involved refluxing cardamonin with an acyl halide/acetic anhydride in DCM. DMAP was added as a catalyst in some of the acylation reactions. In some cases, these alkylation/acylation reactions resulted in a mixture of mono- and di-substituted products, but only the products that showed adequate yields were considered. It is crucial to note that in cases where mono-substitution primarily occurred such as in **2** and **6**, 4'-OH was always the one substituted, and it seems that the intramolecular hydrogen bonding between 2'-OH and the carbonyl oxygen made it more difficult to substitute as opposed to 4'-OH.

Importance of the alkene group for bioactivity was investigated by reducing it, and this was performed by the synthesis of dihydrochalcone **7** and flavanone **17**. The reduction of cardamonin *via* $NaBH_4$ in order to produce **7** resulted in a mixture of products that proved difficult to separate, and according to the product's 1H -NMR spectrum, it seemed that the product mixture consisted of a dihydrochalcone,

tetrahydrochalcone and allylic alcohol. Therefore, selective reduction of cardamonin's alkene group *via* the $\text{NiCl}_2/\text{NaBH}_4$ system at $0\text{ }^\circ\text{C}$ was considered and that produced **7** but in low yield. As for **17**, it was produced by refluxing cardamonin with concentrated HCl in methanol for 72 h.

Cardamonin's ketone group was modified by Schiff base formation and cyclisation reactions. Schiff bases were formed by reacting cardamonin with primary amine hydrochlorides, therefore pyridine was initially added to the reactants to scavenge HCl and produce free primary amines. However, some amines, such as methylamine and ethylamine, did not react with cardamonin. *S*-benzyl dithiocarbazate (SBDTC) was also reacted with cardamonin. SBDTC (**Figure 3.1**) is a bioactive amine that is often used to form highly active Schiff bases (Break *et al.* 2013). It was synthesised as previously reported (Break *et al.* 2013) and was considered due to its well-known bioactivity, so it was thought that it would enhance cardamonin's activity. Cyclic rings were produced by reacting cardamonin with $\text{NH}_2\text{NH}_2 \cdot \text{H}_2\text{O}$ and NH_2OH to yield pyrazoline **11** and isoxazoline **12**, respectively. Furthermore, pyrimidine rings were also produced by reacting cardamonin with urea and thiourea in the presence of NaOH to synthesise **13** and **14**, respectively.

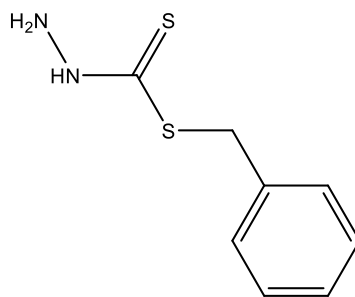
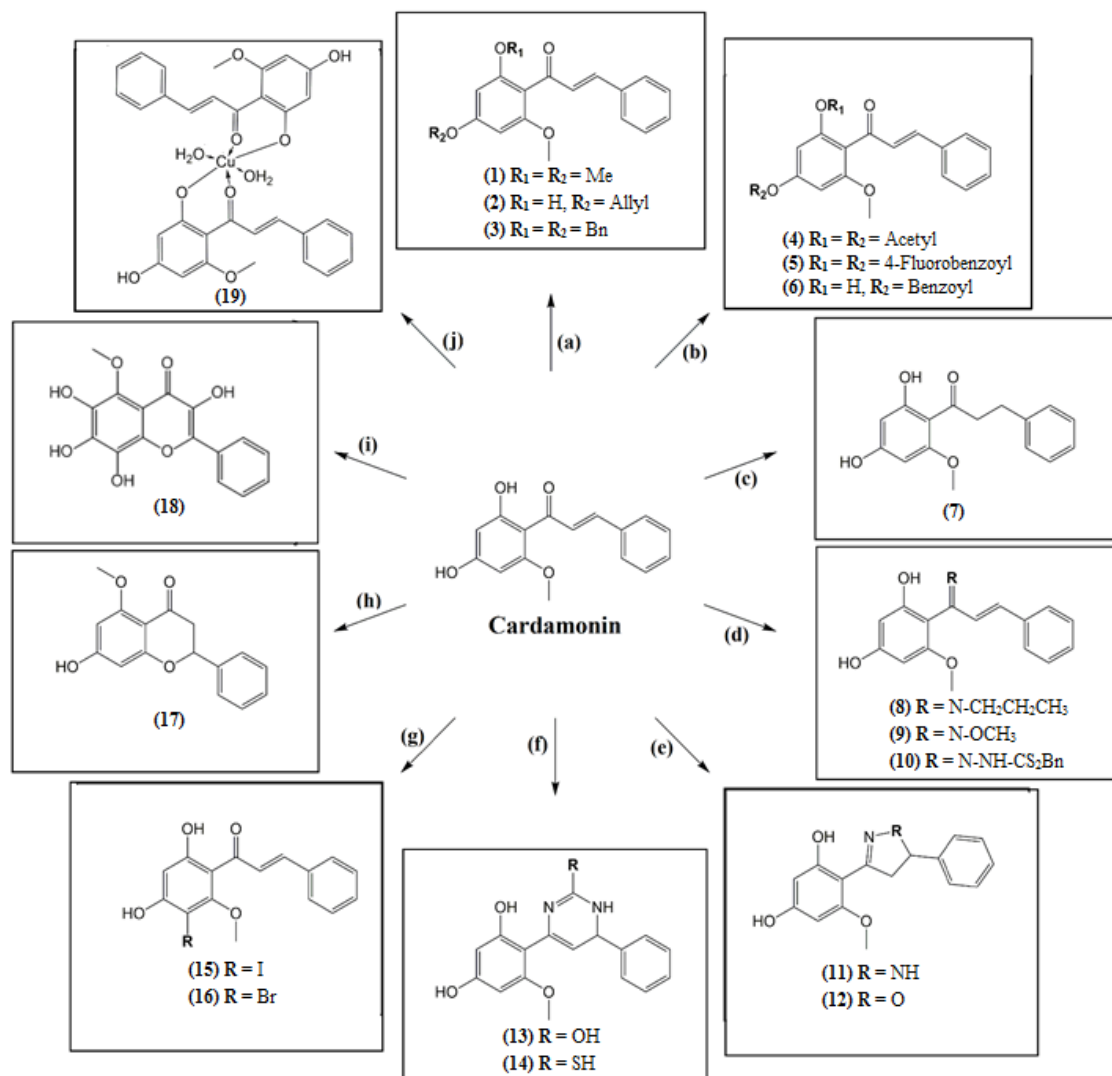


Figure 3.1 Structure of SBDTC

Synthesis of flavanone **17** encouraged us to synthesise the flavone analogue of cardamonin by reacting the chalcone with I₂-DMSO, in order to compare and further investigate the importance of the alkene group. Surprisingly, no flavone was obtained, rather nuclear halogenation occurred at ring A resulting in **15**. The case was similar when bromine was initially reacted with cardamonin in chloroform with the intention of halogenating the alkene group, but nuclear bromination at ring A occurred instead, resulting in **16**. Flavone synthesis was attempted again using FeCl₃ (Hemanth and Perumal 2007) but was still unsuccessful. It has been deduced from these incidents that a method excluding the use of halogens might finally result in successfully synthesising the flavone, as alkene halogenation seems to fail with cardamonin and this step is vital in flavone synthesis. Therefore, a previously reported method that used oxalic acid for flavone synthesis (Zambare *et al.* 2009) was considered but the attempt failed, and interestingly another study also reported the failure of this method (Ndoile and Heerden 2013) which might raise some concerns about the method's efficiency. It seems that substituents at ring A affected the side-chain halogenation of cardamonin. This assumption is strengthened by the fact that the intended dibromo and flavone derivatives have been obtained in previous studies with no reported complications when there were no 6'-OCH₃ or 4'-OH (Dinesha *et al.* 2015; Song *et al.* 1999). However, the unexpected bromination and iodination of ring A encouraged us to perform chlorination and that was attempted using *N*-chlorosuccinimide but the reaction resulted in a mixture of products that proved challenging to separate, as deduced from the NMR spectrum. Moreover, further attempts at purification would have resulted in very low yields of

the pure compounds, and such amounts would not allow further characterisation and bioassays to be performed. Synthesis of flavonol **18** proceeded smoothly and involved reacting cardamonin with 30% H_2O_2 and NaOH.

Cu (II) complex of cardamonin (**19**) required the addition of a base as no reaction occurred without it, this suggested that deprotonation of 2'-OH was crucial for complexation in this case. Imidazole was initially used as a mild base and this produced **19** in low yields, so NaOH was used instead resulting in a much higher yield. Imidazole was initially used as a base instead of NaOH in order to prevent the potential conversion of some of the copper acetate to CuO which would contaminate the desired metal complex (**19**). It is crucial to note that coordinating cardamonin to other metal ions, such as Fe^{2+} , Co^{2+} and Ni^{2+} *via* reacting cardamonin with FeCl_2 , CoCl_2 and NiCl_2 in ethanol, was not successful.



Scheme 3.1 Semi-synthesis of cardamonin analogues. Reagents and conditions: (a) K_2CO_3 , alkyl halide, acetone, reflux; (b) pyridine, DMAP, acyl halide/acetic anhydride, DCM, reflux; (c) NiCl_2 , NaBH_4 , methanol, ice-bath; (d) HCl , primary amine, methanol, reflux; (e) $\text{NH}_2\text{NH}_2 \cdot \text{H}_2\text{O}$ / NH_2OH , methanol, reflux; (f) urea/thiourea, NaOH , 80% ethanol, reflux; (g) I_2 , DMSO, reflux for **(15)**/ Br_2 , CHCl_3 , reflux for **(16)**; (h) HCl , methanol, reflux; (i) 30% H_2O_2 , NaOH , methanol, rt; (j) $\text{Cu}(\text{OAc})_2$, 0.18% NaOH , methanol, reflux

3.1.2 Structure and Characterisation

- **IR Spectral Analysis**

The IR spectra of the compounds have provided valuable structural information which aided in confirming the identity of the synthetic compounds. The IR spectra have been placed in the **Appendix** section and the most crucial peaks were labelled for each compound.

Firstly, it is crucial to note that generally the peak at around 3400 cm^{-1} can be attributed to 4'-OH of the structure or it could be due to residual water from surrounding moisture, but NMR studies further confirmed whether 4'-OH was present or not.

The IR spectrum for cardamonin (**Figure 8.19**) is the most crucial one as the spectra for the analogues are similar to it with slight differences. Cardamonin's spectrum showed two broad peaks at 3448 cm^{-1} and 3170 cm^{-1} , and these have been attributed to 4'-OH and 2'-OH groups of the structure, respectively. The lower absorption frequency observed for 2'-OH was suggested to be due to lengthening of the (O-H) bond as a result of the intramolecular hydrogen-bonding interaction between the 2'-OH and adjacent carbonyl group (**Figure 3.2**).

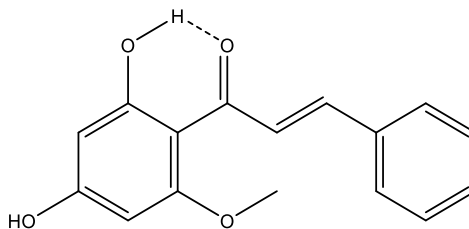


Figure 3.2 Intramolecular hydrogen bonding in cardamonin

The peak at 1630 cm^{-1} was assigned to (C=O) group of the structure and this relatively low absorption frequency value for a carbonyl group is due to the presence of an α,β -unsaturated carbonyl system possessing conjugated double bonds. The conjugated system present in the structure results in lengthening of the (C=O) due to resonance causing it to possess a more single-bond character which results in lower absorption frequencies. The peaks at 1609 cm^{-1} and 1475 cm^{-1} were attributed to (C=C) of the aromatic rings, while the peak at 2926 cm^{-1} was assigned to the (C-H) groups of the molecule. The peaks at 1114 cm^{-1} and 1225 cm^{-1} indicated the presence of (C-O) groups with the former being assigned to the methoxy group and the latter attributed to the phenolic (C-O) of the structure.

IR analysis of cardamonin's acylated/alkylated analogues (**1-6**) (**Figure 8.20 - Figure 8.25**) aided in confirming their formation. The disappearance of the peak at around 3170 cm^{-1} , assigned to 2'-OH, indicated that substitution has occurred at 2'-OH, however, confirming substitution at 4'-OH using IR spectra was not possible due to interference from the residual moisture peak. However, further NMR analysis showed that substitution only occurred at 4'-OH for compounds **2** and **6**, but the IR spectrum of **2** (**Figure 8.21**) and **6** (**Figure 8.25**) still showed no peak for 2'-OH. This might have been due to the wide residual moisture peak at around 3400 cm^{-1} which obscured the 2'-OH peak. The IR spectra of the acylated compounds (**Figure 8.23 - Figure 8.25**) showed a further characteristic peak at around $1690\text{--}1776\text{ cm}^{-1}$ corresponding to an ester (C=O) which proves that the desired compound has been successfully obtained. It is crucial to mention that the IR spectrum of **3** (**Figure 8.22**) showed a set of overlapping peaks between $2700\text{ cm}^{-1} - 3200\text{ cm}^{-1}$

that were not found in the spectra of the other compounds. These extra overlapping peaks have been attributed to the aromatic and alkyl (C-H) stretches of the benzyl groups, and this actually further proves the successful *O*-benzylation of cardamonin.

The IR spectra of Schiff bases **8**, **9** and **10** (**Figure 8.27** - **Figure 8.29**) showed a peak at around 1632 cm^{-1} and this has been assigned to the imine (C=N) group of the structures. Moreover, it was still possible to observe the 2'-OH peak at around 3200 cm^{-1} as a result of the intramolecular hydrogen bonding between 2'-OH and the nitrogen of the imine group leading to (OH) bond lengthening. It is interesting to note that 2'-OH peaks of the Schiff bases were found to be at higher absorption frequencies than that of cardamonin, and that might have been due to the weaker (N---H) hydrogen bond present in the Schiff bases relative to the stronger (O---H) hydrogen bond of cardamonin. This weaker hydrogen bond in Schiff bases is suggested to be due to the lower electronegativity of nitrogen compared to that of oxygen, resulting in lesser bond lengthening. This observation further proves the successful replacement of the carbonyl group with an imine group indicating that the desired Schiff bases have been successfully obtained. However, it is crucial to note that in some cases the 2'-OH peak was clearly visible such as in the spectrum of **8** (**Figure 8.27**), while in the spectrum of **9** (**Figure 8.28**) the peak was barely visible. This happens due to the peak at 3400 cm^{-1} which is affected by residual moisture from the atmosphere, so if moisture content was high in the compound, then that would result in an intense wide peak that would overlap with the 2'-OH peak. Moreover, the slight differences in the absorption frequencies of the 2'-OH peak for compounds **8** and **9**, might mean that in some cases the 2'-OH peak is

nearer to the peak at 3400 cm^{-1} resulting in higher chances of overlap. The spectrum of **10** (**Figure 8.29**) was very different from the spectra of the other Schiff bases due to the SBDTC moiety present in the structure. The spectrum showed the typical imine peak at 1627 cm^{-1} in addition to a peak at 1487 cm^{-1} that has been assigned to aromatic (C=C) of the structure. The spectrum also showed peaks that were specific to the SBDTC moiety of the structure, such as the thione (C=S) peak at 950 cm^{-1} , the (N-N) peak at 1042 cm^{-1} and the (NH) peak at 3173 cm^{-1} . There was also the peak for 2'-OH from the structure's cardamonin moiety at 3213 cm^{-1} , however this peak overlapped with the adjacent (NH) peak and was challenging to detect.

The IR spectra for pyrazoline **11** (**Figure 8.30**) and isoxazoline **12** (**Figure 8.31**) showed characteristic peaks for (C=N) at 1618 cm^{-1} and 1610 cm^{-1} , respectively. This drop in the absorption frequency of (C=N), relative to that of imines in general, has been attributed to the lone pair of electrons present on the secondary amine nitrogen of **11** and oxygen of **12** (Ioffe 1968). This causes lengthening of the (C=N) bond through resonance, thus giving it a more single-bond character. Moreover, the spectra for **13** (**Figure 8.32**) and **14** (**Figure 8.33**) show peaks at 1661 cm^{-1} which was attributed to (C=N) of the pyrimidine ring, while the peaks at around 3222 cm^{-1} and 1601 cm^{-1} have been assigned to (N-H) stretch and bend, respectively. Compounds **13** and **14** exist as tautomers, and their IR spectral data along with their NMR data enable the identification of the tautomeric state each of these molecules exist in, but that would be discussed later after discussing their NMR spectral data.

The IR spectrum of flavanone **17** (**Figure 8.36**) shows a peak at 1657 cm^{-1} , and this has been attributed to the carbonyl group of the structure, while this higher

absorption value relative to that of cardamonin shows that the carbonyl group is no longer conjugated which indicates the disappearance of the adjacent double bond. Moreover, there is an absence of a peak for 2'-OH which is thought to be a result of its conversion into an ether. These characteristic peaks found in the IR spectrum of the flavanone prove the formation of the intended compound. The case was similar for **18** whereby the IR spectrum (**Figure 8.37**) is very similar to that of cardamonin except that there is no peak for 2'-OH which indicates that cyclisation might have occurred.

The IR spectrum of **19** (**Figure 3.3** and **Figure 8.38**) showed a peak at around 1598 cm^{-1} assigned to (C=O) and this negative shift in the absorption frequency relative to that of cardamonin suggested coordination of the carbonyl oxygen with the metal ion. This negative shift is thought to be due to enhancement of the mesomeric effect upon complexation which results in lengthening of (C=O). Moreover, the peak assigned for 2'-OH at 3173 cm^{-1} has disappeared from the spectrum of **19** which indicates that the phenolic group has coordinated with the metal ion in its deprotonated form. This was further confirmed by the appearance of a peak at 1230 cm^{-1} which was assigned to the phenolic (C-O) of **19**, and this positive shift in the absorption frequency relative to that of cardamonin further indicated the coordination of the phenolic oxygen of deprotonated 2'-OH to the metal ion.

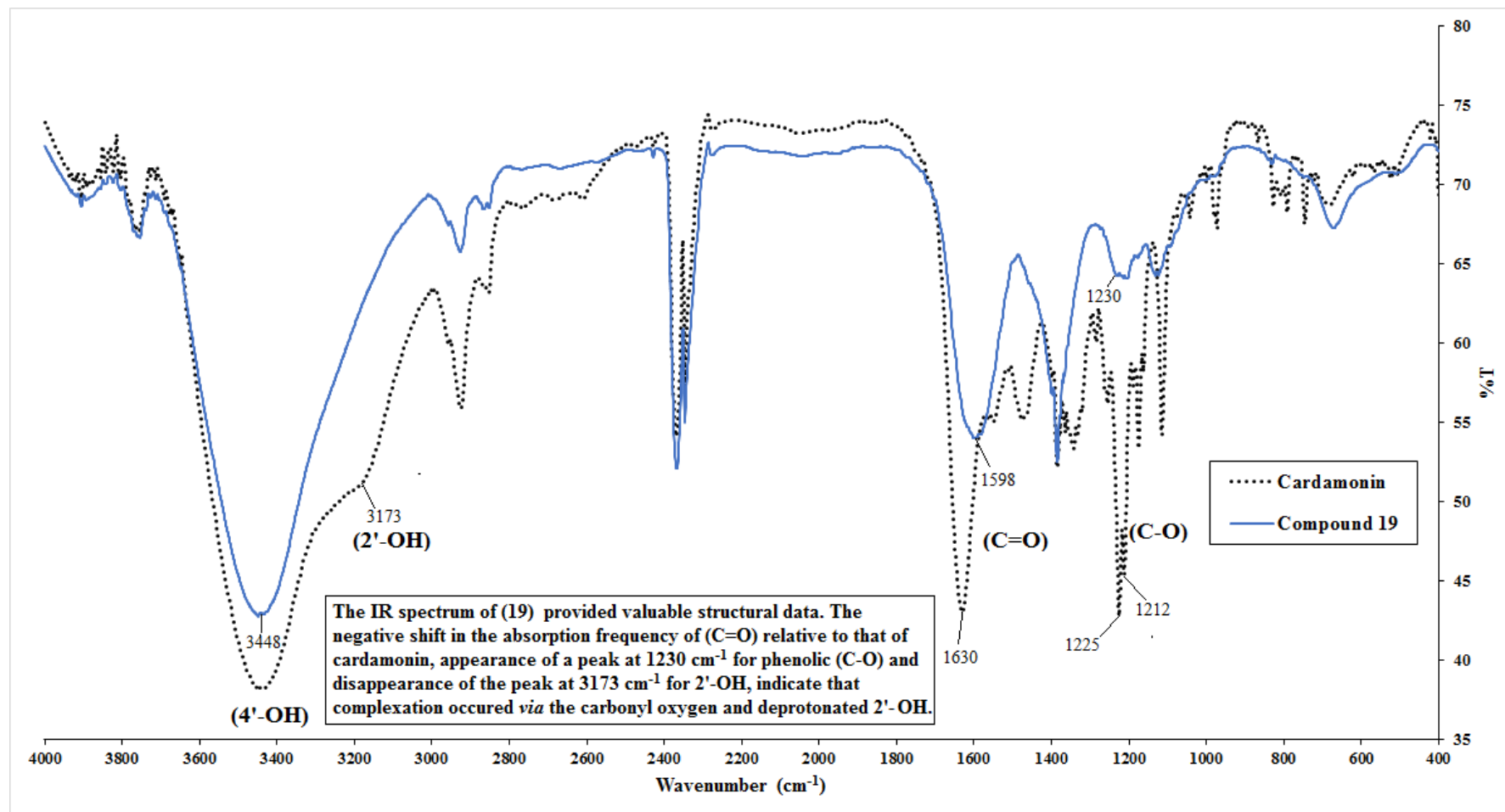


Figure 3.3 Overlaid IR spectra of cardamonin and **19**

Finally, it is crucial to mention that it was not possible to fully deduce the structures of **7**, **15** and **16** *via* IR spectroscopy. This was due to the fact that these analogues possessed IR spectra that were too similar to that of cardamonin and characteristic peaks proved difficult to identify. Therefore, it was decided that further analysis *via* NMR spectroscopy would be needed to confirm the analogues' structures. However, it was possible to observe the appearance of an extra peak in the IR spectrum of **15** (**Figure 8.34**) and **16** (**Figure 8.35**) at the fingerprint region. The peak at 847 cm^{-1} in the spectrum of **15** was attributed to the newly formed (C-I), while the peak at 498 cm^{-1} in the spectrum of **16** was attributed to the newly formed (C-Br). This could indicate the successful halogenation of the compounds, but further analysis *via* NMR spectroscopy is required to confirm these structural findings.

- **NMR Spectral Analysis**

Cardamonin

Discussion of cardamonin's NMR spectrum is highly crucial as the spectra of the other derivatives are very similar to it with the exception of some extra peaks corresponding to the groups that were added. Therefore, a thorough discussion would be provided for cardamonin's NMR spectrum while only new peaks corresponding to newly added groups would be discussed for the analogues.

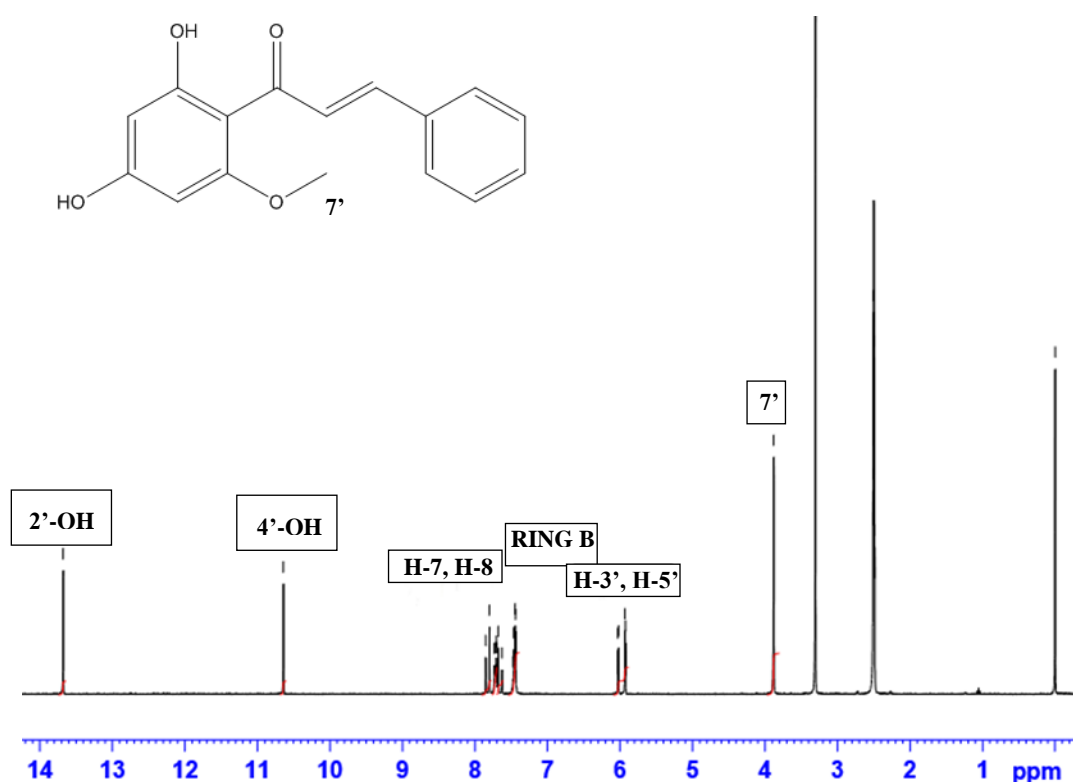


Figure 3.4 NMR spectrum of cardamonin

The singlet peak at 3.96 ppm corresponded to the methyl protons of the methoxy group (7') and this relatively high absorption is a result of deshielding effect on the methyl protons by the adjacent electronegative oxygen atom. H-3' and H-5' of ring

A showed a doublet for each due to long range coupling interactions with each other and they showed lower absorption values than those of aromatic protons in general at 6.03 ppm and 5.98 ppm, respectively; this upfield absorbance might be due to the shielding effect provided by the adjacent methoxy and hydroxyl groups which directed electrons to the *ortho* and *para* positions of the ring. Methine protons H-7 and H-8 have been assigned the peaks 7.89 ppm and 7.82 ppm, respectively, and the higher absorption peak of the former is due to deshielding by resonance effect which also results in further shielding of H-8. **Figure 3.5** illustrates the resonance effect phenomenon.

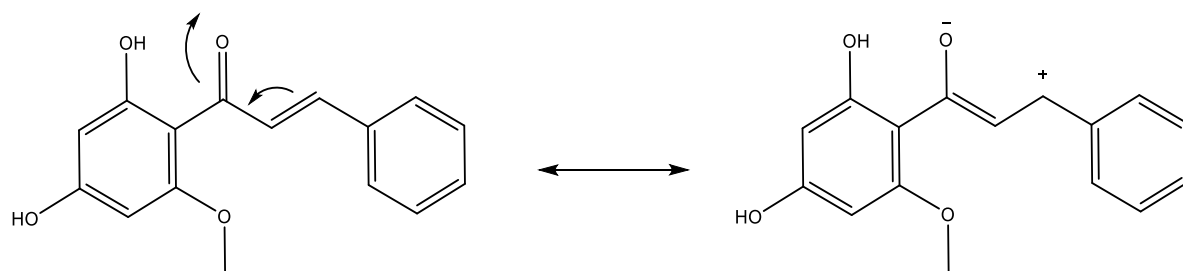


Figure 3.5 Resonance effect of cardamonin

It is important to note that the coupling constant (J) for the doublets of H-7 and H-8 is almost 16 Hz which is large and has been suggested to indicate the existence of the chalcone as a *trans* isomer (Tran *et al.* 2012). This is usually characteristic to chalcones and can be used as a proof for their formation.

Finally, the singlet peak at 14.16 ppm has been attributed to 2'-OH as this relatively high absorption for a hydroxyl proton is a result of further deshielding of the proton due to intramolecular hydrogen bonding between it and the adjacent carbonyl oxygen. This hydrogen bond meant that the electronegative carbonyl oxygen would further deshield the hydroxyl proton resulting in a further downfield shift.

Compound 1

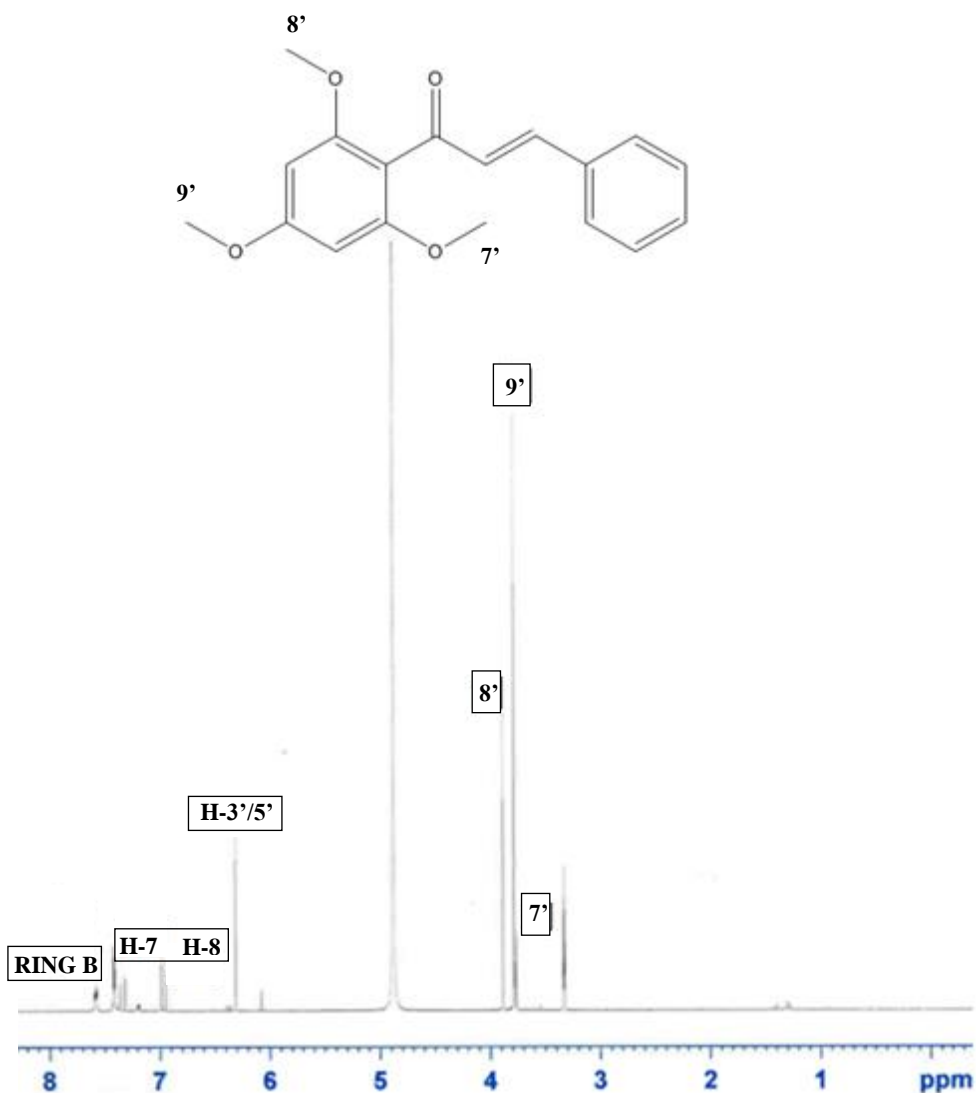


Figure 3.6 NMR spectrum of **1**

The characteristic singlet at 6.31 ppm in the spectrum of **1** belonging to aromatic protons H-3' and H-5' prove that the substitution reaction was successful and the intended di-alkylated compound has been obtained. This is due to the fact that these protons can only be equivalent if the hydroxyl groups of the parent compound cardamonin were successfully methylated as that would result in a 2',4',6'-

trimethoxy ring and that makes H-3' and H-5' chemically equivalent. Furthermore, it is crucial to note that these protons are shielded by the resonance effect of the electron-donating methoxy groups causing them to absorb further upfield. Finally the 3 singlet peaks at around 3.85 ppm were assigned to methyl protons 7', 8' and 9' which further proves the formation of the analogue.

Compound 2

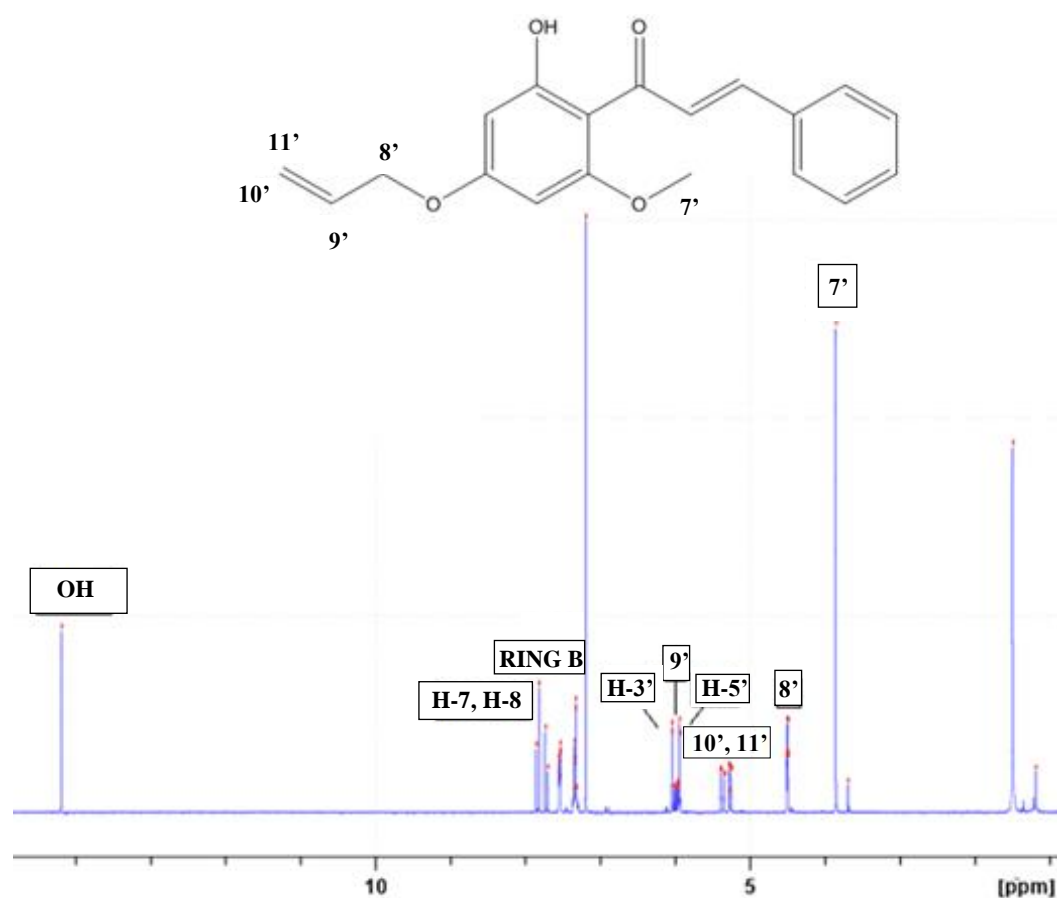


Figure 3.7 NMR spectrum of **2**

The spectrum of **2** showed the formation of the desired product *via* the multiplet at around 5.98 ppm which was attributed to the methine proton of the allyl group (9'), as this proton experiences couplings with all the surrounding protons resulting in a

complex multiplet which is characteristic to the allyl group. There was also a pair of doublet of doublets, belonging to protons of the methylene group (**10'**, **11'**) in the allyl fragment at around 5.26 ppm and 5.35 ppm due to geminal and vicinal couplings with the neighbouring protons. Finally, the presence of a doublet for protons of the methylene bridge of the allyl group (**8'**) at 4.50 ppm indicated the successful allylation of cardamonin. However, the presence of a peak at 14.19 ppm assigned to 2'-OH indicated that allylation occurred only at 4'-OH.

Compound 3

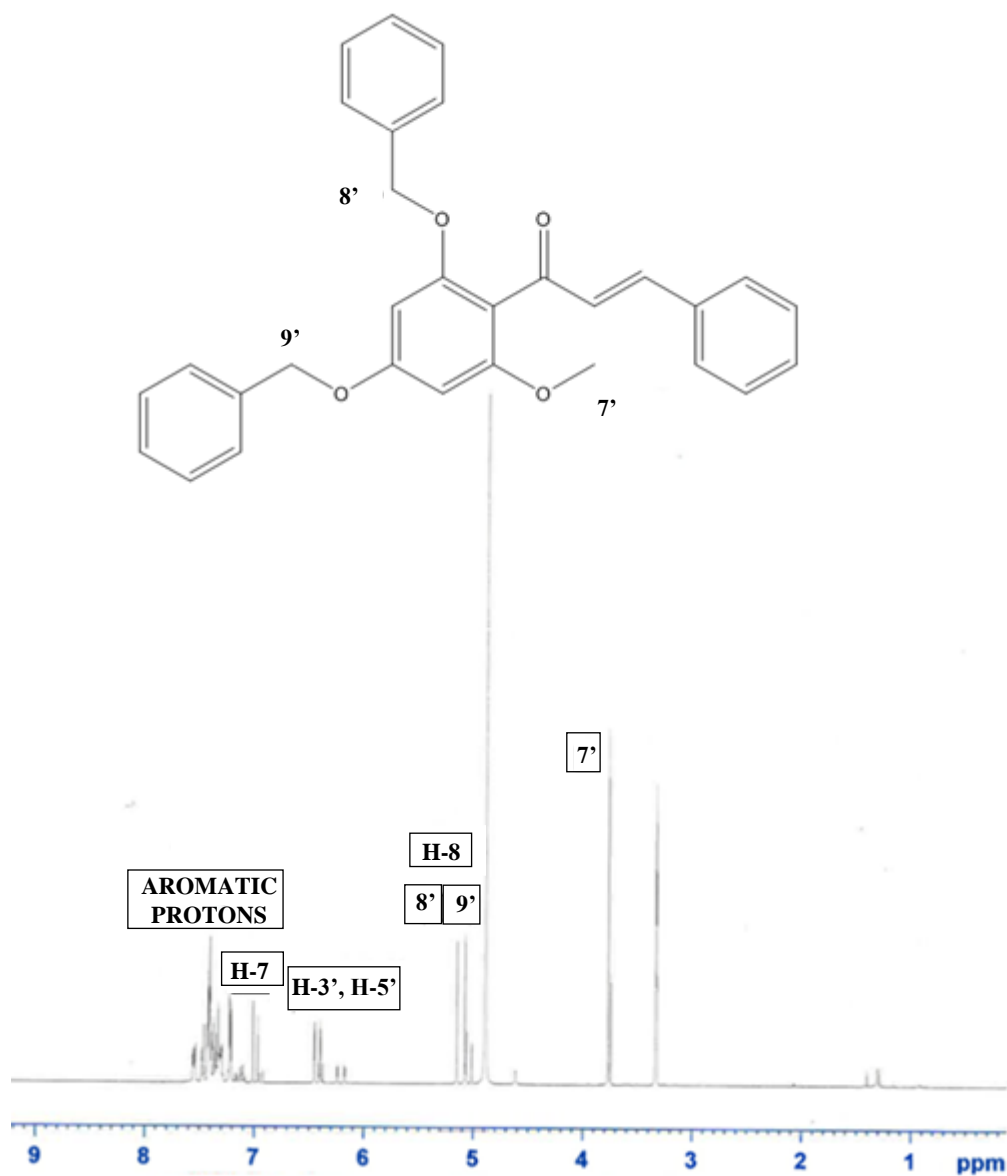


Figure 3.8 NMR spectrum of **3**

The spectrum for compound **3** showed a relatively large number of overlapping peaks in the range between 7 and 8 ppm, and this indicates the presence of a large number of aromatic protons which proves that cardamomin has been successfully benzylated. Moreover, the peaks around 5 ppm attributed to the methylene protons

of the benzyl group (**8'** and **9'**) further confirm the formation of the intended product, and this relatively higher chemical shift is due to the high electronegativity of the adjacent oxygen which enhanced the deshielding effect. It was difficult to assign each peak to its corresponding aromatic proton due to the extensive overlapping of peaks resulting from the 4 benzene rings present in the structure.

Compound 4

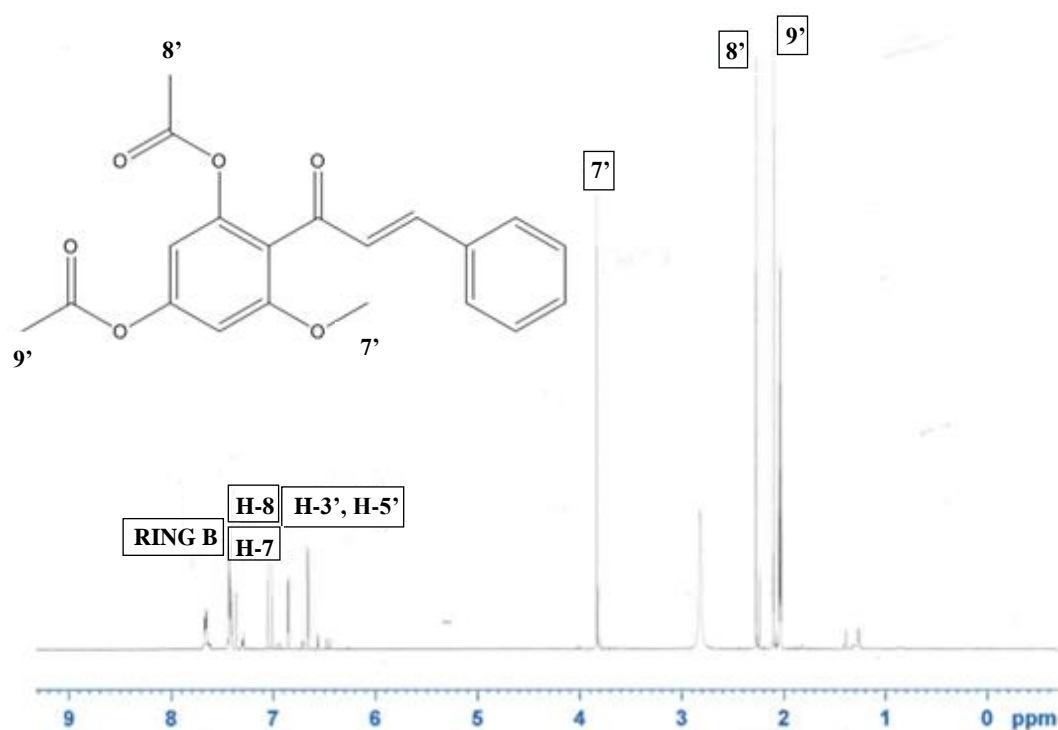


Figure 3.9 NMR spectrum of **4**

The spectrum for **4** has characteristic singlet peaks corresponding to methyl protons of the acetyl groups (**9'** and **8'**) at 2.11 ppm and 2.28 ppm which confirms the successful di-acetylation of cardamonin.

Compound 5

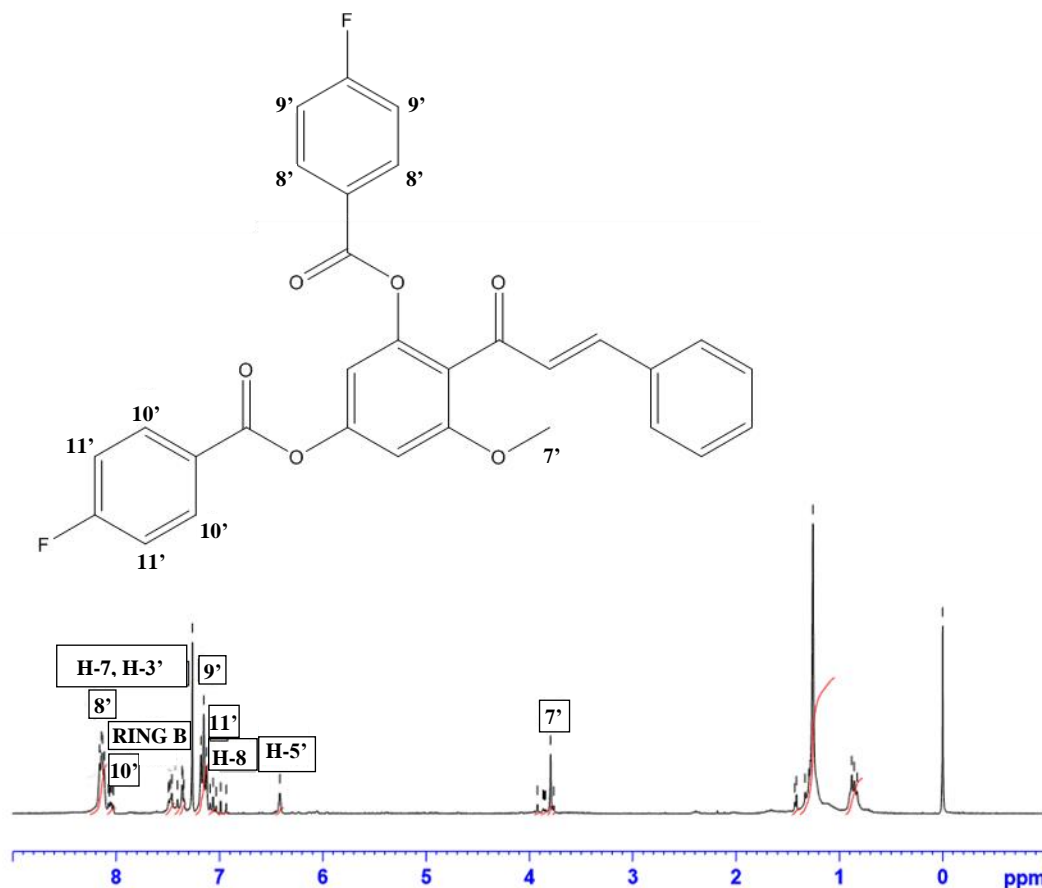


Figure 3.10 NMR spectrum of **5**

The spectrum has proven the formation of the 4-fluorobenzoylated analogue of cardamonin by peaks characteristic to the 4-fluorobenzoyl moiety along with peaks belonging to the cardamonin moiety. The triplet and doublet of doublet peaks at around 7.10 ppm and 8.10 ppm have been assigned to *meta* (**9'**, **11'**) and *ortho* (**8'**, **10'**) protons of the 4-fluorobenzene ring, respectively, and these splitting patterns have been a result of coupling of the protons with each other in addition to the neighbouring fluorine atom, as fluorine has a nuclear spin similar to hydrogen, thus it can couple with the adjacent protons. Moreover, the presence of these splitting

patterns as duplicates in addition to the disappearance of a peak at 14 ppm for 2'-OH, indicate that disubstitution of cardamonin has taken place resulting in two 4-fluorobenzoyl moieties that are magnetically non-equivalent.

Compound 6

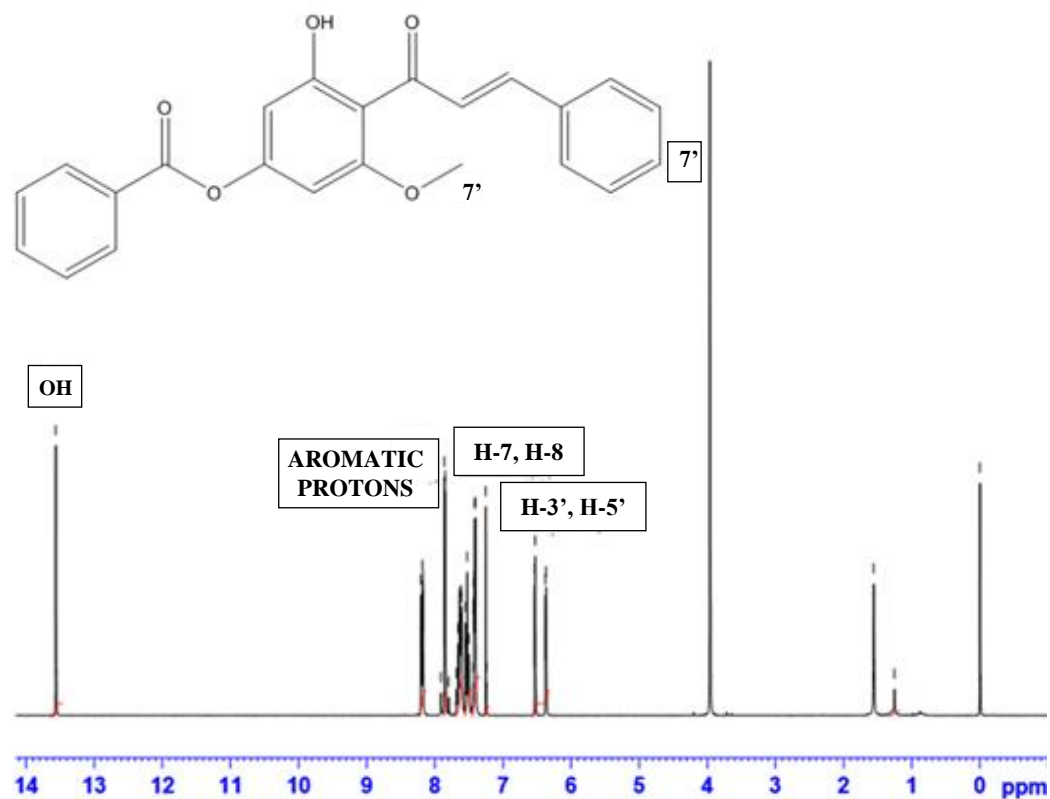


Figure 3.11 NMR spectrum of **6**

The spectrum of the benzoylated compound shows a higher number of peaks around 7-8 ppm relative to that of cardamonin due to contribution from the benzoyl group protons. Furthermore, the peak at 13.56 ppm corresponding to 2'-OH shows that benzoylation occurred at the *para* position of ring A only.

Compound 7

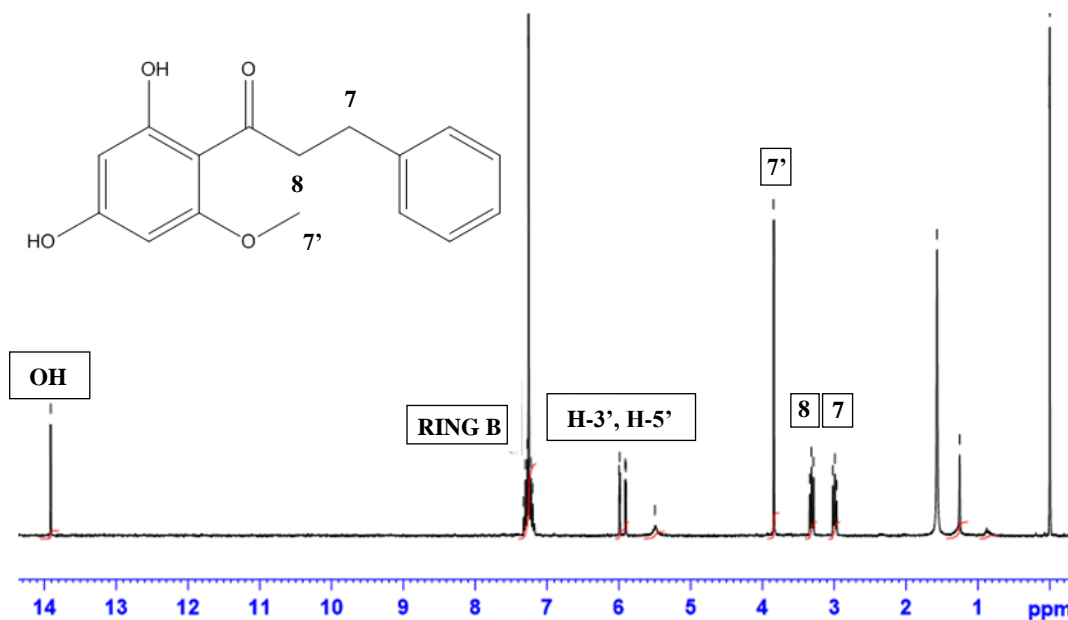


Figure 3.12 NMR spectrum of **7**

The NMR spectrum of compound **7** shows that reduction of cardamonin *via* the NaBH₄/ Ni²⁺ system resulted in a dihydrochalcone whereby the alkene group of the chalcone was selectively reduced. This is evident from the appearance of a pair of triplets at 2.99 ppm and 3.32 ppm corresponding to the methylene protons **7** and **8** respectively, which shows that the alkene group has been converted. Moreover, the disappearance of a pair of doublets with large coupling constants at around 7.70 ppm corresponding to methine protons H-7 and H-8 further confirms the reduction of the alkene group. This structure assignment was further strengthened and complemented by data obtained from the IR spectrum which showed a peak corresponding to the ketone group, thus confirming that the ketone group was unaffected by the reduction reaction and the product is a dihydrochalcone.

Compound 8

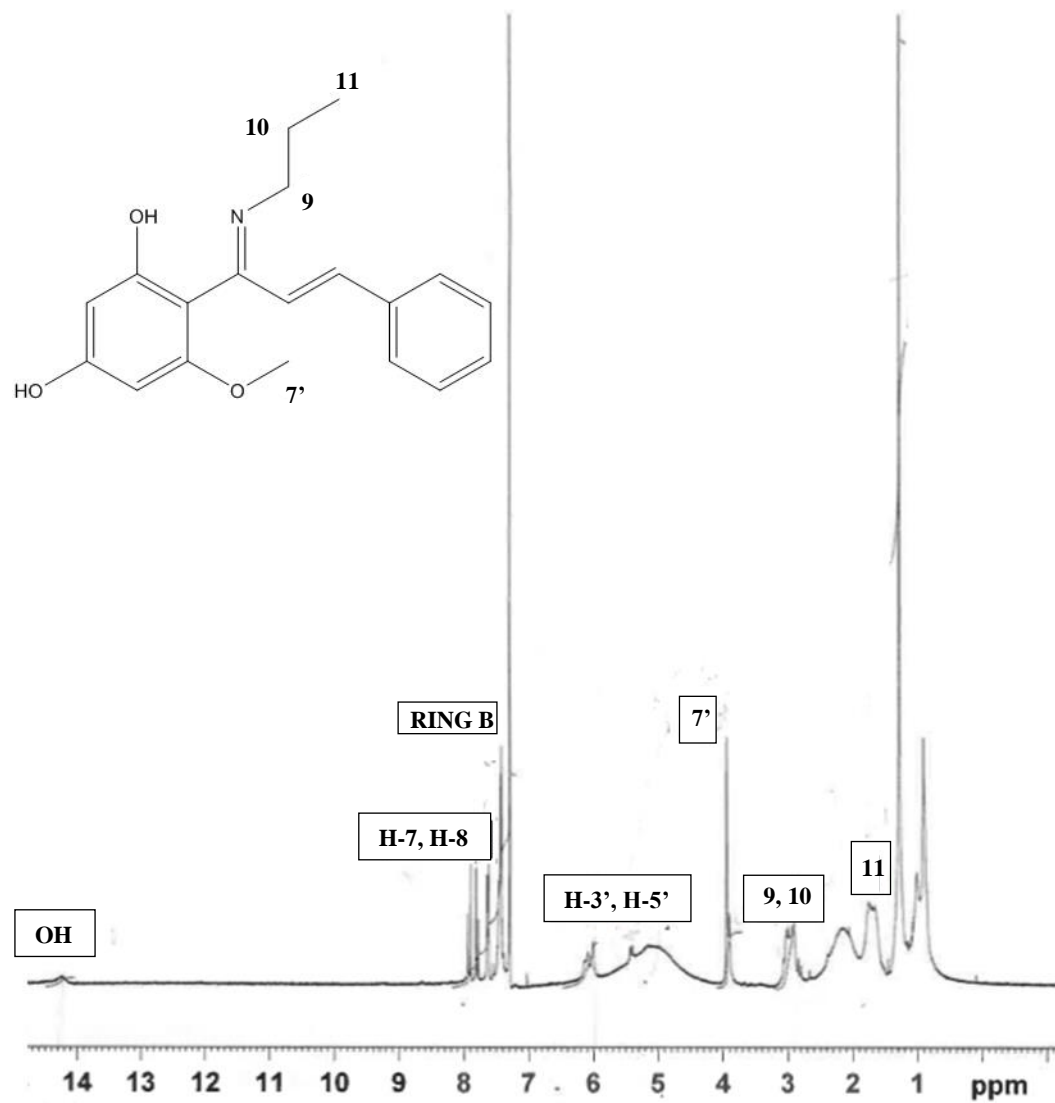


Figure 3.13 NMR spectrum of **8**

Compound 9

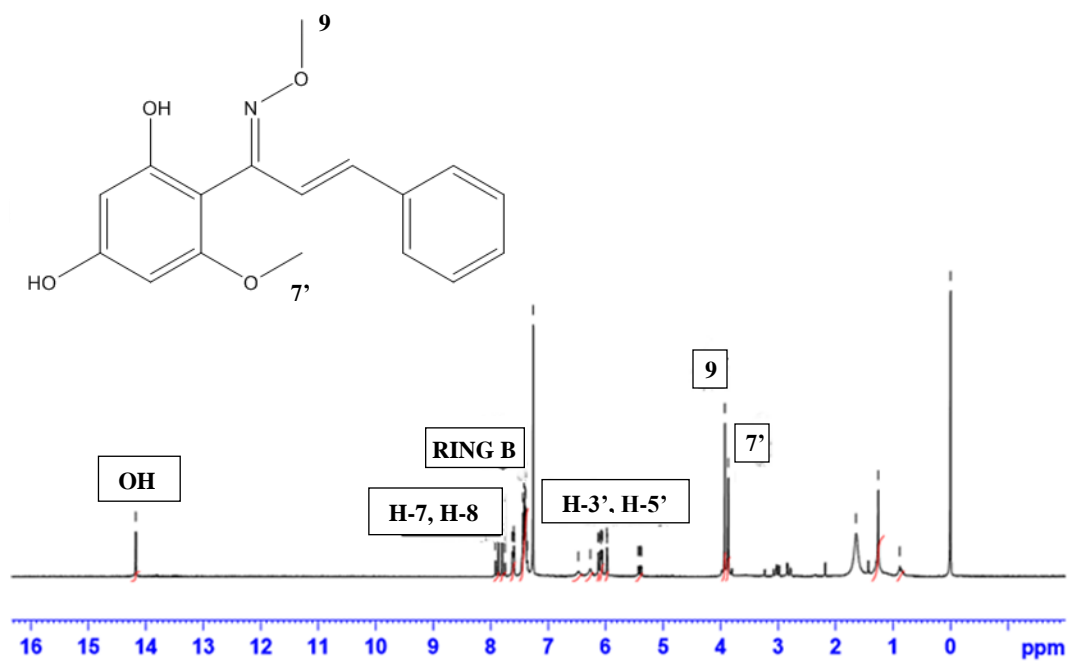


Figure 3.14 NMR spectrum of 9

Compound 10

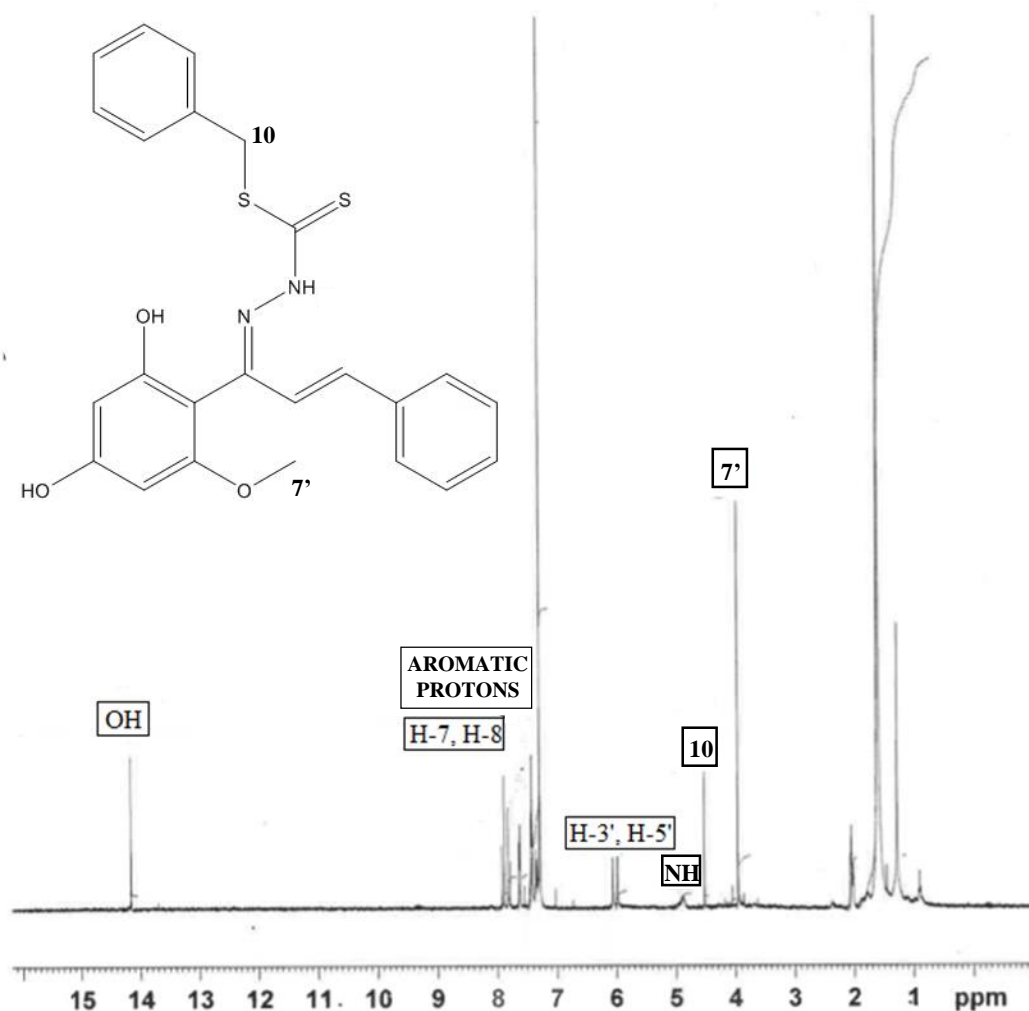


Figure 3.15 NMR spectrum of **10**

The spectra for Schiff bases **8**, **9** and **10** show little variation from that of cardamomin and the extra peaks shown are due to the alkyl groups that have been attached to them. The spectrum for **8** shows a triplet peak at 3.00 ppm assigned for the methylene bridge protons adjacent to the nitrogen atom (**9**) while the peaks at 2.82 ppm and 1.70 ppm have been assigned to the adjacent methylene bridge protons (**10**) and methyl protons (**11**), respectively, which further proves that the

condensation reaction was successful and resulted in the formation of the desired structure. The spectrum for **9** is very similar to that of cardamonin except for one characteristic peak at around 3.93 ppm assigned to C=NOCH₃ (**9**) which proves the formation of the intended Schiff base. Finally, the spectrum for **10** has shown a characteristic singlet at 4.52 ppm assigned to the methylene bridge (**10**) of the SBDTC moiety and these protons have been deshielded by the adjacent sulphur atom, moreover, there were several overlapping peaks at around 7.5 ppm with an integral of about 10 protons assigned to ring B of the cardamonin moiety and the benzene ring of the SBDTC moiety, which further prove the formation of the SBDTC-derived Schiff base. It is also crucial to note that the presence of a peak for NH at 4.92 ppm in the spectrum of **10** proves that the structure exists as the thione tautomer, as such a structure can actually undergo thione-thiol tautomerism (**Figure 3.16**)

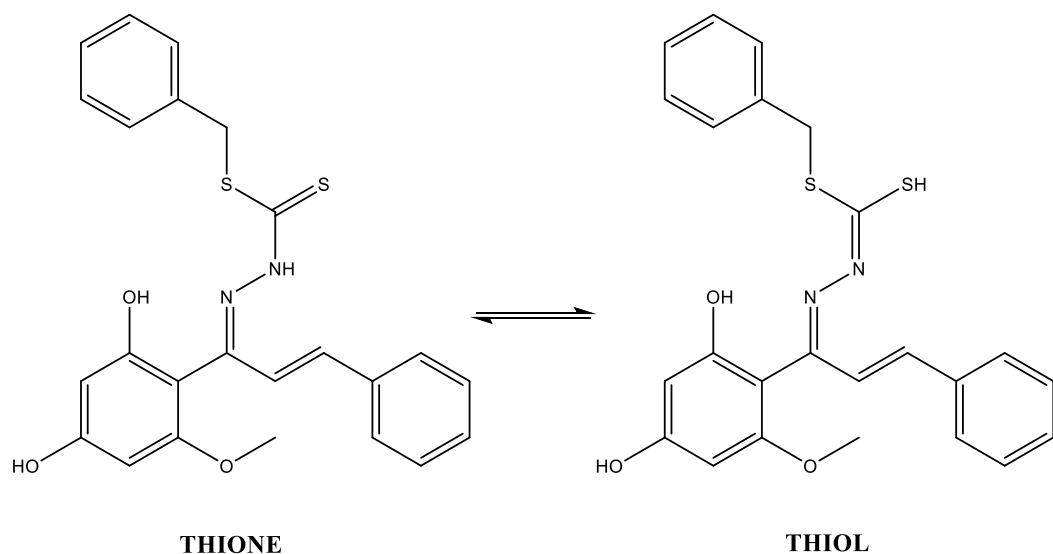


Figure 3.16 thione-thiol tautomerism in **10**

Compound 11

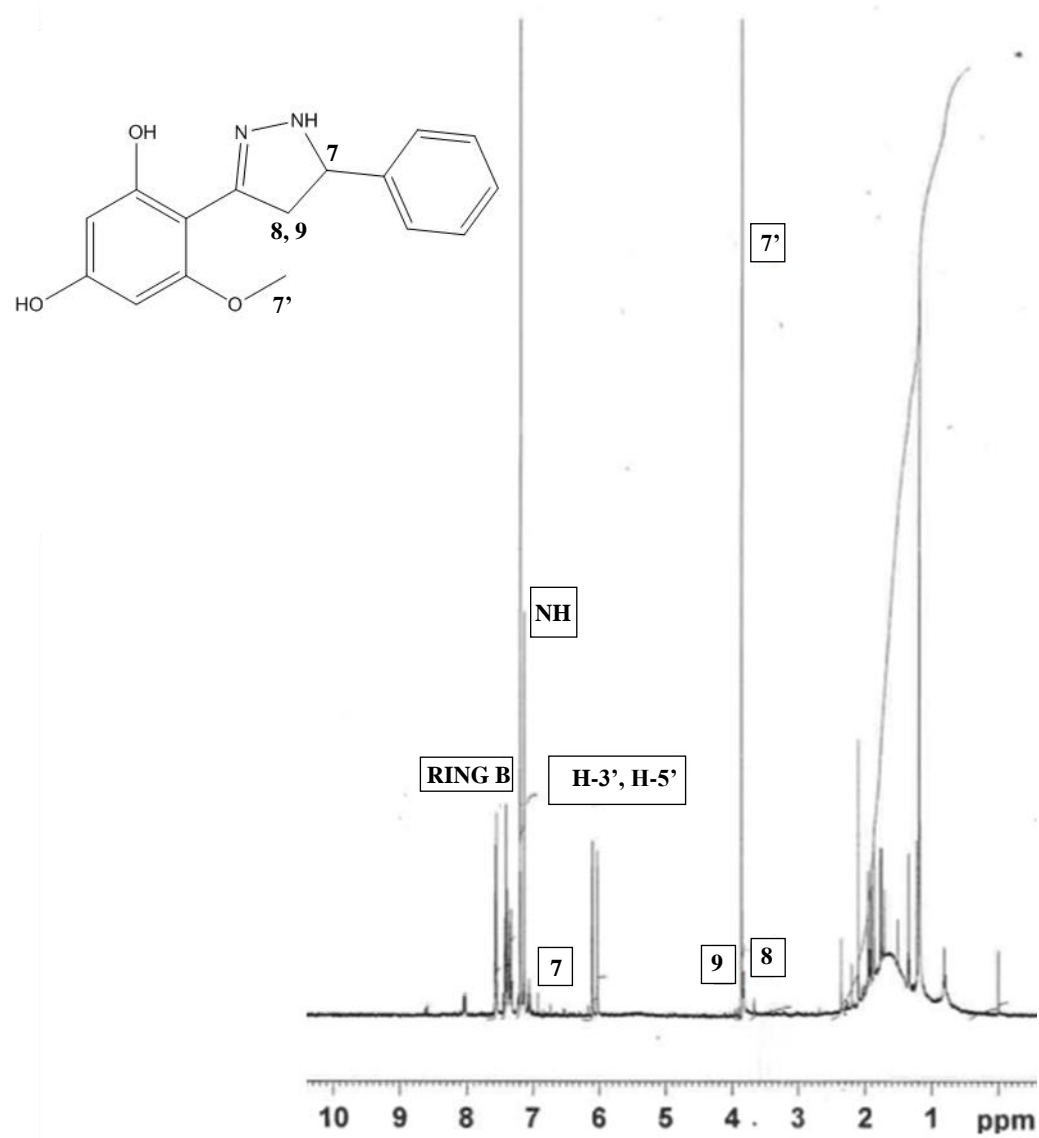


Figure 3.17 NMR spectrum of **11**

Compound 12

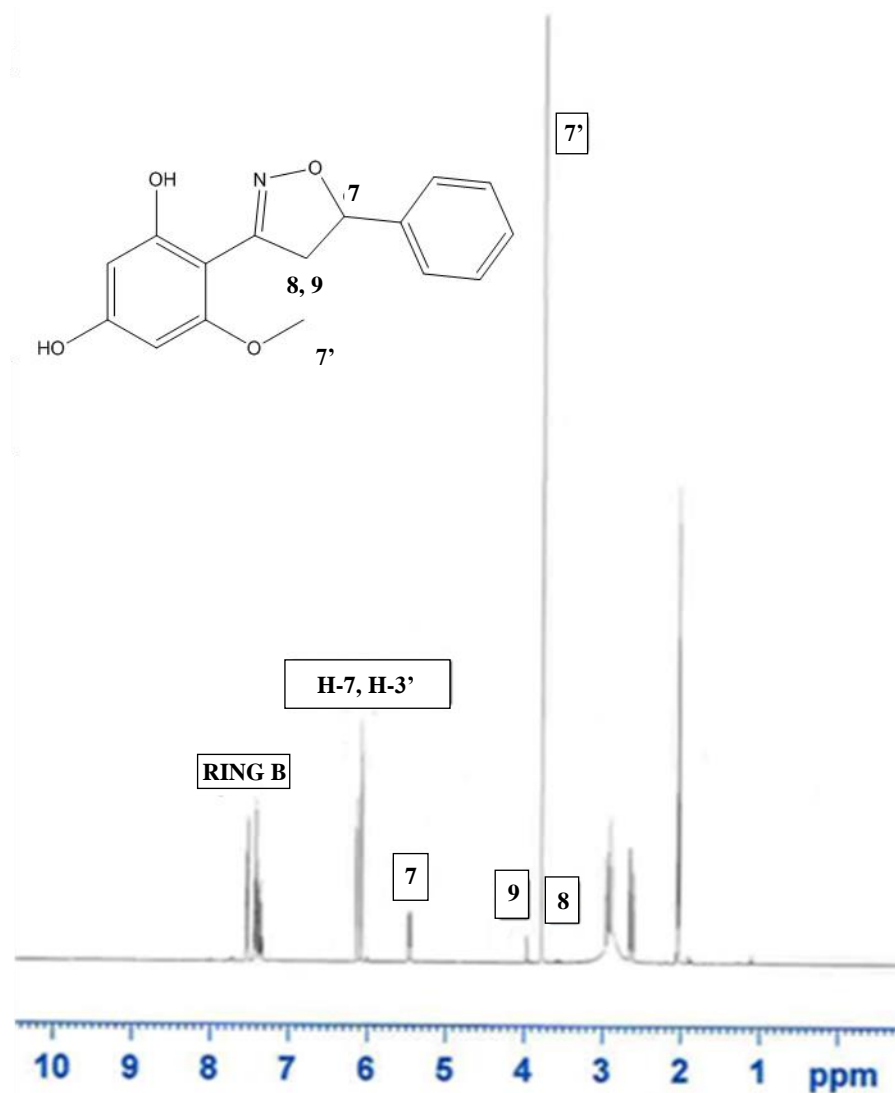


Figure 3.18 NMR spectrum of **12**

The spectra have clearly proven that the cyclisation reactions were successful and resulted in the formation of the desired pyrazoline and isoxazoline compounds. The disappearance of doublets corresponding to the α and β methine protons of chalcones indicated that the alkene double bond is no longer present. Formation of the pyrazoline/isoxazoline ring was proven by the presence of three doublet of doublets at 3.83 ppm, 3.94 ppm and 6.52 ppm for **11** and 3.58 ppm, 3.93 ppm and

5.46 ppm for **12** corresponding to the methylene (**8, 9**) and methine (**7**) protons of the pyrazoline/isoxazoline rings. These three doublet of doublets found in each of the compounds arise due to restricted rotation of the C-C sigma bond of the pyrazoline/isoxazoline rings resulting in two magnetically inequivalent protons which can couple with each other peak as well as the adjacent methine (**7**) proton resulting in doublet of doublets for each of the three protons. The relatively high absorption frequency of the methine proton (**7**) is suggested to be as a result of deshielding by the adjacent electronegative nitrogen/oxygen atom in addition to the flow of electrons towards the adjacent benzene ring. Finally, the singlet at 7.13 ppm found only in the spectrum of **11** was assigned to (NH) of the pyrazoline ring moiety.

Coupling constants have also managed to provide valuable structural data. The relatively large coupling constants for pyrazoline/isoxazoline ring protons is generally due to *trans* coupling. Based on that, the peak at 3.94 ppm for **11** and 3.93 for **12** was attributed to the *trans* proton of the pyrazoline/isoxazoline ring's methylene group (**8, 9**), and this was due to their large coupling constants of 20.2 Hz and 24 Hz, respectively. These large coupling constants are characteristic for pyrazoline/isoxazoline protons and further prove the formation of the desired product.

Compound 13

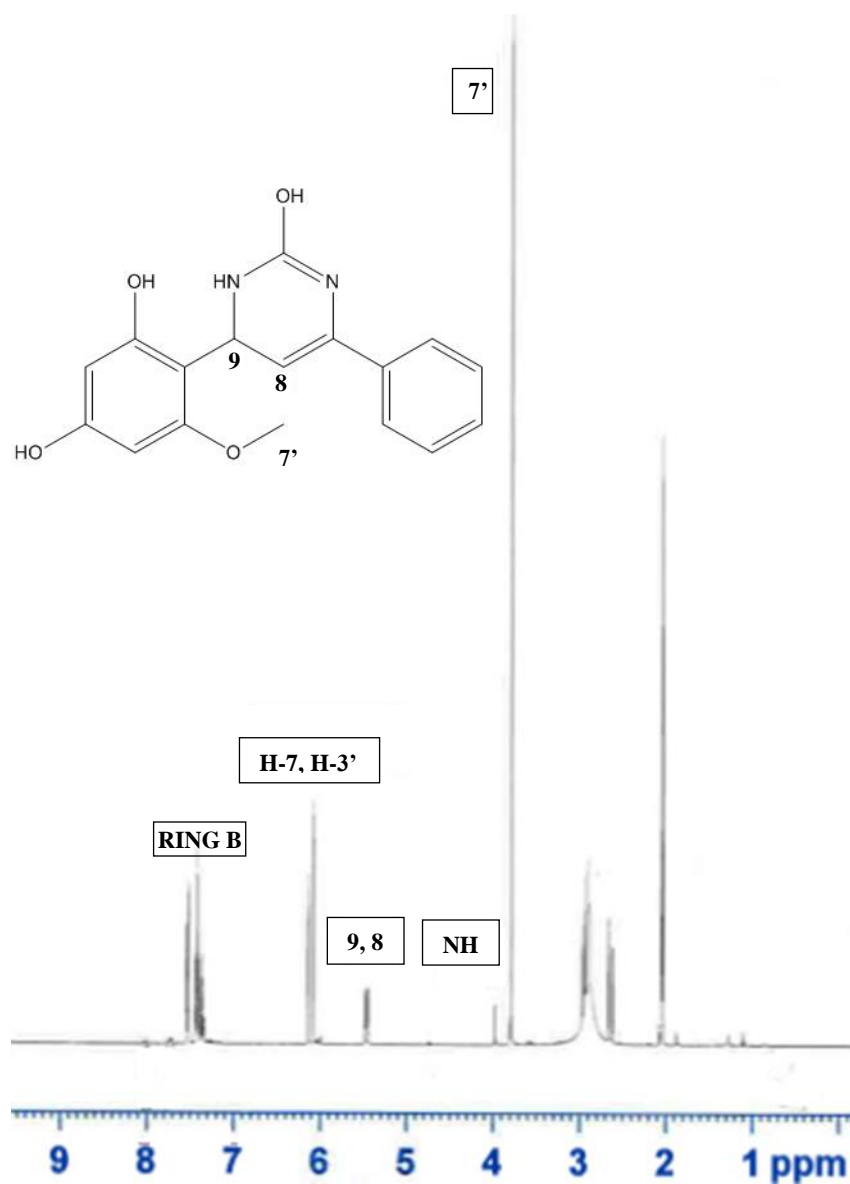


Figure 3.19 NMR spectrum of **13**

Compound 14

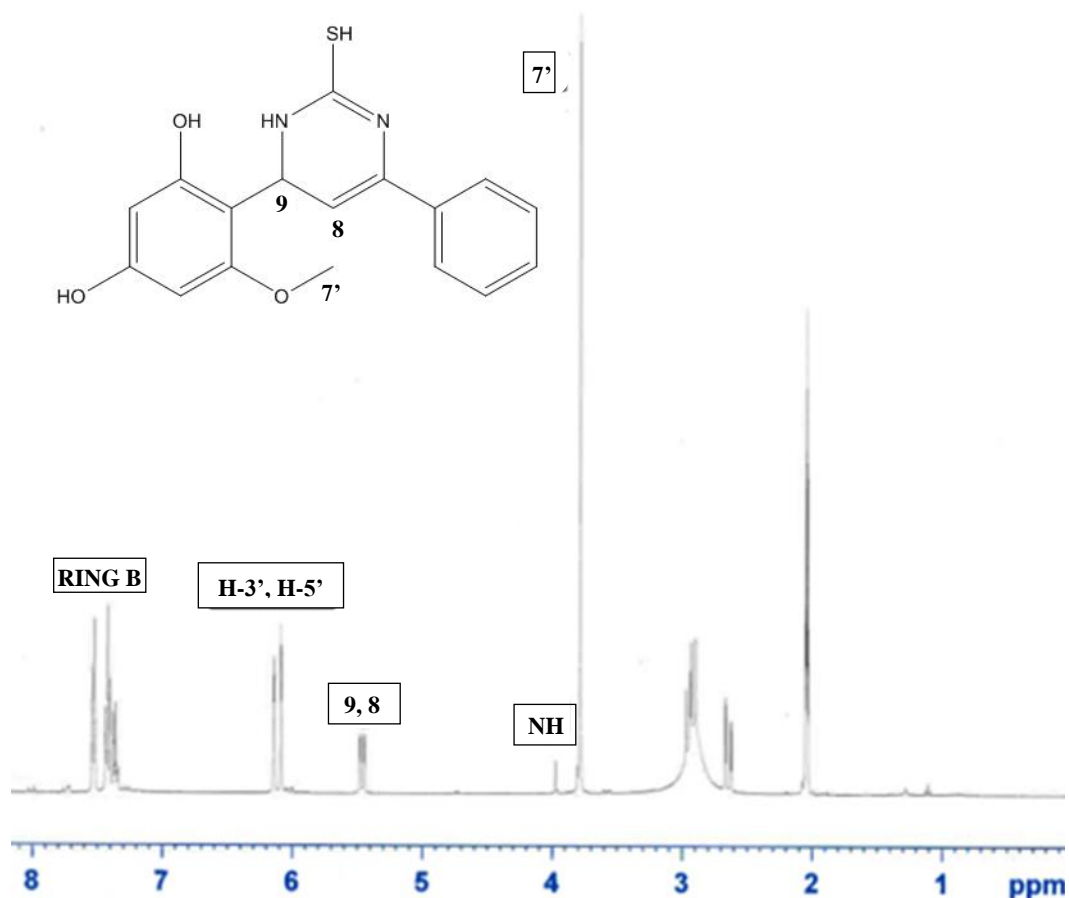
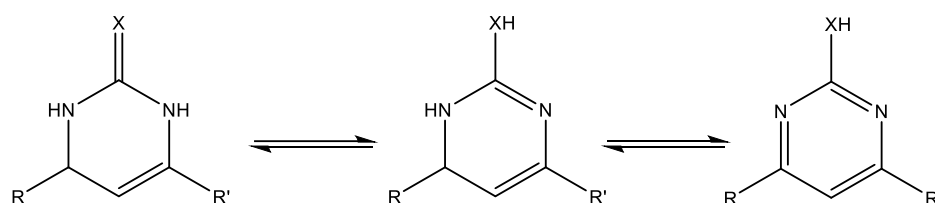


Figure 3.20 NMR spectrum of **14**

The spectra of **13** and **14** appear very similar to each other with the majority of peaks typical of those found in cardamonin, so both spectra would be analysed simultaneously. The absence of doublets possessing large coupling constants corresponding to H-7 and H-8, at around 7 ppm, indicates that one of these protons no longer exists and cyclisation was thus successful. Moreover, the pair of doublets at around 5.5 ppm have been attributed to the methine protons (**8**, **9**) of the pyrimidine group which further proves the formation of the intended pyrimidone/pyrimidthione derivative. Pyrimidone and pyrimidthiones are known to

exhibit tautomerism similar to that shown in **Figure 3.21** and presence of a pair of doublets at about 5.5 ppm suggests that the methine proton (**9**) of the pyrimidine ring is coupled with an adjacent proton (-CH-CH-NH); combining this spectral data with that obtained from IR analysis enabled the correct determination of the structure along with the tautomeric state of the synthetic compounds.



Pyrimidones: X = O ; Pyrimidithione: X = S

Figure 3.21 Tautomerism in pyrimidones/pyrimidthiones

Compound 15

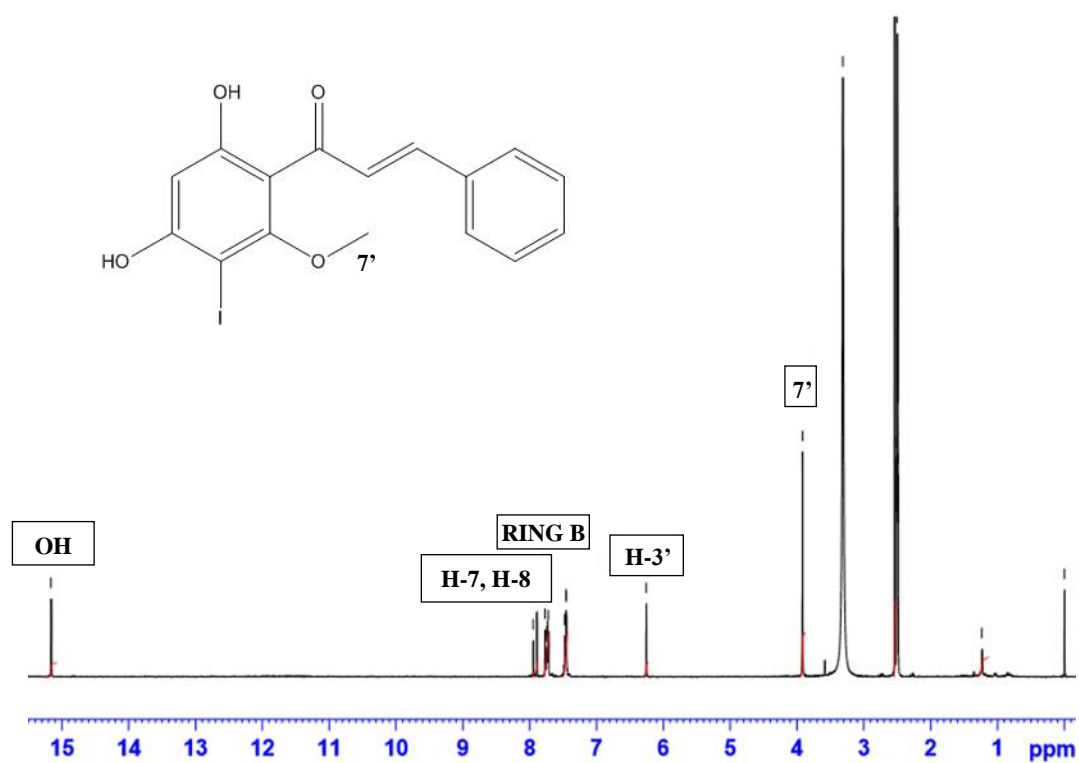


Figure 3.22 NMR spectrum of **15**

Compound 16

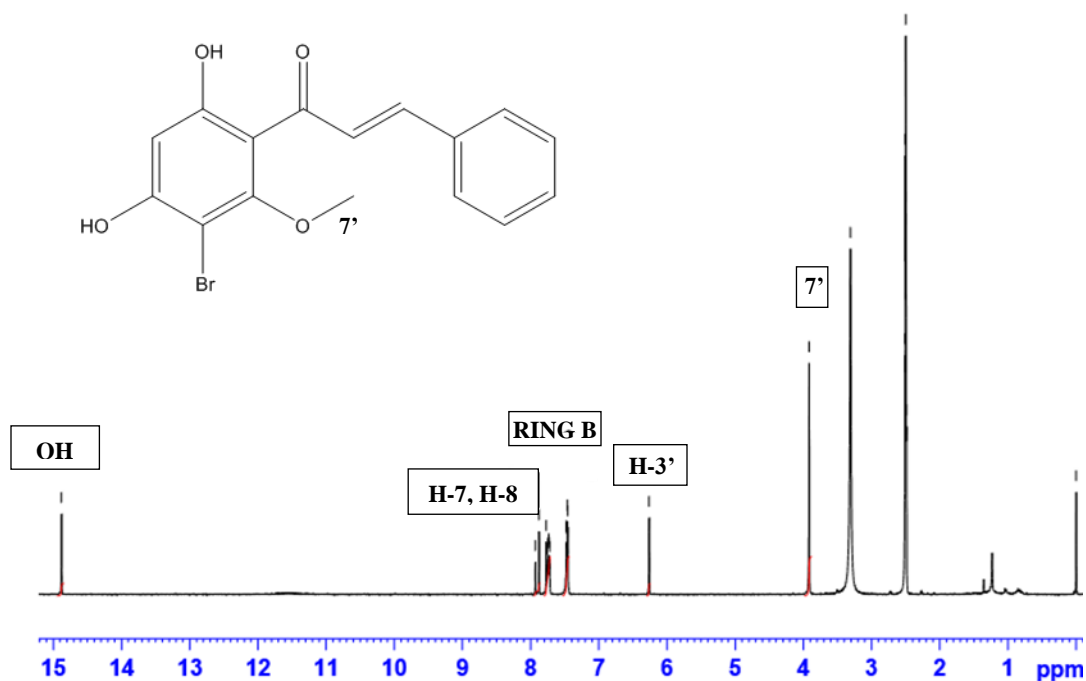


Figure 3.23 NMR spectrum of **16**

The spectra for **15** and **16** are very similar to that of the parent compound cardamonin. However, the presence of a singlet in both spectra at 6.26 ppm for H-3' rather than a doublet, and the absence of a peak for H-5' at around 5.9 ppm shows that aromatic halogenation took place at the *meta* position of ring A.

Compound 17

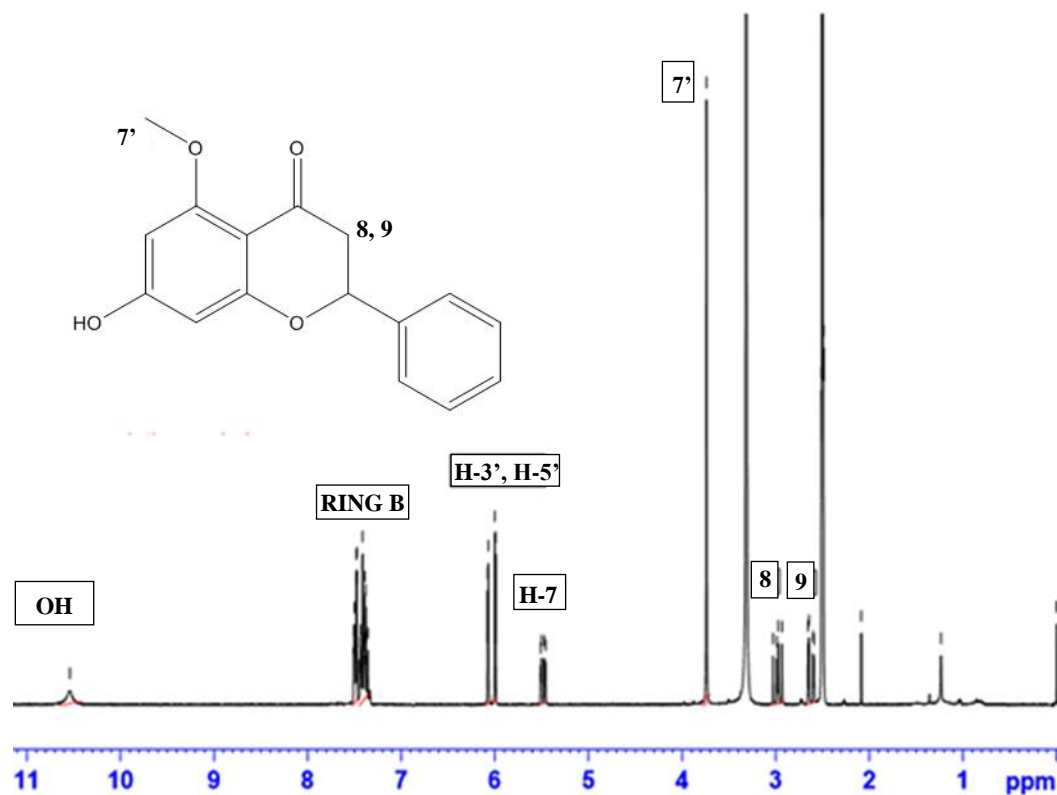


Figure 3.24 NMR spectrum of **17**

The absence of a peak at around 13-14 ppm corresponding to 2'-OH shows that cyclisation into the intended flavanone has occurred. Moreover, the absence of a pair of doublets with large coupling constants for methine protons H-7 and H-8 shows that the double bond is no longer present, this is further supported by the appearance of 3 sets of doublet of doublets peaks attributed to the methylene protons adjacent to the carbonyl group (**8, 9**), and H-7. These sets of doublet of doublets are a result of geminal and vicinal couplings between the adjacent protons. All these peaks prove the formation of the intended product.

Compound 18

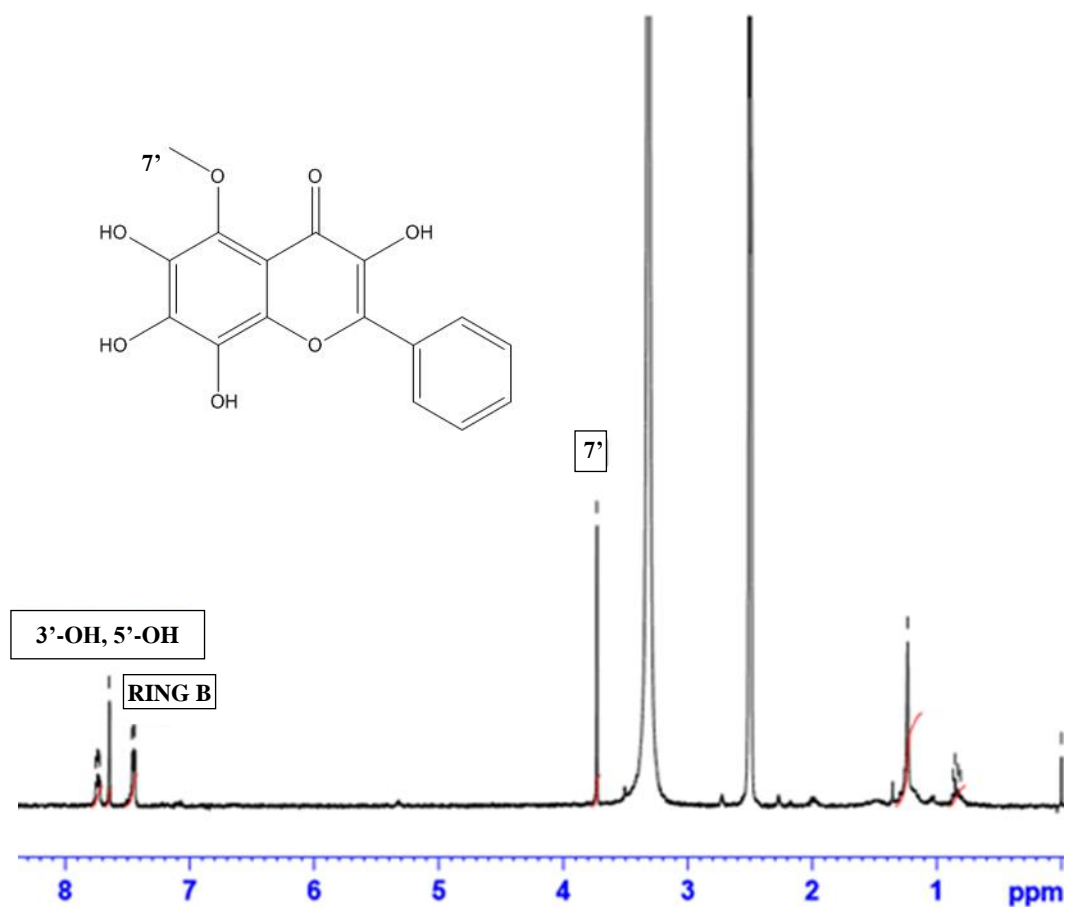


Figure 3.25 NMR spectrum of **18**

The spectrum of flavonol showed the absence of peaks corresponding to the methine protons of cardamonin which proves the formation of the flavonol. However, there was also an absence of a pair of doublets corresponding to H-3' and H-5' which meant that hydroxylation at these positions of ring A has also taken place. This is further supported by the singlet peak at 7.65 ppm which integrated to 2 protons corresponding to 3' and 5'-OH, and this singlet peak is due to these hydroxyl groups being in a similar chemical environment, each having an ether and a hydroxyl group

adjacent to them. Finally, the disappearance of a peak at around 13-14 ppm corresponding to 2'-OH shows that cyclisation has taken place as predicted.

Compound 19

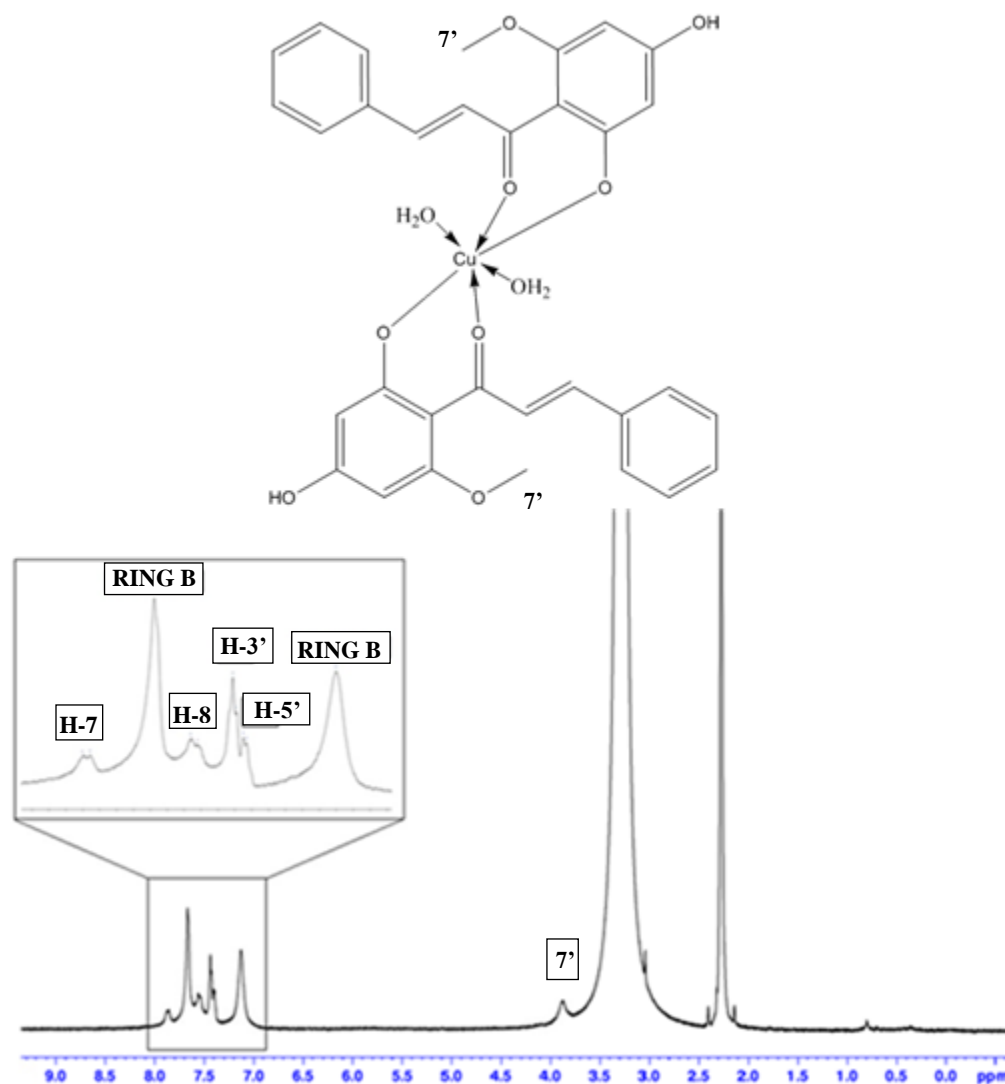


Figure 3.26 NMR spectrum of **19**

NMR analysis for **19** resulted in a spectrum with low-intensity broad peaks and this was due to the paramagnetic nature of copper (II) ion (**Figure 3.26**). These broad peaks of **19** are actually an indication for formation of the desired copper complex

(**19**). The spectrum showed no peak for 2'-OH suggesting the involvement of the group's deprotonated form in complexation. Moreover, the peaks assigned to the aromatic protons of ring A (H-3' and H-5') were found to be shifted downfield after complexation, to 7.45 ppm and 7.42 ppm, respectively. This downfield shift observed was attributed to the electron withdrawing mesomeric effect exerted by Cu²⁺ after bonding with cardamonin's deprotonated 2'-OH. These characteristic peaks further prove the formation of **19** and provide further information about its structure.

- **Further supporting characterisation of 19**

It was intended to elucidate the structure of **19** *via* X-ray crystallography, however, that was not possible. This was due to the inability to grow crystals of the metal complex despite attempts to grow them using a variety of solvents, such as methanol, isopropanol and DMSO. Moreover, more than one method was investigated for growing the crystals, such as the slow evaporation method and crystallisation by the cooling down of a heated saturated solution of **19**. It is also crucial to note that small vials and NMR tubes were used in order to initiate crystallisation. Interestingly, a survey of the available literature showed that chalcone metal complexes mostly lacked structure elucidation *via* X-ray crystallography, unless the chalcone was initially derivatised. Therefore, the metal complex was analysed *via* HRMS, elemental analysis, TGA and UV-Vis spectral analysis, in addition to the previously discussed IR and NMR analyses.

HRMS spectrum showed a very clear and high-intensity peak at 624.0783 (**Figure 3.27**) which was attributed to the sodium adduct of compound **19** at a ligand to metal stoichiometric ratio of 2:1. This experimental m/z value (624.0783) closely matches the theoretical/calculated value for a sodium adduct of **19** at a ligand to metal stoichiometric ratio of 2:1 (624.0829). The deduced structure of **19** from HRMS data was further confirmed *via* elemental analysis whereby the obtained percentage of carbon and hydrogen [%C (57.02), %H (4.47)] closely matches the theoretical/calculated value of **19** with a ligand to metal stoichiometric ratio of 2:1 [%C (57.01), %H (5.08)]. However, the experimental value obtained from elemental analysis matches the theoretical value only when it is assumed that there would be 4 water molecules in the structure of **19**, otherwise both values actually do not match. To summarise, HRMS and elemental analysis confirmed that **19** exists at a ligand to metal stoichiometric ratio of 2:1, however, it was deduced from elemental analysis data that there should be water molecules. The reason that the presence of these water molecules was not detected by HRMS might have been due to the extreme conditions, such as very high temperatures, used in the process which resulted in the loss of those water molecules. Therefore, to further confirm the presence of these water molecules and investigate their nature a thermogravimetric analysis (TGA) was conducted on compound **19**. The TGA curve (**Figure 3.28**) showed a 4.1% loss in weight between 30 - 200 °C corresponding to a loss of 2 moles of lattice water, while a 5.6% weight loss was observed between 206-262 °C attributed to the loss of 2 moles of coordinated water. Therefore, it was concluded that the general formula for **19** would be $[\text{Cu}(\text{C}_{16}\text{H}_{13}\text{O}_4)_2(\text{H}_2\text{O})_2] \cdot 2\text{H}_2\text{O}$.

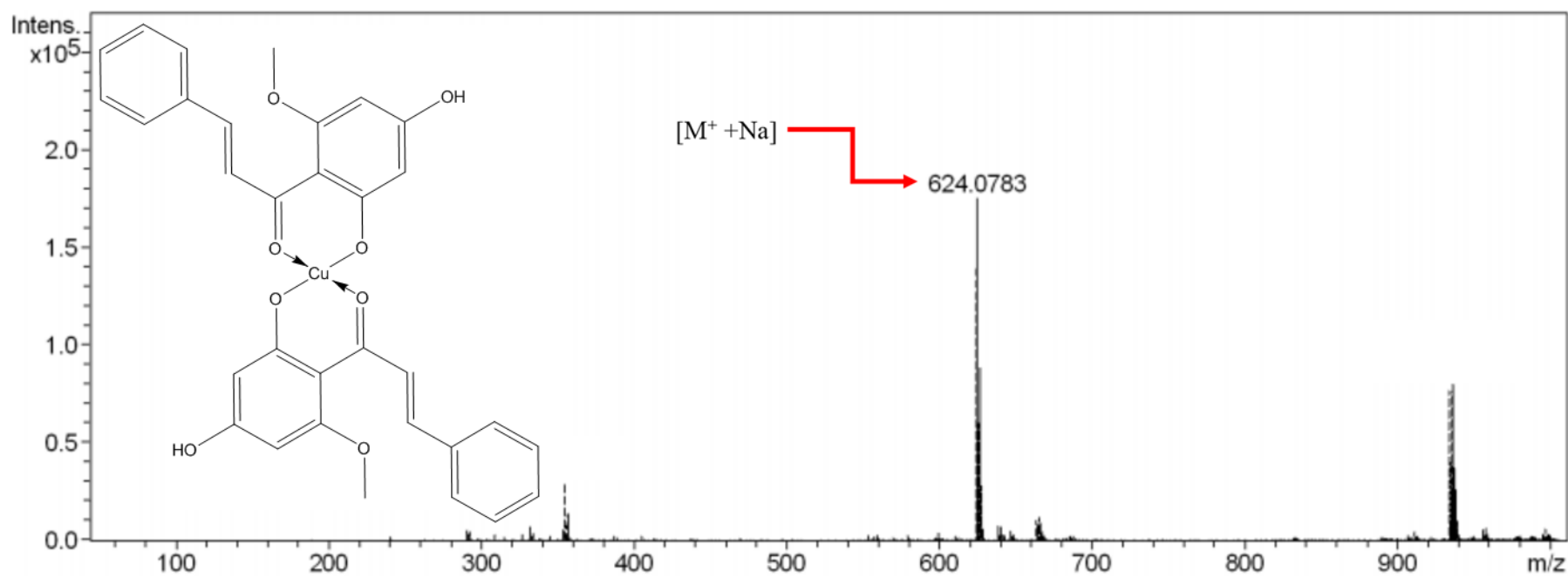


Figure 3.27 HRMS spectrum of **19**

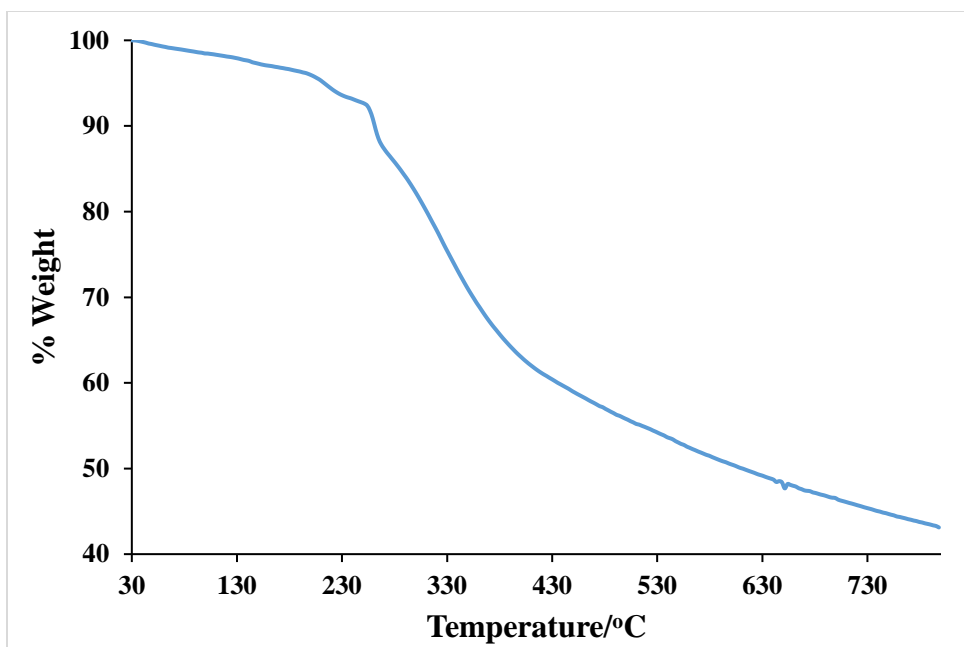


Figure 3.28 TGA curve of **19**

Cardamonin and compound **19** were analysed *via* UV-Vis spectroscopy in order to compare and prove the formation of the metal complex. The UV-Vis spectrum for **19** (**Figure 3.29**) showed bands at 291 nm, 352 nm and 432 nm which were attributed to $n \rightarrow \pi^*$ and $\pi \rightarrow \pi^*$ transitions involving the molecular orbitals of (C=O) and benzene rings. The slight shift observed in the absorption band of **19** at 432 nm relative to that of cardamonin is most likely resulting from the coordination of cardamonin to the metal ion causing an increase in the delocalisation of the compound's electron system which consequently led to a change in the transitions' energies (Kalanithi *et al.* 2012). The formation of **19** was mostly proven by the bands at 506 nm and 600 nm. The band observed at 506 nm has been assigned to ligand-to-metal charge transfer (LMCT), while the broad band at 600 nm was attributed to d-d transitions and indicates an octahedral arrangement (Raman *et al.* 2004).

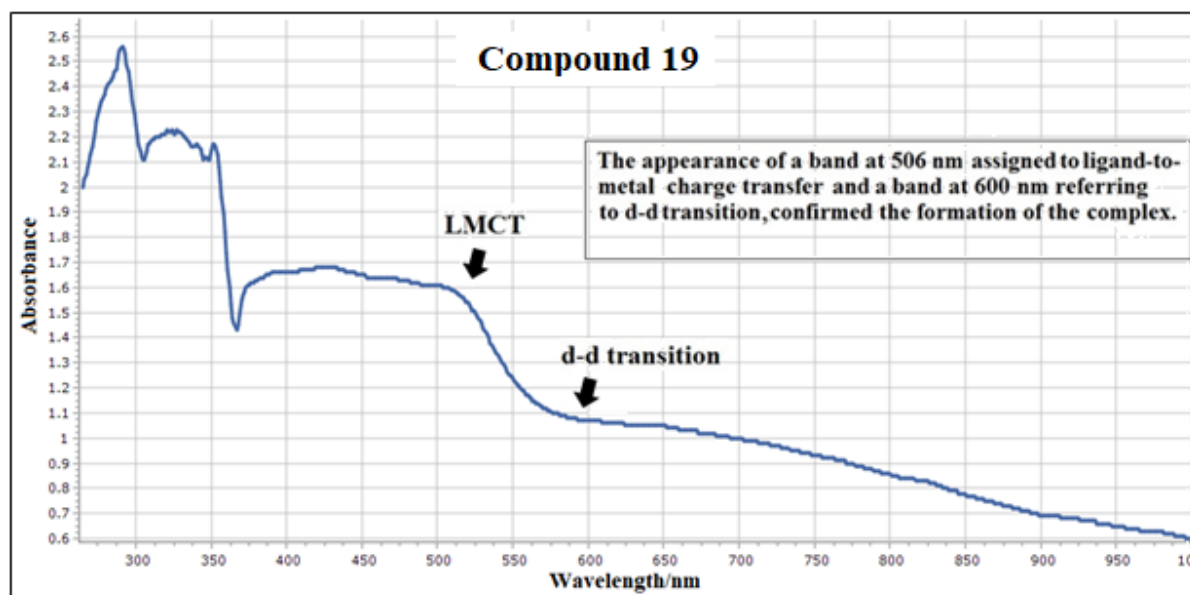
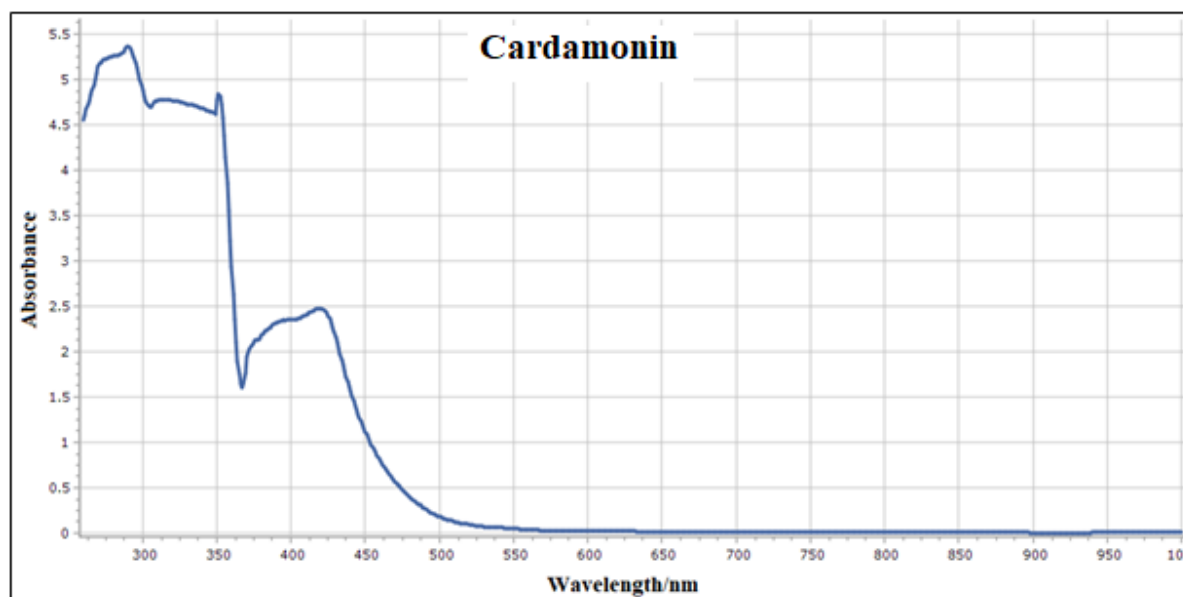


Figure 3.29 UV-Vis spectrum of cardamonin and 19

3.2 Biological Studies

3.2.1 Cell Viability and Structure-activity Relationship Studies

Table 3.1 IC₅₀ values of cardamonin and its analogues against HK1 and A549

cells. Active analogues have been shaded.

Compound	IC ₅₀ (μM) ^a	
	A549	HK1
Cardamonin	67.0 ± 7.0	22.6 ± 5.4
(1)	>100	>100
(2)	35.1 ± 9.9	4.95 ± 0.9
(3)	>100	>100
(4)	27.3 ± 4.3	21.7 ± 5.9
(5)	>100	89.5 ± 7.1
(6)	37.6 ± 3.1	29.4 ± 1.1
(7)	>100	>100
(8)	>100	>100
(9)	>100	>100
(10)	23.9 ± 5.7	36.6 ± 14.2
(11)	63.8 ± 6.5	46.8 ± 10.3
(12)	>100	>100
(13)	29.9 ± 1.3	66.5 ± 3.3
(14)	>100	>100
(15)	36.1 ± 1.3	49.7 ± 3.6
(16)	>100	>100
(17)	>100	>100
(18)	83.9 ± 16.2	60.4 ± 3.7
(19)	13.2 ± 4.8	0.7 ± 0.3

^a IC₅₀ values are reported as the mean (IC₅₀ ± SEM) of duplicates of three independent experiments.

Results of the bioassay were summarised in **Table 3.1**, and analogues demonstrating activities higher than cardamonin were regarded as active. The active analogues were shaded in grey colour in **Table 3.1**. The results showed that cardamonin and its analogues exerted higher activity against HK1 than A549 cells with the exception of **10**, **13** and **15**. It is possible that compounds **10**, **13** and **15** are actually acting in a different manner than the other analogues in each cell-line. So it is possible that they are acting on different receptors or possessing completely different modes of action from the other analogues, which might explain the reason behind these three compounds not following the general trend observed with the other analogues. It has been also observed that the active analogues showed greater enhancement, relative to cardamonin, when tested against A549 than HK1 cells. Finally, it can be deduced from the results that compound **19** possessed the highest cytotoxic activity followed by **2**.

It is also crucial to note that the IC₅₀ values obtained for cardamonin against A549 cells are actually different from the results obtained in previous studies in the literature (**Table 2.2**) and this is due to many factors. One of the main factors is that this study used MTS assay for assessing cell viability, while these previous studies used MTT as shown in **Table 2.2**. Moreover, the duration of treatment for A549 cells was different whereby the cells were treated for 72 h in this study, while a 48 h treatment duration was used in the previous studies.

SAR analysis revealed that substituting cardamonin's hydroxyl groups with non-polar groups resulted in loss of cytotoxic activity, while substitution with more polar groups enhanced activity. This was deduced primarily by comparing the

bioactivities of **1**, **2**, **3** and **4**, whereby there was a loss in activity when the hydroxyl groups were methylated and benzylated, but acetylation of the same groups and allylation of 4'-OH resulted in activity enhancement. However, it seems that loss of activity upon *O*-benzylation might not only be due to polarity alone, as activity was also lost when the hydroxyl groups were substituted by the more polar 4-fluorobenzoyl group. Therefore, it has been suggested that steric hindrance could be the main reason behind the loss of activity for **3** and **5**, whereby the bulky benzene ring at the *ortho* position of ring A might be preventing any potential interactions between the ketone group and the receptor. This steric hindrance effect does not seem to exist when only benzylation of 4'-OH occurred as in analogue **6**, which further shows that bulky substituents might negatively affect bioactivity if substitution occurred at 2'-OH specifically. Thus, it can be concluded that avoiding bulky substituents at cardamonin's 2'-OH and substituting the hydroxyl groups with more polar fragments is expected to enhance bioactivity.

There was a loss in the cytotoxic activity of **7** and **17** which lacked the alkene double bond; these results show that the alkene double bond is crucial for bioactivity. Importance of the ketone group to bioactivity was investigated by Schiff base formation and cyclisation reactions at the group. Results have shown that Schiff bases of cardamonin, **8** and **9**, had no bioactivity while only the SBDTC-derived analogue, **10**, had high activity but it was not considered due to its low purity. Furthermore, **11**, **12** and **14** were generally found to have no activity indicating that cyclisation at the ketone group also results in loss of activity. However, **13** was an exception, whereby high activity was demonstrated against A549 cells despite

chemical modification at cardamonin's ketone group, and this activity was attributed to the formation of a pyrimidinone moiety as a result of the tautomerisation (**Figure 3.21**) of **13** at its target receptor; thus the analogue would still possess a ketone group in this case resulting in enhanced activity. On the other hand, the clearly observed loss in activity of **13** against HK1 cells might be due to the presence of the compound in its enol form in this case. Therefore, it can be generally concluded that cardamonin's alkene double bond and its ketone group are crucial, as their absence led to a loss in activity.

Halogenation of cardamonin resulted in compounds **15** and **16**. The good bioactivity of **15** showed that iodination of cardamonin enhanced bioactivity, however, bromination resulted in loss of activity as can be seen in **16**. **18** demonstrated very weak bioactivity, but it has been suggested that the compound could act as an antioxidant for cancer prevention due to its high phenolic content.

Copper complex of cardamonin (**19**) showed highly potent activity and was the most active analogue with an interesting IC_{50} of 13.2 μ M and 0.7 μ M against A549 and HK1 cells respectively, demonstrating an enhancement in activity of 5 and 32 fold relative to cardamonin, respectively. These results indicate that complexation of cardamonin to metal ions enhances activity.

Results of the SAR study have been summarised in **Figure 3.30**.

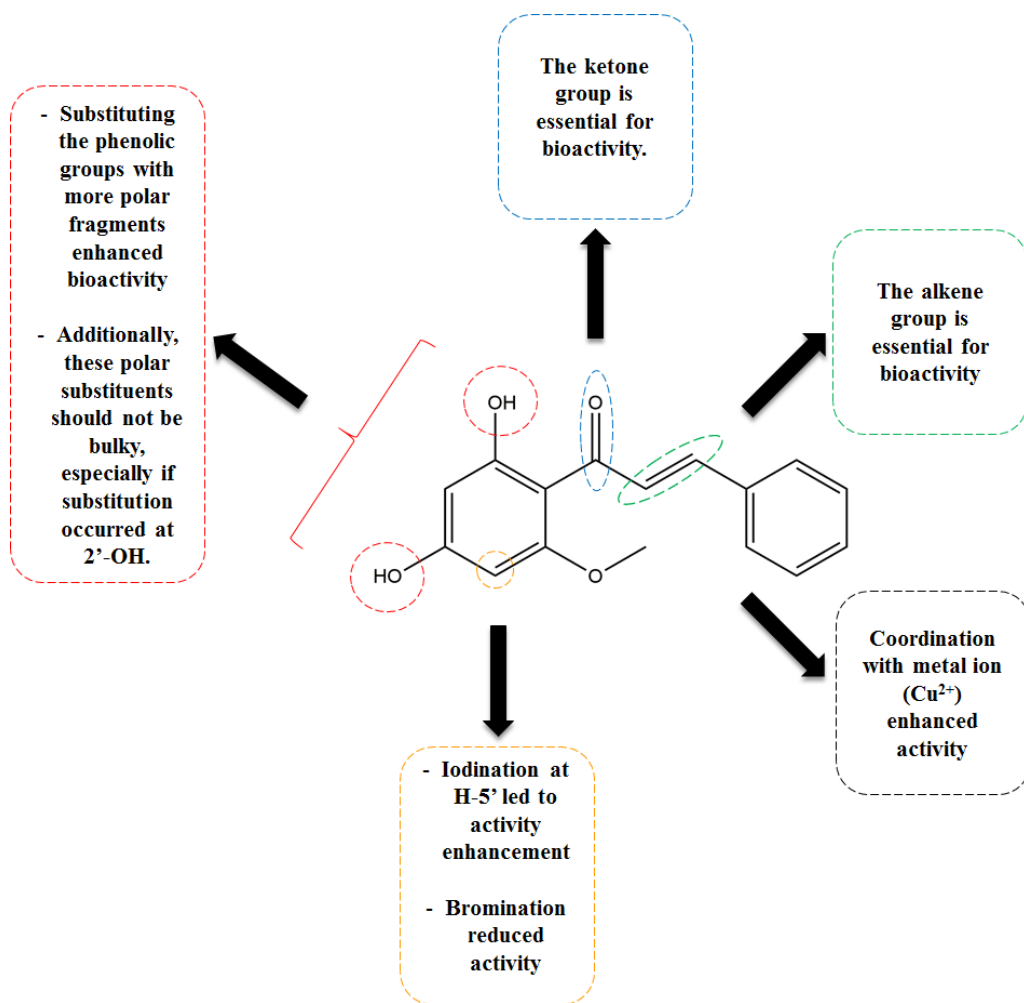


Figure 3.30 A summary of the anticancer SAR study results of cardamonin

3.2.2 Active Analogues Showed More Selectivity Towards the Cancer Cells

In order to determine the selectivity of the active analogues to cancer cells, the bioactive analogues were further screened against human normal lung fibroblast cells (MRC-5) (**Table 3.2**). The results showed that almost all active analogues showed greater selectivity towards the cancer cell lines and demonstrated lower cytotoxicity towards normal MRC-5 cells, such as the highly active compound **19**, which was almost 29 times more selective towards HK1 cells. Such data further reflected the potential of **19** as an anticancer agent. Therefore, since **19** was the most active compound with high selectivity to cancer cells, it was decided to further investigate its bioactivity and mode of action; the following experiments will be addressing that.

Table 3.2 Cytotoxic activity of the bioactive analogues against MRC-5 cells

Compound	IC ₅₀ (μM) ^a (MRC-5)	Selectivity index (SI) ^b	
		A549	HK1
(2)	17.1 ± 4.2	0.5	3.5
(4)	39.9 ± 7.8	1.5	1.8
(6)	>100	NA	NA
(13)	>100	NA	NA
(15)	>100	NA	NA
(19)	20.6 ± 3.3	1.6	28.6

^a IC₅₀ values are reported as the mean (IC₅₀ ± SEM) of duplicates of three independent experiments.

^b SI = (IC₅₀ of MRC-5)/(IC₅₀ of A549 “or” HK1).

3.2.3 Compound 19 Inhibited the Migration of A549 and HK1 Cells

A wound healing scratch assay has been implemented in order to investigate the effect of **19** on the migration of A549 and HK1 cells and compare it to that of cardamonin (**Figure 3.31** and **Figure 3.32**). The cells were treated either with solvent alone to act as the control, or with compound **19**.

In the present study, migration assay was performed to investigate the migration inhibitory effect of compound **19** relative to cardamonin after a treatment duration of 24 h and 48 h. It has been decided to determine the treatment concentration for the assay by using IC₅₀. Therefore, the IC₅₀ of **19** at 24 h was used as a reference to determine the concentration to be used for this migration assay, and this IC₅₀ was calculated from the cell viability data of **19** at 24 h. The cell viability data of **19** and cardamonin at 24 h have been placed in the **Appendix** section (**Figure 8.39** and **Figure 8.40**). In the case of A549, the IC₅₀ of **19** at 24 h was 54.6 μ M (**Figure 8.40**), but at this relatively high concentration there was risk of cytotoxicity and cell death which would lead to an incorrect interpretation of the assay results. Therefore, 25 μ M (~0.5 x IC₅₀ of **19**) was used for the assay. Cardamonin was also investigated in order to compare the inhibitory effect of **19** relative to cardamonin, and this necessitated that cardamonin also gets investigated at the same concentration of **19**. This would enable a more accurate and fair comparison between the inhibitory effects of **19** and cardamonin. As for HK1, the IC₅₀ of **19** at 24 h was 12 μ M (**Figure 8.40**) which means that cardamonin would also have to be investigated at 12 μ M. However, cardamonin's IC₅₀ at 24 h is (>100 μ M) (**Figure 8.39**) which means that a concentration of 12 μ M would be very low to show any activity. To solve this

issue, **19** and cardamonin were investigated against HK1 cells at 25 μM ($\sim 2 \times \text{IC}_{50}$ of **19**). Therefore, a concentration of 25 μM was decided to be used for compound **19** and cardamonin against A549 and HK1 cells.

Compared with the control treatment, **19** has significantly reduced the migration of A549 and HK1 cells by around 2-fold and >3 -fold, respectively. Furthermore, the inhibitory effect of **19** on the migration of both cell lines was generally 2-3 times stronger than that of cardamonin, which further highlights the enhanced bioactivity possessed by **19**. Cell death did not occur in this experiment as the investigated cells were still attached to the 6-well plate, otherwise the cells would have detached. Moreover, no visible change in cell morphology was observed which further indicates that the cells did not die throughout the experiment. The potential of cancer cells to metastasise depends on several properties such as their migration ability, so these positive results demonstrate the potential ability of **19** in preventing cancer metastasis in patients, such as those suffering from lung and breast cancer (Doan *et al.* 2016; Nandakumar *et al.* 2017).

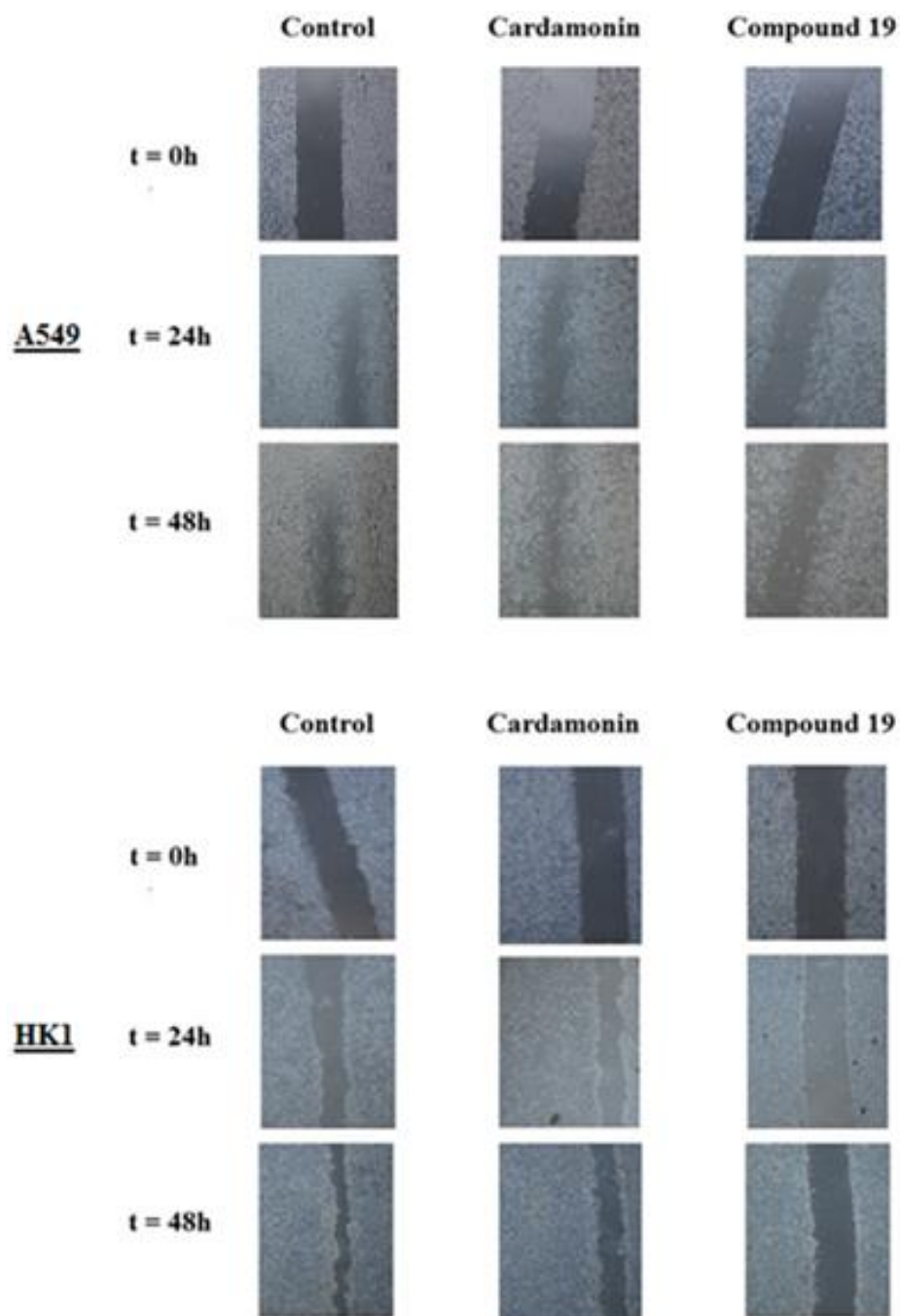


Figure 3.31 Compound **19** inhibited the migration of A549 and HK1 cells. Migration assay was conducted in a 6-well plate by forming a “wound” across a layer of cells followed by treatment with either solvent control, 25 μ M cardamonin or 25 μ M compound **19**. The figure shows representative wound closure images from three experiments.

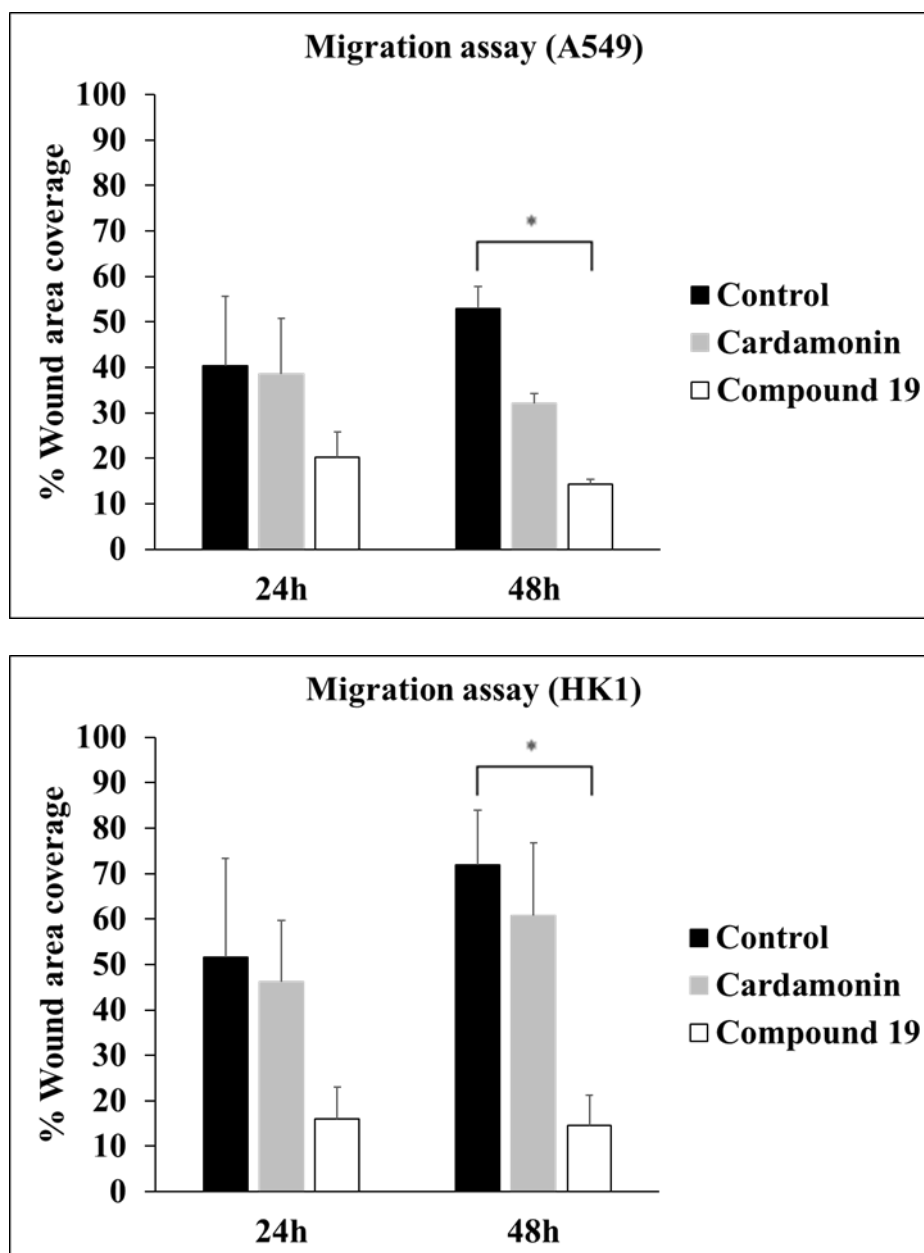


Figure 3.32 Quantification of cell migration assay results for A549 and HK1 cells was performed using the software ImageJ. Cell migration was calculated and expressed as the percentage of “wound” area covered by the cells to the initial cell-free “wound” area. The assay was repeated three times, and bars and error bars refer to mean \pm SEM. * $p < 0.05$, analysed using a two-tailed unpaired t-test.

3.2.4 Induction of G2/M-phase Arrest by Compound 19 in A549 and HK1 Cells

Cell-cycle is the series of events that occur in order to enable cell division and replication, and consists of four distinct phases: G1-phase which involves the preparation of material and energy for replication, S-phase (synthesis) where DNA replication occurs, G2-phase (interphase) where the new replicated DNA is checked and errors are repaired, and M-phase (mitosis) which involves the nuclear and cytoplasmic division of the cell. Many cytotoxic agents work by stopping this cell-cycle at a certain phase which eventually affects the cell's division (Fares *et al.* 2014).

Therefore, a cell-cycle analysis was conducted in order to investigate if compound **19** results in cell death *via* disrupting or arresting the cell-cycle in A549 and HK1 cells. A549 and HK1 cells were treated either with solvent alone to act as the control, or with compound **19** at IC₅₀ concentrations. Cells treated with **19** for 24 h showed a profound increase in the fraction of cells in the G2/M-phase (37.38% compared to 10.52% in the untreated cells for A549 cells; 39.15% compared to 15.48% in the untreated cells for HK1 cells). This was accompanied by a decrease in the number of cells in the G1-phase for both cell lines and S-phase for A549 only (**Figure 3.33**). Therefore, this indicated that **19** induced G2/M-phase cell-cycle arrest in both A549 and HK1 cells.

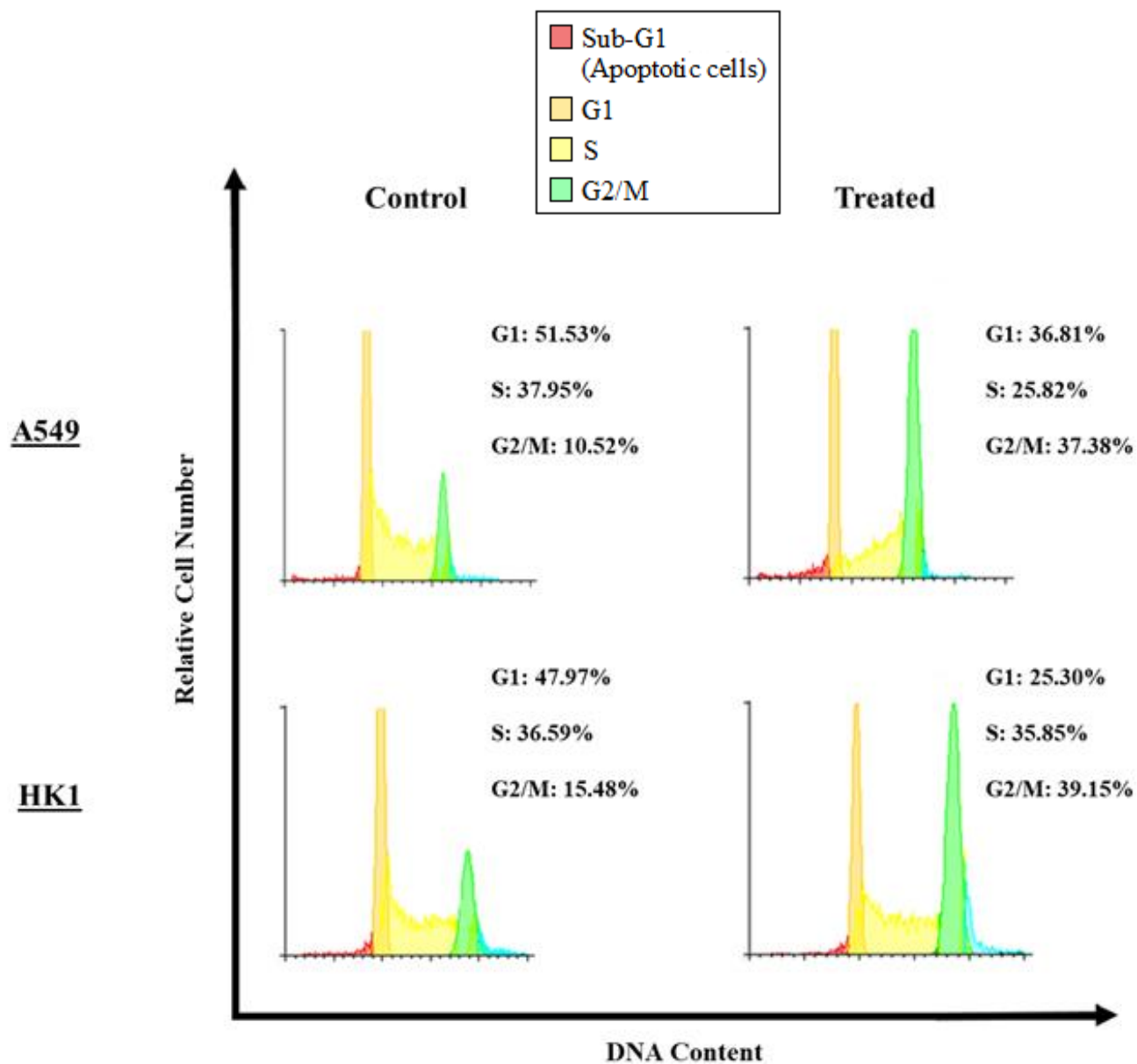


Figure 3.33 Flow cytometric analysis of cell-cycle parameters following 24 h of treatment with either solvent control or **19** at IC₅₀ concentrations in A549 and HK1 cells. Data were gated to exclude apoptotic cells from calculations of the fraction of cells in G1, S and G2/M phases. Results are representative of two independent experiments for each cell-line.

3.2.5 Compound 19 causes DNA damage in A549 and HK1 cells

Cell-cycle arrest at G2/M phase is a common cellular response for agents that cause DNA damage (Qiu *et al.* 2013), and since **19** induced a G2/M-phase cell cycle arrest, we reasoned that it might be able to cause DNA damage. DNA damage that results in the formation of double-strand breaks (DSB) is always followed by phosphorylation of the histone H2AX to γ -H2AX (Kuo and Yang 2008). Therefore, γ -H2AX is considered a DNA double-strand breaks (DSB) marker which can be quantified in order to assess DNA damage.

The induction of DNA damage by **19** was assessed by detecting the number of cells expressing γ -H2AX after treatment. A549 and HK1 cells were treated either with solvent alone to act as the control, or with compound **19** at IC₅₀ concentrations. It was decided to treat the cells with **19** at IC₅₀ concentrations because this assay is based on the cell-cycle data, whereby the G2/M cycle arrest caused by **19** was the reason behind suspecting that DNA damage also took place in the cells. Therefore, it was decided to use the same treatment concentration of **19** for cell-cycle analysis and DNA damage assay. Flow cytometry was used to detect γ -H2AX formation. As demonstrated in **Figure 3.34**, **19** significantly increased the formation of γ -H2AX in A549 and HK1 cells by 7- and 5-fold relative to the control, respectively. This indicated that the activity of **19** involved the induction of DNA damage in both cell lines as has been predicted.

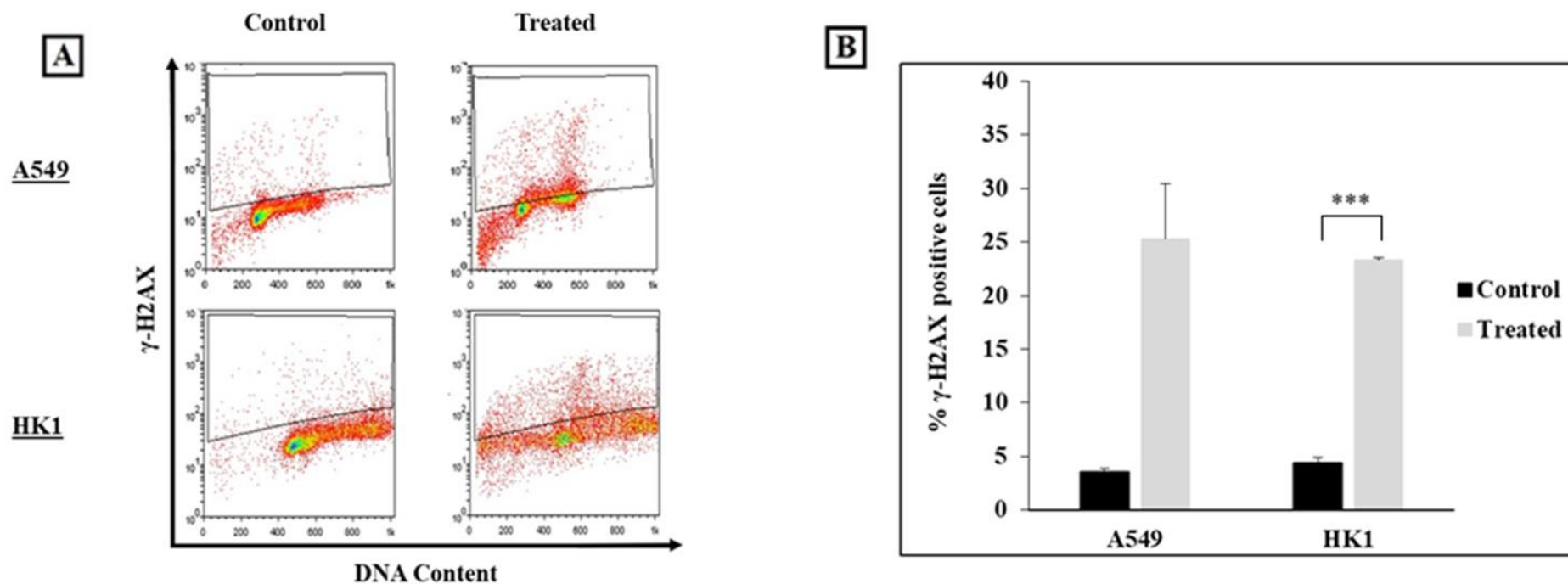


Figure 3.34 Flow cytometric detection of γ -H2AX formation following 24 h of treatment with either solvent control or **19** at IC₅₀ concentrations in A549 and HK1 cells. **(A)** Representative dot-plots illustrating γ -H2AX abundance versus total cellular DNA content of each cell. **(B)** Bar chart summarising results of the flow cytometry analysis. Results represent the mean \pm SEM of 2 independent experiments. ***p<0.001, analysed using a two-tailed unpaired t-test.

3.2.6 Induction of Apoptosis by Compound 19 via Activation of Caspase-3/7

The activation of caspases is considered to be the hallmark of apoptosis, especially caspase-3 which is considered to be the most important of the executioner caspases. It is activated by any of the initiator caspases which results in direct activation of enzymes responsible for DNA fragmentation (Nomura *et al.* 2008). Therefore, the induction of apoptosis by the most active compound, **19**, in A549 and HK1 cells was investigated *via* a Caspase-Glo 3/7 Assay. The assay uses a reagent which emits luminescence or glows after being cleaved by caspase-3/7. This luminescence can be then read by a luminometer.

This assay is very sensitive and is affected by the treatment concentration of the compound, duration of incubation of the cells after treatment and even duration of incubation of the cells after adding the Caspase-Glo reagent (Piazza *et al.* 2009; Ramanan *et al.* 2011; Lee *et al.* 2015). These factors affect the assay because of a main issue, which is the fact that the time of caspase activation is unknown, so it is possible that the caspase was actually activated but because the reading was taken later, the luminescent signal would have diminished by that time resulting in a low reading. However, as can be seen from the studies cited earlier, if a certain compound activates a certain caspase, a signal would usually always be detected even if it is small, and optimising the treatment concentration would just strengthen the signal.

In the present experiment, several attempts were made in order to determine the concentration of compound **19** and duration of treatment that would result in detection of the strongest luminescent signal. The amount of Caspase-Glo reagent

was very limited so that also limited the number of attempts that could be performed. Results of these attempts have been summarised in **Table 8.1** and **Table 8.2** in the **Appendix** section. Based on these attempts, it has been deduced that a concentration of 10 μ M for compound **19** produces the strongest luminescence signal. The optimum duration of treatment and incubation were also determined and outlined in **Section 6.8**.

The experiment was finally performed whereby A549 and HK1 cells were treated either with solvent alone to act as the control, or with compound **19** (10 μ M). This was followed by the addition of Caspase-Glo reagent to the control and treatment groups. Results of the assay showed that A549 and HK1 cells treated with **19** resulted in the activation of caspase-3 and -7 within 12 h of treatment by about 1.4- and 2-fold, respectively (**Figure 3.35**). This suggested that **19** induced cell death through caspase-dependent apoptosis in both cell lines. It is also interesting to note that caspase-3/7 was more activated in HK1 cells than A549 cells, which might explain the results of the MTS assay which showed that **19** exerted higher cytotoxic activity against HK1 cells than it did against A549 cells.

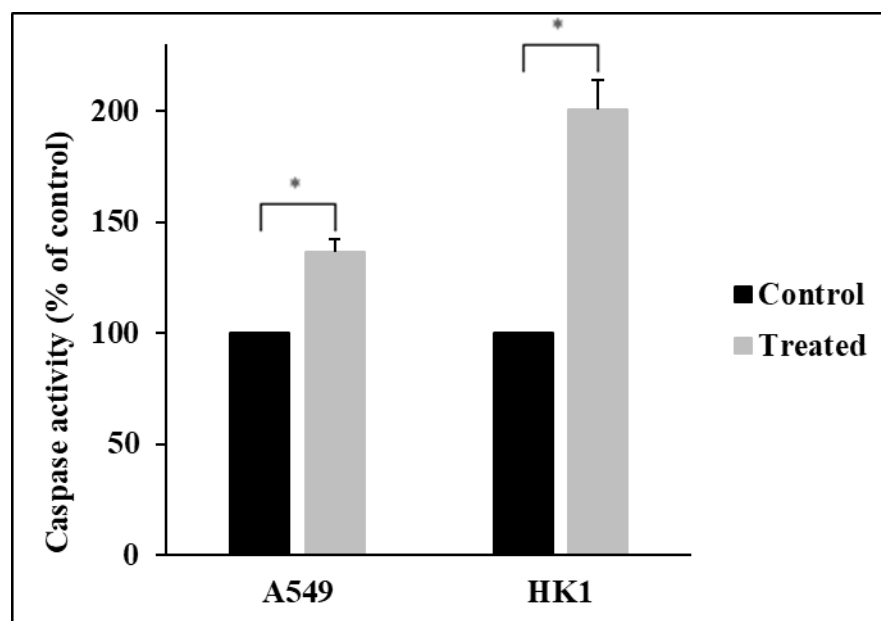


Figure 3.35 Caspase-3/7 activity of A549 cells and HK1 cells, treated with solvent control or **19** at about 10 μ M for 12 h. The experiment was performed in duplicate for each cell line and bars and error bars refer to mean \pm SEM. * $p < 0.05$, analysed using a two-tailed unpaired t-test.

3.2.7 Compound 19 Activated Caspase-9 Leading to Apoptosis via the Mitochondrial Pathway

Apoptosis in cells can be activated *via* extrinsic (death receptor) and intrinsic (mitochondrial) apoptotic pathways, and initiator caspases-8 and 9 play a significant role in these pathways (**Figure 3.36**). The extrinsic pathway involves the binding of ligands to death receptors, such as the binding of tumor necrosis factor-related apoptosis-inducing ligand (TRAIL) to its death receptors DR4 and DR5, resulting in the activation of caspase-8 which in turn activates caspase-3/7. On the other hand, the intrinsic pathway is initially activated *via* a range of stimuli such as DNA damage, oxidative stress and ischemia. Furthermore, intrinsic pathway induction is also affected by members of a group of proteins bound to the outer membrane of the mitochondria called the bcl family group. The bcl group consists of pro-apoptotic proteins (bax and bad) in addition to anti-apoptotic proteins (bcl-2 and bcl-XL), and coordination between these protein types affects the induction of apoptosis. Therefore, intrinsic apoptosis occurs when pro-apoptotic signalling prevails and this results in mitochondrial membrane perturbation followed by release of cytochrome C. Cytochrome C then forms a complex with apoptotic protease activating factor (APAF-1) to form a complex that later activates caspase-9. Caspase-9 later activates caspase-3/7 resulting in apoptosis (Loreto *et al.* 2014; Ichim and Tait 2016).

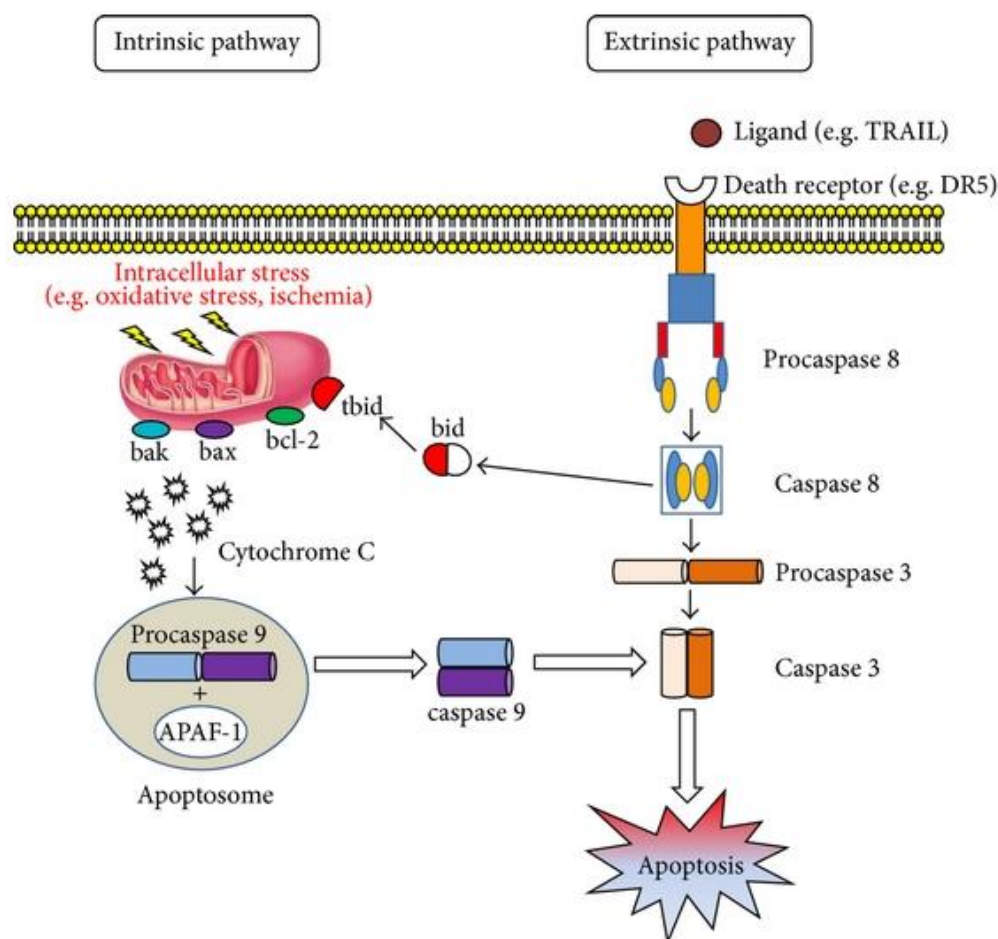


Figure 3.36 Intrinsic apoptosis and Extrinsic apoptosis signalling pathways (adapted from: Loreto *et al.* 2014)

Therefore, Caspase-Glo 8 and 9 assays were conducted in order to investigate the apoptotic pathway that is induced by the most active compound, **19**. The assays work in a similar manner to the Caspase-Glo 3/7.

The way to determine the concentration of **19** that should be used in the assay is the same as the one for Caspase-Glo 3/7. However, the amount of Caspase-Glo 8 and Caspase-Glo 9 was limited and it was not possible to run several attempts in order to optimise the conditions that would result in the emittance of the strongest luminescence signal. Therefore, it was decided to use the same conditions that were

used with Caspase-Glo 3/7. However, the treatment time was reduced to 6 h, because caspase-8 and 9 are initiator caspases, so it was reasoned that they would be activated at an earlier time-point

A549 and HK1 cells were treated either with solvent alone to act as the control, or with compound **19** (10 μ M). This was followed by the addition of Caspase-Glo 8 reagent to the control and treatment groups in the case of Caspase-8 assay while Caspase-Glo 9 reagent was added to the control and treatment groups in the case of Caspase-9 assay. Results of the assay showed that **19** activated only caspase-9 in A549 and HK1 cell lines within 6 h of treatment (**Figure 3.37**). This indicated that **19** caused apoptosis *via* the intrinsic (mitochondrial) pathway. However, the results also indicated that **19** inhibited caspase-8 which could mean that **19** is actually an inhibitor of caspase-8, but then cell-death occurred *via* a different pathway resulting in the observed increase of caspase-9 activity. This alternative cell-death pathway *via* caspase-9 would have most probably involved a very complex signalling pathway that would need further studies to elucidate (Vandenabeele, Berghe and Festjens 2006; Jeong *et al.* 2011; Li *et al.* 2017).

It can be seen from the data that the detected luminescence signals were not very strong and this is because the experiment was not fully optimised due to the limited amount of Caspase-Glo 8 and 9 reagents. It seems that a different treatment concentration for **19** or a different time-point for signal detection should have been used. However, the fact that there was an increased luminescence signal detected, even if it was not very strong, surely indicates that caspase-9 was activated.

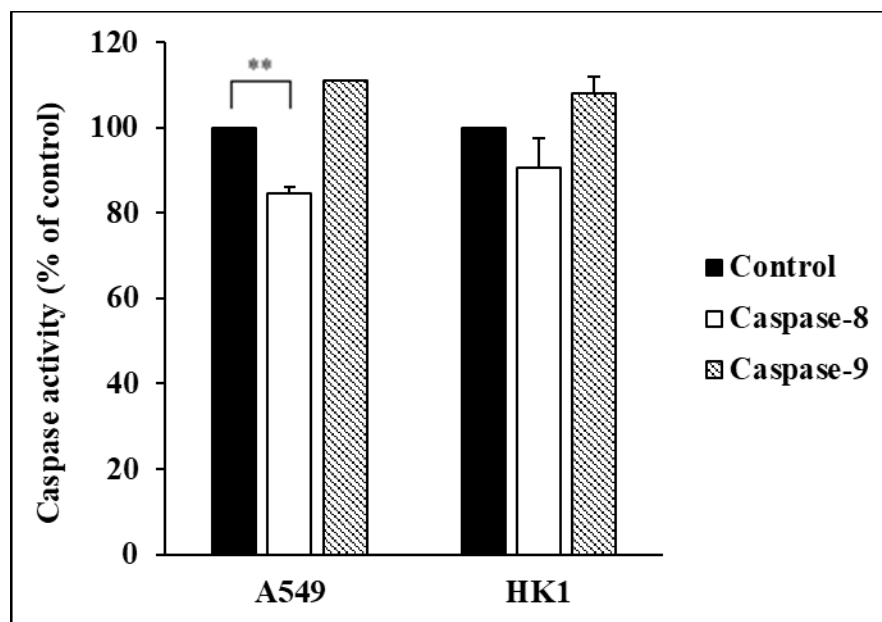


Figure 3.37 Caspase-8 and caspase-9 activity of A549 cells and HK1 cells, treated with either solvent control or **19** at about 10 μ M for 6 h. The experiment was performed in duplicate for each cell line and bars and error bars refer to mean \pm SEM. ** $p < 0.01$, analysed using a two-tailed unpaired t-test.

3.2.8 Compound 19 Inhibited mTOR Expression in A549 and HK1 Cells

The mTOR pathway is usually activated in several types of cancers and regulates cell proliferation, metabolism, apoptosis and metastasis. mTOR pathway is initially activated by ligand stimulation of certain membrane-bound receptors which results in the phosphorylation of phosphatidylinositol 3-kinase (PI3-K) which in turn activates a downstream effector known as Akt. Akt mainly acts as a regulator of cell-survival and is responsible for the eventual phosphorylation of mTOR. mTOR later phosphorylates downstream effectors, S6K1 and 4E-BP1, resulting in eIF4E-mediated protein synthesis and increased cell growth, metabolism and proliferation (Ekman, Wynes and Hirsch 2012; Porta, Paglino and Mosca 2014). This pathway is known as the PI3-K/Akt/mTOR signalling pathway (**Figure 3.38**).

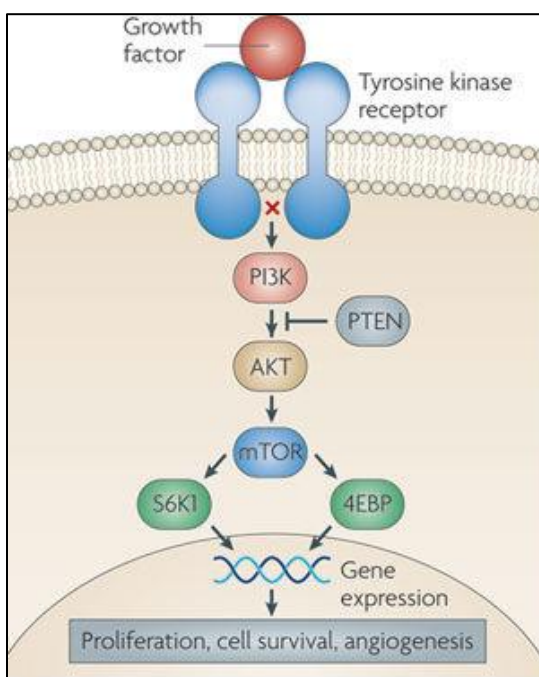


Figure 3.38 PI3-K/Akt/mTOR signalling pathway (*adapted from: Holmes 2011*)

In the case of lung cancer, there is an abnormal activation of the PI3-K/Akt/mTOR pathway and this higher activation contributes to cancer cell growth and maintenance. The role of mTOR in advancing lung cancer has been linked to its effect on a downstream effector known as eIF-4E. Moreover, several negative regulators of the mTOR pathway, such as PTEN, have been found to be mutated in lung cancer, while the upstream regulator of mTOR, Akt, is often highly activated in lung cancer cells (Ekman, Wynes and Hirsch 2012). As for NPC, the abnormal activation of the PI3-K/Akt/mTOR signalling pathway has also been found to be one of the reasons for cancer progression. Moreover, Akt, S6K1 and 4E-BP1, were all found to be further activated in NPC cells (Wang *et al.* 2014; Li *et al.* 2017). A study performed on NPC patients also found that mTOR and its downstream effector, S6K1, were highly activated in NPC cells of the patients (Yang *et al.* 2013). Therefore, all these studies suggest a very crucial role for the mTOR signalling pathway in NPC and lung cancer progression, and inhibition of this pathway could be a key step for treating these cancer types (Yang *et al.* 2013).

Several previous studies stated that cardamonin exerted its cytotoxic effect *via* mTOR pathway inhibition (Tang *et al.* 2014; Nui *et al.* 2015; Xue *et al.* 2015). Therefore, it was decided to investigate whether the most active analogue, **19**, also exerted its anticancer effect *via* a similar pathway. The effect of **19** on the expression levels of mTOR was assessed *via* a qPCR analysis.

The cells were treated either with solvent alone to act as the control, or with compound **19** prior to running the assay. Similar to the migration assay, there is no specific protocol with regards to treatment concentrations for qPCR assay and

different studies across literature have used different treatment concentrations without providing justifications (Martí-Centelles *et al.* 2015; Szychowski *et al.* 2017; Baud *et al.* 2018). This experiment was performed in order to investigate if **19** affects mTOR activity resulting in the death of A549 and HK1 cells. Therefore, it has been decided to use 50 μ M of compound **19** which is **twice** the concentration that has been used for the migration assay. This is because the 25 μ M concentration of **19** used for the migration assay did not result in significant cell death which could mean a lower inhibition of mTOR signalling by **19** which might prove challenging to detect. So it was thought that if **19** was actually involved in mTOR pathway inhibition, then a 50 μ M concentration would result in significant inhibition of mTOR signalling, enabling a more accurate and clearer assessment of mTOR inhibition by **19**. It is interesting to note that several qPCR studies have also reported treatment concentrations that are significantly higher than the compounds' IC₅₀ values, and this further supports the choice of treatment concentration that have been used in this present experiment (Duan *et al.* 2017; Baud *et al.* 2018).

Results of the assay showed that **19** downregulated the expression of mTOR by almost 3 and 4-fold in A549 and HK1 cells, respectively (**Figure 3.39**). Therefore, this indicated that **19** might have exerted its cytotoxic effect *via* inhibition of mTOR activity. It can also be noticed that mTOR expression was more inhibited by **19** in HK1 cells than A549 cells which could further explain the observed higher cytotoxic activity exerted by **19** against HK1 cells. Therefore, these results indicate that **19** could potentially act as an anticancer agent for NPC and lung cancer due to its role in mTOR pathway inhibition. However, several additional tests are required

such as Western blotting and kinase assays, to further investigate the effect of **19** on mTOR.

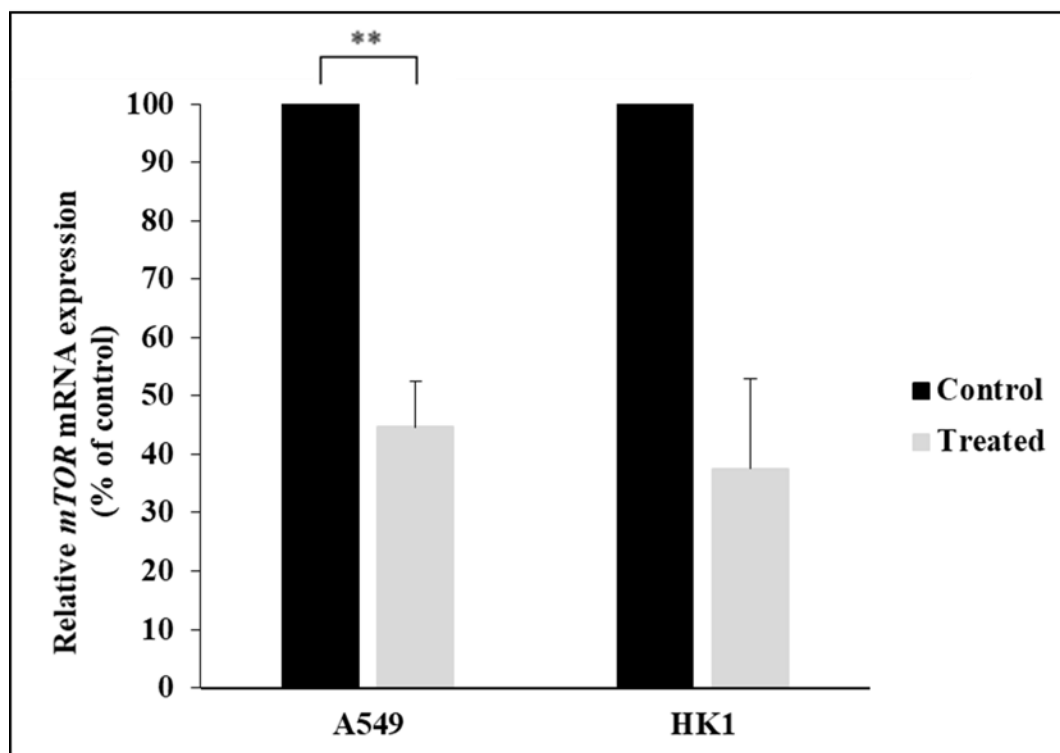


Figure 3.39 mRNA expression of *mTOR* in A549 and HK1 cells after treatment with either solvent control or 50 μ M of compound **19** for 24 h, as determined by qPCR. mRNA expression levels were normalised to GAPDH and compared with the untreated solvent control. The qPCR experiment was repeated three times, and bars and error bars refer to mean \pm SEM. ** $p < 0.01$, analysed using a two-tailed unpaired t-test.

3.3 *In Silico* Studies

3.3.1 *Drug-likeness and ADMET Studies*

A certain active compound cannot be developed into a medicinal drug unless it goes through the body successfully from the moment of administration until it is removed from the body. This journey is usually assessed *via* four dimensions; **A**bsorption, **D**istribution, **M**etabolism and **E**limination. These four parameters are usually referred to as ADME. So a successful oral drug will be fully or largely **absorbed** from the gut and then **distributed** across the body. The drug will be distributed across various sites of the body, but it should largely be distributed towards its intended site of action and in the process it should ideally not interact non-specifically with other targets such as related receptors or serum protein. A large portion of the drug then goes through the liver and gets **metabolised** by enzymes such as the P450 oxygenases, however, a successful drug should avoid inducing or inhibiting these enzymes as that could lead to drug-drug interactions. Moreover, the metabolism of an ideal drug candidate should not result in toxic metabolites. Finally, the drug or its metabolites pass through the kidneys and get **eliminated** or removed from the body. In addition to these parameters, **toxicology** studies are usually conducted in order to ensure that the drug would not be **toxic** to the body. These properties that define a certain drug are collectively known as **ADMET** properties (Hodgson 2001).

ADMET properties can usually be only fully confirmed after clinical studies have been taken, but there have been studies conducted to enable the prediction of a compound's properties from its structure, and software have been developed for that

purpose. This was performed by studying the properties of established drugs in the market and observing general chemical properties that make a compound more “Drug-like” with desirable ADMET properties. This was later followed by feeding the information to a computer or software. The software then uses the parameters and information that have been stored in it to predict the “Drug-likeness” of new molecules.

In this present experiment, the “Drug-likeness” of analogues possessing biological activities equivalent to that of cardamonin and higher were assessed *in silico* using calculations made by the software Molsoft. The software predicts oral bioavailability of compounds based on parameters from the ‘Lipinski’s rule of 5’ in addition to other parameters and reports the final assessment in the form of a ‘Drug-likeness score’. A desirable ‘Drug-likeness score’ range has been defined by the software after calculating the scores of established marketed drugs and a summary of this range has been shown in **Figure 3.40**.

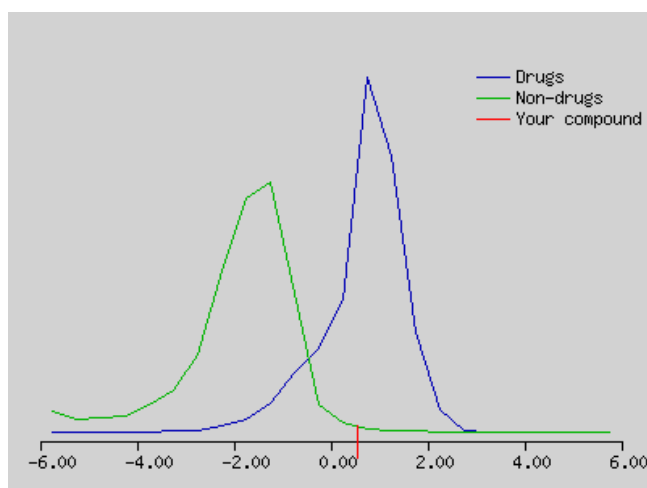


Figure 3.40 Drug-likeness graph used by Molsoft. Drug-likeness score for **6** has been shown in this image as a red vertical line.

Table 3.3 shows the predicted physicochemical properties of the compounds investigated by Molsoft. Results of the analysis revealed that the analogues are generally predicted to possess good drug-like properties with **6** having the most optimum properties.

Table 3.3 ‘Lipinski’s rule of 5’ with additional parameters for selected analogues

Compound	MWT ^a	LogP ^b	HBA ^c	HBD ^d	PSA ^e	LogS ^f	Drug-likeness score
Cardamonin	270	3.21	4	2	55.01	-3.56	-0.25
2	296	3.90	4	1	44.79	-4.22	-0.37
4	354	3.21	6	0	62.43	-4.32	-0.21
6	374	4.88	5	1	57.77	-5.75	0.56
13	312	2.50	5	4	81.01	-3.00	0.16
15	396	3.77	4	2	54.03	-3.90	-0.19
19	655	6.41	10	7	74.65	-6.95	-0.01

^a *Molecular weight*

^b *Calculated lipophilicity*

^c *Number of hydrogen bond acceptors*

^d *Number of hydrogen bond donors*

^e *Polar surface area (Å²)*

^f *Solubility parameter [in log(moles/L)]*

In silico prediction of further ADMET properties was partially performed via “Pre-ADMET” and results of the online tool’s predictions for the most active compounds were summarised in **Table 3.4**. The online tool managed to predict the ADMET properties of all active compounds except that of **19**, because the software was not able to process organometallic compounds. “Pre-ADMET” can aid in assessing bioavailability by predicting a compound’s permeability to Caco-2 cells and its percentage human intestinal absorption (%HIA). Caco-2 cells are derived from human colon adenocarcinoma and these cells are usually used to assess a compound’s *in vitro* permeability. A value of (<4) indicates low Caco-2 permeability, while (4-70) indicates moderate permeability and (>70) indicates high permeability (Valasani *et al.* 2013). %HIA is the sum of bioavailability and absorption of a compound; a value of (0%-20%) indicates low absorption while (20%-70%) moderate absorption and (70%-100%) indicates high absorption (Valasani *et al.* 2013). Cardamonin and its analogues have been predicted to generally have moderate Caco-2 cell permeability and high %HIA.

Percentage Plasma Protein Binding (PPB) refers to the percentage of drug that is bound to plasma proteins, and a value of (>90%) indicates strong binding while (<90%) indicates weak binding (Valasani *et al.* 2013). The online tool predicted that %PPB would be generally high for cardamonin and its active analogues which indicates that the compounds’ drug action, efficacy and disposition might be negatively affected, as usually the unbound concentration of a drug is the one available for drug diffusion/transport across membranes and interaction with the target. However, **13** was the only active analogue predicted to have low %PPB.

Therefore, in general it is predicted that the bioactive cardamonin analogues would have improved bioavailability over their parent compound, however it seems that appropriate doses would have to be administered to account for the predicted high plasma protein binding.

Toxicity of the compounds was predicted by assessing their risk towards inhibition of the cardiac Human ether-a-go-go-related gene (hERG) ion channel, by their ability to penetrate the Blood-Brain Barrier (BBB) and if they inhibit Cytochrome P450 3A4 (CYP3A4). It was predicted that there was no high risk of hERG inhibition by cardamonin and its analogues, therefore, it seems that the analogues would not induce cardiotoxicity. As for the compounds' ability to penetrate the BBB, analogues were predicted to have moderate to low penetration ability with a much lower penetration ability than that of cardamonin, except for **15**. This was deduced by treating BBB penetration values of (>2.0) as an indication of high penetration ability, while ($0.1-2.0$) indicated moderate ability and (<0.1) indicated low penetration ability (Gonçalves *et al.* 2012). Thus, it can be deduced that the analogues would probably possess no Central nervous system (CNS) side-effects. Finally, the software predicted that cardamonin and its active analogues would all act as inhibitors of CYP3A4 which is an enzyme responsible for the metabolism of many drugs, and this might result in drug-drug interactions leading to side-effects. This would mean that further studies might be required to identify which drugs should not be co-administered with cardamonin or its analogues to avoid potential drug-drug interactions. Therefore in general, these results further reflect the

potential improvement in ADMET properties of cardamonin analogues relative to cardamonin itself.

Table 3.4 *In silico* prediction of further ADMET properties of cardamonin and its most active analogues

Compound	Plasma Protein Binding (%)	Caco-2 Cell Permeability (nm/sec)	Human Intestinal Absorption (%)	hERG Inhibition	Blood-Brain Barrier Penetration
Cardamonin	92.70	15.98	92.83	Medium risk	0.56
2	94.10	41.82	95.75	Low risk	0.41
4	93.02	35.16	99.04	Medium risk	0.02
6	94.60	28.19	96.28	Low risk	0.06
13	84.79	20.93	84.62	Medium risk	0.70
15	90.88	20.86	96.15	Medium risk	1.20

3.3.2 Molecular Docking Studies

Molecular docking studies were considered in order to study the binding poses and possible interactions of the most active compound, **19**, with the mTOR protein target and examine the compound's potential as an mTOR inhibitor. mTOR was chosen as the protein target based primarily on my results that showed the inhibition of mTOR expression by **19**. This protein target has been also chosen due to previous studies which showed that cardamonin exerted its cytotoxic activity *via* the inhibition of mTOR signalling, so it was expected that its analogues would also have a similar mechanism (Tang *et al.* 2014; Niu *et al.* 2015). Cardamonin was also docked to mTOR in order to compare its binding affinity and interactions to that of **19** which might aid in providing a possible explanation for the difference found in their bioactivities. Moreover, studying cardamonin's interactions with mTOR might provide possible explanations to the observed activities of the other synthetic analogues and SAR that was deduced from them.

Docking studies were performed *via* AutoDock Vina and visualisation of results was performed using Accelrys Discovery Studio 4.0. The X-ray crystal structure of mTOR complexed with a ligand has been downloaded from the RCSB protein data bank (<http://www.rcsb.org>) with PDB code 4JT5. Initially the docking protocol was validated by redocking the co-crystallised ligand onto the target (mTOR) and the best generated binding pose was compared to that of the co-crystallised ligand. The binding pose generated by Autodock Vina was similar to that of the co-crystallised ligand with an RMSD value of 1.66 Å, which indicated that the software was suitable for conducting docking experiments with mTOR (Figure 3.41)

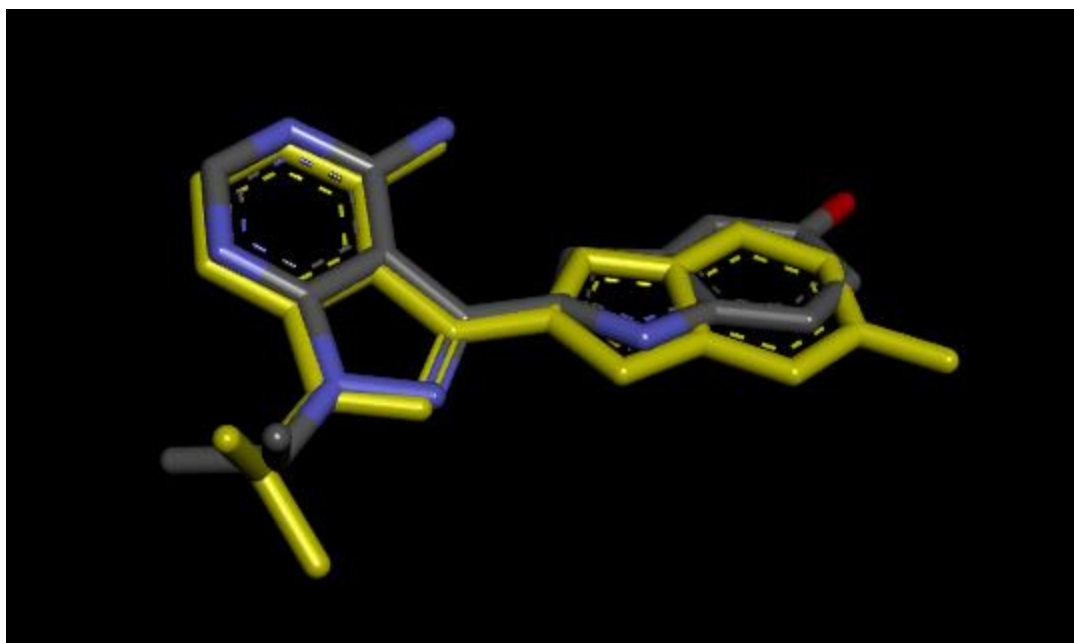


Figure 3.41 Binding pose of the co-crystallised ligand compared to the highest binding energy pose of the ligand generated by Autodock Vina (Yellow). The binding poses were found to be similar

Cardamonin was then docked onto mTOR (**Figure 3.42**) and the docking results showed a binding affinity of -8.1 kcal/mol whereby cardamonin interacted with mTOR *via* hydrophobic interactions and hydrogen bonds. Hydrophobic interactions included Pi-alkyl and Pi-sigma interactions between cardamonin's rings and mTOR. The 2'-OH and 4'-OH of cardamonin formed hydrogen bonds with ASP2195 (2.06 Å) and GLU2190 (2.57 Å) residues of mTOR, moreover, the ketone group formed a hydrogen bond with ASP2357 (3.27 Å). In light of such information it seems that to maintain good binding, substituents at cardamonin's phenolic groups should be polar groups capable of forming hydrogen bonds or polar interactions with mTOR. Therefore, that might explain the reason behind the general enhancement of bioactivity when *O*-acylation of cardamonin's phenols was

performed, while at the same time explaining the loss of activity when non-polar groups were added *via O*-alkylation reactions. The hydrogen bond formed by the carbonyl oxygen of cardamonin might explain the loss of activity when the oxygen was substituted by alkyl amines, whereby the non-polar alkyl groups prevented the formation of any hydrogen bonds. Moreover, this hydrogen bond interaction might also explain the enhancement in activity when urea moiety was introduced in place of the ketone group, whereby **13** is thought to have tautomerised to form a pyrimidinone moiety whose ketone group is capable of forming hydrogen bonds with the receptor.

Compound **19** was then docked onto mTOR (**Figure 3.42**) since the compound has been the most biologically active analogue, so it was expected that it would bind with high affinity. The water molecules have been omitted for a better assessment of the complex's interactions. Docking analysis results revealed that **19** interacted more efficiently than cardamonin with mTOR, and had a binding free energy of -9.8 kcal/mol. Rings B of the ligands formed Pi-alkyl, Pi-sigma and Pi-Pi interactions with ILE 2356, ILE 2237 and HIS 2247, respectively. Moreover, the binding of **19** to mTOR was enhanced by hydrogen bonds with LYS 2187 and ASP 2357; the carbonyl oxygen atom of **19** formed hydrogen bonds with LYS 2187 (6.8 Å), while the same amino acid formed hydrogen bonds with the *ortho* phenolic oxygen atoms of **19** (6.2 Å and 6.5 Å), as for ASP 2357, it formed a hydrogen bond with 4'-OH (4.8 Å). A detailed summary of the interactions has been shown in **Figure 3.42**.

Docking results indicate that the metal ion might have enhanced activity indirectly by its ability to coordinate two cardamonin ligands which enabled further

interactions with mTOR, unlike in the case of cardamonin alone. Moreover, it is possible that **19** possessed better permeability into cells due to its enhanced lipophilicity as can be explained by the Overtone's concept and chelation theory (Break *et al.* 2013). According to the Overtone's concept of cell permeability, the membrane surrounding cells favours the passage of lipophilic compounds, and chelation enhances lipophilicity by allowing the delocalisation of π -electrons over the whole chelate ring, while positive charge on the metal ion is partially shared with the donor groups resulting in better penetration. Therefore, these might be the reasons behind the increased bioactivity of **19** despite the probability of no interactions between the copper (II) ion and its receptor as per the docking results.

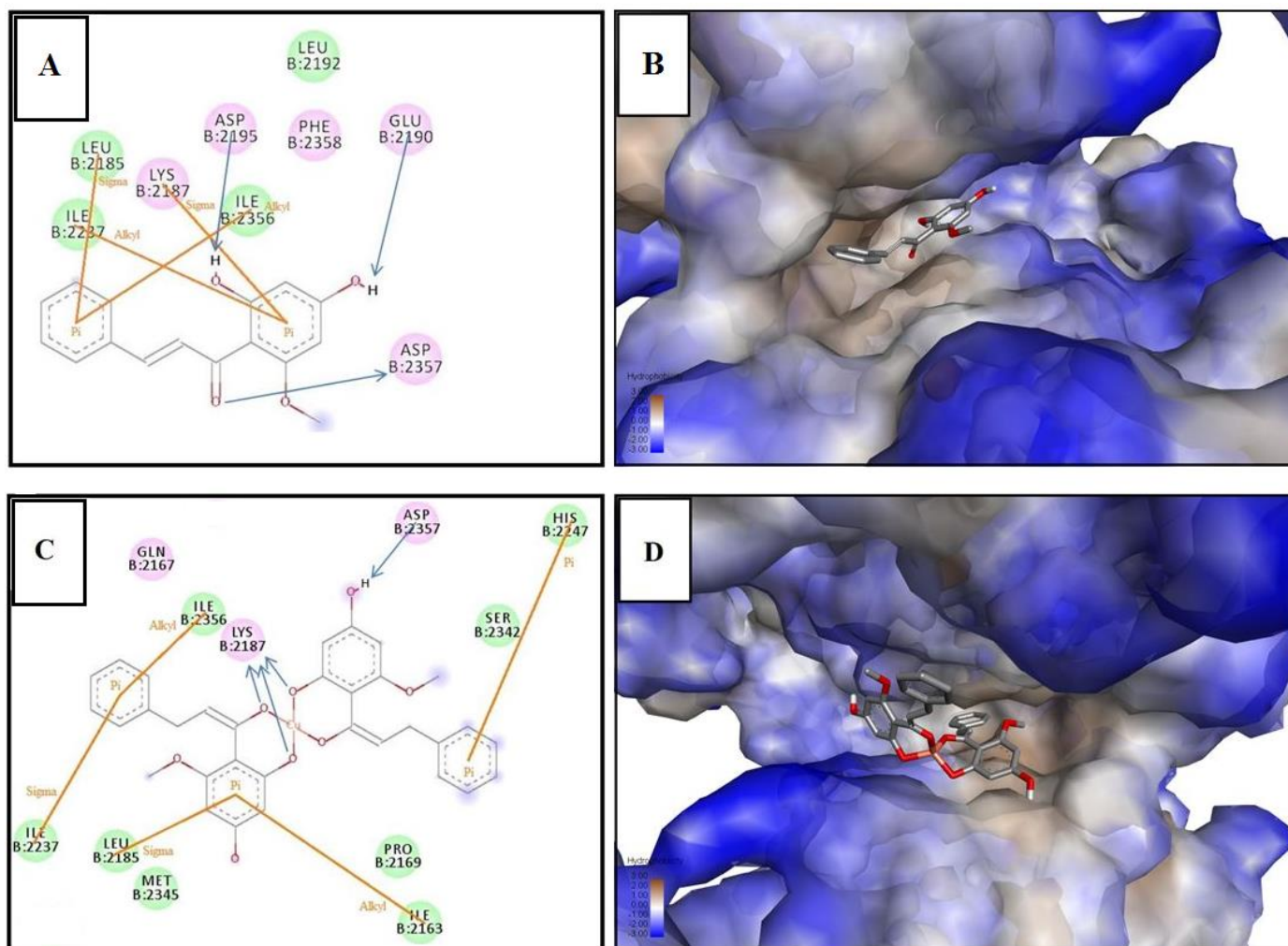


Figure 3.42 (A and C): 2D diagram showing the interactions between mTOR and: (A) Cardamomin; (C) Compound **19**, the orange lines represent hydrophobic interactions, while the blue arrows represent hydrogen bonds. **(B and D):** 3D interaction map of mTOR, which has been mapped according to hydrophobicity, and: (B) Cardamomin; (D) Compound **19**

4 Conclusion

In the present study, 19 analogues of cardamonin were synthesised and tested against A549 and HK1 cell lines. One of the contributions of this study is in exploring the chemistry and reactivity of cardamonin. Several reactions were attempted to produce the cardamonin analogues and every effort was made in order to maximise product yields by reducing the reaction steps for each analogue to only one step. Such short reaction routes have also proven to be economical as less reagents were required. It was found that cardamonin reacted differently from other conventional chalcones in some cases, such as in the synthesis of halogenated derivatives **15** and **16**, in addition to the synthesis of flavonol **18**. Moreover, attempts to coordinate cardamonin with metal ions were all unsuccessful; except in the case of Cu^{2+} which resulted in the formation of a metal complex with a Cardamonin:metal ion ratio of 2:1 (Compound **19**).

However, the main contribution of this study is in conducting an SAR study on cardamonin and its analogues for the first time, in addition to the discovery of the highly active copper (II) complex of cardamonin (**19**). The SAR study identified the importance of the ketone, alkene and polar groups for bioactivity. As for **19**, it demonstrated potent activity against A549 and HK1 cell lines with an IC_{50} of 13.2 μM and 0.7 μM , respectively, while also showing lower toxicity towards healthy MRC5 cells with an IC_{50} of 20.6 μM . Moreover, **19** possessed a migration inhibitory effect on cancer cells that is higher than cardamonin. Studies on its mode of action revealed that **19** managed to activate caspase-9 and caspase-3/7 leading to apoptosis

and induced G2/M-phase cell-cycle arrest. Furthermore, it induced its anticancer effect *via* inhibiting the expression of mTOR. **Figure 4.1** shows an overall summary of the proposed mode of action of **19** in both A549 and HK1 cells based on the experimental data that were generated from the assays performed. Finally, *In silico* studies managed to provide a plausible explanation for the observed bioactivity of the analogues; especially compound **19**, whereby molecular docking of the compound to mTOR showed that **19** formed further interactions with the receptor which might have resulted in enhanced activity. Therefore, it can be clearly seen that the objectives set for the study have been fully fulfilled.

Such results have never been reported earlier and this study is the first one to attempt to optimise the bioactivity of cardamonin and explore its SAR, chemistry and reactivity further. This would aid in guiding future optimisation studies on cardamonin, in addition to performing further studies on the active analogues that were discovered in this study.

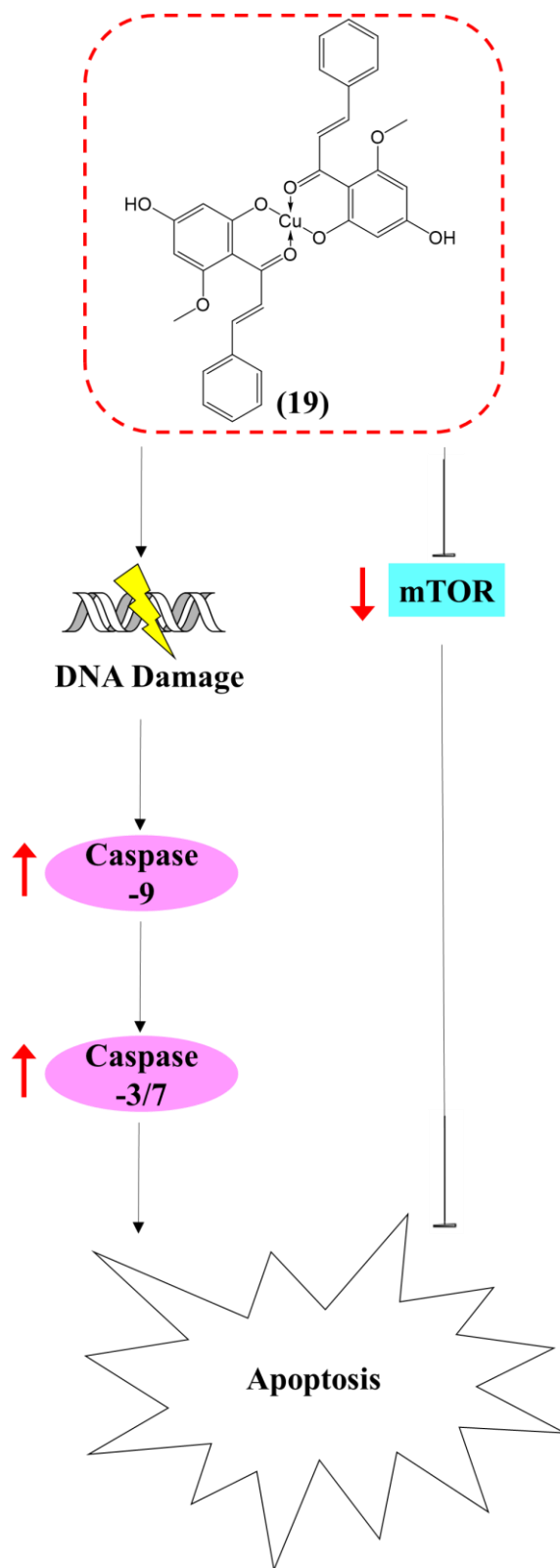


Figure 4.1 Schematic representation of the proposed signalling pathways induced by **19** in the cancer cells to cause apoptosis

5 Future Studies

Future work would include investigating the anticancer activity of **19** on further cell lines such as Jurkat, MCF-7 and HepG2 cells. These further studies would also include studying the mode of action of **19** on these cell lines. Later studies could include *in vitro* ADMET studies on **19**, as this would enable a better prediction of the compound's pharmacokinetics and increase its success rate as a medicinal product. Such studies would involve investigating the solubility, permeability, bioavailability and percentage plasma protein binding of **19**. Finally, it is planned to study the anticancer activity of **19** *in vivo* using mice, and the compound's pharmacokinetics would also be investigated at this stage.

There are also other plans, and these include the synthesis of molecular hybrids involving cardamonin and other bioactive natural product molecules. Molecular hybridisation is a known technique used to enhance the bioactivity of a certain compound by chemically linking it to another bioactive compound. There were several successful studies that used molecular hybridisation to enhance bioactivity. It is predicted that this technique would produce highly active analogues of cardamonin and it seems to be a promising future work that can be conducted in parallel with the further studies that are planned to be conducted on **19**.

6 Materials and Methods

6.1 General

Reagents of analytical grade were used as received from their commercial sources, while cardamonin (98% purity) was obtained from Shanghai Yuanye Bio-Technology Co. Ltd (Shanghai, China). Elemental analysis was performed on a Vario MACRO CUBE CHNS analyser, while thermogravimetric analysis (TGA) was performed *via* a Mettler Toledo TGA analyser up to 800 °C with a heating rate of 10 °C/min in an atmosphere of N₂. IR spectra were recorded by a Perkin Elmer FTIR spectrophotometer within the range (4000–400 cm⁻¹) using KBr discs while melting points have been measured using an Electrothermal IA9100 digital m.p. apparatus measuring within a range of (0 °C–400 °C). HRMS spectrum was recorded using a Bruker micrOTOF-Q LCMS (ESI positive) at UKM CRIM lab. HPLC purity analysis was performed using an Agilent 1260 Infinity system equipped with a Zorbax 300SB-C18 column (5 µm, 250 mm x 4.6 mm). Mobile solvent A was water, while B was acetonitrile and the flow rate used was 1.25 ml/min. The time program used for the HPLC analysis was 55% B (0-5 min), 55% - 85% B (5-25 min) and 99% B (25-30 min).

¹H NMR spectra were obtained *via* a Bruker FT-NMR 300 MHz, 400 MHz and 600 MHz. TLC was performed using 60F aluminium silica gel aluminium plates with 254 nm fluorescent indicator from Merck. UV-Vis spectra were obtained *via* an UltroSpec 8000 spectrophotometer.

6.2 Synthesis

Cardamonin

IR (KBr, cm^{-1}): 3448, 3173 (2'-OH), 2926 (C-H), 1630 (C=O), 1609 and 1475 (aromatic C=C), 1384, 1225 and 1212 (phenolic C-O), 1112 (O-CH₃), 972, 790, 744; ¹H NMR (300 MHz, DMSO, δ (ppm)): 13.69 (s, 1H, 2'-OH), 7.83 (d, 1H, H-7, $J = 15.6$ Hz), 7.65 (d, 1H, H-8, $J = 15.9$ Hz), 7.73-7.44 (m, 5H, aromatic protons of ring B), 6.02 (d, 1H, H-3', $J = 2.1$ Hz), 5.92 (d, 1H, H-5', $J = 2.4$ Hz), 3.88 (s, 3H, 6'-OCH₃); UV-Vis (λ_{max} , nm) in DMSO: 290, 351, 419

General method for synthesis of **(1)**, **(2)** and **(3)**

Cardamonin (30 mg, 0.11 mmol) was dissolved in acetone followed by the addition of K₂CO₃ (0.14 g, 1 mmol). The alkyl halide was later added and the reaction mixture was left to stir under reflux for 24 h. K₂CO₃ was removed by filtration while the solvent was evaporated *in vacuo*. The remaining solid was finally purified *via* preparative TLC using a mobile phase of cyclohexane:chloroform in a ratio of 6:4.

The alkyl halides used were methyl iodide (2 ml, 0.032 mol), allyl bromide (0.2 ml, 2.31 mmol) and BnCl (2 ml, 0.017 mol) for the synthesis of **(1)**, **(2)** and **(3)**, respectively.

(E)-3-Phenyl-1-(2,4,6-trimethoxyphenyl)prop-2-en-1-one (1)

Yield: 7.4 mg (22.5%); Mp: 55-61 °C; IR (KBr, cm^{-1}): 3449, 2938 (C-H), 1633 (C=O), 1606 and 1458 (aromatic C=C), 1336, 1228 (phenolic C-O), 1128 (O-CH₃), 974, 815, 742; ¹H NMR (400 MHz, methanol-*d*₄, δ (ppm)): 7.59-7.42 (m, 5H, aromatic protons of ring B), 7.35 (d, 1H, H-7, $J = 16.4$ Hz), 6.97 (d, 1H, H-8, $J =$

16 Hz), 6.31 (s, 2H, H-3'/5'), 3.89 (s, 3H, 2'-OCH₃), 3.79 (s, 3H, 4'-OCH₃), 3.76 (s, 3H, 6'-OCH₃); Purity: 95% (HPLC, R_t = 4.243 min)

(E)-1-(4-(Allyloxy)-2-hydroxy-6-methoxyphenyl)-3-phenylprop-2-en-1-one (2)

Yield: 21.2 mg (62%); Mp: 106-108 °C; IR (KBr, cm⁻¹): 3448, 3190 (2'-OH), 2927 (C-H), 1628 (C=O), 1573 (allylic C=C), 1422 (aromatic C=C), 1340, 1220 (phenolic C-O), 1114 (O-CH₃), 980, 790, 743; ¹H NMR (400 MHz, CDCl₃, δ(ppm)): 14.19 (s, 1H, 2'-OH), 7.54-7.34 (m, 5H, aromatic protons of ring B), 7.83 (d, 1H, H-7, *J* = 15.6 Hz), 7.72 (d, 1H, H-8, *J* = 15.6 Hz), 6.04 (d, 1H, H-3', *J* = 2.4 Hz), 5.98 (m, 1H, CH₂-CH=CH₂), 5.94 (d, 1H, H-5', *J* = 2.3 Hz), 5.35 (dd, 1H, CH₂-CH=CH-H, *J* = 1.4 Hz), 5.26 (dd, 1H, CH₂-CH=CH-H, *J* = 1.3 Hz), 4.50 (d, 2H, CH₂-CH=CH₂, *J* = 5.4 Hz), 3.85 (s, 3H, 6'-OCH₃); Purity: 95% (HPLC, R_t = 8.750 min).

(E)-1-(2,4-Bis(benzyloxy)-6-methoxyphenyl)-3-phenylprop-2-en-1-one (3)

Yield: 10.6 mg (21%); Mp: 57-60 °C; IR (KBr, cm⁻¹): 3449, 2930 (C-H), 1634 (C=O), 1618 and 1444 (aromatic C=C), 1385, 1227 (phenolic C-O), 1122 (O-CH₃), 974, 812, 770; ¹H NMR (400 MHz, methanol-*d*₄, δ(ppm)): 7.56-7.20 (m, 15H, aromatic protons), 6.98 (d, 1H, H-7, *J* = 16 Hz), 6.45 (d, 1H, H-3', *J* = 2 Hz), 6.39 (d, 1H, H-5', *J* = 2 Hz), 5.15 (s, 2H, 2'-OCH₂-Ar), 5.08 (s, 2H, 4'-OCH₂-Ar), 5.04 (d, 1H, H-8, *J* = 18.8 Hz), 3.77 (s, 3H, 6'-OCH₃); Purity: 97% (HPLC, R_t = 11.806 min)

4-Cinnamoyl-5-methoxy-1,3-phenylene diacetate (4)

Cardamonin (40 mg, 0.15 mmol) was dissolved in dichloromethane by constant heating and stirring followed by the addition of acetic anhydride (0.2 ml, 2.12 mmol), pyridine (0.2 ml, 2.47 mmol) and DMAP (7.2 mg, 0.059 mmol). The reaction mixture was left to stir for 24 h under reflux. The mixture was later washed with 4.5% HCl and saturated aqueous sodium bicarbonate, followed by drying with MgSO₄. The solvent was then evaporated and the resulting solid was purified using preparative TLC with a solvent system of chloroform:cyclohexane at 4:6.

Yield: 10.7 mg (20%); Mp: 183-186 °C; IR (KBr, cm⁻¹): 3449, 2919 (C-H), 1772 (C=O), 1642 (C=O of cardamonin moiety), 1419 (aromatic C=C), 1385, 1213 (phenolic C-O), 1119 (O-CH₃), 830, 689, 614; ¹H NMR (400 MHz, acetone-*d*₆, δ(ppm)): 7.68-7.42 (m, 5H, aromatic protons of ring B), 7.38 (d, 1H, H-7, *J* = 16.4 Hz), 7.03 (d, 1H, H-8, *J* = 16.4 Hz), 6.86 (d, 1H, H-3', *J* = 2 Hz), 6.66 (d, 1H, H-5', *J* = 2 Hz), 3.83 (s, 3H, 6'-OCH₃), 2.28 (s, 3H, 4'-OCOCH₃), 2.11 (s, 3H, 2'-OCOCH₃); Purity: 98% (HPLC, R_t = 4.414 min)

4-Cinnamoyl-5-methoxy-1,3-phenylene bis(4-fluorobenzoate) (5)

Cardamonin (30 mg, 0.11 mmol) was dissolved in dichloromethane by constant heating and stirring followed by the addition of 4-fluorobenzoyl chloride (1 ml, 8.46 mmol), pyridine (0.2 ml, 2.47 mmol) and DMAP (0.05 g, 0.41 mmol). The reaction mixture was left to stir for 24 h under reflux. The mixture was later washed with 4.5% HCl and saturated aqueous sodium bicarbonate followed by drying with

MgSO₄. Finally, the solvent was evaporated and the product purified using preparative TLC with a solvent system of chloroform:cyclohexane at 4:6.

Yield: 18.4 mg (43%); Mp: 168-171 °C; IR (KBr, cm⁻¹): 3083 (C-H), 1683 (C=O), 1623 (C=O of cardamonin moiety), 1609 and 1428 (aromatic C=C), 1363, 1238 (phenolic C-O), 1131 (O-CH₃), 924, 855, 770; ¹H NMR (300 MHz, CDCl₃, δ(ppm)): 8.14 (dd, 2H, *ortho*-H of 4-fluorobenzoyl moiety at position 2', *J* = 7.6, 10.8 Hz), 8.05 (dd, 2H, *ortho*-H of 4-fluorobenzoyl moiety at position 4', *J* = 7.2, 12.4 Hz), 7.49-7.35 (m, 5H, aromatic protons of ring B), 7.44 (d, 1H, H-7, *J* = 22.4 Hz), 7.34 (d, 1H, H-3', *J* = 2 Hz), 7.15 (t, 2H, *meta*-H of 4-fluorobenzoyl moiety at position 2', *J* = 11.2 Hz), 7.06 (t, 2H, *meta*-H of 4-fluorobenzoyl moiety at position 4', *J* = 11.2 Hz), 6.96 (d, 1H, H-8, *J* = 21.2 Hz), 6.41 (d, 1H, H-5', *J* = 2 Hz), 3.80 (s, 3H, OCH₃); Purity: 98% (HPLC, R_t = 2.176 min).

4-Cinnamoyl-3-hydroxy-5-methoxyphenyl benzoate (6)

Cardamonin (36 mg, 0.15 mmol) was dissolved in dichloromethane by constant heating and stirring followed by the addition of benzoyl bromide (0.1 ml, 0.78 mmol) and pyridine (0.1 ml, 1.2 mmol). The reaction mixture was left to stir for 24 h under reflux. The solvent was evaporated and the crude product was purified using preparative TLC with a solvent system of ethylacetate:hexane at 7:3 followed by further purification using a solvent system of chloroform:cyclohexane at 1:1.

Yield: 9.4 mg (13%); Mp: 105-106 °C; IR (KBr, cm⁻¹): 2930 (C-H), 1733 (C=O), 1636 (C=O of cardamonin moiety), 1541 (aromatic C=C), 1340, 1243 (phenolic C-O), 1139 (O-CH₃), 998, 871, 705; ¹H NMR (300 MHz, CDCl₃, δ(ppm)): 13.57 (s,

1H, 2'-OH), 8.20-7.25 (m, 10H, aromatic protons ring B and benzoyl group), 7.63 (d, 1H, H-7, $J = 15.9$ Hz), 7.57 (d, 1H, H-8, $J = 18$ Hz), 6.53 (d, 1H, H-3', $J = 2.4$ Hz), 6.38 (d, 1H, H-5', $J = 2.1$ Hz), 3.97 (s, 3H, 6'-OCH₃); Purity: 98% (HPLC, $R_t = 9.410$ min).

1-(2,4-Dihydroxy-6-methoxyphenyl)-3-phenylpropan-1-one (7)

Cardamonin (30 mg, 0.11 mmol) was dissolved in methanol and NiCl₂ (2 equivalent) was added to the mixture. The mixture was stirred and placed in an ice-bath. NaBH₄ (6 equivalent) was later added and the mixture was left to stir for 5-10 min followed by dilution with HCl (37%). Methanol was evaporated followed by the addition of water and the organic product was extracted by dichloromethane. Dichloromethane was finally evaporated and the crude product was purified *via* preparative TLC using a mobile phase of ethyl acetate:hexane in a ratio of 1:1.

Yield: ~2 mg (7%); IR (KBr, cm⁻¹): 3437, 2919 (C-H), 1628 (C=O), 1455 (aromatic C=C), 1382, 1270, 1217 (phenolic C-O), 1114 (O-CH₃), 952, 816, 746; ¹H NMR (300 MHz, CDCl₃, δ (ppm)): 13.91 (s, 1H, 2'-OH), 7.33-7.20 (m, 5H, aromatic protons of ring B), 5.99 (d, 1H, H-3', $J = 2.1$ Hz), 5.91 (d, 1H, H-5', $J = 2.1$ Hz), 3.84 (s, 3H, 6'-OCH₃), 3.32 (t, 2H, -CH₂-CH₂-Ar, $J = 7.5$ Hz), 2.99 (t, 2H, -CH₂-CH₂-Ar, $J = 7.5$ Hz); Purity: 97% (HPLC, $R_t = 5.167$ min)

General method for synthesis of (8) and (9)

The amine hydrochloride was initially fully dissolved in methanol followed by the addition of pyridine (~0.5 ml, 6.18 mmol) and the mixture was left to stir under heating for 15 min. Cardamonin (20-30 mg, 0.11 mmol) was later added followed

by 2-3 drops of HCl and the reaction mixture was left to stir under reflux for 24 h. Methanol was finally evaporated to obtain the product. In some cases further purification *via* preparative TLC was performed using a solvent system of chloroform:cyclohexane at 4:6.

The amines used were propylamine hydrochloride (0.1 g, 1.05 mmol) and methoxyamine hydrochloride (0.1 g, 1.20 mmol) for the synthesis of compounds **(8)** and **(9)**.

(Z)-5-Methoxy-4-(3-phenyl-1-(propylimino)propyl)benzene-1,3-diol (8)

Yield: 10 mg (29%); Mp: 145-150 °C; IR (KBr, cm⁻¹): 3448, 3190 (2'-OH), 2967 (C-H), 1628 (C=N), 1490 (aromatic C=C), 1383, 1225 (phenolic C-O), 1114 (O-CH₃), 990, 788, 744; ¹H NMR (400 MHz, CDCl₃, δ(ppm)): 14.28 (s, 1H, OH), 7.91 (d, 1H, H-7, *J* = 15.2 Hz), 7.79 (d, 1H, H-8, *J* = 15.6 Hz), 7.64-7.29 (m, 5H, aromatic protons of ring B), 6.14 (d, 1H, H-3', *J* = 1.5 Hz), 6.02 (d, 1H, H-5', *J* = 1.4 Hz), 3.92 (s, 3H, 6'-OCH₃), 3.00 (t, 2H, C=NCH₂, *J* = 1.7 Hz), 2.82 (m, 2H, NCH₂CH₂), 1.70 (t, 3H, NCH₂CH₂CH₃, *J* = 1.6 Hz); Purity: 96% (HPLC, R_t = 3.888 min)

(Z)-1-(2,4-Dihydroxy-6-methoxyphenyl)-3-phenylpropan-1-one O-methyl oxime (9)

Yield: 5.6 mg (17%); Mp: 233-235 °C; IR (KBr, cm⁻¹): 3451, 3277 (2'-OH), 2919 (C-H), 1636 (C=N), 1457 (aromatic C=C), 1384, 1224 (phenolic C-O), 1116 (O-CH₃), 967, 791, 741; ¹H NMR (300 MHz, CDCl₃, δ(ppm)): 14.17 (s, 1H, OH), 7.89 (d, 1H, H-7, *J* = 15.5 Hz), 7.77 (d, 1H, H-8, *J* = 15.5 Hz), 7.62-7.39 (m, 5H, aromatic protons of ring B), 6.12 (d, 1H, H-3', *J* = 1.7 Hz), 5.97 (d, 1H, H-5', *J* = 1.7 Hz),

3.93 (s, 3H, C=NOCH₃), 3.87 (s, 3H, 6'-OCH₃); Purity: 98% (HPLC, R_t = 2.115 min).

Benzyl-2-(1-(2,4-dihydroxy-6-methoxyphenyl)-3-phenylpropylidene)hydrazine-1-carbodithioate (10)

Cardamonin (8 mg, 0.03 mmol) was dissolved in ethanol by constant heating and stirring followed by the addition of SBDTC (0.018 g, 0.09 mmol). 2-4 drops of HCl were later added and the mixture was left to stir under reflux for 24 h. The mixture was then cooled and the resulting solid precipitate was filtered, washed with ethanol and dried over silica gel.

Yield: 10.7 mg (79%); Mp: 189-192 °C; IR (KBr, cm⁻¹): 3415, 3213 (2'-OH), 3173 (NH), 2926 (C-H), 1627 (C=N), 1487 (aromatic C=C), 1384, 1042 (N-N), 950 (C=S), 866, 826, 790, 744, 705; ¹H NMR (400 MHz, CDCl₃, δ(ppm)): 14.16 (s, 1H, OH), 7.90 (d, 1H, H-7, *J* = 15.6 Hz), 7.80 (d, 1H, H-8, *J* = 15.6 Hz), 7.64-7.31 (m, 10H, aromatic protons of ring B and ring of SBDTC moiety), 6.06 (d, 1H, H-3', *J* = 2.2 Hz), 5.99 (d, 1H, H-5', *J* = 2.2 Hz), 4.91 (s, 1H, NH), 4.52 (s, 2H, -CH₂-S), 3.96 (s, 3H, 6'-OCH₃); Purity: <90% (HPLC, R_t = 4.398 min).

5-Methoxy-4-(5-phenyl-4,5-dihydro-1H-pyrazol-3-yl)benzene-1,3-diol (11)

Cardamonin (20 mg, 0.078 mmol) was dissolved in methanol and was left to stir under constant heating for 5 min. To this solution was added excess 100% hydrazine hydrate (0.3 ml, 9.64 mmol) and the reaction mixture was left to stir under reflux for 24 h. The solvent and hydrazine hydrate were evaporated, and the solid obtained

was further purified by preparative TLC using a solvent system of chloroform:cyclohexane at 4:6, which resulted in a flaky brown solid product.

Yield: 22 mg (99%); Mp: 135-140 °C; IR (KBr, cm^{-1}): 3423, 2919 (C-H), 1618 (C=N), 1463 (aromatic C=C), 1384, 1213 (phenolic C-O), 1158 (O-CH₃), 956, 816, 765; ¹H NMR (400 MHz, CDCl₃, δ (ppm)): 7.57-7.35 (m, 5H, aromatic protons of ring B), 7.13 (s, 1H, NH), 6.52 (dd, 1H, H-C-Ar of pyrazoline ring, $J = 2, 8$ Hz), 6.10 (d, 1H, H-3', $J = 2.3$ Hz), 6.03 (d, 1H, H-5', $J = 2.4$ Hz), 3.94 (dd, 1H, CH-H of pyrazoline, $J = 3.8, 20.2$ Hz), 3.83 (dd, 1H, CH-H of pyrazoline ring, $J = 3.8, 10$ Hz), 3.86 (s, 3H, 6'-OCH3); Purity: 95% (HPLC, $R_t = 2.771$ min)

5-Methoxy-4-(5-phenyl-4,5-dihydroisoxazol-3-yl)benzene-1,3-diol (12)

To a mixture of cardamonin (30 mg, 0.11 mmol) and NH₂OH·HCl (17 mg, 0.24 mmol) in ethanol, NaOH (40 mg, 1 mmol) was added. The mixture was left to stir for 24 h, and it was then left in a freezer overnight. Crushed ice and 2 ml of HCl (37%) were later added to the mixture resulting in the formation of a pale yellow precipitate which was collected *via* vacuum filtration.

Yield: 16 mg (51%); Mp: 220-221 °C; IR (KBr, cm^{-1}): 3448, 3220 (2'-OH), 2923 (C-H), 1610 (C=N), 1582 and 1482 (aromatic C=C), 1375, 1221 (phenolic C-O), 1109 (O-CH₃), 987, 838, 770; ¹H NMR (400 MHz, acetone-*d*₆, δ (ppm)): 7.55-7.35 (m, 5H, aromatic protons of ring B), 6.14 (d, 1H, H-3', $J = 2$ Hz), 6.09 (d, 1H, H-5', $J = 2$ Hz), 5.46 (dd, 1H, H-C-Ar of isoxazoline ring, $J = 3, 12.8$ Hz), 3.93 (dd, 1H, CH-H of isoxazoline ring, $J = 2, 24$ Hz), 3.79 (s, 3H, 6'-OCH3), 3.58 (dd, 1H, CH-H of isoxazoline, $J = 4, 14$ Hz); Purity: 95% (HPLC, $R_t = 26.287$ min)

General method for synthesis of (13) and (14)

Cardamonin (30 mg, 0.11 mmol) and, urea (40 mg, 0.67 mmol) for synthesis of (13) or thiourea (40 mg, 0.53 mmol) for synthesis of (14), were added together in a round bottom flask. To this was added NaOH (0.2 g, 0.005 moles) dissolved in 80% ethanol, and the mixture was left to stir under reflux for more than 24 h. 1 ml of HCl (37%) was later added to neutralise the mixture and crushed ice was finally added resulting in the formation of a precipitate which was collected *via* vacuum filtration.

4-(2-Hydroxy-6-phenyl-1,6-dihydropyrimidin-4-yl)-5-methoxybenzene-1,3-diol (13)

Yield: 34 mg (99%); Mp: 220-221 °C; IR (KBr, cm⁻¹): 3437, 3226 (NH), 2965 (C-H), 1661 (C=N), 1601 (NH bend), 1591 and 1475 (aromatic C=C), 1384, 1221 (phenolic C-O), 1119 (O-CH₃), 969, 847, 766; ¹H NMR (400 MHz, acetone-*d*₆, δ(ppm)): 7.54-7.34 (m, 5H, aromatic protons of ring B), 6.14 (d, 1H, H-3', *J* = 2.4 Hz), 6.08 (d, 1H, H-5', *J* = 2.4 Hz), 5.48 (d, 1H, CH of pyrimidine, *J* = 2.8 Hz), 5.45 (d, 1H, CH of pyrimidine, *J* = 3.2 Hz), 3.98 (s, 1H, NH), 3.79 (s, 3H, 6'-OCH3); Purity: 95% (HPLC, R_t = 4.445 min).

4-(2-Mercapto-6-phenyl-1,6-dihydropyrimidin-4-yl)-5-methoxybenzene-1,3-diol (14)

Yield: 35 mg (97%); Mp: 213-216 °C; IR (KBr, cm⁻¹): 3437, 3222 (NH), 2965 (C-H), 1662 (C=N), 1601 (NH bend), 1591 and 1475 (aromatic C=C), 1384, 1222 (phenolic C-O), 1119 (O-CH₃), 969, 847, 766; ¹H NMR (400 MHz, acetone-*d*₆, δ(ppm)): 7.54-7.36 (m, 5H, aromatic protons of ring B), 6.14 (d, 1H, H-3', *J* = 2.4

Hz), 6.09 (d, 1H, H-5', $J = 2.4$ Hz), 5.48 (d, 1H, CH of pyrimidine, $J = 3.2$ Hz), 5.45 (d, 1H, CH of pyrimidine, $J = 2.8$ Hz), 3.97 (s, 1H, NH), 3.79 (s, 3H, 6'-OCH₃); Purity: 95% (HPLC, $R_t = 2.741$ min).

(E)-1-(4,6-Dihydroxy-3-iodo-2-methoxyphenyl)-3-phenylprop-2-en-1-one (15)

Cardamonin (50 mg, 0.19 mmol) and iodine (42 mg, 0.16 mmol) were added to a round bottom flask followed by the addition of 10 ml of DMSO. The reaction mixture was left to stir under reflux for 6 h. Water was then added to the mixture and the solid formed was filtered and washed with sodium thiosulfate in order to remove the excess iodine. The resulting solid was finally purified *via* preparative TLC using a mobile phase of cyclohexane:chloroform in a ratio of 6:4.

Yield: 4.2 mg (6%); Mp: 257-259 °C; IR (KBr, cm^{-1}): 3450, 3165 (2'-OH), 2920 (C-H), 1639 (C=O), 1625 and 1483 (aromatic C=C), 1384, 1281, 1222 (phenolic C-O), 1115 (O-CH₃), 972, 847 (C-I), 790; ¹H NMR (300 MHz, DMSO, $\delta(\text{ppm})$): 15.16 (s, 1H, OH), 7.92 (d, 1H, H-7, $J = 15.6$ Hz), 7.76-7.45 (m, 5H, aromatic protons of ring B), 7.75 (d, 1H, H-8, $J = 15.3$ Hz), 6.26 (s, 1H, H-3'), 3.92 (s, 3H, 6'-OCH₃); Purity: 95% (HPLC, $R_t = 7.781$ min)

(E)-1-(3-Bromo-4,6-dihydroxy-2-methoxyphenyl)-3-phenylprop-2-en-1-one (16)

Cardamonin (30 mg, 0.11 mmol) was dissolved in chloroform. This was followed by the addition of 1.2 ml of bromine water and the reaction mixture was left to stir at room temperature for 24 h. Chloroform was separated from the aqueous phase and later evaporated. The resulting solid was finally purified *via* preparative TLC using a mobile phase of cyclohexane:chloroform in a ratio of 1:1.

Yield: 1.4 mg (4%); Mp: 176-178 °C; IR (KBr, cm^{-1}): 3464, 3173 (2'-OH), 2921 (C-H), 1649 (C=O), 1528 (aromatic C=C), 1384, 1281, 1224 (phenolic C-O), 1118 (O-CH₃), 972, 848, 745, 498 (C-Br); ¹H NMR (300 MHz, DMSO, δ (ppm)): 14.89 (s, 1H, 2'-OH), 7.90 (d, 1H, H-7, $J = 15.6$ Hz), 7.76-7.46 (m, 5H, aromatic protons of ring B), 7.74 (d, 1H, H-8, $J = 15.6$ Hz), 6.26 (s, 1H, H-3'), 3.92 (s, 3H, 6'-OCH₃); Purity: 99% (HPLC, $R_t = 5.570$ min)

7-Hydroxy-5-methoxy-2-phenylchroman-4-one (17)

Cardamonin (30 mg, 0.11 mmol) was dissolved in methanol followed by the addition of 10 ml of HCl (37%). The reaction mixture was heated under reflux and left to stir for 72 h. The solvent was later evaporated followed by the addition of purified water. The solid precipitate that formed was collected *via* filtration and further purified *via* preparative TLC using a mobile phase of cyclohexane:chloroform in a ratio of 1:9.

Yield: 2.2 mg (7%); Mp: 226-227 °C; IR (KBr, cm^{-1}): 3438, 2919 (C-H), 1657 (C=O), 1620 and 1441 (aromatic C=C), 1383, 1298, 1229 (phenolic C-O), 1116 (O-CH₃), 773; ¹H NMR (300 MHz, DMSO, δ (ppm)): 10.54 (s, 1H, 4'-OH), 7.51-7.36 (m, 5H, aromatic protons of ring B), 6.07 (d, 1H, H-3', $J = 2.1$ Hz), 6.00 (d, 1H, H-5', $J = 2.1$ Hz), 5.48 (dd, 1H, O-CH₂-Ar, $J = 3, 12.3$ Hz), 3.74 (s, 3H, 6'-OCH₃), 2.98 (dd, O=C-CH₂-H-C, $J = 12.3, 16.2$ Hz), 2.62 (dd, O=C-CH₂-H-C, $J = 3.3, 16.4$ Hz); Purity: 95% (HPLC, $R_t = 2.607$ min)

3,6,7,8-Tetrahydroxy-5-methoxy-2-phenyl-4H-chromen-4-one (18)

Cardamonin (30 mg, 0.19 mmol) was dissolved in methanol followed by the addition of 0.2 ml 4% NaOH. The mixture was stirred at 0 °C for 30 min. 0.3 ml of 30% H₂O₂ was later added and the reaction mixture was left to stir for 24 h at room temperature. 10-12 ml of HCl (37%) was then added and the reaction mixture was left to stand in the freezer for another 24 h. The solid precipitate was finally collected and purified *via* preparative TLC using a mobile phase of ethyl acetate:hexane in a ratio of 6:4 followed by further purification using ethyl acetate:hexane in a ratio of 4:6

Yield: 18 mg (30%); Mp: 143-145 °C; IR (KBr, cm⁻¹): 3450, 2925 (C-H), 1638 (C=O), 1541 (aromatic C=C), 1373, 1238, 1219 (phenolic C-O), 1100 (O-CH₃), 955, 782; ¹H NMR (300 MHz, DMSO, δ(ppm)): 7.76-7.44 (m, 5H, aromatic protons of ring B), 7.65 (s, 2H, 3'-OH & 5'-OH), 3.73 (s, 3H, 6'-OCH₃); Purity: 98% (HPLC, R_t = 4.007 min)

[Cu(C₁₆H₁₃O₄)₂(H₂O)₂].2H₂O (19)

Cardamonin (40 mg, 0.11 mmol) was dissolved in methanol by constant heating and stirring while copper (II) acetate (30 mg, 0.15 mmol) was separately dissolved in methanol in another beaker under the same conditions. 3 ml of dilute NaOH was added to the cardamonin mixture followed by the addition of the copper (II) acetate solution. The reaction was left for 6-8 h with stirring under reflux. Finally, a brown precipitate formed and was collected *via* suction filtration.

Yield: 33.5 mg (48%); Mp: >300 °C; IR (KBr, cm⁻¹): 3448, 2926 (C-H), 1598 (C=O), 1460 (aromatic C=C), 1384, 1230 and 1213 (phenolic C-O), 1117 (O-CH₃), 972, 827, 744; ¹H NMR (600 MHz, DMSO, δ(ppm)): 7.88 (d, 1H, H-7, *J* = 10.8 Hz), 7.69-7.15 (m, 5H, aromatic protons of ring B), 7.57 (d, 1H, H-8, *J* = 12 Hz), 7.45 (d, 1H, H-3', *J* = 6.6 Hz), 7.42 (d, 1H, H-5', *J* = 6.0 Hz), 3.90 (s, 3H, 6'-OCH₃); HRMS calculated for C₃₂H₂₆CuNaO₈ [M⁺ + Na]: 624.0829, found: 624.0783; Analytical calculated for [Cu(C₁₆H₁₃O₄)₂(H₂O)₂]·2H₂O: %C (57.01), %H (5.08), found: %C (57.02), %H (4.47); UV-Vis (λ_{max}, nm) in DMSO: 291, 352, 432, 506, 600.

6.3 Cell Culture

Cardamonin and its analogues were tested against A549 (lung cancer cells) and HK1 cells (NPC cells). A549 cells were obtained from the American Type Culture Collection (ATCC) while HK1 cells were donated by Prof. GSW Tsao (Faculty of Medicine, The University of Hong Kong) (Huang *et al.* 1980). Cell cultures were generally maintained using RPMI 1640 (Gibco) supplemented with 10% fetal bovine serum (FBS) (Gibco), penicillin (100 U/ml, Gibco), streptomycin (100 µg/ml, Gibco) and 2 mM L-Glutamine (Gibco) under humidified atmosphere containing 5% CO₂ in air at 37 °C. 10% FBS was replaced with 1% FBS for treatment medium while adherent cells were dissociated using Trypsin-EDTA solution (Gibco).

6.4 Cell Viability Assay

The spectrophotometric MTS (3-(4,5-dimethylthiazol-2-yl)-5-(3-carboxymethoxyphenyl)-2-(4-sulfophenyl)-2H-tetrazolium) assay was used to assess cell viability. Aliquots of 100 µl of 10,000 cells in an appropriate medium were dispensed into 96-well plates. Cells were incubated for 24 h at 37 °C prior to treatment to allow cell attachment. 100 µl of treatment medium were later added and the cells were incubated for 72 h. 10 µl of MTS reagent (Promega) was finally added to each well including the control and blank. The plate was wrapped in aluminium foil to protect from light and incubated at 37 °C for 1 h before reading the absorbance at 490 nm using a Tecan 200 ELISA plate reader.

6.5 Migration Assay

Cells were seeded in 6-well plates and left to grow until around 80% confluency. This was followed by forming a scratch or “wound” in the layer of cells using a sterile 200 μ l pipette. The cells were washed with PBS and incubated with cardamonin (25 μ M) and compound **19** (25 μ M) in the presence of 10% FBS for 24 h and 48 h. Magnified cells under the microscope were photographed at 0 h, 24 h and 48 h. The images were analysed *via* the software “ImageJ” in order to measure the area of the wound that has been occupied by the migrating cells. Results of the different treatment groups were then expressed as a percentage of the original area of the wound.

6.6 Cell-cycle Analysis

Cell-cycle analysis of A549 and HK1 cells has been performed according to a previously reported method using a fluorochrome solution containing 50 mg/mL of propidium iodide (PI), 0.1 mg/mL of ribonuclease A, 0.1% *v/v* Triton X-100 and 0.1% *w/v* sodium citrate in *d*-H₂O (Yap *et al.* 2016). A549 and HK1 cells were each seeded in six-well plates at a density of 1×10^6 cells/well and treated for 24 h with **19** at its IC₅₀ concentrations. There were also cells treated with DMSO (control). Cells were then harvested followed by washing with ice-cold PBS twice. Later, the pelleted cells were resuspended in 0.3-0.5 ml of the fluorochrome solution and stored overnight in the dark at 4 °C. Finally, the measurements were conducted using a Beckman Coulter Cytomics FC500 MCL flow cytometer and data analysis was performed *via* Weasel flow cytometry analysis software.

6.7 Flow Cytometric Detection of γ -H2AX

Cells were seeded at a density of $1-1.5 \times 10^6$ in 10 cm^2 dishes and allowed to adhere for 24 h at 37°C . The cells were treated with **19** for 24 h at its IC_{50} concentrations and then trypsinised, collected and fixed with 1% methanol-free formaldehyde in PBS. Following a 5 min incubation at room temperature, cells were permeabilised by adding 500 μl of 0.4% Triton-X-100 in PBS and mixed gently. Cells were then rinsed with PBS, centrifuged and resuspended in 200 μl of H2AX antibody (1:3333 dilution) at room temperature for 1.5 h. Secondary antibody (goat anti-mouse Alexa Fluor 488; 1:1750 dilution) was later added and cells were incubated for 1 h at room temperature in the dark. Cells were washed with PBS and then resuspended in 300 μl of 50 $\mu\text{g/ml}$ propidium iodide/ 0.1 mg/ml RNase A in PBS followed by incubation for at least 10 min at room temperature. Finally, the measurements were conducted using a Beckman Coulter Cytomics FC500 MCL flow cytometer and data analysis was performed *via* Weasel flow cytometry analysis software.

6.8 Caspase-Glo 3/7 Apoptosis Assay

A549 and HK1 cells were treated with 10 μM of **19** for 12 h and caspase activation was investigated using a Caspase-Glo 3/7 assay (Promega) following the directions provided by the kit's manufacturer. Briefly, after the 12 h treatment, Caspase-Glo 3/7 reagent was added to the cells in a 1:1 ratio of reagent to cell culture media, and mixed with a shaker followed by incubation at room temperature for a duration of 60 min for A549 cells and 30 min for HK1 cells. The resulting luminescence was read using a Varioscan flash multiplate reader.

6.9 Caspase-Glo 8 and Caspase-Glo 9 Assays

The protocol followed was similar to that of the Caspase-Glo 3/7 assay. However, Caspase-Glo 8 and Caspase-Glo 9 assays involved treating A549 and HK1 cells with 10 μ M of **19** for 6 h followed by adding the caspase reagent, shaking and incubating for 30 min for both A549 and HK1 cells. Each caspase assay was performed separately.

6.10 qPCR Assay

Total RNA was isolated from the cancer cells using TRIsure (Bioline), according to the manufacturer's instructions. This was followed by cDNA synthesis using Tetro cDNA Synthesis Kit (Bioline) according to the manufacturer's protocol.

qPCR was performed on an ECO Illumina qPCR machine using a KAPA SYBR FAST qPCR Kit (Kapa Biosystems). Gene expression data were normalised to the endogenous control, GAPDH. The primer sequences were as follows: **GAPDH**: 5'-GCACCGTCAAGGCTGAGAAC-3' (Forward), 5'-ATGGTGGTGAAGACGCCAGT-3' (Reverse); **mTOR**: 5'-CGCTGTCATCCCTTTATCG-3' (Forward), 5'-ATGCTCAAACACCTCCACC-3' (Reverse).

The PCR cycling profile was as follows: One cycle at 50 °C for 2 min followed by another cycle at 95 °C for 3 min. Then 40 cycles of 95 °C for 3 s, 63 °C (A549 cDNA)/59 °C (HK1 cDNA) for 30 s and 72 °C for 15 s. Relative gene expression levels were calculated using the comparative C_T method.

6.11 In Silico Studies

6.11.1 Drug-likeness and ADMET Studies

Drug-likeness studies for the most active analogues were performed using “MolSoft” (<http://www.molsoft.com/>), while ADMET studies were mostly conducted using the software “Pre-ADMET” (<https://preadmet.bmdrc.kr/>).

6.11.2 Molecular Docking Studies

X-ray crystal structure of mTOR complexed with a ligand has been downloaded from the RCSB protein data bank (<http://www.rcsb.org>) with PDB code 4JT5. Molecular structures of the ligands, cardamonin and **19**, were prepared by Chem3D and their energy was minimised followed by the addition of Gasteiger charges using AutoDock Tools. Water molecules of **19** were excluded. The receptor was prepared for docking using AutoDock Tools whereby water molecules and heteroatoms were removed followed by the addition of hydrogen atoms and charges. Search space for docking was determined by a grid box placed around the position of the co-crystallised ligand with a grid size of 32x18x22 and a grid spacing of 0.375 Å. Finally, docking was performed using AutoDock Vina. Analysis and visualisation of docking results were performed *via* Accelrys Discovery Studio Visualizer 4.0, moreover, 2D interaction diagrams were generated using the same software followed by slight additions in order to include all relevant interactions.

7 References

Aderogba, M. A., D. T. Kgatle, L. J. McGaw and J. N. Eloff (2012). "Isolation of antioxidant constituents from *Combretum apiculatum* subsp. *apiculatum*." South African Journal of Botany **79**: 125-131.

Akihisa, T., T. Kikuchi, H. Nagai, K. Ishii, K. Tabata and T. Suzuki (2011). "4-Hydroxyderricin from *Angelica keiskei* Roots Induces Caspase-dependent Apoptotic Cell Death in HL60 Human Leukemia Cells." Journal of Oleo Science **60**(2): 71-77.

Albuquerque, H. M. T., C. M. M. Santos, J. A. S. Cavaleiro and A. M. S. Silva (2014). "Chalcones as versatile synthons for the synthesis of 5- and 6-membered nitrogen heterocycles." Current Organic Chemistry **18**(21): 2750-2775.

American Cancer Society (2015). "Learn about cancer." [ONLINE] Available at: <http://www.cancer.org/cancer/index>. [Accessed 26 August 15].

American Cancer Society (2018). "Risks of Cancer Surgery." [ONLINE] Available at: www.cancer.org/treatment/treatments-and-side-effects/treatment-types/surgery/risks-of-cancer-surgery.html. [Accessed 7 June 18].

Bajgai, S. P., V. Prachyawarakorn, C. Mahidol, S. Ruchirawat and P. Kittakoop (2011). "Hybrid flavan-chalcones, aromatase and lipoxygenase inhibitors, from *Desmos cochinchinensis*." Phytochemistry **72**(16): 2062-2067.

Baud, M. G. J., M. R. Bauer, L. Verduci, F. A. Dingler, K. J. Patel, D. Horil Roy, A. C. Joerger and A. R. Fersht (2018). "Aminobenzothiazole derivatives stabilize the thermolabile p53 cancer mutant Y220C and show anticancer activity in p53-Y220C cell lines." European Journal of Medicinal Chemistry **152**: 101-114.

Break, M. K. b., M. I. M. Tahir, K. A. Crouse and T.-J. Khoo (2013). "Synthesis, Characterization, and Bioactivity of Schiff Bases and Their Cd^{2+} , Zn^{2+} , Cu^{2+} , and Ni^{2+} Complexes Derived from Chloroacetophenone Isomers with S-Benzylidithiocarbazate and the X-Ray Crystal Structure of S-Benzyl- β -N-(4-chlorophenyl)methylenedithiocarbazate." Bioinorganic Chemistry and Applications **2013**: 13.

Cancer Research UK (2014). "Nasopharyngeal cancer risks and causes." [ONLINE] Available at: <http://www.cancerresearchuk.org/about-cancer/type/nasopharyngeal-cancer/about/nasopharyngeal-cancer-risks-and-causes>. [Accessed 26 August 15].

Cancer Research UK (2018). "Side effects of cisplatin." [ONLINE] Available at: <http://www.cancerresearchuk.org/about-cancer/cancer-in-general/treatment/cancer-drugs/drugs/cisplatin/side-effects>. [Accessed 7 June 18].

Carvalho, A. M., L. M. Gonçalves, I. M. Valente, J. A. Rodrigues and A. A. Barros (2012). "Analysis of cardamonin by square wave voltammetry." Phytochemical Analysis **23**(4): 396-399.

Chan Sylvia, Y. Y., K. W. Choy, S. W. Tsao, Q. Tao, T. Tang, T. Y. Chung Grace and K. W. Lo (2008). "Authentication of nasopharyngeal carcinoma tumor lines." International Journal of Cancer **122**(9): 2169-2171.

Cheung Siu, T., P. Huang Dolly, B. Y. Hui Angela, W. Lo Kwok, W. Ko Chuen, S. Tsang Yuen, N. Wong, M. Whitney Bruce and C. K. Lee Joseph (1999). "Nasopharyngeal carcinoma cell line (C666-1) consistently harbouring Epstein-Barr virus." International Journal of Cancer **83**(1): 121-126.

Chow, Y. L., K. H. Lee, S. Vidyadaran, N. H. Lajis, M. N. Akhtar, D. A. Israf and A. Syahida (2012). "Cardamonin from *Alpinia rafflesiana* inhibits inflammatory responses in IFN- γ /LPS-stimulated BV2 microglia via NF- κ B signalling pathway." International Immunopharmacology **12**(4): 657-665.

Damião Mariana, C. F. C. B., F. M. Pasqualoto Kerly, K. Ferreira Adilson, F. Teixeira Sarah, A. Azevedo Ricardo, A. M. Barbuto José, F. Palace-Berl, C. Franchi-Junior Gilberto, E. Nowill Alexandre, T. Tavares Maurício and R. Parise-Filho (2014). "Novel Capsaicin Analogues as Potential Anticancer Agents: Synthesis, Biological Evaluation, and In Silico Approach." Archiv der Pharmazie **347**(12): 885-895.

De Spirt, S., A. Eckers, C. Wehrend, M. Micoogullari, H. Sies, W. Stahl and H. Steinbrenner (2016). "Interplay between the chalcone cardamonin and selenium in the biosynthesis of Nrf2-regulated antioxidant enzymes in intestinal Caco-2 cells." Free Radical Biology and Medicine **91**: 164-171.

Derita, M. and S. Zacchino (2011). "Chemotaxonomic importance of sesquiterpenes and flavonoids in five argentinian species of Polygonum Genus." Journal of Essential Oil Research **23**(5): 11-14.

Dinesha, S. Viveka, B. K. Priya, K. S. R. Pai, S. Naveen, N. K. Lokanath and G. K. Nagaraja (2015). "Synthesis and pharmacological evaluation of some new fluorine containing hydroxypyrazolines as potential anticancer and antioxidant agents." European Journal of Medicinal Chemistry **104**: 25-32.

Doan, P., A. Karjalainen, J. G. Chandraseelan, O. Sandberg, O. Yli-Harja, T. Rosholm, R. Franzen, N. R. Candeias and M. Kandhavelu (2016). "Synthesis and biological screening for cytotoxic activity of N-substituted indolines and morpholines." European Journal of Medicinal Chemistry **120**: 296-303.

Duan, Y.-C., Y.-Y. Guan, X.-Y. Zhai, L.-N. Ding, W.-P. Qin, D.-D. Shen, X.-Q. Liu, X.-D. Sun, Y.-C. Zheng and H.-M. Liu (2017). "Discovery of resveratrol derivatives as novel LSD1 inhibitors: Design, synthesis and their biological evaluation." European Journal of Medicinal Chemistry **126**: 246-258.

Ekman, S., M. W. Wynes and F. R. Hirsch (2012). "The mTOR Pathway in Lung Cancer and Implications for Therapy and Biomarker Analysis." Journal of Thoracic Oncology **7**(6): 947-953.

Fares, M., S. M. Abou-Seri, H. A. Abdel-Aziz, S. E. S. Abbas, M. M. Youssef and R. A. Eladwy (2014). "Synthesis and antitumor activity of pyrido [2,3-d]pyrimidine and pyrido[2,3-d] [1,2,4]triazolo[4,3-a]pyrimidine derivatives that induce apoptosis through G1 cell-cycle arrest." European Journal of Medicinal Chemistry **83**: 155-166.

Fu, Y., T.-c. Hsieh, J. Guo, J. Kunicki, M. Y. W. T. Lee, Z. Darzynkiewicz and J. M. Wu (2004). "Licochalcone-A, a novel flavonoid isolated from licorice root (*Glycyrrhiza glabra*), causes G2 and late-G1 arrests in androgen-independent PC-3 prostate cancer cells." Biochemical and Biophysical Research Communications **322**(1): 263-270.

Fusi, F., M. Cavalli, D. Mulholland, N. Crouch, P. Coombes, G. Dawson, S. Bova, G. Sgaragli and S. Saponara (2010). "Cardamonin is a bifunctional vasodilator that inhibits Cav1.2 current and stimulates KCa1.1 current in rat tail artery myocytes." Journal of Pharmacology and Experimental Therapeutics **332**(2): 531-540.

Gazdar, A. F., P. A. Bunn and J. D. Minna (2017). "Small-cell lung cancer: what we know, what we need to know and the path forward." Nature Reviews Cancer **17**: 725.

Gonçalves, C. J., A. S. Lenoir, P. Padaratz, R. Corrêa, R. Niero, V. Cechinel-Filho and F. d. Campos Buzzi (2012). "Benzofuranones as potential antinociceptive agents: Structure–activity relationships." European Journal of Medicinal Chemistry **56**: 120-126.

Gonçalves, L. M., I. M. Valente and J. A. Rodrigues (2014). "An overview on cardamonin." Journal of Medicinal Food **17**(6): 633-640.

He, W., Y. Jiang, X. Zhang, Y. Zhang, H. Ji and N. Zhang (2014). "Anticancer cardamonin analogs suppress the activation of NF-kappaB pathway in lung cancer cells." Molecular and Cellular Biochemistry **389**(1-2): 25-33.

He, Y. Q., Y. Liu, J. W. Zhang, J. Tang, J. Su, Y. Y. Li, Y. L. Lu, C. H. Wang, L. Yang and Z. T. Wang (2009). "Characterization of cardamonin metabolism by P450 in different species via HPLC-ESI-ion trap and UPLC-ESI-quadrupole mass spectrometry." Acta Pharmacologica Sinica **30**(10): 1462-1470.

Hemanth Kumar, K. and P. T. Perumal (2007). "A novel one-pot oxidative cyclization of 2'-amino and 2'-hydroxychalcones employing FeCl₃·6H₂O-methanol. Synthesis of 4-alkoxy-2-aryl-quinolines and flavones." Tetrahedron **63**(38): 9531-9535.

Herbst, R. S., D. Morgensztern and C. Boshoff (2018). "The biology and management of non-small cell lung cancer." Nature **553**: 446.

Holmes, D. (2011). "PI3K pathway inhibitors approach junction." Nature Reviews Drug Discovery **10**: 563.

Hodgson, J. (2001). "ADMET—turning chemicals into drugs." Nature Biotechnology **19**: 722.

Huang, D. P., J. H. C. Ho, Y. F. Poon, E. C. Chew, D. Saw, M. Lui, C. L. Li, L. S. Mak, S. H. Lai and W. H. Lau (1980). "Establishment of a cell line (NPC/HK1) from a differentiated squamous carcinoma of the nasopharynx." International Journal of Cancer **26**(2): 127-132.

Ichim, G. and S. W. G. Tait (2016). "A fate worse than death: apoptosis as an oncogenic process." Nature Reviews Cancer **16**(8): 539-548.

Ioffe BV (1968). "Characteristic frequencies in the infrared spectra of pyrazolines". Chemistry of Heterocyclic Compounds **4**: 791–793.

Itokawa, H., M. Morita, and S. Mihashi (1981). "Phenolic compounds from the rhizomes of *Alpinia speciosa*." Phytochemistry **20**: 2503-2506.

Jackman, D. M. and B. E. Johnson (2005). "Small-cell lung cancer." The Lancet **366**(9494): 1385-1396.

Jaipetch, T., S. Kanghae, O. Pancharoen, V. Patrick, V. Reutrakul, P. Tuntiwachwuttikul and A. White (1982). "Constituents of *Boesenbergia pandurata* (syn. *Kaempferia pandurata*): Isolation, Crystal Structure and Synthesis of (±)-Boesenbergin A." Australian Journal of Chemistry **35**(2): 351-361.

Jaiswal, S., A. Sharma, M. Shukla and J. Lal (2015). "Gender-related pharmacokinetics and bioavailability of a novel anticancer chalcone, cardamonin, in rats determined by liquid chromatography tandem mass spectrometry." Journal of Chromatography B: Analytical Technologies in the Biomedical and Life Sciences **986-987**: 23-30.

Jaiswal, S., M. Shukla, A. Sharma, N. Rangaraj, K. Vaghasiya, M. Y. Malik and J. Lal (2016). "Preclinical pharmacokinetics and ADME characterization of a novel anticancer chalcone, cardamonin." Drug Testing and Analysis. Article in Press.

Je, H. D. and J. H. Jeong (2016). "Cardamonin inhibits agonist-induced vascular contractility via Rho-kinase and mEK inhibition." Korean Journal of Physiology and Pharmacology **20**(1): 69-74.

Jeong, H.-S., H. Y. Choi, E.-R. Lee, J.-H. Kim, K. Jeon, H.-J. Lee and S.-G. Cho (2011). "Involvement of caspase-9 in autophagy-mediated cell survival pathway." Biochimica et Biophysica Acta (BBA) - Molecular Cell Research **1813**(1): 80-90.

Jia, D., W. Yang, L. Li, H. Liu, Y. Tan, S. Ooi, L. Chi, L. G. Filion, D. Figeys and L. Wang (2015). " β -Catenin and NF- κ B co-activation triggered by TLR3 stimulation facilitates stem cell-like phenotypes in breast cancer." Cell Death and Differentiation **22**(2): 298-310.

Kalanithi, M., M. Rajarajan, P. Tharmaraj and C. D. Sheela (2012). "Spectral, biological screening of metal chelates of chalcone based Schiff bases of N-(3-aminopropyl) imidazole." Spectrochimica Acta Part A: Molecular and Biomolecular Spectroscopy **87**: 155-162.

Kim, N.-Y., H.-O. Pae, G.-S. Oh, T.-H. Kang, Y.-C. Kim, H.-Y. Rhew and H.-T. Chung (2001). "Butein, a Plant Polyphenol, Induces Apoptosis Concomitant with Increased Caspase-3 Activity, Decreased Bcl-2 Expression and Increased Bax Expression in HL-60 Cells." Pharmacology & Toxicology **88**(5): 261-266.

Kim, S. M., N. Neuendorff, R. S. Chapkin and D. J. Earnest (2016). "Role of Inflammatory Signaling in the Differential Effects of Saturated and Polyunsaturated Fatty Acids on Peripheral Circadian Clocks." EBioMedicine **7**: 100-111.

Kim, Y. J., H. Ko, J. S. Park, I. H. Han, E. C. Amor, J. W. Lee and H. O. Yang (2010). "Dimethyl cardamonin inhibits lipopolysaccharide-induced inflammatory factors through blocking NF- κ B p65 activation." International Immunopharmacology **10**(9): 1127-1134.

Kim, Y. J., K. S. Kang, K. C. Choi and H. Ko (2015). "Cardamonin induces autophagy and an antiproliferative effect through JNK activation in human colorectal carcinoma HCT116 cells." Bioorganic and Medicinal Chemistry Letters **25**(12): 2559-2564.

Ko, H., Y. J. Kim, E. C. Amor, J. W. Lee, H. C. Kim, H. J. Kim and H. O. Yang (2011). "Induction of autophagy by dimethyl cardamonin is associated with proliferative arrest in human colorectal carcinoma HCT116 and LOVO cells." Journal of Cellular Biochemistry **112**(9): 2471-2479.

Koparal, A. T. and M. Zeytinoglu (2003). "Effects of Carvacrol on a Human Non-Small Cell Lung Cancer (NSCLC) Cell Line, A549." Cytotechnology **43**(1-3): 149-154.

Kuete, V., A. H. L. Nkuete, A. T. Mbaveng, B. Wiench, H. K. Wabo, P. Tane and T. Efferth (2014). "Cytotoxicity and modes of action of 4'-hydroxy-2',6'-dimethoxychalcone and other flavonoids toward drug-sensitive and multidrug-resistant cancer cell lines." Phytomedicine **21**(12): 1651-1657.

Kuo, L. J. and L.-X. Yang (2008). " γ -H2AX - A Novel Biomarker for DNA Double-strand Breaks." In Vivo **22**(3): 305-309.

Lee, J. H., S. J. Haeng, M. G. Phan, X. Jin, S. Lee, T. S. Phan, D. Lee, Y. S. Hong, K. Lee and J. L. Jung (2006). "Blockade of nuclear factor- κ B signaling pathway and anti-inflammatory activity of cardamomin, a chalcone analog from *Alpinia conchigera*." Journal of Pharmacology and Experimental Therapeutics **316**(1): 271-278.

Lee, M. Y., C. B. Seo, J. A. Lee, I. S. Shin, S. J. Kim, H. Ha and H. K. Shin (2012). "Alpinia katsumadai H AYATA seed extract inhibit LPS-induced inflammation by induction of heme oxygenase-1 in RAW264.7 cells." Inflammation **35**(2): 746-757.

Lee, S.-h., J.-s. Kim, K. Ravichandran, H.-W. Gil, H.-y. Song and S.-y. Hong (2015). "P-Glycoprotein Induction Ameliorates Colistin Induced Nephrotoxicity in Cultured Human Proximal Tubular Cells." PLOS ONE **10**(8): e0136075.

Li, C., Y. Zhang, Y. Lu, Z. Cui, M. Yu, S. Zhang and X. Xue (2011). "Evidence of the cross talk between Wnt and Notch signaling pathways in non-small-cell lung cancer (NSCLC): Notch3-siRNA weakens the effect of LiCl on the cell cycle of NSCLC cell lines." Journal of Cancer Research and Clinical Oncology **137**(5): 771-778.

Li, N., J. H. Liu, J. Zhang and B. Y. Yu (2008). "Comparative evaluation of cytotoxicity and antioxidative activity of 20 flavonoids." Journal of Agricultural and Food Chemistry **56**(10): 3876-3883.

Li, P., L. Zhou, T. Zhao, X. Liu, P. Zhang, Y. Liu, X. Zheng and Q. Li (2017). "Caspase-9: structure, mechanisms and clinical application." Oncotarget **8**(14): 23996-24008.

Li, Q., W. Ni, Z. Deng, M. Liu, L. She and Q. Xie (2017). "Targeting nasopharyngeal carcinoma by artesunate through inhibiting Akt/mTOR and inducing oxidative stress." Fundamental & Clinical Pharmacology **31**(3): 301-310.

Li, Y. Y., S. S. Huang, M. M. Lee, J. S. Deng and G. J. Huang (2015). "Anti-inflammatory activities of cardamonin from *Alpinia katsumadai* through heme oxygenase-1 induction and inhibition of NF- κ B and MAPK signaling pathway in the carrageenan-induced paw edema." International Immunopharmacology **25**(2): 332-339.

Liao, Q., D. H. Shi, W. Zheng, X. J. Xu and Y. H. Yu (2010). "Antiproliferation of cardamonin is involved in mTOR on aortic smooth muscle cells in high fructose-induced insulin resistance rats." European Journal of Pharmacology **641**(2-3): 179-186.

Lin, E., W. H. Lin, S. Y. Wang, C. S. Chen, J. W. Liao, H. W. Chang, S. C. Chen, K. Y. Lin, L. Wang, H. L. Yang and Y. C. Hseu (2012). "Flavokawain B inhibits growth of human squamous carcinoma cells: Involvement of apoptosis and cell cycle dysregulation in vitro and in vivo." Journal of Nutritional Biochemistry **23**(4): 368-378.

Liu, L., X. Chen and Z. Hu (2007). "Separation and determination of alpinetin and cardamonin in *Alpinia katsumadai* Hayata by flow injection-micellar electrokinetic chromatography." Talanta **71**(1): 155-159.

López, S. N., R. L. E. Furlan and S. A. Zacchino (2011). "Detection of antifungal compounds in *Polygonum ferrugineum* Wedd. extracts by bioassay-guided fractionation. Some evidences of their mode of action." Journal of Ethnopharmacology **138**(2): 633-636.

Loreto, C., G. La Rocca, R. Anzalone, R. Caltabiano, G. Vespasiani, S. Castorina, D. J. Ralph, S. Cellek, G. Musumeci, S. Giunta, R. Djinovic, D. Basic and S. Sansalone (2014). "The Role of Intrinsic Pathway in Apoptosis Activation and Progression in Peyronie's Disease." BioMed Research International **2014**: 10.

Lu, Q.-B., Q.-R. Zhang, N. Ou, C.-R. Wang and J. Warrington (2015). "In Vitro and In Vivo Studies of Non-Platinum-Based Halogenated Compounds as Potent Antitumor Agents for Natural Targeted Chemotherapy of Cancers." EBioMedicine **2**(6): 544-553.

Lu, S., C. Lin, X. Cheng, H. Hua, T. Xiang, Y. Huang and X. Huang (2018). "Cardamonin reduces chemotherapy resistance of coloncancer cells via the TSP50/NF- κ B pathway in vitro." Oncology Letters **15**(6): 9641-9646.

Mahapatra, D. K., S. K. Bharti and V. Asati (2015). "Anti-cancer chalcones: Structural and molecular target perspectives." European journal of medicinal chemistry **98**: 69-114.

Martí-Centelles, R., E. Falomir, J. Murga, M. Carda and J. A. Marco (2015). "Inhibitory effect of cytotoxic stilbenes related to resveratrol on the expression of the VEGF, hTERT and c-Myc genes." European Journal of Medicinal Chemistry **103**: 488-496.

Memon, A. H., Z. Ismail, A. F. A. Aisha, F. S. R. Al-Suede, M. S. R. Hamil, S. Hashim, M. A. A. Saeed, M. Laghari and A. M. S. Abdul Majid (2014). "Isolation, characterization, crystal structure elucidation, and anticancer study of dimethyl cardamonin, isolated from *Syzygium campanulatum* Korth." Evidence-based Complementary and Alternative Medicine **2014**.

Mi, X. G., Z. B. Song, L. G. Sun, Y. L. Bao, C. L. Yu, Y. Wu and Y. X. Li (2016). "Cardamonin inhibited cell viability and tumorigenesis partially through blockade of testes-specific protease 50-mediated nuclear factor-kappaB signaling pathway activation." International Journal of Biochemistry and Cell Biology **73**: 63-71.

National Cancer Institute (2014). "About Cancer." [ONLINE] Available at: <http://www.cancer.gov/about-cancer>. [Accessed 26 August 15].

Nandakumar, N., S. Muthuraman, P. Gopinath, P. Nithya, J. Gopas and R. S. Kumar (2017). "Synthesis of coumapherine derivatives: Their NF- κ B inhibitory effect, inhibition of cell migration and their cytotoxic activity." European Journal of Medicinal Chemistry **125**: 1076-1087.

Ndoile, M. M. and F. R. Van Heerden (2013). "Total synthesis of ochnaflavone." Beilstein Journal of Organic Chemistry **9**: 1346-1351.

Nesello, L. A. N., A. Campos, T. Wagner, A. S. Feliciano, F. De Campos Buzzi and V. C. Filho (2016). "Chemical Composition and Antinociceptive Potential of *Campomanesia reitziana* Fruits." Journal of Medicinal Food **19**(5): 518-520.

Newman, D. J. and G. M. Cragg (2016). "Natural Products as Sources of New Drugs from 1981 to 2014." Journal of Natural Products **79**(3): 629-661.

Niu, P. G., Y. X. Zhang, D. H. Shi, Y. Liu, Y. Y. Chen and J. Deng (2015). "Cardamonin inhibits metastasis of Lewis lung carcinoma cells by decreasing mTOR activity." PLoS ONE **10**(5).

Niu, P. G., Y. X. Zhang, D. H. Shi, Y. Liu, Y. Y. Chen and J. Deng (2015). "Cardamonin inhibits metastasis of Lewis lung carcinoma cells by decreasing mTOR activity." PLoS ONE **10**(5).

Niu, P., Y. Zhang, D. Shi, Y. Chen and J. Deng (2013). "Cardamonin ameliorates insulin resistance induced by high insulin and high glucose through the mTOR and signal pathway." Planta Medica **79**(6): 452-458.

Nomura, M., T. Takahashi, A. Uesugi, R. Tanaka and S. Kobayashi (2008). "Inotodiol, a lanostane triterpenoid, from *Inonotus obliquus* inhibits cell proliferation through caspase-3-dependent apoptosis." Anticancer Research **28**(5 A): 2691-2696.

Nwet, N. W., S. Awale, H. Esumi, Y. Tezuka and S. Kadota (2007). "Bioactive secondary metabolites from *Boesenbergia pandurata* of Myanmar and their preferential cytotoxicity against human pancreatic cancer PANC-1 cell line in nutrient-deprived medium." Journal of Natural Products **70**(10): 1582-1587.

Orlikova, B., D. Tasdemir, F. Golais, M. Dicato and M. Diederich (2011). "Dietary chalcones with chemopreventive and chemotherapeutic potential." Genes and Nutrition **6**(2): 125-147.

Oronsky, B., T. R. Reid, A. Oronsky and C. A. Carter (2017). "What's New in SCLC? A Review." Neoplasia (New York, N.Y.) **19**(10): 842-847.

Park, M. K., H. J. Lee, J. K. Choi, H. J. Kim, J. H. Kang, E. J. Lee, Y. R. Kim, J. H. Kang, J. K. Yoo, H. Y. Cho, J. K. Kim, C. H. Kim, J. H. Park and C. H. Lee (2014). "Novel anti-nociceptive effects of cardamonin via blocking expression of cyclooxygenase-2 and transglutaminase-2." Pharmacology Biochemistry and Behavior **118**: 10-15.

Park, S., J. Gwak, S. J. Han and S. Oh (2013). "Cardamonin suppresses the proliferation of colon cancer cells by promoting β -catenin degradation." Biological and Pharmaceutical Bulletin **36**(6): 1040-1044.

Pascoal, A., C. Ehrenfried, B. Lopez, T. de Araujo, V. Pascoal, R. Gilioli, G. Anhê, A. Ruiz, J. Carvalho, M. Stefanello and M. Salvador (2014). "Antiproliferative Activity and Induction of Apoptosis in PC-3 Cells by the Chalcone Cardamonin from *Campomanesia adamantium* (Myrtaceae) in a Bioactivity-Guided Study." Molecules **19**(2): 1843.

Pastorino, U. (2010). "Lung cancer screening." British Journal Of Cancer **102**: 1681.

Piazza, G. A., A. B. Keeton, H. N. Tinsley, B. D. Gary, J. D. Whitt, B. Mathew, J. Thaiparambil, L. Coward, G. Gorman, Y. Li, B. Sani, J. V. Hobrath, Y. Y. Maxuitenko and R. C. Reynolds (2009). "A Novel Sulindac Derivative That Does Not Inhibit Cyclooxygenases but Potently Inhibits Colon Tumor Cell Growth and Induces Apoptosis with Antitumor Activity." Cancer Prevention Research **2**(6): 572.

Porta, C., C. Paglino and A. Mosca (2014). "Targeting PI3K/Akt/mTOR Signaling in Cancer." Frontiers in Oncology **4**: 64.

Qin, Y., C. Y. Sun, F. R. Lu, X. R. Shu, D. Yang, L. Chen, X. M. She, N. M. Gregg, T. Guo and Y. Hu (2012). "Cardamonin exerts potent activity against multiple myeloma through blockade of NF- κ B pathway in vitro." Leukemia Research **36**(4): 514-520.

Qiu, J., B. Zhao, Y. Shen, W. Chen, Y. Ma and Y. Shen (2013). "A novel p-terphenyl derivative inducing cell-cycle arrest and apoptosis in MDA-MB-435 cells through topoisomerase inhibition." European Journal of Medicinal Chemistry **68**(Supplement C): 192-202.

Raman, N., S. Ravichandran and C. Thangaraja (2004). "Copper(II), cobalt(II), nickel(II) and zinc(II) complexes of Schiff base derived from benzil-2,4-dinitrophenylhydrazone with aniline." Journal of Chemical Sciences **116**(4): 215-219.

Rao, Y. K., T.-Y. Kao, J.-L. Ko and Y.-M. Tzeng (2010). "Chalcone HTMC causes in vitro selective cytotoxicity, cell-cycle G1 phase arrest through p53-dependent pathway in human lung adenocarcinoma A549 cells, and in vivo tumor growth suppression." Bioorganic & Medicinal Chemistry Letters **20**(22): 6508-6512.

Ravanan, P., R. Sano, P. Talwar, S. Ogasawara, S.-i. Matsuzawa, M. Cuddy, S. K. Singh, G. S. R. S. Rao, P. Kondaiah and J. C. Reed (2011). "Synthetic Triterpenoid Cyano Enone of Methyl Boswellate Activates Intrinsic, Extrinsic, and Endoplasmic Reticulum Stress Cell Death Pathways in Tumor Cell Lines." Molecular Cancer Therapeutics **10**(9): 1635.

Ren, G., A. Sun, C. Deng, J. Zhang, X. Wu, X. Wei, S. Mani, W. Dou and Z. Wang (2015). "The anti-inflammatory effect and potential mechanism of cardamonin in DSS-induced colitis." American Journal of Physiology - Gastrointestinal and Liver Physiology **309**(7): G517-G527.

Rodrigues, T., D. Reker, P. Schneider and G. Schneider (2016). "Counting on natural products for drug design." Nature Chemistry **8**: 531.

Ruiz, C., M. Haddad, J. Alban, G. Bourdy, R. Reategui, D. Castillo, M. Sauvain, E. Deharo, Y. Estevez, J. Arevalo and R. Rojas (2011). "Activity-guided isolation of antileishmanial compounds from *Piper hispidum*." Phytochemistry Letters **4**(3): 363-366.

Sambasevam, Y., A. A. Omar Farouk, T. A. S. Tengku Mohamad, M. R. Sulaiman, B. H. Bharatham and E. K. Perimal (2017). "Cardamonin attenuates hyperalgesia and allodynia in a mouse model of chronic constriction injury-induced neuropathic pain: Possible involvement of the opioid system." European Journal of Pharmacology **796**: 32-38.

Shen, H., W. Gao, Y.-j. Wu, H.-r. Qiu and Y.-q. Shu (2009). "Multicolor fluorescence in situ hybridization and comparative genomic hybridization reveal molecular events in lung adenocarcinomas and squamous cell lung carcinomas." Biomedicine & Pharmacotherapy **63**(6): 396-403.

Shi, D., Y. Zhu, P. Niu, J. Zhou and H. Chen (2018). "Raptor mediates the antiproliferation of cardamonin by mTORC1 inhibition in SKOV3 cells." OncoTargets and Therapy **11**: 757-767.

Shigeta, S., S. Mori, F. Watanabe, K. Takahashi, T. Nagata, N. Koike, T. Wakayama and M. Saneyoshi (2002). "Synthesis and Antiherpesvirus Activities of 5-Alkyl-2-

Thiopyrimidine Nucleoside Analogues." Antiviral Chemistry and Chemotherapy **13**(2): 67-82.

Shrivastava, S., M. K. Jeengar, D. Thummuri, A. Koval, V. L. Katanaev, S. Marepally and V. G. M. Naidu (2017). "Cardamonin, a chalcone, inhibits human triple negative breast cancer cell invasiveness by downregulation of Wnt/ β -catenin signaling cascades and reversal of epithelial–mesenchymal transition." BioFactors **43**(2): 152-169.

Simirgiotis, M. J., S. Adachi, S. To, H. Yang, K. A. Reynertson, M. J. Basile, R. R. Gil, I. B. Weinstein and E. J. Kennelly (2008). "Cytotoxic chalcones and antioxidants from the fruits of *Syzygium samarangense* (Wax Jambu)." Food Chemistry **107**(2): 813-819.

Song, L. L., J. W. Kosmeder II, S. K. Lee, C. Gerhäuser, D. Lantvit, R. C. Moon, R. M. Moriarty and J. M. Pezzuto (1999). "Cancer chemopreventive activity mediated by 4'-bromoflavone, a potent inducer of phase II detoxification enzymes." Cancer Research **59**(3): 578-585.

Strong, M. J., M. Baddoo, A. Nanbo, M. Xu, A. Puetter and Z. Lin (2014). "Comprehensive High-Throughput RNA Sequencing Analysis Reveals Contamination of Multiple Nasopharyngeal Carcinoma Cell Lines with HeLa Cell Genomes." Journal of Virology **88**(18): 10696-10704.

Su, X. H., C. Y. Li, Y. J. Zhong, Z. P. Yuan, Y. F. Li and B. Liang (2012). "A new prenylated chalcone from the seeds of *Millettia pachycarpa*." Chinese Journal of Natural Medicines **10**(3): 222-225.

Sukari, M. A., A. Y. L. Ching, G. E. C. Lian, M. Rahmani and K. Khalid (2007). "Cytotoxic constituents from *Boesenbergia pandurata* (Roxb.) Schltr." Natural Product Sciences **13**(2): 110-113.

Tabata, K., K. Motani, N. Takayanagi, R. Nishimura, S. Asami, Y. Kimura, M. Ukiya, D. Hasegawa, T. Akihisa and T. Suzuki (2005). "Xanthoangelol, a Major Chalcone Constituent of *Angelica keiskei*, Induces Apoptosis in Neuroblastoma and Leukemia Cells." Biological and Pharmaceutical Bulletin **28**(8): 1404-1407.

Szychowski, K. A., M. L. Leja, D. V. Kaminsky, A. P. Kryshchyshyn, U. E. Binduga, O. R. Pinyazhko, R. B. Lesyk, J. Tobiasz and J. Gmiński (2017). "Anticancer properties of 4-thiazolidinone derivatives depend on peroxisome proliferator-activated receptor gamma (PPAR γ)." European Journal of Medicinal Chemistry **141**: 162-168.

Tang, Y., Q. Fang, D. Shi, P. Niu, Y. Chen and J. Deng (2014). "MTOR inhibition of cardamonin on antiproliferation of A549 cells is involved in a FKBP12 independent fashion." Life Sciences **99**(1-2): 44-51.

Tewtrakul, S., S. Subhadhirasakul, C. Karalai, C. Ponglimanont and S. Cheenpracha (2009). "Anti-inflammatory effects of compounds from *Kaempferia parviflora* and *Boesenbergia pandurata*." Food Chemistry **115**(2): 534-538.

Tran, T. D., T. T. Nguyen, T. H. Do, T. N. Huynh, C. D. Tran and K. M. Thai (2012). "Synthesis and antibacterial activity of some heterocyclic chalcone analogues alone and in combination with antibiotics." Molecules (Basel, Switzerland) **17**(6): 6684-6696.

Valasani, K. R., G. Hu, M. O. Chaney and S. S. Yan (2013). "Structure-Based Design and Synthesis of Benzothiazole Phosphonate Analogues with Inhibitors of Human ABAD-A β for Treatment of Alzheimer's Disease." Chemical Biology and Drug Design **81**(2): 238-249.

Vandenabeele, P., T. Vanden Berghe and N. Festjens (2006). "Caspase Inhibitors Promote Alternative Cell Death Pathways." Science's STKE **2006**(358): pe44.

Vik, A., Á. Proszenyák, M. Vermeersch, P. Cos, L. Maes and L. L. Gundersen (2009). "Screening of agelasine D and analogs for inhibitory activity against pathogenic protozoa; identification of hits for visceral leishmaniasis and Chagas disease." Molecules **14**(1): 279-288.

Wang, M.-H., R. Sun, X.-M. Zhou, M.-Y. Zhang, J.-B. Lu, Y. Yang, L.-S. Zeng, X.-Z. Yang, L. Shi, R.-W. Xiao, H.-Y. Wang and S.-J. Mai (2018). "Epithelial cell adhesion molecule overexpression regulates epithelial-mesenchymal transition, stemness and metastasis of nasopharyngeal carcinoma cells via the PTEN/AKT/mTOR pathway." Cell Death & Disease **9**(1): 2.

Wang, J., D. Yun, J. Yao, W. Fu, F. Huang, L. Chen, T. Wei, C. Yu, H. Xu, X. Zhou, Y. Huang, J. Wu, P. Qiu and W. Li (2018). "Design, synthesis and QSAR study of novel isatin analogues inspired Michael acceptor as potential anticancer compounds." European Journal of Medicinal Chemistry **144**: 493-503.

Wang, S., C. Zhai, Y. Zhang, Y. Yu, Y. Zhang, M. Lianghui, S. Li and Y. Qiao (2016). "Cardamonin, a novel antagonist of hTRPA1 cation channel, reveals therapeutic mechanism of pathological pain." Molecules **21**(9).

Wang, S., L. Zhou, W. He and Z. Hu (2007). "Separation and determination of alpinetin and cardamonin by reverse micelle electrokinetic capillary chromatography." Journal of Pharmaceutical and Biomedical Analysis **43**(4): 1557-1561.

Wang, W., Q. Wen, L. Xu, G. Xie, J. Li, J. Luo, S. Chu, L. Shi, D. Huang, J. Li and S. Fan (2014). "Activation of Akt/mTOR Pathway Is Associated with Poor Prognosis of Nasopharyngeal Carcinoma." PLOS ONE **9**(8): e106098.

Wang, Z. T., C. W. Lau, F. L. Chan, X. Yao, Z. Y. Chen, Z. D. He and Y. Huang (2001). "Vasorelaxant effects of cardamonin and alpinetin from *Alpinia henryi* K. Schum." Journal of Cardiovascular Pharmacology **37**(5): 596-606.

Wasil, L. R., L. Wei, C. Chang, L. Lan and K. H. Y. Shair (2015). "Regulation of DNA Damage Signaling and Cell Death Responses by Epstein-Barr Virus Latent Membrane Protein 1 (LMP1) and LMP2A in Nasopharyngeal Carcinoma Cells." Journal of Virology **89**(15): 7612-7624.

Wei, W. I. and J. S. T. Sham (2005). "Nasopharyngeal carcinoma." The Lancet **365**(9476): 2041-2054.

Wei, Z., J. Yang, Y. F. Xia, W. Z. Huang, Z. T. Wang and Y. Dai (2012). "Cardamonin protects septic mice from acute lung injury by preventing endothelial barrier dysfunction." Journal of Biochemical and Molecular Toxicology **26**(7): 282-290.

World Health Organization (2017). "Cancer". [ONLINE] Available at: <http://www.who.int/mediacentre/factsheets/fs297/en/>. [Accessed 2 January 2018].

Wu, N., J. Liu, X. Zhao, Z. Yan, B. Jiang, L. Wang, S. Cao, D. Shi and X. Lin (2015). "Cardamonin induces apoptosis by suppressing STAT3 signaling pathway in glioblastoma stem cells." Tumor Biology **36**(12): 9667-9676.

Xiao, X., X. Si, X. Tong and G. Li (2011). "Preparation of flavonoids and diarylheptanoid from *Alpinia katsumadai* Hayata by microwave-assisted extraction and high-speed counter-current chromatography." Separation and Purification Technology **81**(3): 265-269.

Xue, Z. G., P. G. Niu, D. H. Shi, Y. Liu, J. Deng and Y. Y. Chen (2015). "Cardamonin Inhibits Angiogenesis by mTOR Downregulation in SKOV3 Cells." Planta Medica **82**(1-2): 70-75.

Yadav, V. R., S. Prasad, B. Sung and B. B. Aggarwal (2011). "The role of chalcones in suppression of NF- κ B-mediated inflammation and cancer." International Immunopharmacology **11**(3): 295-309.

Yamamoto, N., K. Kawabata, K. Sawada, M. Ueda, I. Fukuda, K. Kawasaki, A. Murakami and H. Ashida (2011). "Cardamonin stimulates glucose uptake through translocation of glucose transporter-4 in L6 myotubes." Phytotherapy Research **25**(8): 1218-1224.

Yang, C., J. Peng, W. Jiang, Y. Zhang, X. Chen, X. Wu, Y. Zhu, H. Zhang, J. Chen, J. Wang, W. C. S. Cho and K. Jin (2013). "mTOR activation in immature cells of primary nasopharyngeal carcinoma and anti-tumor effect of rapamycin in vitro and in vivo." Cancer Letters **341**(2): 186-194.

- Yap, V. A., M. E. Qazzaz, V. J. Raja, T. D. Bradshaw, H. S. Loh, K. S. Sim, K. T. Yong, Y. Y. Low and K. H. Lim (2016). "Fistulopsines A and B antiproliferative septicine-type alkaloids from *Ficus fistulosa*." Phytochemistry Letters **15**: 136-141.
- Ye, H., A. Fu, W. Wu, Y. Li, G. Wang, M. Tang, S. Li, S. He, S. Zhong, H. Lai, J. Yang, M. Xiang, A. Peng and L. Chen (2012). "Cytotoxic and apoptotic effects of constituents from *Millettia pachycarpa* Benth." Fitoterapia **83**(8): 1402-1408.
- Yit, C. C. and N. P. Das (1994). "Cytotoxic effect of butein on human colon adenocarcinoma cell proliferation." Cancer Letters **82**(1): 65-72.
- Yu, W. G., H. He, J. Y. Yao, Y. X. Zhu and Y. H. Lu (2015). "Dimethyl cardamonin exhibits anti-inflammatory effects via interfering with the PI3K-PDK1-PKC α signaling pathway." Biomolecules and Therapeutics **23**(6): 549-556.
- Zambare, A. S., J. N. Sangshetti, N. D. Kokare and D. B. Shinde (2009). "Development of mild and efficient method for synthesis of substituted flavones using oxalic acid catalyst." Chinese Chemical Letters **20**(2): 171-174.
- Zappa, C. and S. A. Mousa (2016). "Non-small cell lung cancer: current treatment and future advances." Translational Lung Cancer Research **5**(3): 288-300.

Zhang, E.-H., R.-F. Wang, S.-Z. Guo and B. Liu (2013). "An Update on Antitumor Activity of Naturally Occurring Chalcones." Evidence-Based Complementary and Alternative Medicine **2013**: 22.

Zhang, J., S. Sikka, K. S. Siveen, J. H. Lee, J. Y. Um, A. P. Kumar, A. Chinnathambi, S. A. Alharbi, Basappa, K. S. Rangappa, G. Sethi and K. S. Ahn (2017). "Cardamonin represses proliferation, invasion, and causes apoptosis through the modulation of signal transducer and activator of transcription 3 pathway in prostate cancer." Apoptosis **22**(1): 158-168.

Zhang, Q., A. Myint, H. Cui, X. Ge, L. Liu and G. Chou (2005). "Determination of cardamonin using a chemiluminescent flow-injection method." Phytochemical Analysis **16**(6): 440-445.

Zhao, Y. F., H. T. Lü and L. B. Xu (2017). "Rapid Analysis of Alpinetin and Cardamonin in *Alpinia katsumadai* Hayata Using Short-End Injection Microemulsion Electrokinetic Capillary Chromatography Combined with Microwave-Assisted Extraction." Chromatographia **80**(2): 347-352.

Zheng, W., D. Shi, X. Ji, Y. Han and Q. Liao (2010). "Antiproliferation of cardamonin associated with mRNA expression of mTOR, Raptor and Rictor." Zhongguo Zhongyao Zazhi **35**(17): 2318-2323.

Zhu, J. T. T., R. C. Y. Choi, G. K. Y. Chu, A. W. H. Cheung, Q. T. Gao, J. Li, Z. Y. Jiang, T. T. X. Dong and K. W. K. Tsim (2007). "Flavonoids possess neuroprotective effects on cultured pheochromocytoma PC12 cells: A comparison of different flavonoids in activating estrogenic effect and in preventing β -amyloid-induced cell death." Journal of Agricultural and Food Chemistry **55**(6): 2438-2445.

Zi, X. and A. R. Simoneau (2005). "Flavokawain A, a Novel Chalcone from Kava Extract, Induces Apoptosis in Bladder Cancer Cells by Involvement of Bax Protein-Dependent and Mitochondria-Dependent Apoptotic Pathway and Suppresses Tumor Growth in Mice." Cancer Research **65**(8): 3479-3486.

8 Appendix

8.1 HPLC Chromatograms

(Early solvent peaks were removed for clarity purposes)

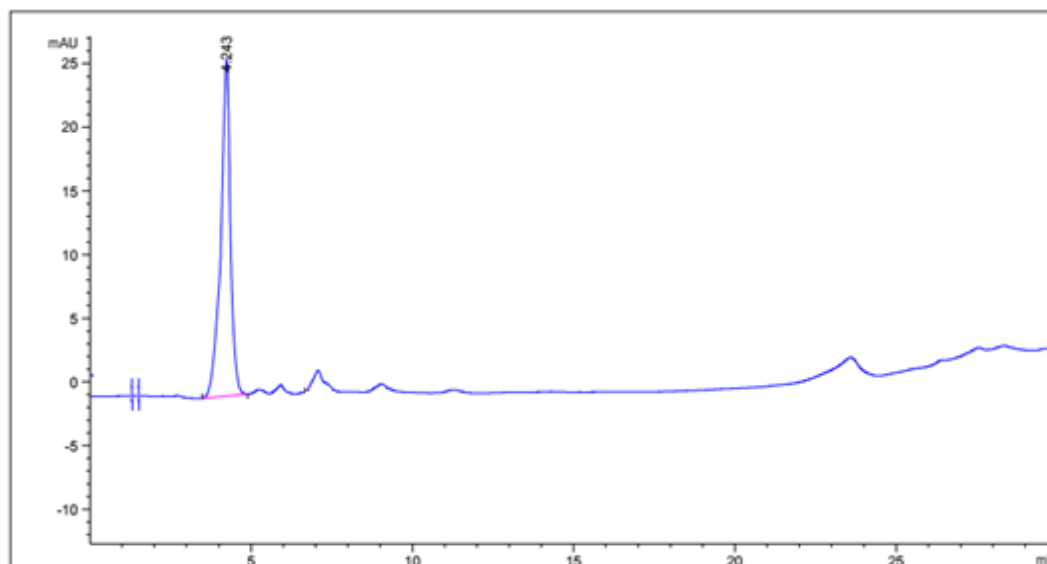


Figure 8.1 HPLC chromatogram of **1**

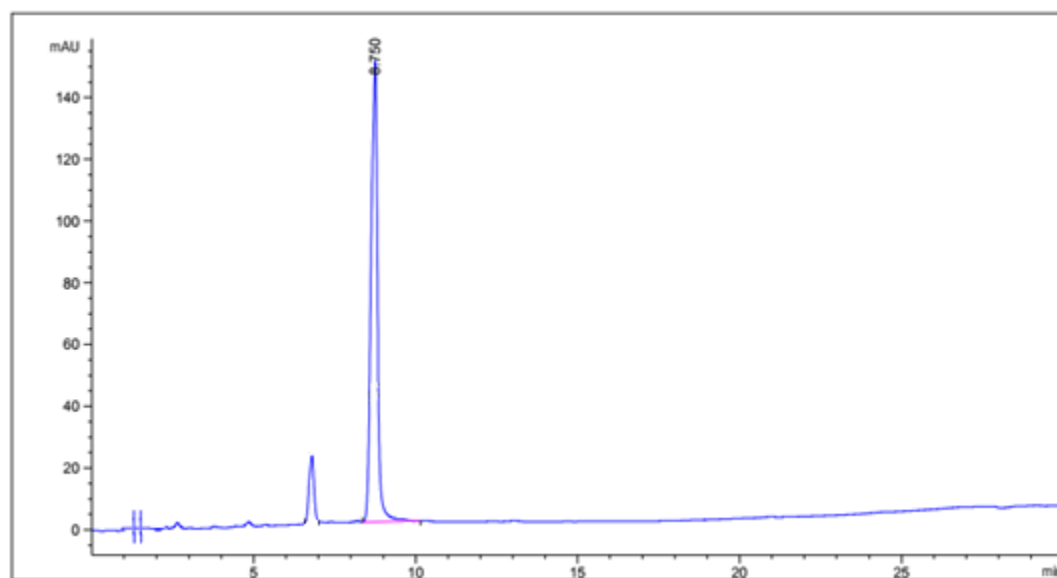


Figure 8.2 HPLC chromatogram of **2**

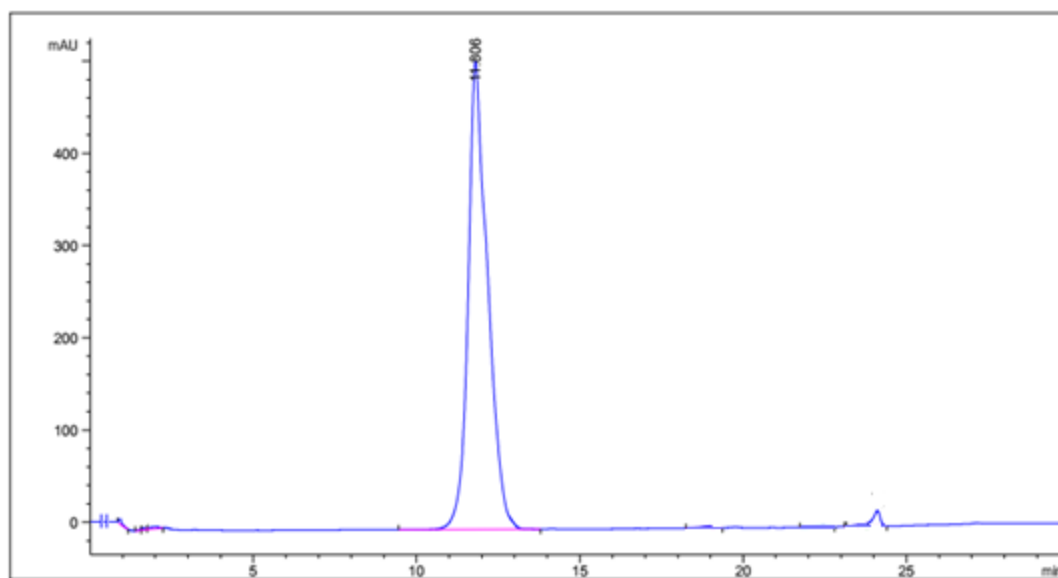


Figure 8.3 HPLC chromatogram of **3**

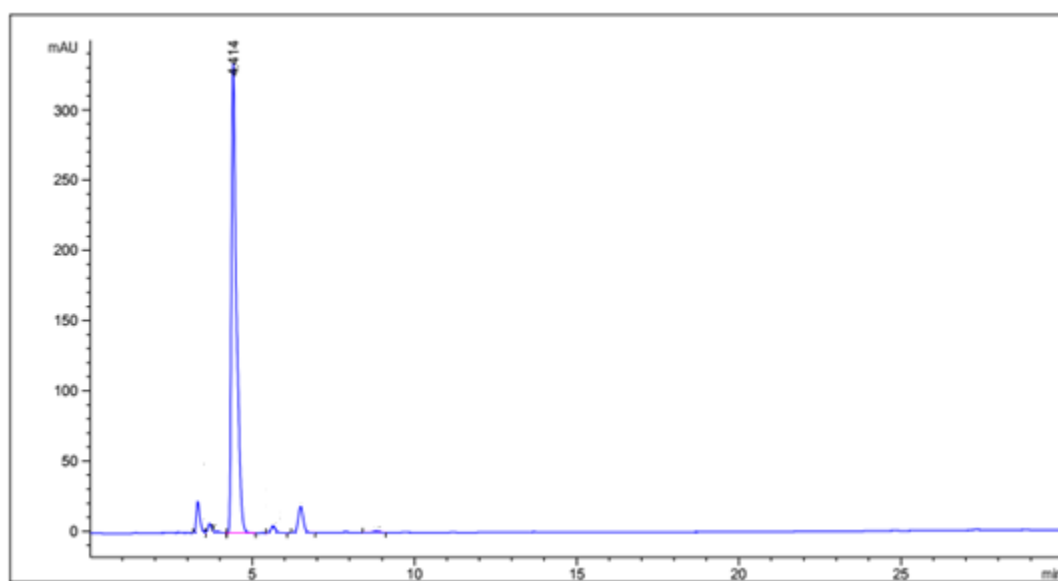


Figure 8.4 HPLC chromatogram of **4**

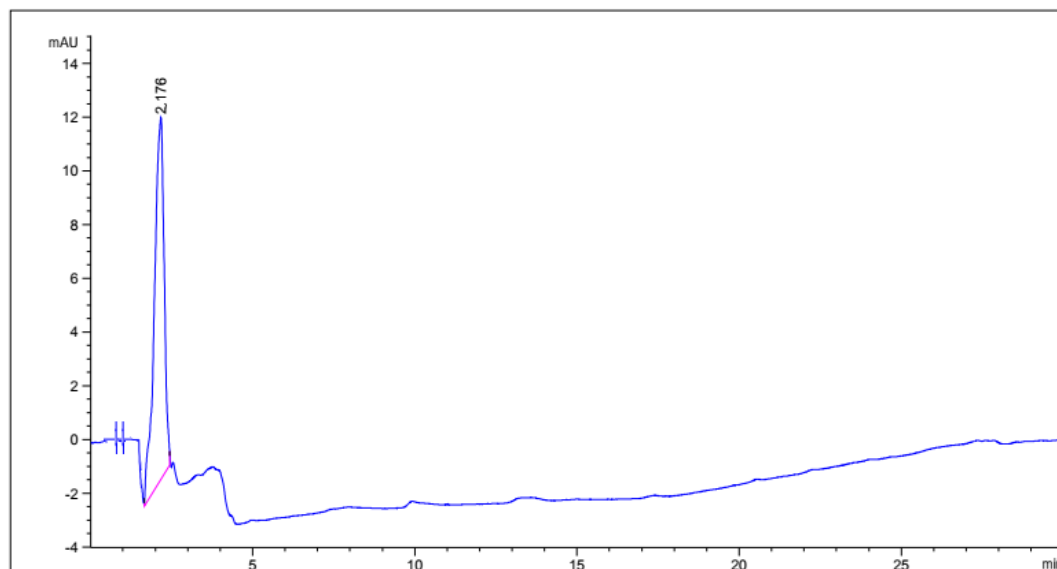


Figure 8.5 HPLC chromatogram of **5**

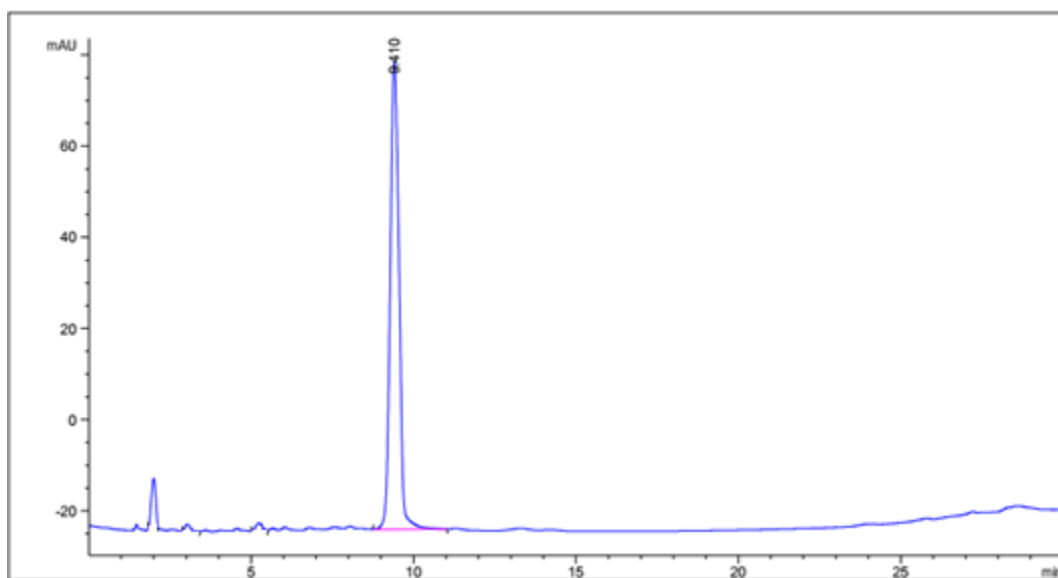


Figure 8.6 HPLC chromatogram of **6**

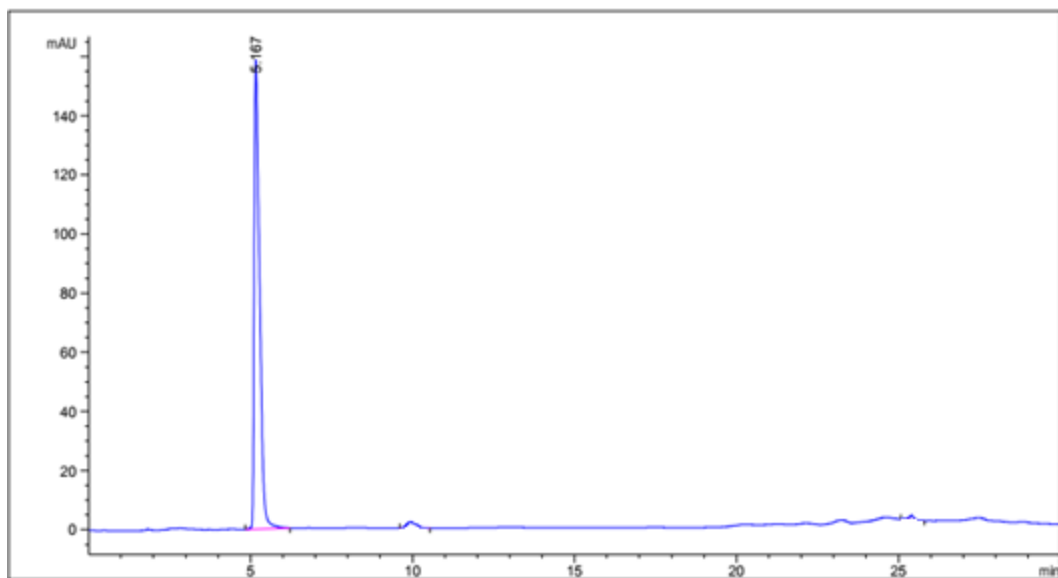


Figure 8.7 HPLC chromatogram of **7**

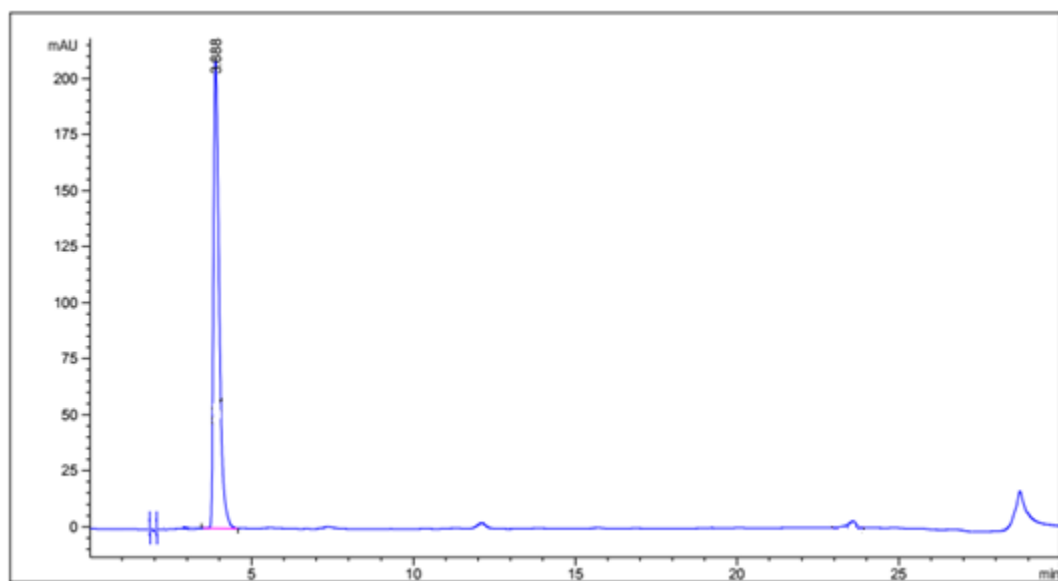


Figure 8.8 HPLC chromatogram of **8**

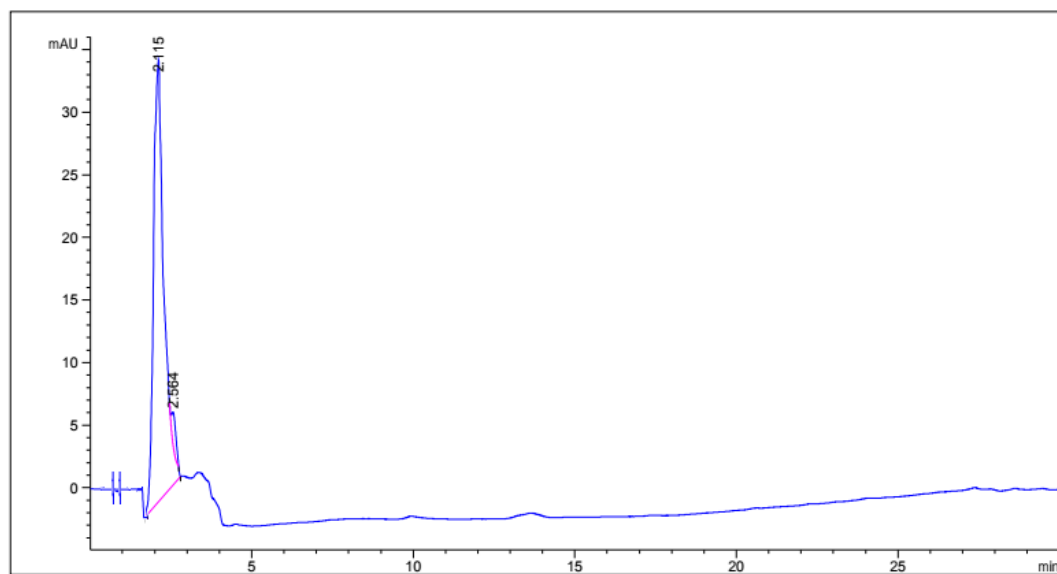


Figure 8.9 HPLC chromatogram of **9**

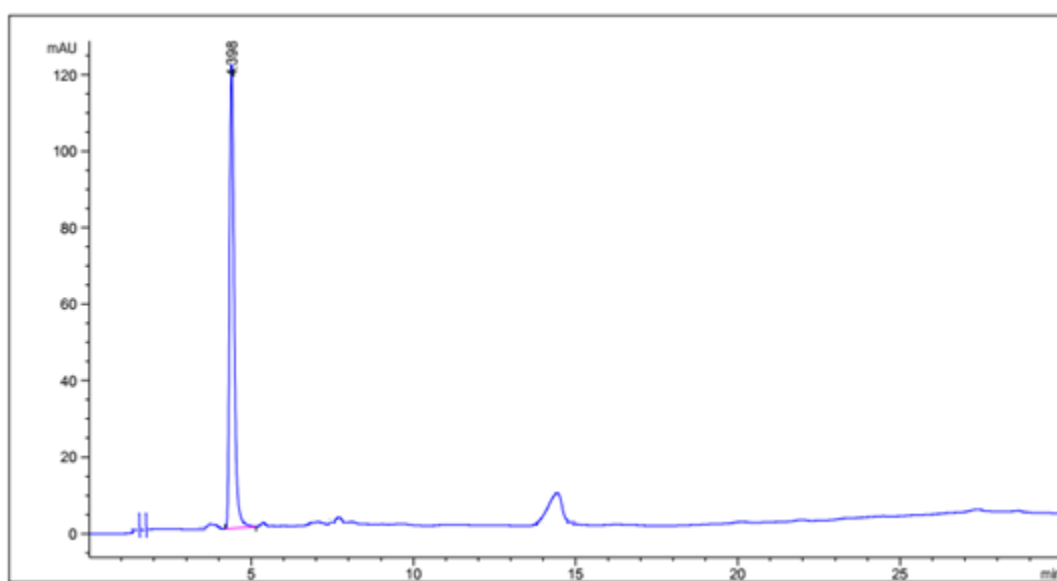


Figure 8.10 HPLC chromatogram of **10**

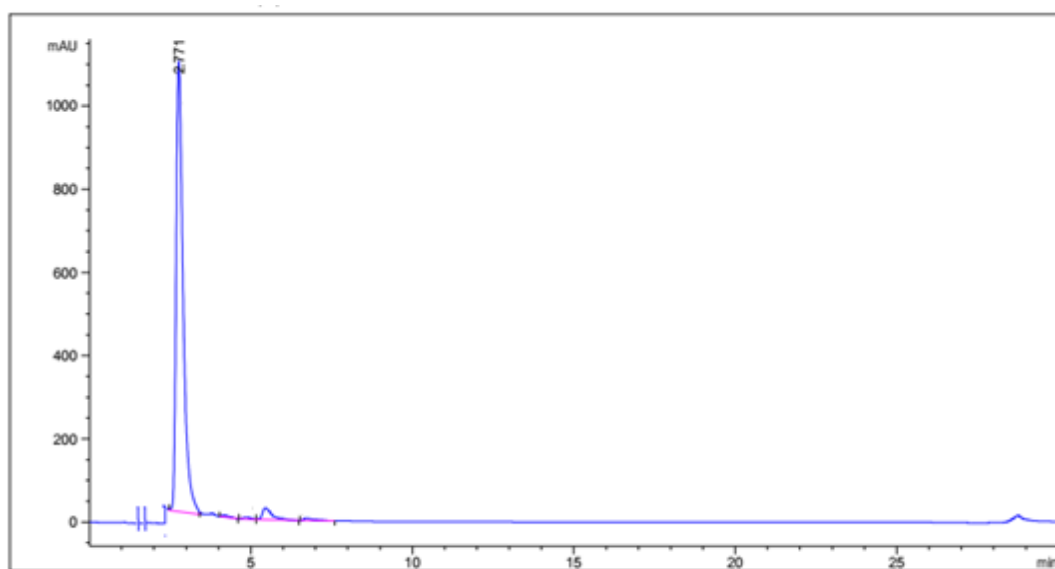


Figure 8.11 HPLC chromatogram of **11**

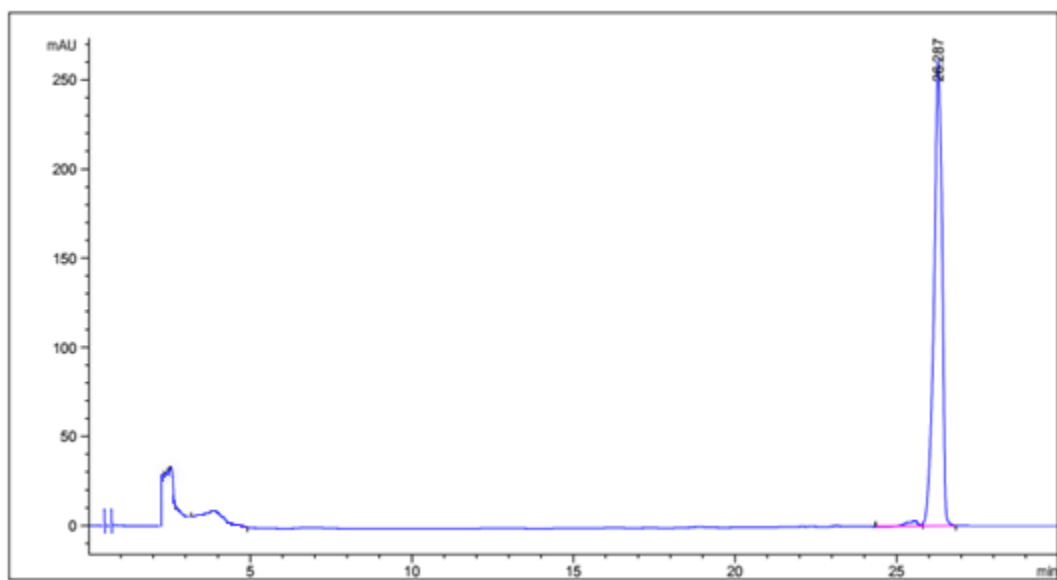


Figure 8.12 HPLC chromatogram of **12**

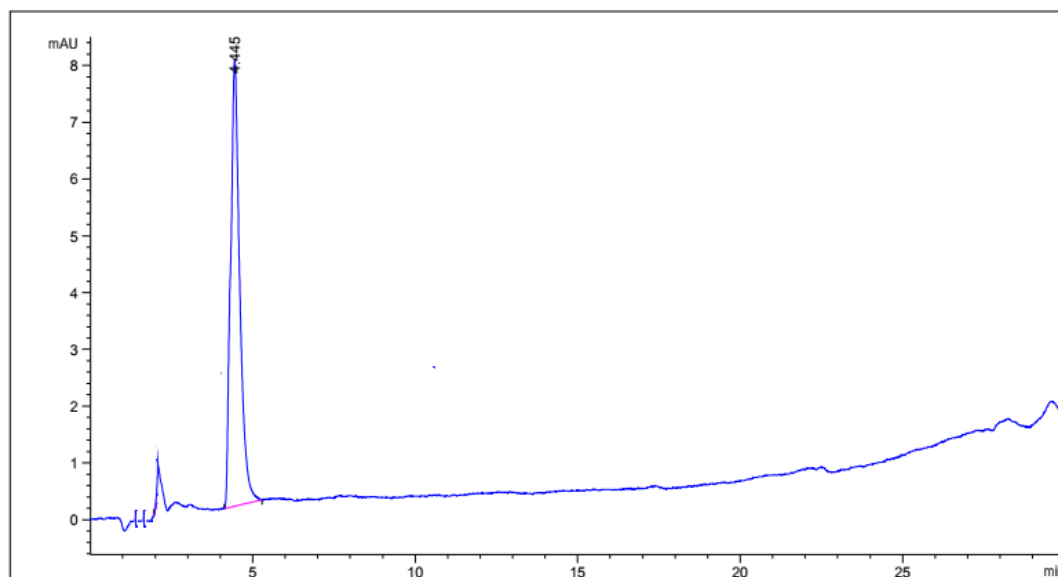


Figure 8.13 HPLC chromatogram of **13**

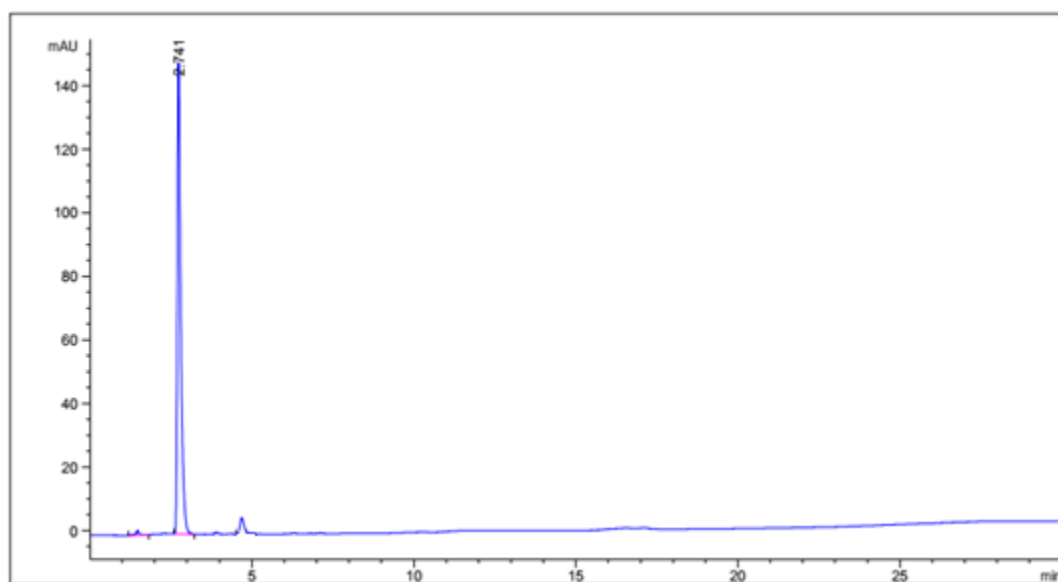


Figure 8.14 HPLC chromatogram of **14**

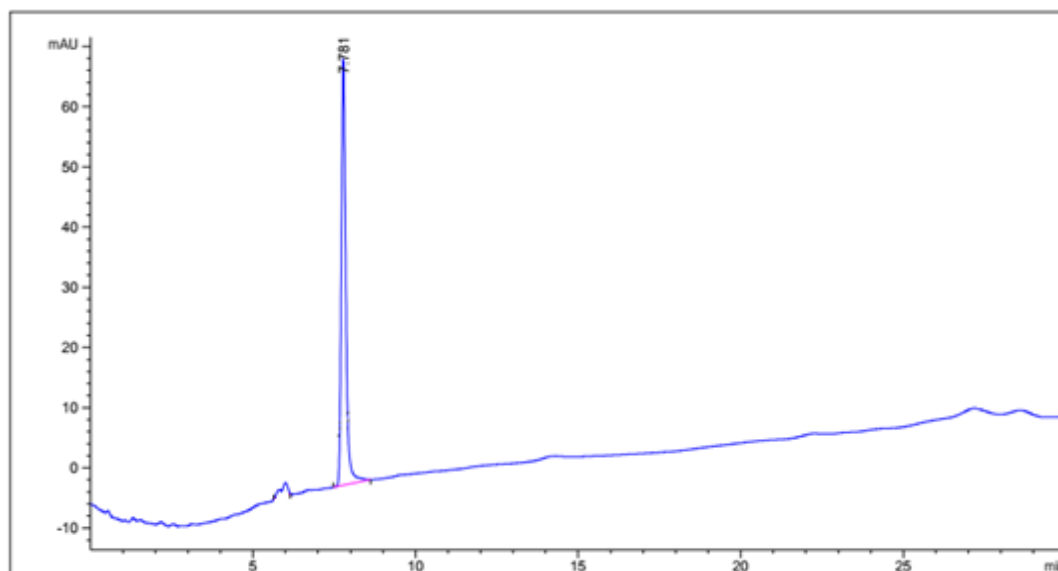


Figure 8.15 HPLC chromatogram of **15**

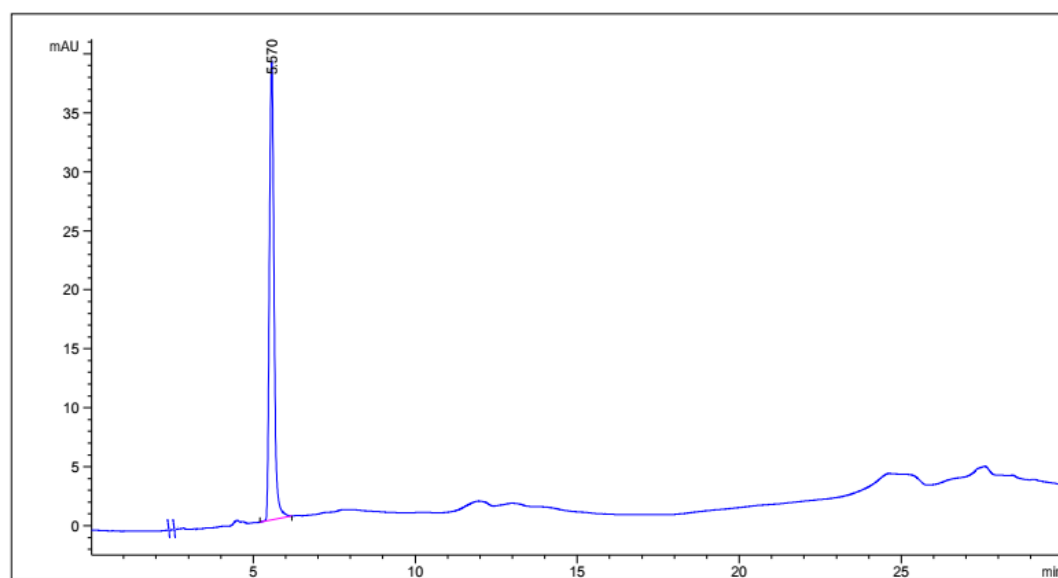


Figure 8.16 HPLC chromatogram of **16**

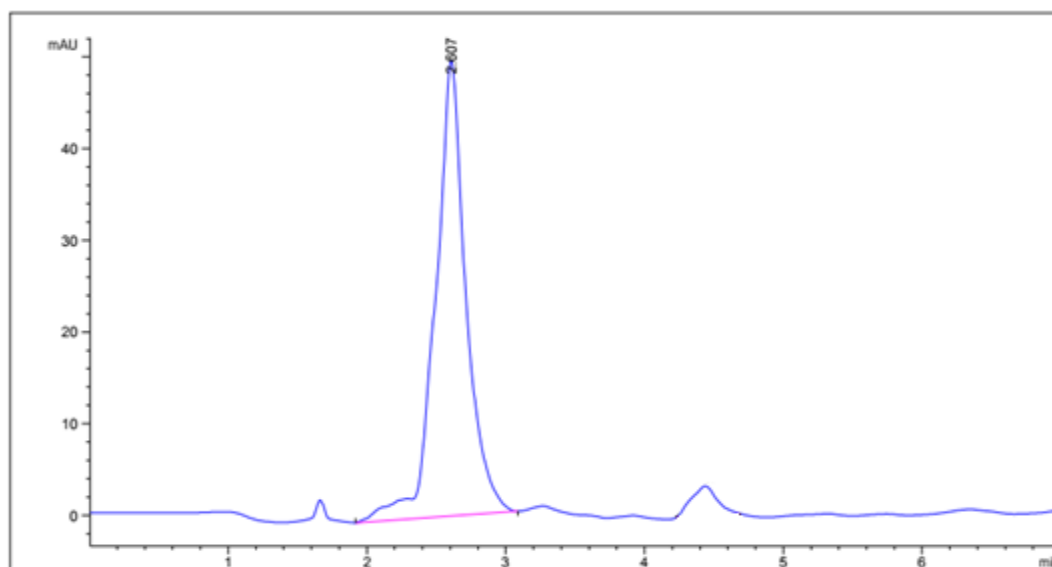


Figure 8.17 HPLC chromatogram of **17**

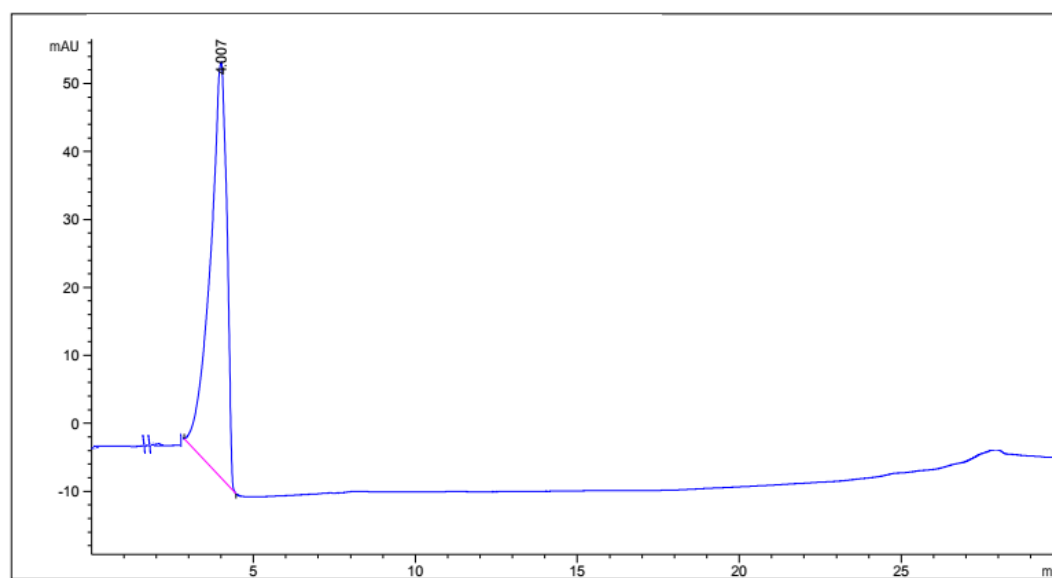


Figure 8.18 HPLC chromatogram of **18**

8.2 IR Spectra

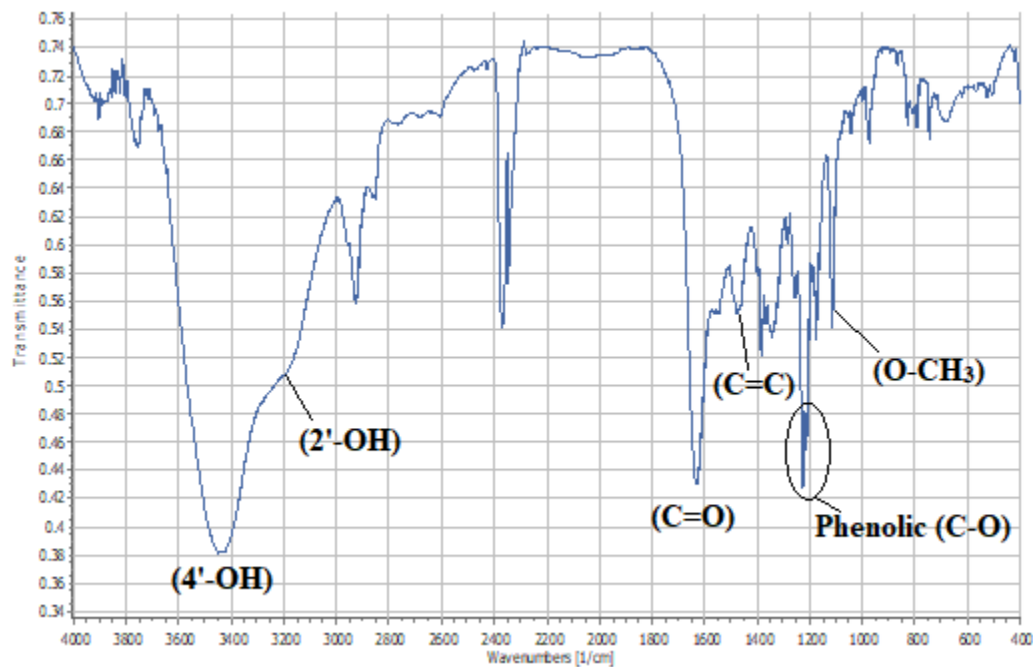


Figure 8.19 IR spectrum of Cardamomin

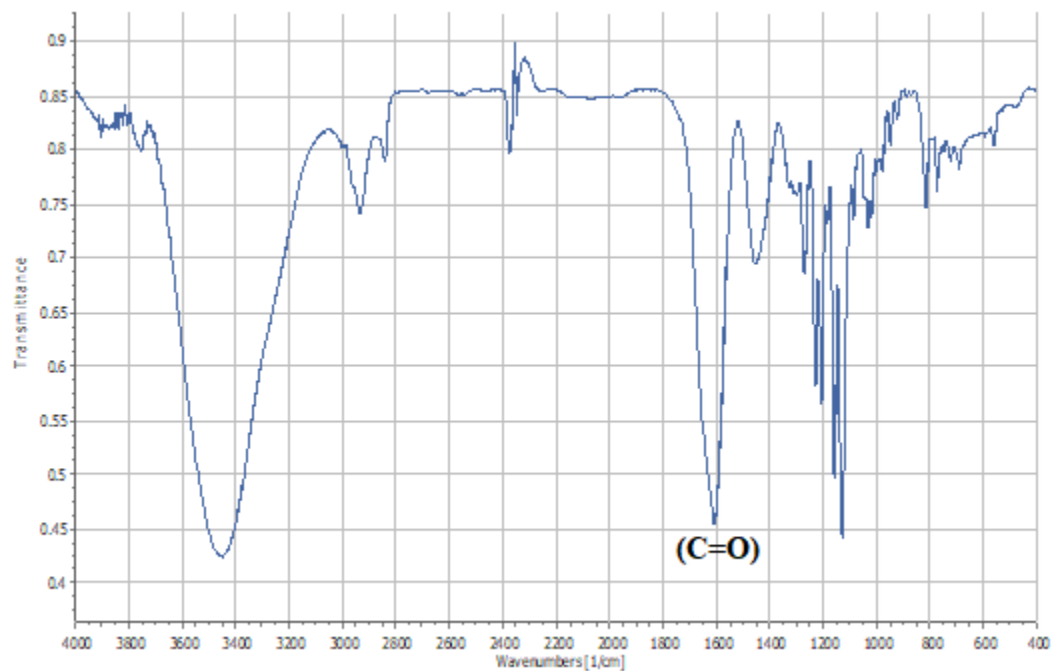


Figure 8.20 IR spectrum of 1

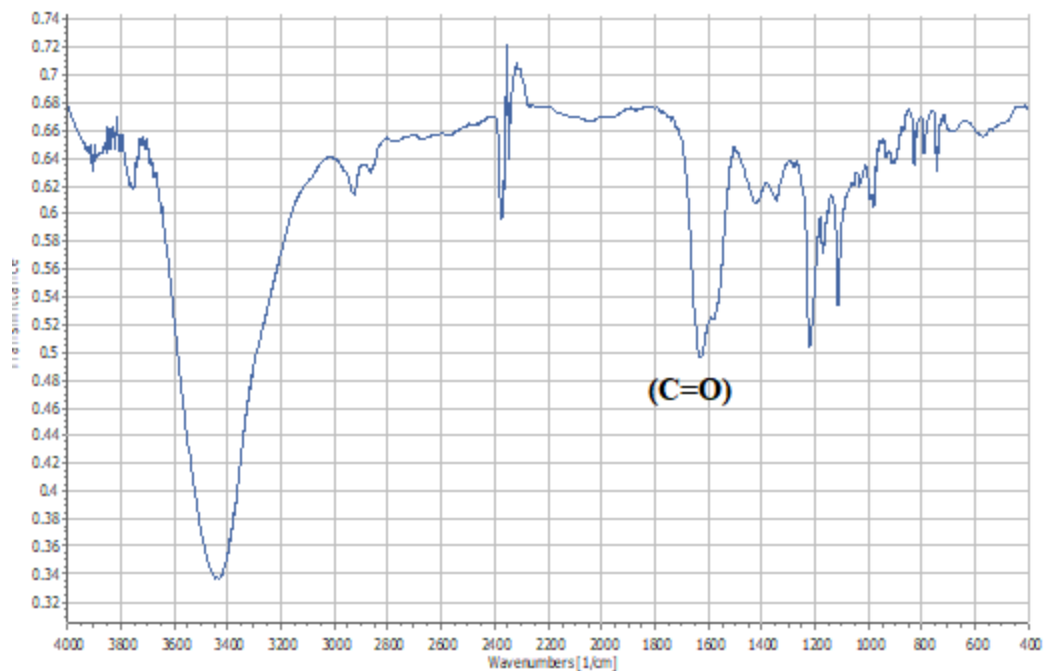


Figure 8.21 IR spectrum of 2

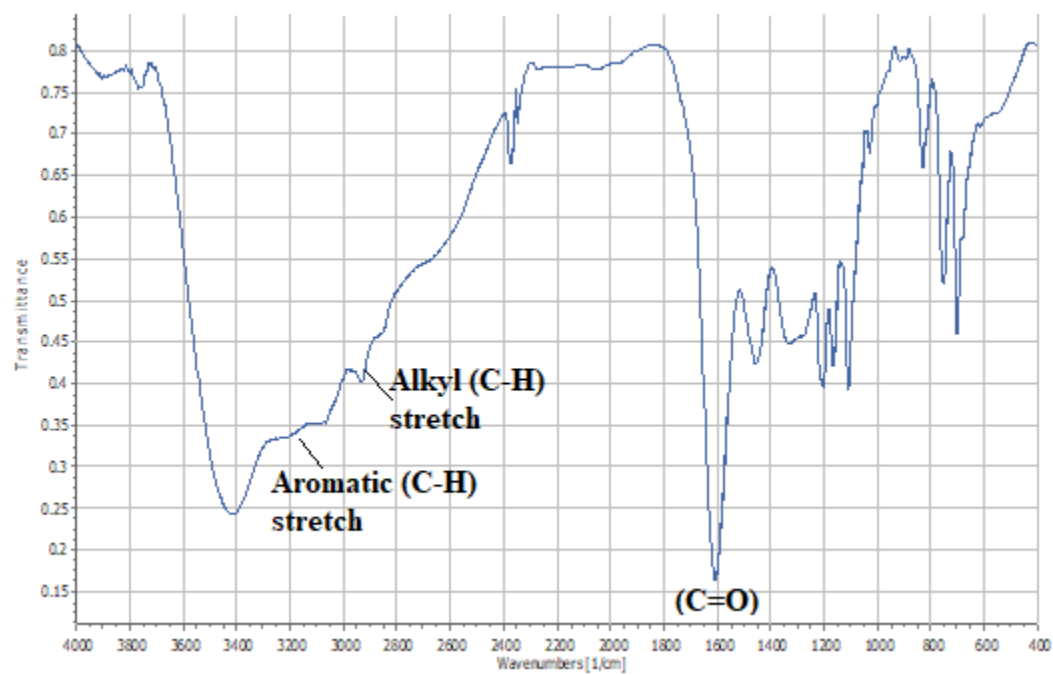


Figure 8.22 IR spectrum of 3

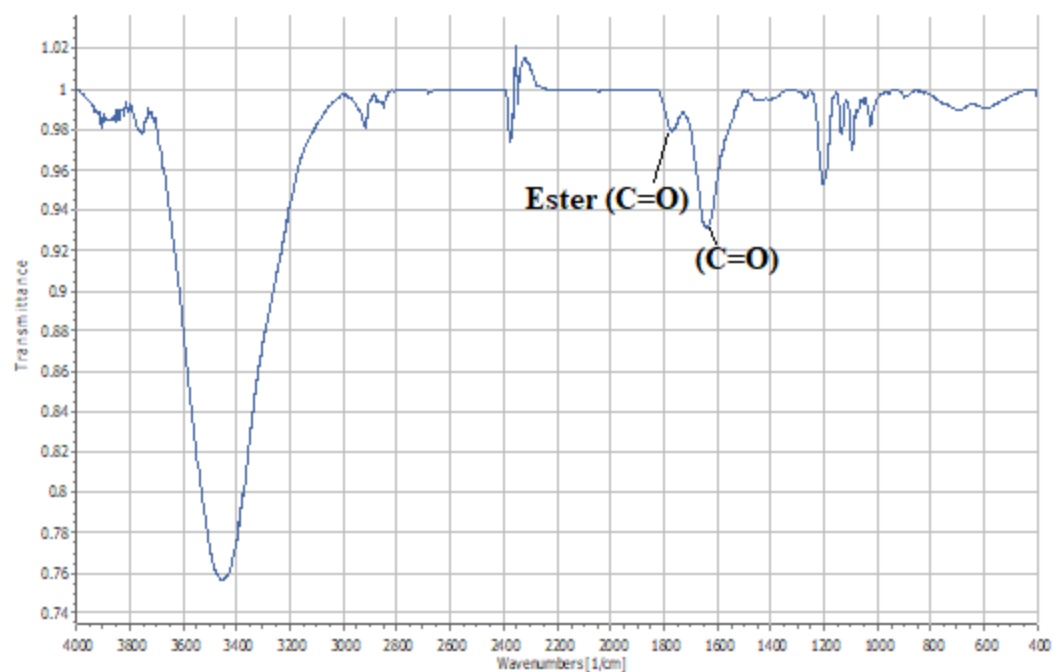


Figure 8.23 IR spectrum of 4

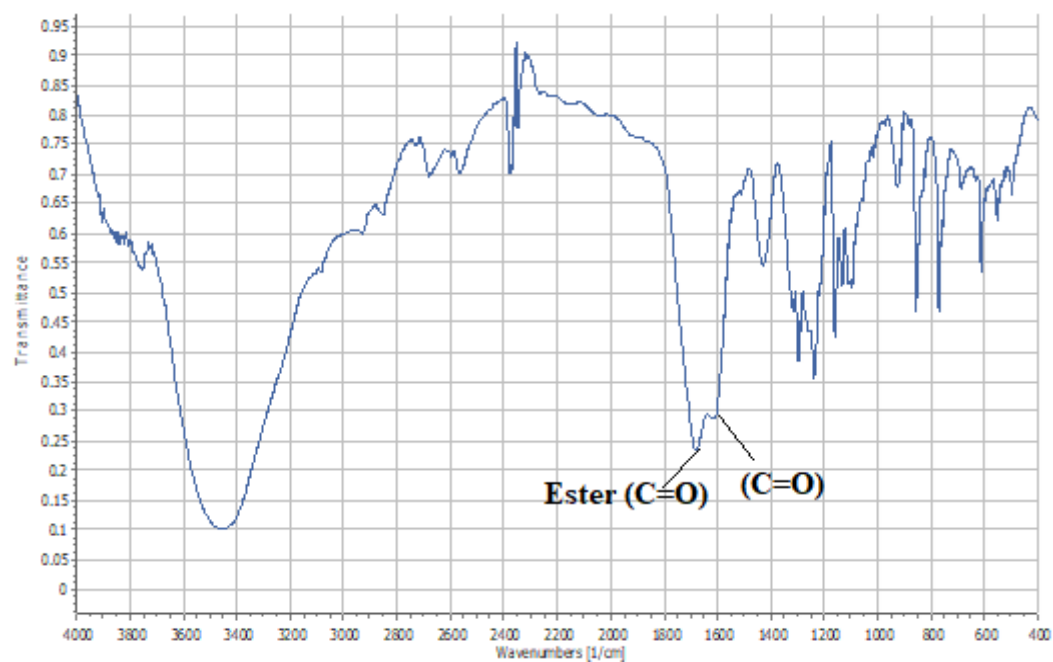


Figure 8.24 IR spectrum of 5

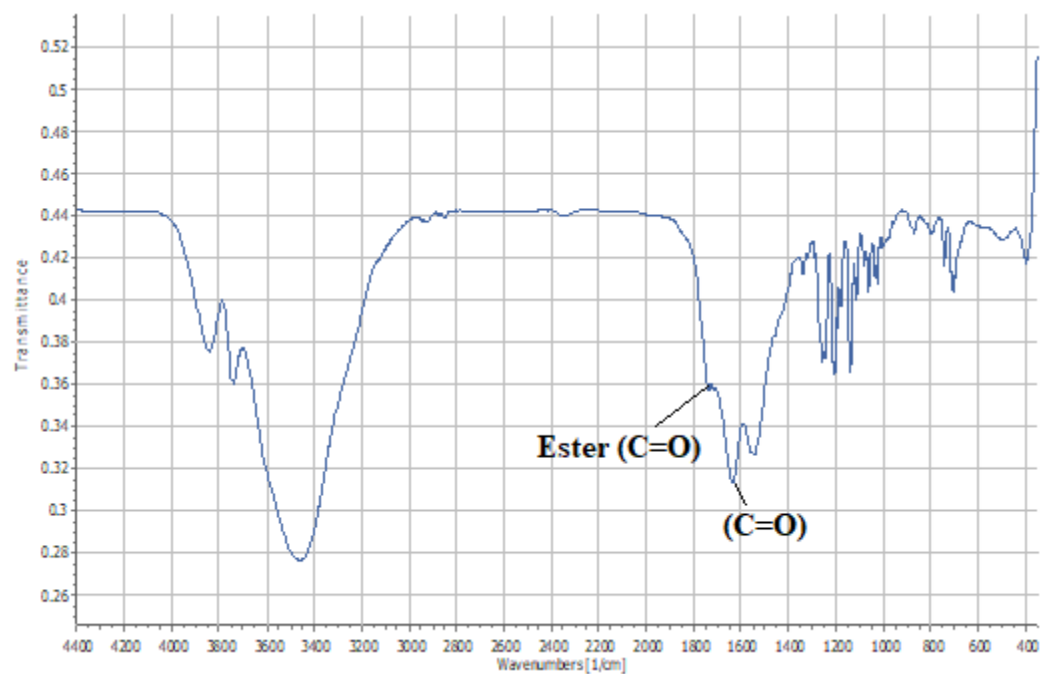


Figure 8.25 IR spectrum of **6**

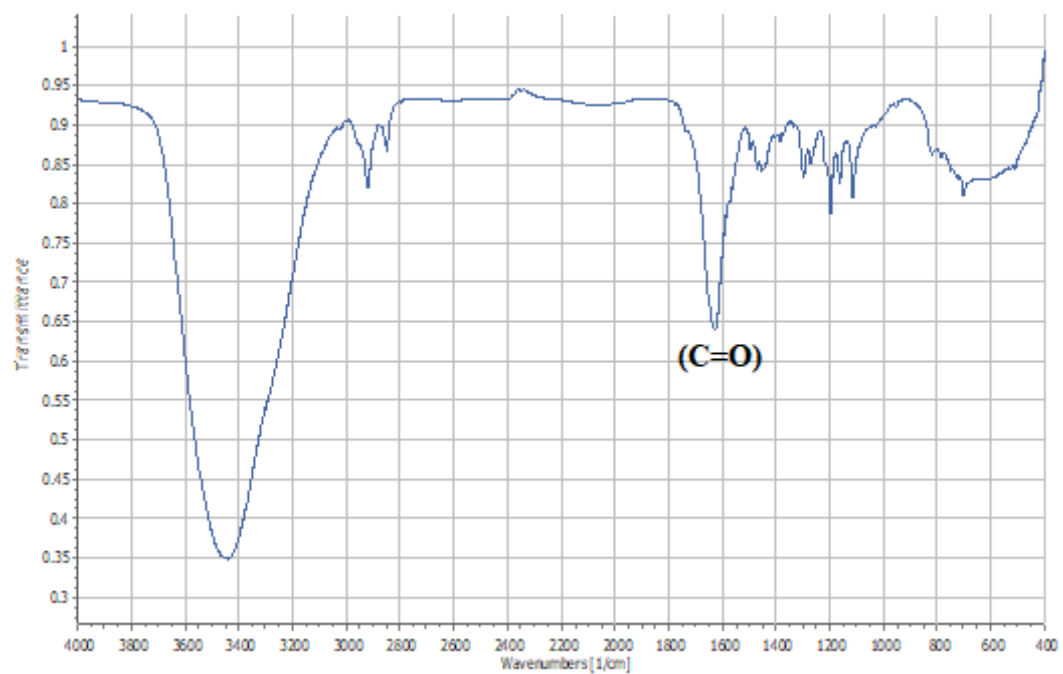


Figure 8.26 IR spectrum of **7**

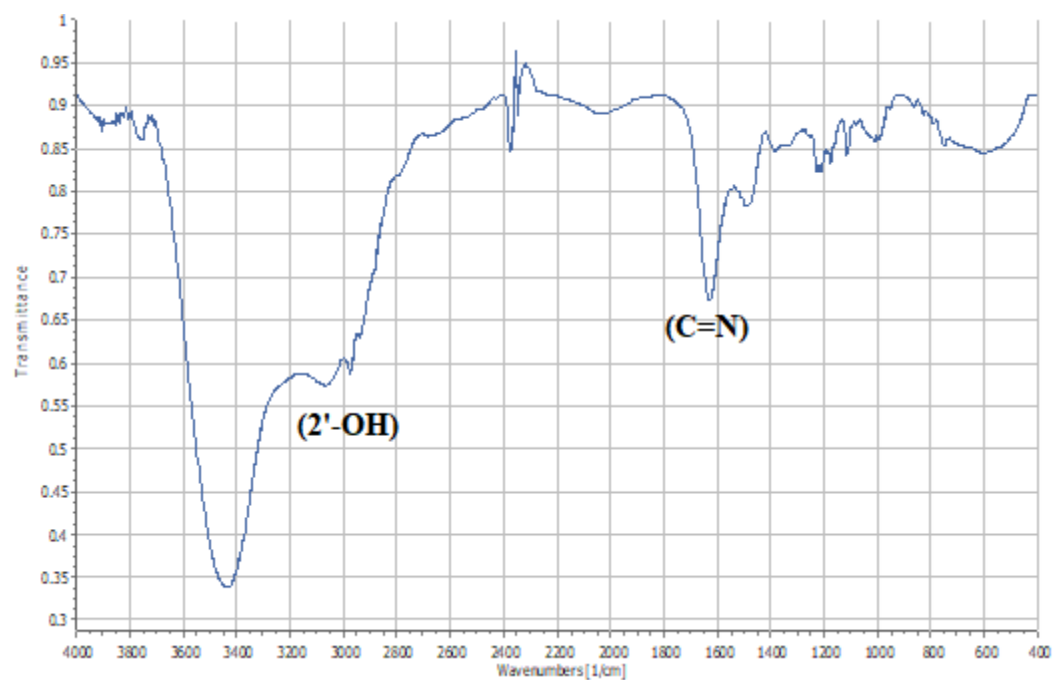


Figure 8.27 IR spectrum of **8**

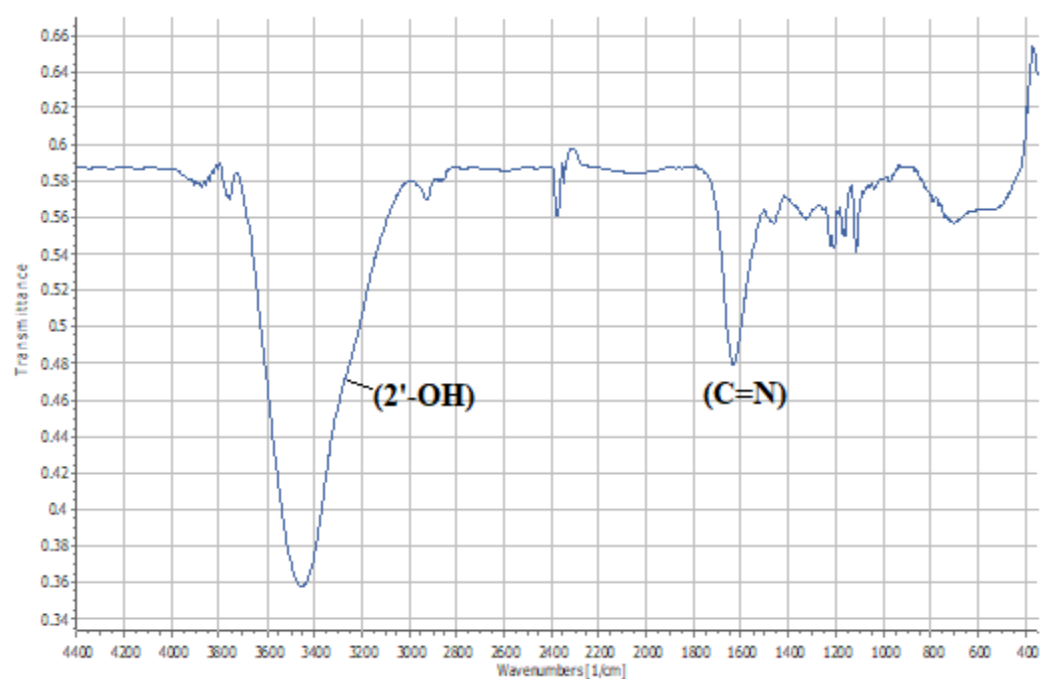


Figure 8.28 IR spectrum of **9**

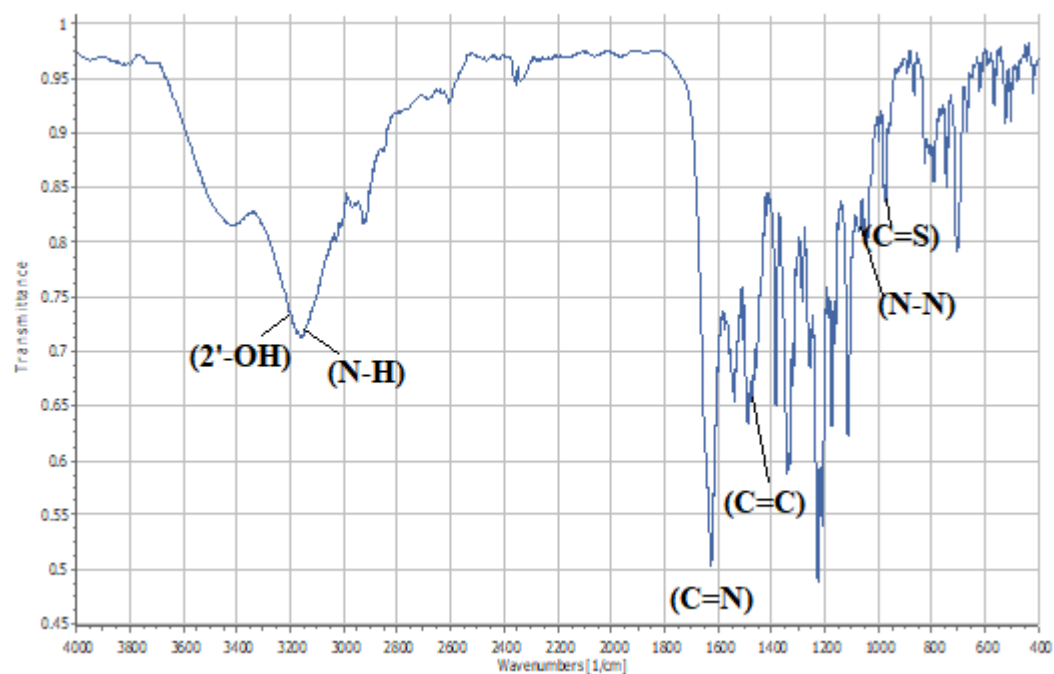


Figure 8.29 IR spectrum of **10**

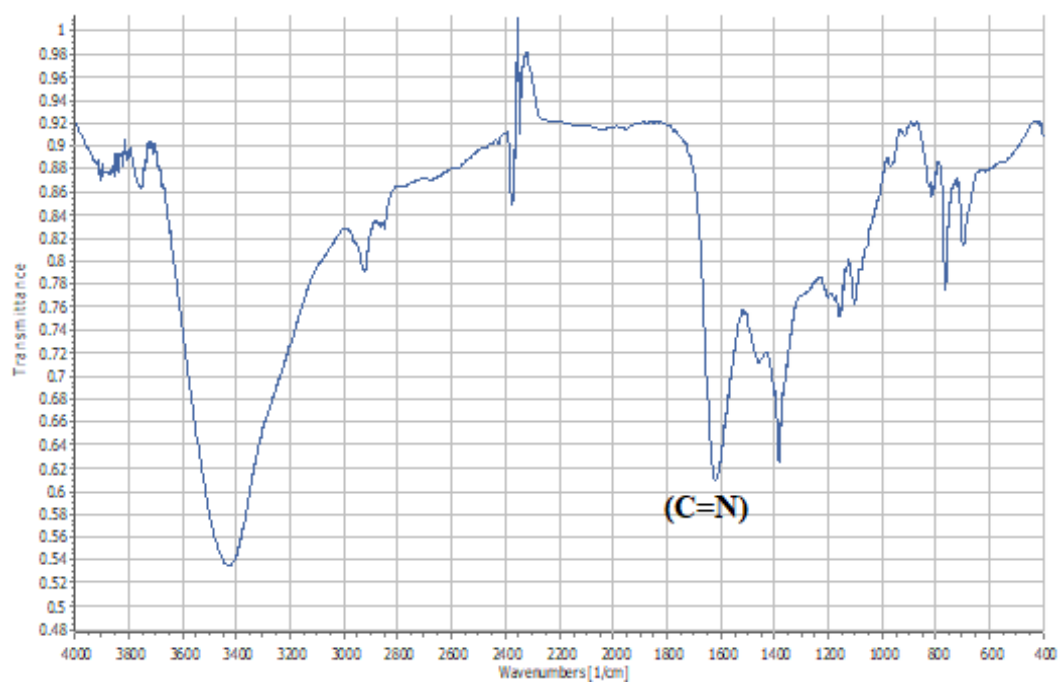


Figure 8.30 IR spectrum of **11**

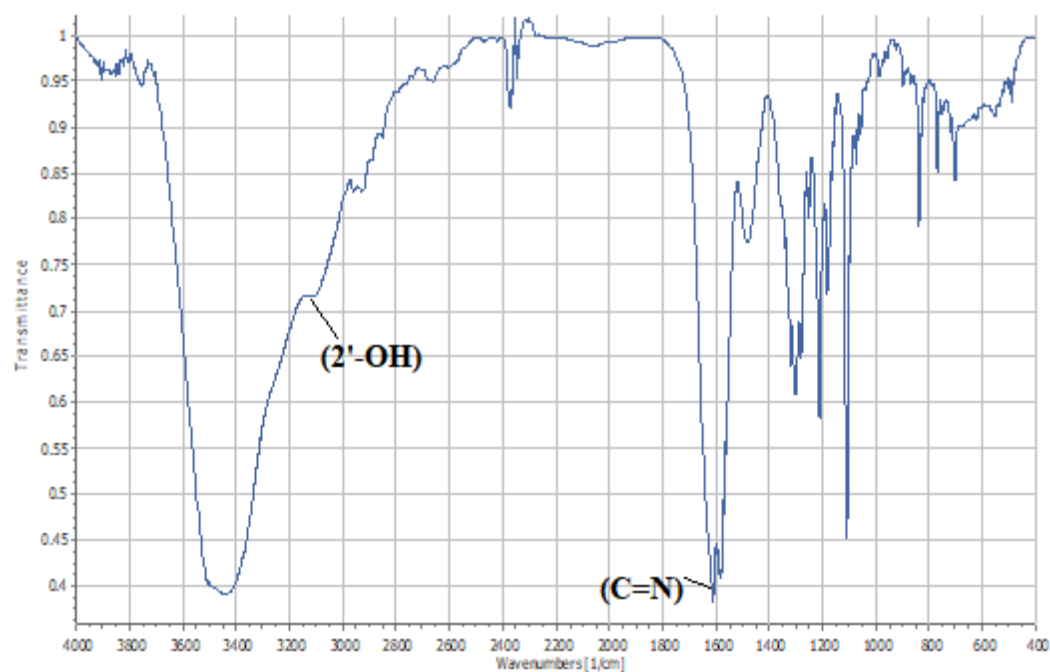


Figure 8.31 IR spectrum of **12**

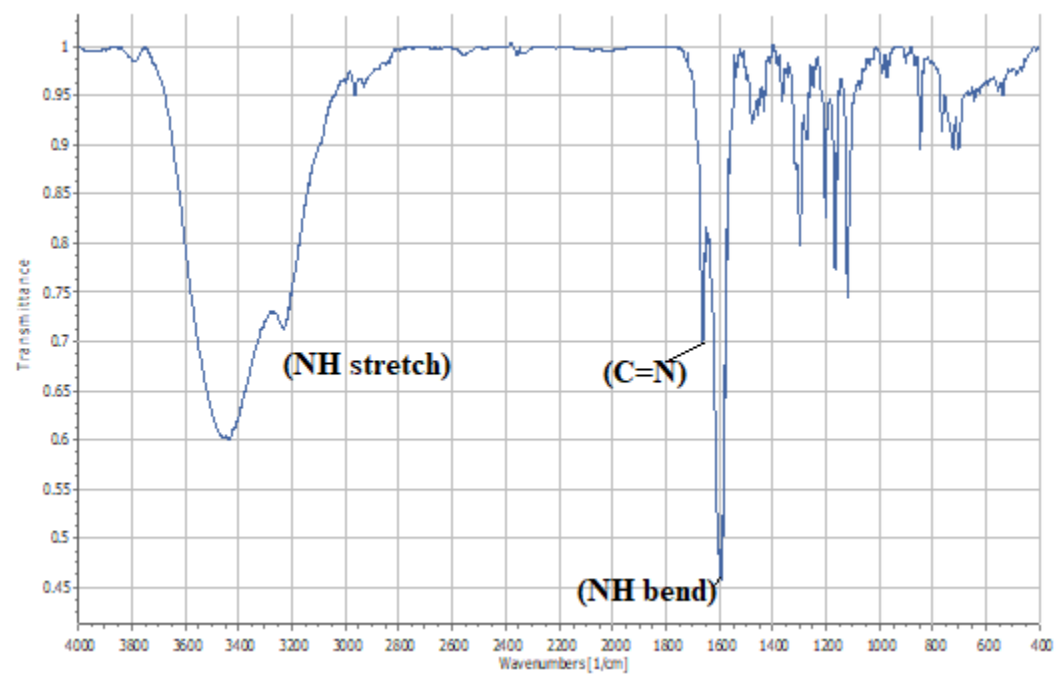


Figure 8.32 IR spectrum of **13**

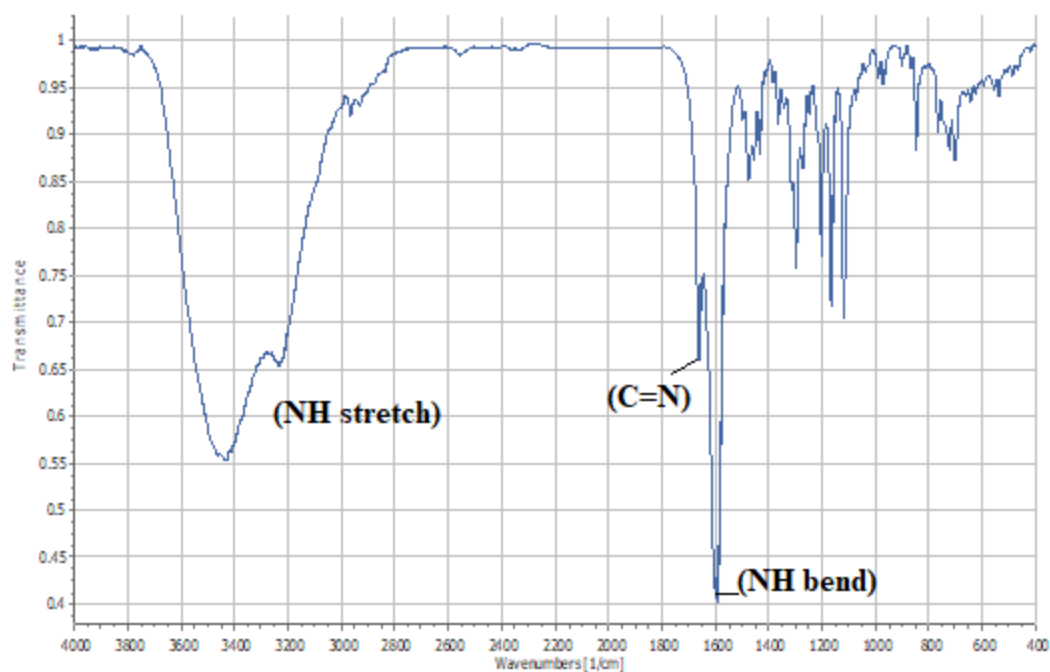


Figure 8.33 IR spectrum of **14**

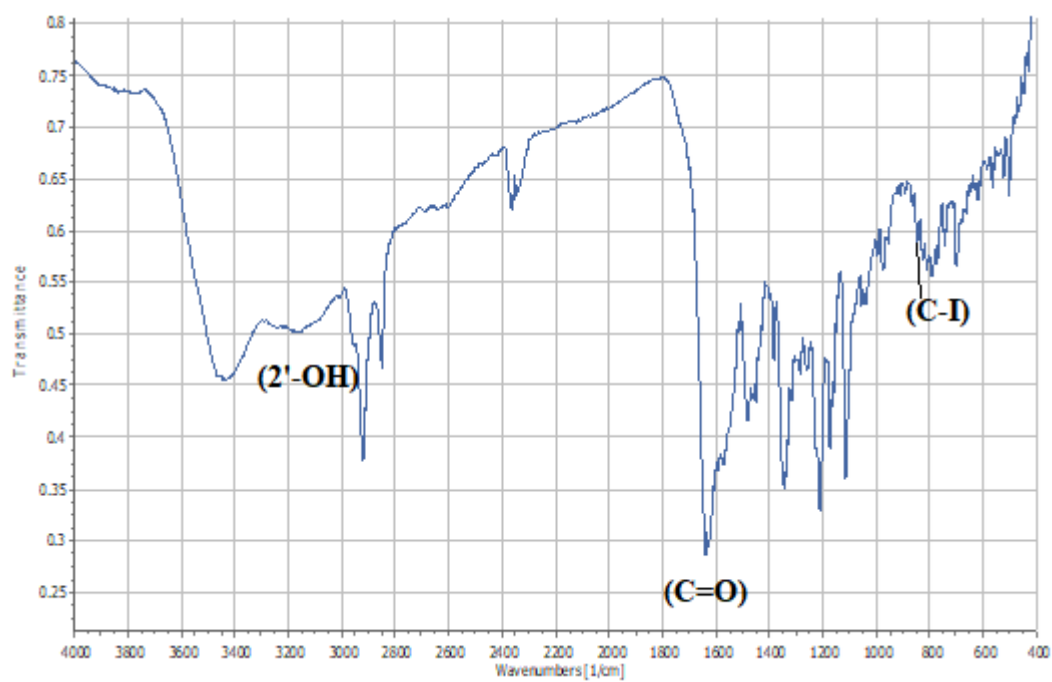


Figure 8.34 IR spectrum of **15**

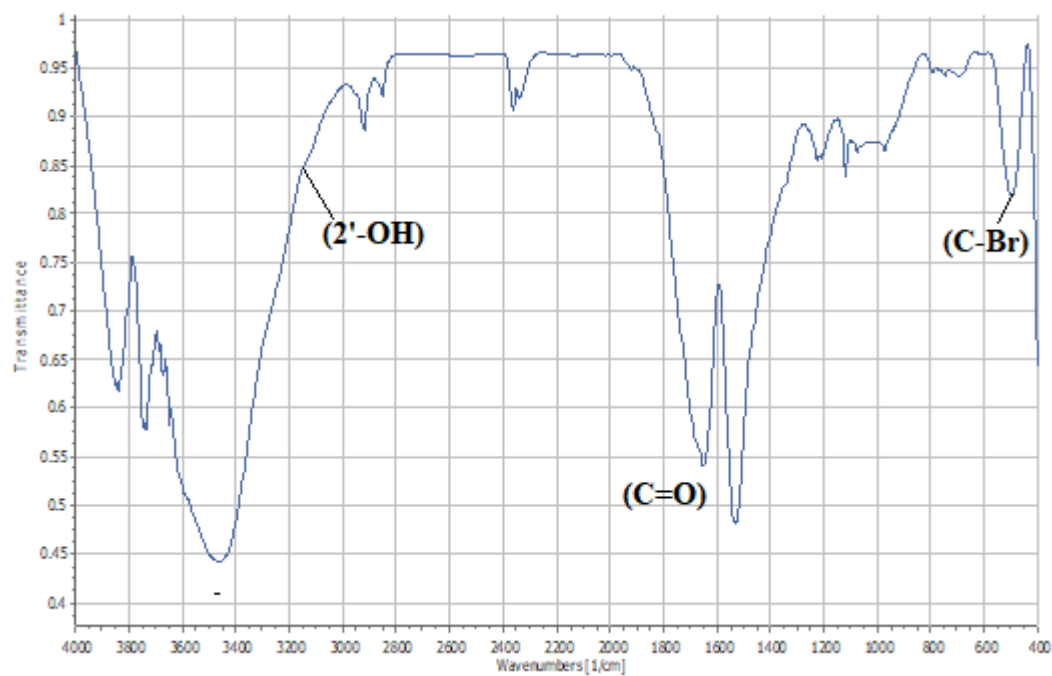


Figure 8.35 IR spectrum of **16**

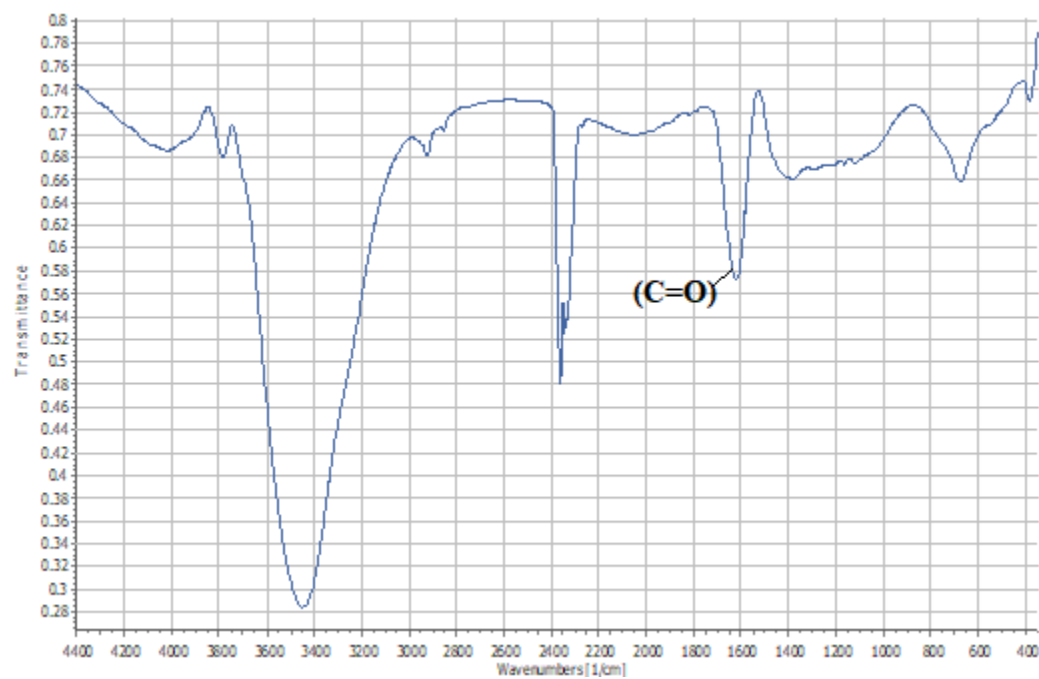


Figure 8.36 IR spectrum of **17**

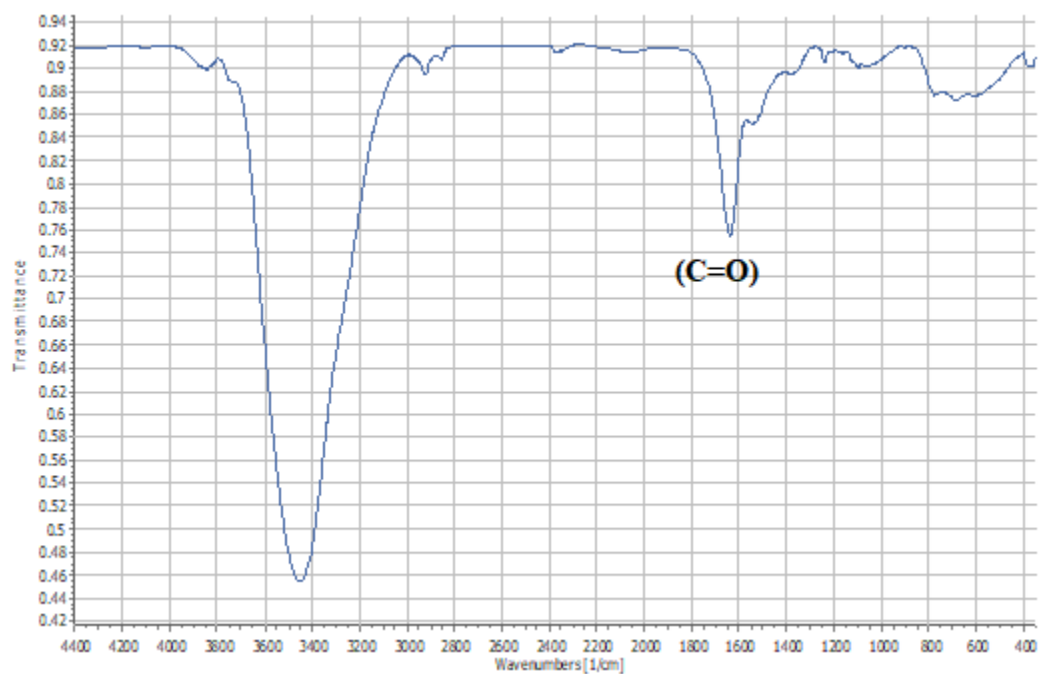


Figure 8.37 IR spectrum of **18**

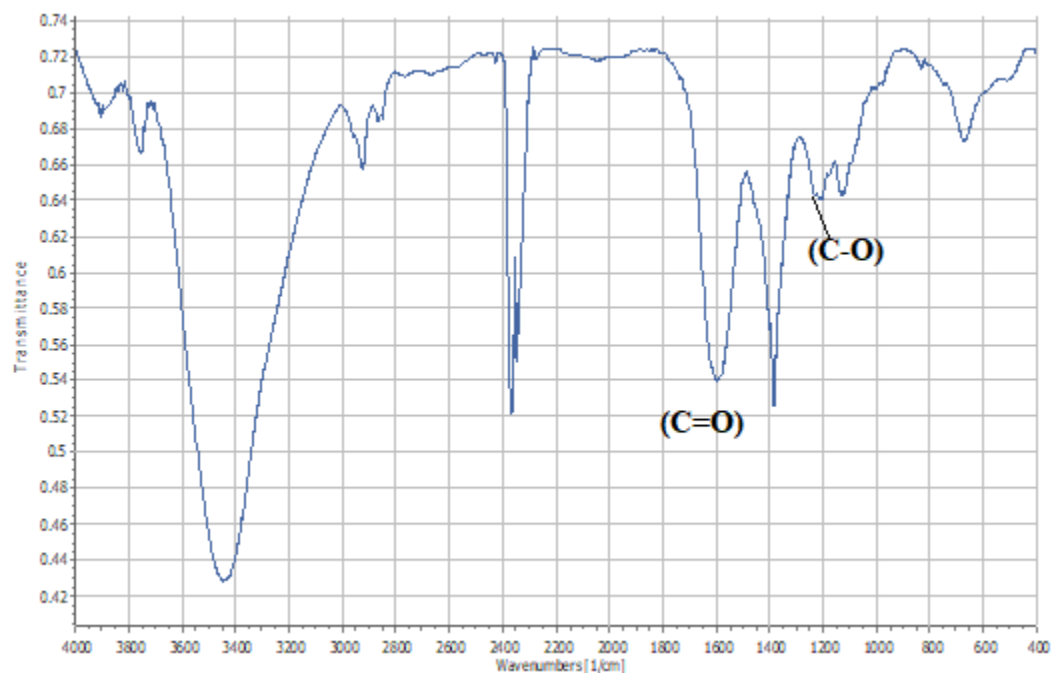


Figure 8.38 IR spectrum of **19**

8.3 Cell Viability Data for Compound 19 and Cardamonin at 24 h

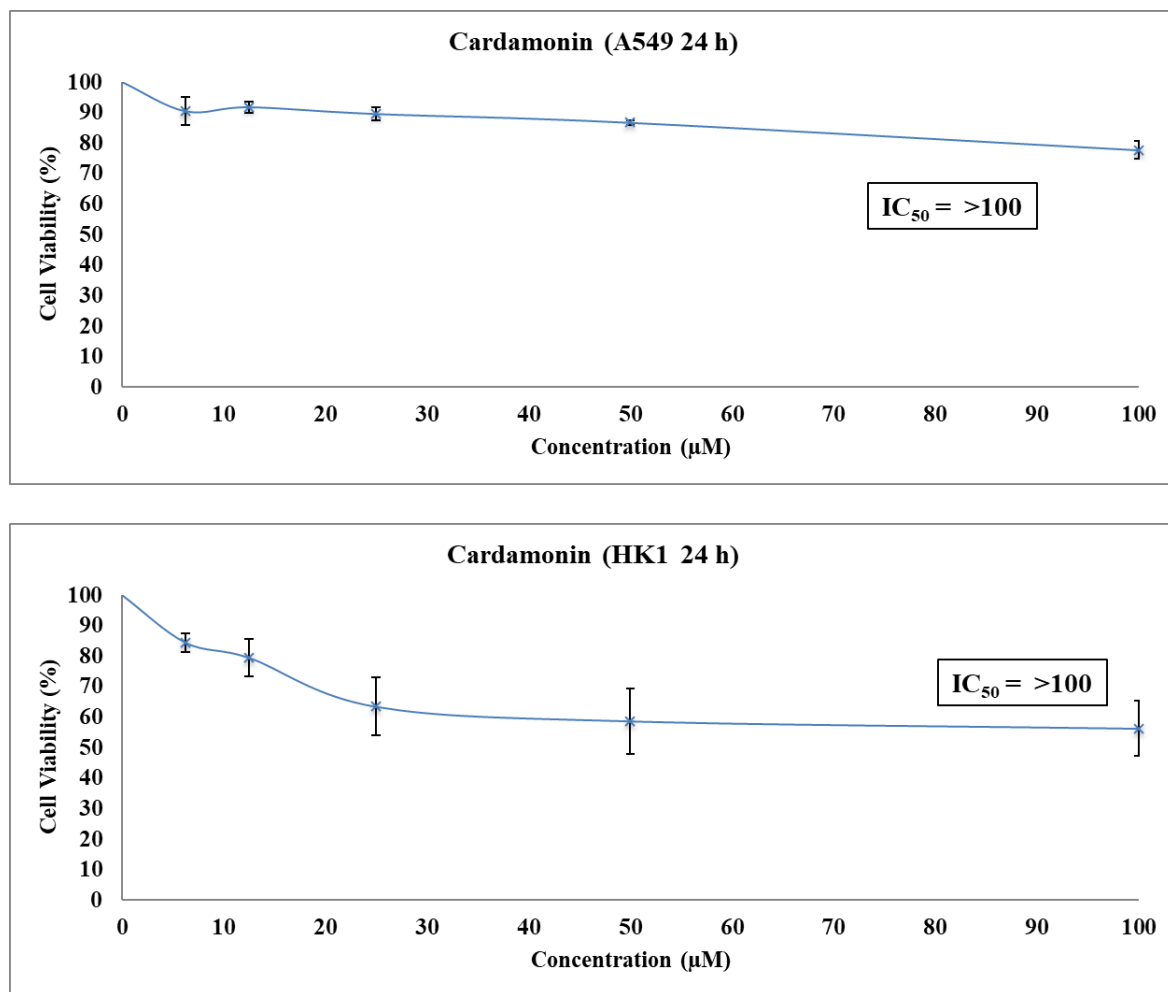


Figure 8.39 Cell viability (MTS assay) of A549 and HK1 cells pre-treated with cardamonin at different concentrations for 24 h. The assay was repeated three times, and bars and error bars refer to mean \pm SEM.

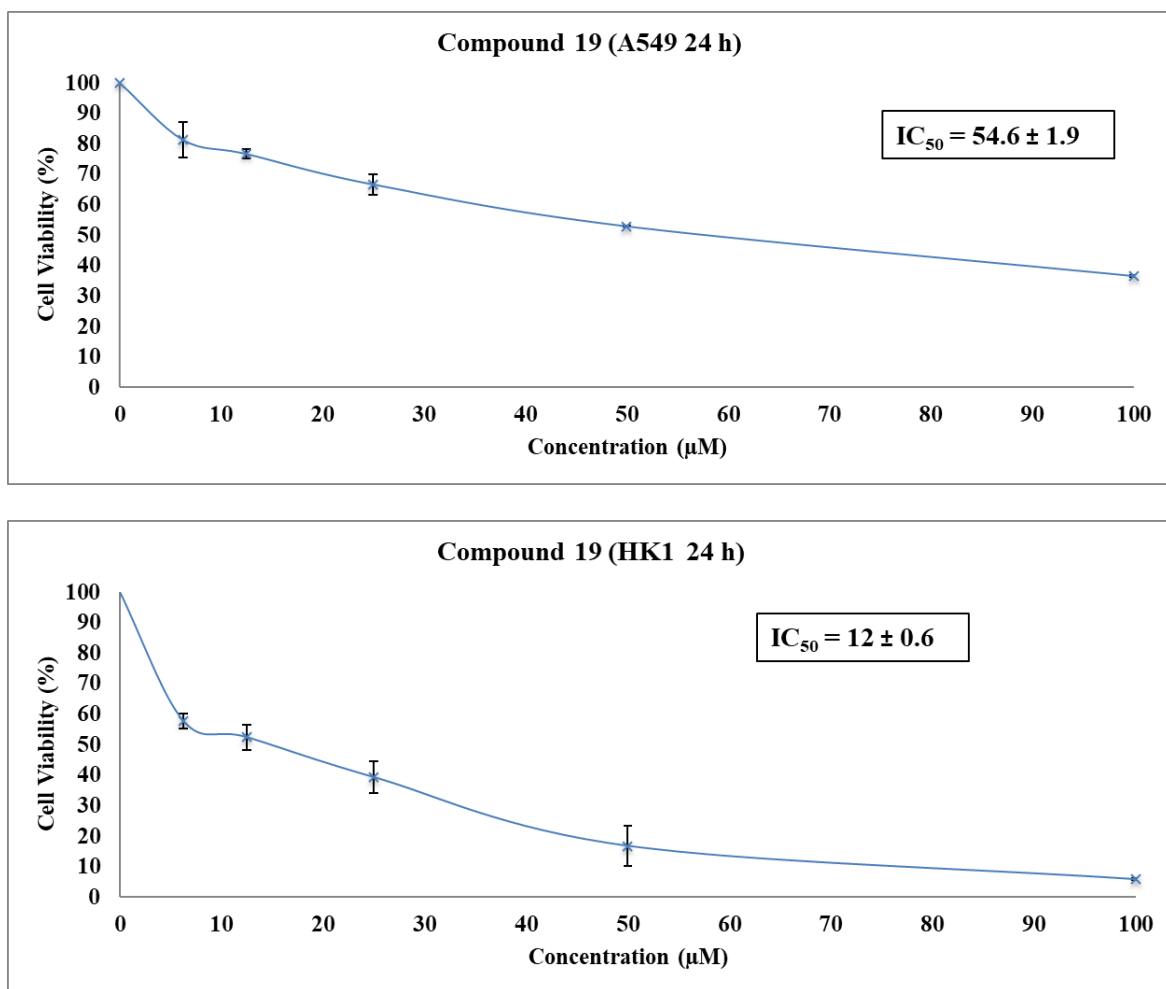


Figure 8.40 Cell viability (MTS assay) of A549 and HK1 cells pre-treated with compound **19** at different concentrations for 24 h. The assay was repeated three times, and bars and error bars refer to mean \pm SEM.

8.4 Caspase-Glo 3/7 Assay Attempts in A549 and HK1 Cells

Table 8.1 Caspase-3/7 activity of A549 cells and HK1 cells, treated with **19** at about 10 μ M. The experiment was performed in duplicate for each cell line and mean results are reported

	A549				HK1			
Duration of treatment (h)	12		24		12		24	
Duration of Incubation after Caspase-Glo addition (min)	30	60	30	60	30	60	30	60
% Caspase activity relative to control	130	137	117	119	200	189	103	105

Table 8.2 Caspase-3/7 activity of A549 cells and HK1 cells, treated with **19** at about 30 μ M. The experiment was performed in duplicate for each cell line and mean results are reported

	A549				HK1			
Duration of treatment (h)	12		24		12		24	
Duration of Incubation after Caspase-Glo addition (min)	30	60	30	60	30	60	30	60
% Caspase activity relative to control	121	122	71	73	181	169	85	86